UNIVERSITY OF OKLAHOMA

GRADUATE COLLEGE

# ADVANCEMENT OF NATURAL PRODUCTS: OPTIMIZATION OF INSTRUMENTATION AND EXAMPLES OF THEIR APPLICATION TO THE ISOLATION OF NEW COMPOUNDS

A DISSERTATION

SUBMITTED TO THE GRADUATE FACULTY

in partial fulfillment of the requirements for the

Degree of

DOCTOR OF PHILOSOPHY

By

ALLISON OLIVIA MATTES
Norman, Oklahoma
2019

# ADVANCEMENT OF NATURAL PRODUCTS: OPTIMIZATION OF INSTRUMENTATION AND EXAMPLES OF THEIR APPLICATION TO THE ISOLATION OF NEW COMPOUNDS

A DISSERTATION APPROVED FOR THE
DEPARTMENT OF CHEMISTRY AND BIOCHEMISTRY

BY

Dr. Robert Cichewicz, Chair

Dr. Bradley Stevenson

Dr. Daniel Glatzhofer

Dr. Indrajeet Sharma

Dr. Zhibo Yang

To friends, family, mentors, and peers.

## Acknowledgements

First and foremost, I must acknowledge Dr. Cichewicz for the mentorship and patience of helping me develop my skills. In chapter 3, edits and mentorship was also completed with the aid of Dr. David Russell and Dr. Sarah Robinson while at an internship at Genetech in San Francisco, CA. In chapter 4, the "chemical zoo" team tirelessly worked on all the soil samples to isolate, purify, extract, and sequence each fungus. Most notable of these coming from the work of Sara Helff and Carolyn Le. Jarod King completed all assay work on both the small scale isolation for initial identification as well as the pure compound MICs. In chapter 5, the isolation, purification, and identification of *Sphecaloma* were completed by the endophyte team led by Dr. Shikha Srivastava and the initial chemical extraction of the fungus, initial isolation of the elsinochromes and the isolation of persephacin A were completed by Dr. Saiket Haldar. Structure elucidation was completed in conjunction with both Dr. Saiket Haldar and Dr. Lin Du. Both *in vitro* and *in vivo* assays reported here were completed by Dr. Shikha Srivastava. All NMR data for chapters 4 and 5 was collected using instruments maintained by Dr. Susan Nimmo and her guidance and training on the instruments were essential to this work.

## Table of Contents

## List of Tables

## List of Figures

## Abstract

The world of natural products has a long rich history dating back thousands of years and was the origin of medicine as we know it. Advancements in the field of natural products can be seen not only in the isolation of new molecules, but also in the advancement of new tools that are used to elucidate the structure of new compounds, identify lead compounds, as well as monitor the pharmokinetics of bioactive substances. The third chapter in this dissertation introduces a new tool that could be used in the later steps of drug development by being able to rapidly quantify a fluorinated compound in complex mixtures, the fourth chapter includes a comparison of an advanced spheroid bioassay with the traditional 2D assay that can be used to identify appropriate lead compounds, and the fifth chapter reveals techniques for applying natural products to a less discussed target: agricultural fungicides.

Chapter 3 shows method optimization of quantitative $^{19}F$ NMR for the rapid analysis of fluorinated compounds in complex mixtures without the need for an internal standard such as a deuterated solvent. The resulting method was validated with percent errors below 4% on two different instruments. Future work on this work be to use it for pharmokinetics in biological sera or to help determine the bioavailbility of compounds in complex biological matricies.

Chapter 4 includes the isolation of polyketides that were tested against both monolayer and spheroid models of pancreatic cancer. The advanced *in vitro* spheroid technique shows how a compound (Asteltoxin G) that does not exhibit the most favorable activity on a monolayer assay can have high selectivity against pancreatic tumor cell line when the cells mimic a more tumor-like atmosphere with higher cell-cell interactions, core hypoxia, and a more hydrophobic environment between the cells.

Chapter 5 includes the isolation of three elsinochromes and a cyclic peptide with two analogs from a unique source: the endophytic fungus *Spaceloma corylii*. Two of the cyclic peptides had antifungal properties and were further explored for agriculturalapplications, a target less often analyzed in traditional academic research. These were tested both *in vitro* against possible pathogenic fungi and *in vivo* for systematic mobility was also analyzed and were found to be neither xylem nor phloem mobile. Additionally, due to the slow-growing nature of the fungus, growth conditions, and an isolation procedure was optimized. These optimizations compared variables such ad media components, media volumes, flask types, and methods of mixing/oxygenation. The best conditions were obtained with a bio-reactor or with lower volume baffled flasks.

# Chapter 1: Introduction

## 1.1 What is a Natural Product?

Natural products, in their most general definition, are compounds produced by any living organisms with a molecular weight below 3000 Da.[1] These compounds are further designated into two major categories: primary and secondary metabolites.[1] Primary metabolites are compounds that are essential to a cell's survival,[1] such as lactic acid, amino acids, lipids and carbohydrates, while secondary metabolites are not used in the day-to-day function of cells,[1] but may still contribute to the long-term survival of the organism. They can be relatively simple compounds like *N*-acyl L-homoserine lactones (AHLs),[2] highly complex compounds like azadirachtin,[3] or very large compounds like cyclosporine(Figure 1).[4]

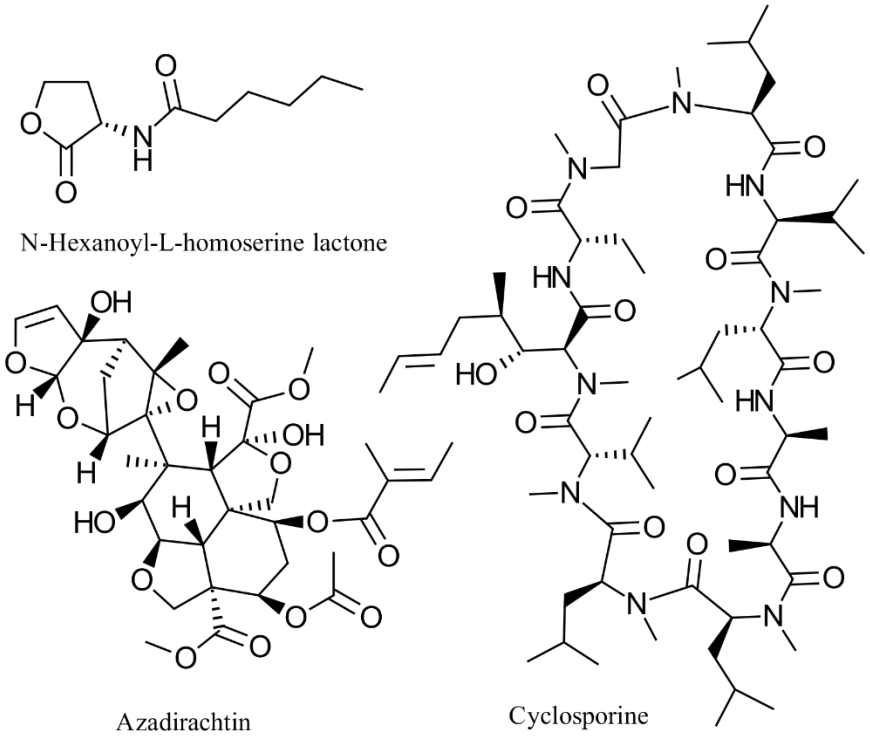


**Figure 1. Diverse Secondary Natural Products**
Examples of natural products highlighting the diversity of functional groups that can be biosynthesized and their complexity.

Typical uses for secondary metabolites vary tremendously, such as intracellular chemical signaling (e.g. hormones, quorum signaling or interkingdom signaling)[5,6] as illustrated by melatonin and AHLs, and agents of chemical warfare as highlighted by compounds like microcystins found as the deadly compounds produced in blue-green algae blooms.[7] In many cases, though, the full extent of the original intent of these secondary metabolites, as well as potential additional uses, remain undetermined.[8,9]

## 1.2 Historic Examples of Natural Products and Their Users

### *1.2.1 Ancient Times to Renaissance*

Modern science has designated procedures to determine the activities of natural products, but humans have been utilizing experimentation to determine the effectiveness of natural products long before the advent of the scientific method. One of the earliest examples of the implementation of natural products for medicinal purposes date back over 5300 years ago in the Alps.[10] Along with the remains of the Hauslabojch mummy, also known as "Ötzi, the Ice Man," were the fruiting bodies of the fungus *Piptoporus betulinus*, which have both antimicrobial and antitumoural properties.[10] Such logic was not limited to a specific region or culture. In the ancient Greek and Roman Empires, a plant called silphium believed to belong to the genus *Ferula*,[11] a genus of flowering plants belonging to the carrot, parsley, and celery family (Apiaceae), was used to treat a variety of ailments such as fever, warts, hair loss, and was most notably one of the most efficient abortifactants of the time. It was noted that feeding it to cattle bestowed a distinct flavor to the meat that made it even more of a prized commodity.[12] This plant was so important to their culture, that images of the plant were depicted on their coinage (Figure 2).[12]

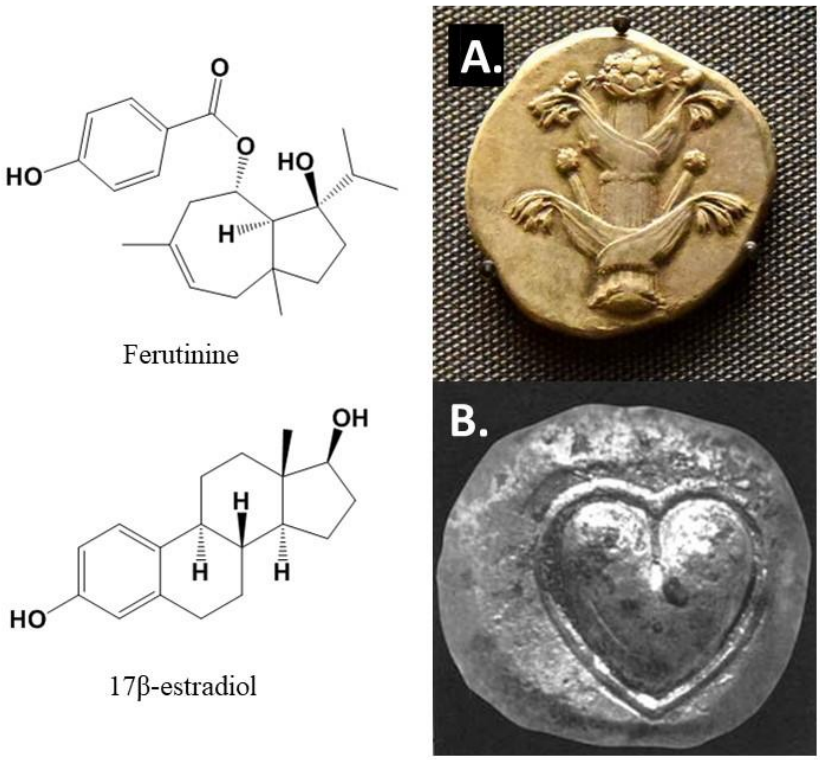


**Figure 2. Examples Highlighting the Importance of Natural Products in Ancient Cultures.** Coinage from the Mediterranean and phytoestrogens. A. Depiction of the silphium plant on coinage found in Cyrene highlighting the importance in ancient Mediterranean societies.[13] B. A representation of the seed from the Silphium plant, believed to be the origination of the heart symbol that has persisted to modern day.[14] The two compounds are phytoestrogens found in modern plants in the Apiaceae family known to target mammalian estrogen sensors.[15]

Figure 2 is one of the few mechanisms scientist have had to determine the likely genus of the plant, because due to the popularity of the plant and the difficulty in culturing it, it quickly succumbed to extinction.[12] It is believed the mechanism of action for the abortifactant is the high levels of phytoestrogens (plant derived compounds that mimic estrogen in mammals) that can been seen in other plants of the Apiaceae.[15–17]

This plant had also been identified in ancient Egyptian medicine, being in a nearby region and part of the Roman empire; however, Egypt had its own rich history with natural products. A document called the Ebers Papyrus was written in 2900 B.C. documenting over 700 natural product plant-based treatments including methods for their administrations.[18]

During the Medieval period, medicinal inquiry was largely completed by monks with the focus of trying to understand how and why the human body succumbed to illness. For this reason, new sources of natural products were identified in the countryside, such as the juniper species, *Juniperus sabina*, as abortifactant, which also was theorized to work through phytoestrogens.[11] Knowledge of these and other plants were usually passed on orally and so written records are scarce. As people emigrated from the countryside, however, many of these recipes were lost.[11]

At the end of the medieval period, began the Renaissance. The Renaissance found scientists focused on the elements of science and medicine, both figuratively and literally. Antoine-Laurent de Lavoisier created the definition of an element with 55 substances listed as potential elements,[19] while anatomy was advanced by human dissections, which helped diagnoses if not with novel medicines.[20] The basis for the modern tools in natural products, the foundations of chemistry and anatomy were developed in this time.

### *1.3 Advancements in the 19$^{th}$-20$^{th}$ Centuries*

Up until the 19$^{th}$ century, medicinal science focused on the describing either how the body ailed or what substances could be used to treat each ailment. That changed when a professor at the University of Dorpat in Estonia, Rudolf Buchheim, began to redefine the field of pharmacology (the study of medicine) into a true experimental science with a focus on specific

pharmacological agents and how they worked.[21,22] His student, Oswald Schmiedeberg, is typically credited with the development of modern pharmacology due to the significant strides he made in defining the field and making Germany a leader in the pharmaceutical industry up until WWII.[21,22] As synthetic chemistry was still in its infancy, (the first instance being the synthesis of urea in 1828[22]) natural product isolation was the preferred method for obtaining many pharmacological agents. During the time between the mid-19$^{th}$ century to the mid-20$^{th}$ century, investigations of the pharmacological effects of natural products helped develop society's understanding of medicine in leaps and bounds. Muscarine from the fly amanita fungus was found to effect electrical signaling in the heart, epinephrine was isolated from adrenal glands, histamine was isolated from pituitary gland extracts, pure insulin was isolated, and morphine was isolated from opium.[22]

Another notable advancement occurred when Alexander Fleming left on vacation and returned to find the inhibition of bacterial growth on plates contaminated with *Penicillium notatum* in 1928.[23,24] While unable to isolate the compound in large quantities himself, in 1940, two other scientists, Howard Florey and Ernst Chain, developed a mass production of the compound in time for WWII.[24] All three scientists received the Nobel Prize in 1945 for the identification of a pharmacological agent that was able to target all gram-positive pathogens.[24] This began the antibiotic revolution, and it is estimated that penicillin and its derivatives have saved over 80 million lives.[25,26]

Discoveries have continued throughout the mid-19$^{th}$ to mid-20$^{th}$ centuries with many new compounds being discovered from natural products that have been described as "truly revolutionary modern medicines with a tremendous impact upon healthcare."[27] For example, there are the immunosuppressants cyclosporine, rapamycin, and FK506 that have helped prevent

the rejection of organ transplants and the avermectins which nearly eliminated the African river blindness.[27] However, natural products are still awaiting their next major revolution since the discovery of antibiotics. On the road to a new major revolution, there are some pitfalls that can delay bringing an extract to market.

### *1.3.1 Pitfalls in Extracts to Market*

While natural products have had a profound impact on the current health system, there are some problems associated with natural product discovery that often cause delays in development. The most significant problems occur with the development of a majority of these natural products, which took 10-20 years to optimize, if the attempt was made to synthetically optimized their structures at all.[27] There are four main reasons for the delay of a drug from discovery to a marketable product. The first is the formulation required. While all drugs require development time for formulations, some of these natural products pose challenges associated with their solubility and stability. The remaining three reasons are all present in the story of Taxol (paclitaxel): source/quantity of the original compound, synthetic reproduction, and biological target identification. Taxol was originally isolated from the bark of the Pacific yew tree, *Taxus brevifolia*,[28] which is very slow-growing and harvesting the bark for Taxol results in tree mortality. Therefore, even after identifying its profound activity in extract form, sourcing enough compound for structure elucidation took 11 years.[28]

Many of the same features that allow natural products to be selectively active targets, the most notable being chiral centers, are what cause problems in both the elucidation of the compound as well as the synthesis. Natural products typically have more chiral centers than synthetic drugs, a feature that can make them more specific towards their biological targets, but

also much more difficult to produce in an efficient manner, sufficient quantity, and reasonable cost. Ultimately, a semisynthetic route was determined using an analogue from another yew tree, but this has been further replaced by being able to grow the plant cells independent of the tree, a feat highlighted in importance with award of a the Presidential Green Chemistry Challenge in 2004.[29–34]

The fourth reason for a delay in the development of natural products into a pharmaceutical agent is the final route to proving the effectiveness in a full system as opposed to single cellular *in vitro* analysis. Since animal testing and clinical trials are costly and have high failure rates (90-95% failure rate between animal testing and clinical trials[35]), many have attempted to identify biological targets before performing such tests. While there are many complex iterations of the route,  the two most common are direct binding to purified proteins or phenotypical evaluations with a variety of cell lines.[36] For Taxol, it took an additional 9 years to determine its biological activity.[28] For some natural product pharmaceutical agents, the biological targets are still unknown.[27] In some cases, following the incorrectly assumed biological target has potentially posed significant cost, wasted unnecessary resources, and delayed discoveries of a treatment as is one theory for the 412 failed clinical trials over 10 years of Alzheimer drugs targeting amyloid-β protein instead of the now theorized root cause of bacterial/fungal infections.[37,38]

### *1.3.2 The Debate of Rational Design Versus Natural Products*

In the 2000s, there was a major push towards synthetic libraries which would eliminate the delays associated with drug discovery as these compounds were already designed with Lapinski's rules[39] and had accessible synthetic routes.[40] However, these synthetic libraries have

not been as fruitful as originally hoped. At the same time, advancements in robotics and computational analysis programs have helped high throughput analysis of drug discovery. These tools have resulted in rapid assay screening, as well as advanced prefractionation, which can be as unique as each drug program sometimes separating a crude fraction into 5-15 samples[41] or into about 200 fractions with an estimated 1-5 compounds each.[42,43] The differences in prefraction are largely tailored to the resources available to the lab and the nature of the extracts, but the general benefit of prefractionation to such an extent allows for rapid dereplication, which prevents a major bottleneck in current drug discovery: scientific labor in isolation and compound elucidation. It also allows detection of highly active yet minute quantities of novel compounds. While some have questioned the usefulness of natural products, computational studies have shown that natural products occupy a more diverse (larger and more complementary) region of chemical space than other (synthetic) sources.[27,44] This has been supported by the continued frequency of natural product and derivative drug approval rates which have been consistently occupying 39% of approved drugs from 1981-2010.[44]

### *1.3.3 Prospects for the Future*

As natural product drug discovery progresses into the future, soil microorganisms and marine sources are prime sources for novel drug candidates. Between 1981-2006, there were 24 new natural product entities that made it past phase II clinical studies, 16 of which were from soil microorganisms.[27] One possible reason for this is that soil is "extraordinarily rich in unique species."[45] Since there is an estimated 2-5 million different fungal species, of which only 100,000 have been identified,[46,47] there is significant promise for discovery of new compounds as

advanced culturing techniques are developed, as this dissertation shows with the isolation of new analogues of asteltoxin with increased stability and activity within a spheroid assay.

There is a new frontier that is further being explored by natural product drug discovery scientists: endophytes.[48–52] Endophytes, organisms that coexist within a plant's tissues without being pathogenic for at least part of their life cycle, can behave symbiotically as well.[53–55] Often, this symbiosis manifests by producing compounds that are antimicrobial to eliminate other pathogens that threaten their host environment.[51] They have also been theorized to produce nutrients for the host plants as well as modify the plant's own antimicrobial compounds to either increase toxicity or specificity towards organisms other than themselves.[53–55] Not only are these endophytes a new frontier as a source for novel organisms and novel compounds, endophytes have begun to be utilized in other aspects of drug development. For instance, recent fermentation practices have used endophytes produce the precursors for paclitaxel to be able to meet the clinical demand without harvesting the host plants to extinction.[29–34] For complex natural products that are difficult to obtain through total synthesis, these fermentation practices are also a new frontier of natural product technologies.

One area these fermentation-only practices lack is with the incorporation of certain atoms, like fluorine, which has unique electronic properties. When placed in the correct location, the small size yet high electronegativity and potential to accept hydrogen bonds of fluorine can cause compounds to increase their half-life by resisting proteolysis as well as changing binding affinities. As new compounds are identified from unique sources such as endophytes, another frontier is to logically substitute these fluorine atoms into key locations using synthetic chemistry. These syntheses have been more attainable following the organometallic synthetic revolution when reactions such as the Negishi coupling had been discovered that allow facile

formation of carbon-carbon bonds. More recently, organometallic synthesis have begun finding regioselective routes for the formation of carbon-fluorine bonds.[56] These practices of incorporating fluorine into known APIs (active pharmaceutical ingredients) have already begun making an impact on the market. In fact, in 2015, approximately one in five drugs (including immunoglobulin drugs) contained fluorine and its incorporation has increased to nearly one-third of the newly approved small-molecule drugs.[57]

With the new atom comes a new benefit to drug discovery. Fluorine's only isotope, $^{19}F$, is NMR active. While this dissertation covers the rapid quantification of $^{19}F$ with an external standard, and this is applicable in the synthetic/medicinal chemistry area of drug discovery, this technique may eventually be applied to one of the most difficult transitions of specialties in drug discovery, the *in vitro* to *in vivo.* It has long been argued[58] that animal studies are not adequate predictors of efficacy in humans, and genetically modified mice for a phenotypic response might not have the same irregularity as the human disease state. For that reason, low-dose clinical trials have become more commonly accepted for drug submissions before full *in vivo* testing.[58,59] These low-dose preclinical trials are directly benefitted by the $^{19}F$ NMR development presented here as more and more drugs become fluorinated. Eventually, pharmokinetics and bioavailability will be able to be quantified directly in biological media with fluorinated compounds without the need of animal testing and potentially decreasing the failure rate in clinical trials with adequate analysis during pre-clinical trials.

Other potential advances to decrease the failure rate between *in vitro* and *in vivo* testing can include advanced assays such as the spheroid assay (discussed within chapter 4) or the organ-on-a-chip, small chips containing specialized human cells in an environment that better mimics a whole organ procedures.[59–61] New reliable and reproducible assays that can bridge that

gap between the fields are lacking in the field. For instance, a paper by Amgen analyzed 53 "landmark" studies and found that only 11% were reproducible.[62] Its concluded that since the majority of these failures occurred between switching of project experts (eg. drug discovery to medicinal chemists to clinical), it is important that the communication between the lines of clinical, medicinal chemists, and drug discovery chemists improve their communication, and proper preclinical validations of primary scientific data before engaging in clinical trials is necessary.[62]

### *1.3.4 Summary and Relevance to Dissertation*

In summary, natural products have been the source of medicine throughout the ages, being found with remains over 5300 year ago,[10] in written records of applications over 2900 years ago,[18] and influencing cultures which have in turn created symbols that have persevered through modern days.[12] Applications of natural products have only become more successful with the advent of new technologies that can be isolated for the specific active compounds as seen with penicillin, be modified for quantity as is seen with the semi-synthesis and now fermentation of paclitaxel, and be predicted as is seen with *in silico* modeling and exploring chemical space.

This work helps advance the field for the future of natural products by developing quantitative $^{19}$F NMR to help in the development of the analysis in fluorinating natural products. The fluorination of natural products is a trend already seen in FDA approvals due to $^{19}$F unique characteristics such as being relatively small for a hydrogen bond acceptor and its electronegativity which has been shown to be able to increase inherent stability of compound when substituted at specific locations as well as help molecules resist enzymatic degradation. This work adds an additional benefit to those compounds, namely in including additional tools to

monitor these compounds in environments that would originally be difficult to analyze (*via* $^{19}F$ NMR). Further development on this would might allow direct analysis in media, such as blood, that would be unsuitable to analyze unprocessed samples such as HPLC or MS.

Additionally, seen in this work are isolations of a polyketide with anticancer properties and a cyclic peptide with antifungal properties. Both compounds come from fungi, a source underexplored with only an estimated 2% of species isolated. These fungi were isolated from a soil sample and a leaf respectively. The organism from the leaf, *Spaceloma corylii*, was behaving as an endophyte which are relatively unexplored for chemical constituents due to their difficult isolation in high-throughput methods. Both chapters also investigate non-traditional assays designed to increase the likelihood of success in determining a potential lead compound.

# Chapter 2: Hypothesis and Chapter Overviews

## 2.1 Introduction

This chapter introduces the prevalent hypothesis mentioned in the following section, as well as the hypothesis for each of the following chapters distinguished in individual sections. After the hypothesis, an overview is presented summarizing the content of the chapter.

## 2.2 Research Questions

The natural product pipelines to drug discovery have experienced many upgrades to increase productivity; however, new innovations are still needed to overcome backlogs that arise in identifying appropriate lead compounds. These backlogs can occur from culturing new sources of organisms, creating appropriate assays to limit failed *in vivo* or clinical trials, or quantifying bioavailability during pre-clinical trials. Advancements in the tools used within natural product pipelines can lead to new potentially active pharmaceutical ingredients. Due to the diverse background of fungi and that only an estimated 2-10% of potential fungi have even been characterized, fungi represent an ideal source for new natural products. **Can advancement in the proper tools be used to identify better lead compounds prior to clinical trials**?

The primary research question was tested using the following specific research questions:

1. Can an external standard be used to rapidly yet accurately quantitate active pharmaceutical ingredients (APIs) containing fluorine via a $^{19}F$ NMR method?
2. Can a spheroidal assay identify a potential lead compound that a monolayer assay would miss?

3. Can a high-throughput laser cutting device isolate an endophyte with a previously unidentified natural products?

### 2.2 Chapter 3. Applications of $^{19}F$ Quantitative NMR to Pharmaceutical Analysis

Incorporation of fluorine into active pharmaceutical ingredients can be beneficial to important properties such as metabolism, stability, and selectivity. This has resulted in nearly one-third of the newly approved small molecule drugs containing at least one fluorine atom. This 100% naturally abundant isotope, $^{19}F$, can therefore be easily identified even in complex mixtures. Despite the potential, $^{19}F$ quantitative NMR (qNMR) has been slow to develop. Herein is presented experimental methodologies utilizing optimized parameters for uniform quantification of fluorine containing drugs. Validation has been confirmed using both gravimetric and absolute concentration data reduction. The specific research question was found to be supported as an external standard can be used to accurately quantitate fluorinated compounds rapidly. This has a far-reaching impact as this technique may currently be implemented in medicinal and synthetic chemistry by quantitating synthesized compounds within non-deuterated solvents that would otherwise be unquantifiable in $^{1}H$ NMR quantitation. After further minor optimization, this method may be used during pharmokinetic analyses to quantitate bioavailability within blood without modification to the sample.

### 2.3 Chapter 4. Asteltoxin G Is a Selective Toxin of Pancreatic Cancer Line Spheroids While Preserving Normal Fibroblasts and Normal Pancreas Spheroids.

In this project, a fungal extract screening program was initiated on cells grown in monolayers, looking for compounds with selective toxicity that killed MIA PaCa-2 and Panc-1

pancreatic cancer cell lines while remaining safe to NIH/3T3 normal mouse fibroblasts and hTERT-HPNE normal pancreas ductal cells. One extract out of 3,588, isolated from a soil sample from a forest near Mt. Hood, Oregon and later identified as *Pochonia suchlasporia,* distanced itself from all others in its selectivity for cancer cell lines. It was subjected to bioassay-guided fractionation, which yielded a new asteltoxin derivative, named here as asteltoxin G, as well as 2 other polyenic alpha-pyrones: asteltoxin and AB5529. Two known compounds from other classes were also isolated, sclerotinin A, and (-)-terpestacin. To further examine the *in vivo* applicability of this set of compounds, a three-dimensional spheroid assay, was developed using the Perkin Elmer Operetta High Content Imaging System. Asteltoxin G caused a more than five-fold reduction in MIA PaCa-2 tumor spheroid volume at doses as low as 6.25 μM, while NIH/3T3 fibroblast spheroids and hTERT-HPNE E6/E7 spheroids were unaffected at the highest concentration tested (50 μM). A selectivity index of >15 was found for the MIA PaCa-2 spheroids compared to spheroids made of normal cells. These results indicate that asteltoxin G may be a more attractive chemical lead with regard to its *in vivo* efficacy, as well as illustrates the power of 3-D spheroid assays in drug development.

### 2.4 Chapter 5. Isolation of Cyclic Peptide

In this project, endophytes, organisms living within plants without being pathogenic, were isolated from a variety of sources via a new laser cutting apparatus. During the fungal isolation procedure, an inhibition zone was noted between two neighboring fungal colonies. The organism responsible for creating the inhibition zone was purified and shown to have an exceptionally slow growth rate. Three new cyclic peptides, herein termed persephacins A-C were isolated along with three elsinochromes (A, D and the new analogue E) via bioassay guided

fractionation. The resulting pure compounds were tested for activity against a variety of agricultural pathogens *in vitro* and *in vivo*, and the cyclic peptides were found to be the source of the antifungal activity. Additional studies assessed the potential application of the most active compound, persephacin A, as an agricultural antifungal compound. The bioassay data suggested there is a potential for developing this compound as an agricultural antifungal; however, its lack of mobility within plants may limit its applications.

### 2.5 Other Noteworthy Contributions

While this dissertation is highlighting three projects accomplished during my graduate career, there have been other noteworthy contributions on projects that have been accomplished in collaboration with other scientist and have led to publications/paper submissions. These will be addressed chronologically.

Early work included my effort to culture fungi on increasingly deuterium rich media to isolate natural products with incorporated deuterium and LCMS analysis of metabolite profiles. Isolation, elucidation and paper composing was accomplished by Bin Wang and assays were completed by Jarrod King. The results were published in the Journal of Natural Products.[63]

A second study involved compounds as potential countermeasures against liver toxicity from Alfatoxin B1, a potent carcinogen from the *Aspergillus* genus.[64,65] Adam Carter isolated three compounds from *Alternaria alternaria*, and I identified two active compounds from *Aspergillus niger*. Semi-synthesis and structure activity relationships were explored by Adam Carter. Jarrod King developed and executed the assays. Paper submission pending Journal of Natural Products peer review.

# Chapter 3: Improving Development of Natural Products with $^{19}F$ NMR

## 3.1: Abstract

Incorporation of fluorine into active pharmaceutical ingredients (APIs) can be beneficial to improve its properties such as metabolism, stability, and selectivity. This has resulted in nearly one-third of the newly approved small molecule drugs containing at least one fluorine atom. The 100% naturally abundant isotope, $^{19}F$, can therefore be readily detected in complex mixtures by NMR. Despite the potential for applying this method, $^{19}F$ quantitative NMR (qNMR) has been slow to develop. Herein presents experimental methodologies utilizing optimized parameters for uniform quantification of fluorine in drugs. Validation has been confirmed using both gravimetric and absolute concentration data reduction. This chapter was published with minor formatting changes in Concepts in Magnetic Resonance Part A.[66]

## 3.2: Acknowledgements

This work was completed on instrumentation and with materials provided by Genentech, corp. Experiments were performed, and data analyzed by Allison Mattes under the supervision and guidance of Drs. Sarah Robinson and David Russell. The manuscript was prepared by Allison Mattes and Drs. Sarah Robinson, David Russell, and Robert Cichewicz.

## 3.3 Introduction

Quantitative NMR (qNMR) is a well-established technique that has been adopted for a variety of uses.[67–69] QNMR studies often rely on the use of hydrogen ($^{1}H$) atoms due to their relatively high NMR sensitivity and ubiquitous presence in organic compounds. However, there are certain drawbacks to using $^{1}H$ NMR for qNMR. First, the chemical shift range for hydrogen

is compressed into a relatively narrow band of 10 – 12 parts per million (ppm). Given the structural complexity of most analytes and analyte mixtures, signal overlap can be a significant problem. Second, accurately determining analyte concentrations by qNMR is challenging and prone to inaccuracies when samples consist of component mixtures that span wide dynamic range (e.g. pharmaceutical formulations that contain high concentrations of excipients relative to the active pharmaceutical ingredient).

In comparison, $^{19}F$ NMR has several advantages that make it well suited for use in qNMR. The sensitivity of the $^{19}F$ isotope in NMR is comparable to $^{1}H$ since it has a natural abundance of 100%, its Larmor frequency is nearly that of hydrogen, and it has a nuclear spin of ½. Fluorine is also highly responsive to changes in its electronic environment; which equates to significant spectral dispersion and a functional chemical shift range of >200 ppm (Figure 3).[70] Moreover, the limited appearance of $^{19}F$ in most natural and many synthetic compounds means that in most samples, the spectral region for $^{19}F$ will be free from interfering resonances. This attribute imparts excellent selectivity for the technique, making it suitable for low level quantification of fluorinated isomers that are challenging to separate and quantify by traditional separation techniques including HPLC or GC. Finally, a $^{19}F$ qNMR purity assessment can be performed on sub-milligram amounts of material in less than an hour including sample preparation, data acquisition, and analysis.

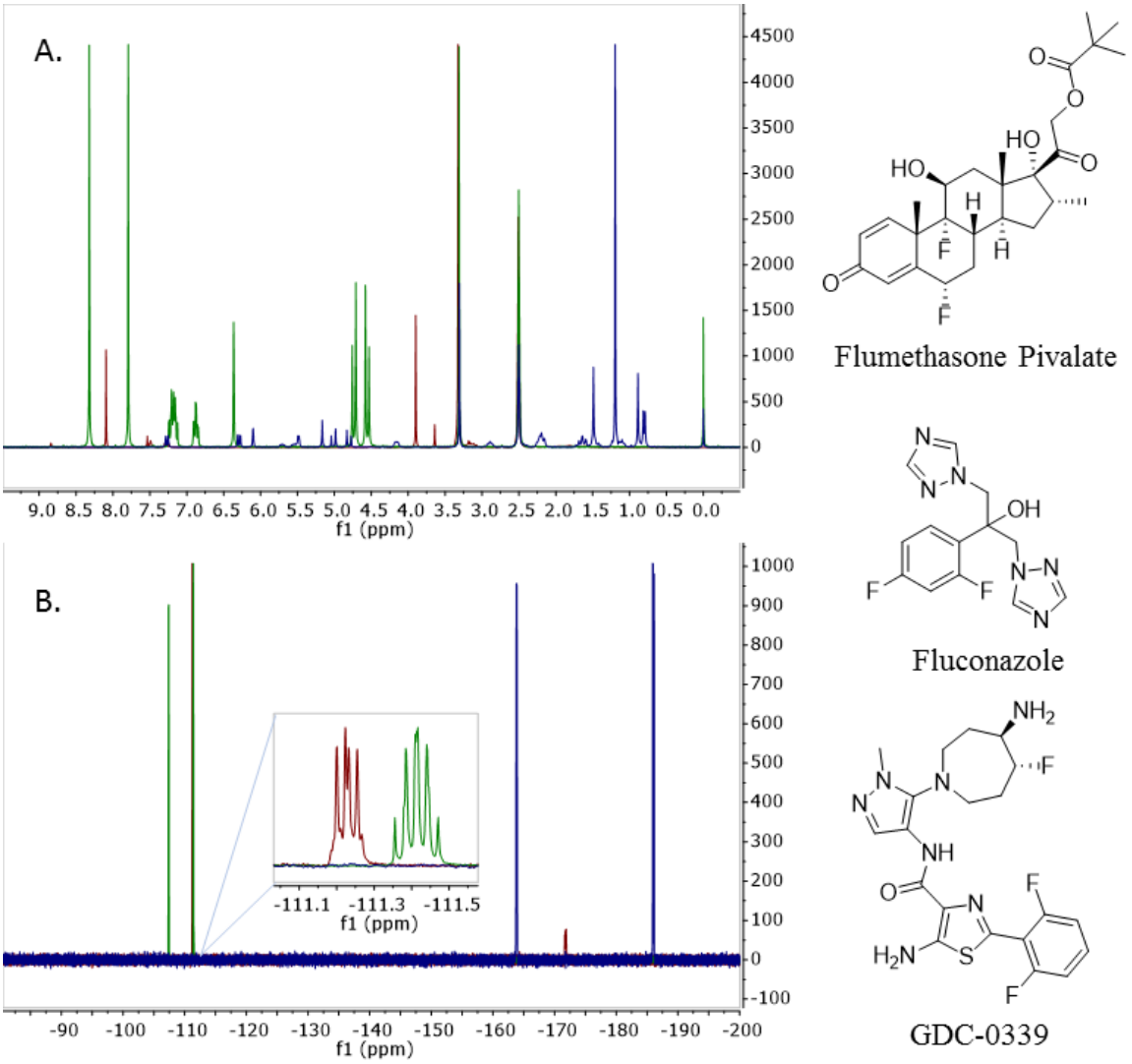


**Figure 3. Overlaid $^{1}$H NMR Spectra**
(A, top) and overlaid $^{19}$F NMR spectra (B, bottom) of flumethasone pivalate (blue), fluconazole (green) and GDC-0339 (red)

Assessment of an API, an active pharmaceutical ingredient, purity is critical throughout the drug development process. Traditionally, a battery of analyses utilizing GC and LC methods are utilized to detect organic impurities in the sample. Water content must usually be confirmed with a Karl Fisher analysis and synthetic routes depending, inorganic element concentrations

measured using an ICP technique. The time and material required for this purity characterization can reach upwards of weeks and hundreds of milligrams.

Given these considerations, the use of $^{19}F$ for qNMR in pharmaceutical analysis settings is quite promising. This is based in part on the fact that in 2015, approximately one in five drugs (including immunoglobulin drugs) contained fluorine and its incorporation has increased to nearly one-third of the newly approved small-molecule drugs.[57] There are multiple reasons for the growing use of fluorine in drug substances, many of which are based on fluorine's ability to alter the physical and electronic properties of an API.

Despite its potential utility, comparatively few qNMR studies have been reported that utilize $^{19}F$ nuclei for analyses in the pharmaceutical industry. Among the reports which have appeared, research has been focused on using $^{19}F$ for polymorph analysis,[71] reaction monitoring,[72] and mass balance measurements.[73] However, the requirements for accurate qNMR measurements necessistate the evaluation of additional experimental constraints including excitation bandwidth and digital resolution, which to date have not received in-depth experimental evaluations.

Presented herein is the analysis of several critical features of $^{19}F$ NMR that must be controlled to collect quantitative NMR data. Data were presented comparing results obtained using two methodologies: traditional internal reference approach and single point calibration with absolute intensity method.[74,75] Additionally, several important data processing parameters are highlighted, as well as application of the Mnova qNMR package to expedite sample analyses.

## 3.4 Results and Discussion

### *3.4.1 Acquiring Quantitative $^{19}F$ NMR Spectra - T1 Relaxation*

One of the first parameters to optimize is the T1 relaxation. The spin-lattice relaxation time, or T1, is a measurement of the rate constant for the magnetic vector to return to equilibrium. As with all quantitative NMR experiments, T1 relaxation must be considered. There are several approaches that can be used to ensure that differences in the relative relaxation rates of resonances in the analyte do not negatively impact quantitative analyses.

The simplest method is to remove the impact of relaxation by measuring a single transient for each data set. A limiting factor for this approach is the recoverable signal-to-noise for the data set. Given that relaxation is not a factor using this approach, a 90 degree tip angle can be safely used to maximize the signal available in a single transient.

The most commonly employed technique to provide reliable signal amplitudes is to wait for a period at least 5× longer between acquisitions (acquisition time plus the interpulse delay) and the T1 of the slowest relaxing signal of interest. This provides approximately 99.33% relaxation. To decrease relaxation error, waiting approximately 8 × T1 results in approximately 99.97% relaxation.

For the purpose of demonstrating the effects of T1 relaxation, an inversion recovery T1 analysis was performed on fluconazole, flumethasone pivalate, and GDC-0339. The longest T1s were observed in fluconazole and flumethasone pivalate at approximately 1.1 seconds. Therefore, the relaxation delay was set to 8.25 s and the acquisition time to 1.75 s, yielding a total of 10 s, or 9 × T1 for all measurements.

Pulsing the sample during receiver gain adjustment then acquiring data without full relaxation is another point of consideration that could result in increased T1 relaxation error. To

overcome this problem, it is recommended that the gain is set to a value that is low enough to prevent saturation of the signal and/or waiting a sufficient period of time before starting the experiment to ensure nuclei are fully relaxed.

### *3.4.2 Acquiring Quantitative $^{19}F$ NMR Spectra - Tip Angle*

When a single transient is used to record a qNMR spectrum, the pulse width required for a 90 degree rotation of the magnetization is the best choice to maximize signal to noise (S:N). However, if signal averaging is required to build up acceptable S:N, then the most efficient combination of tip angle and relaxation delay can be calculated based on a predetermined acceptable level of error.[76] For most applications, the optimal values, with respect to signal per unit time, will be just less than the widely accepted 90 degree tip angle and 5 × T1. The selection of a tip angle is not critical; however, smaller tip angles will allow shorter total relaxation times.

### *3.4.3 Acquiring Quantitative $^{19}F$ NMR Spectra - Acquisition Time*

The acquisition time, defined as the time interval during which the receiver is recording data, should be set to the reciprocal of the half-height line width for the signal of interest. For most routine small molecule quantitative $^{19}F$ applications, line widths will be on the order of 0.5 Hz. Therefore, acquisition times of 2 – 2.5 s are appropriate. Increasing the acquisition time beyond the time it takes for the FID to decay to zero decreases the S:N of the measurement.

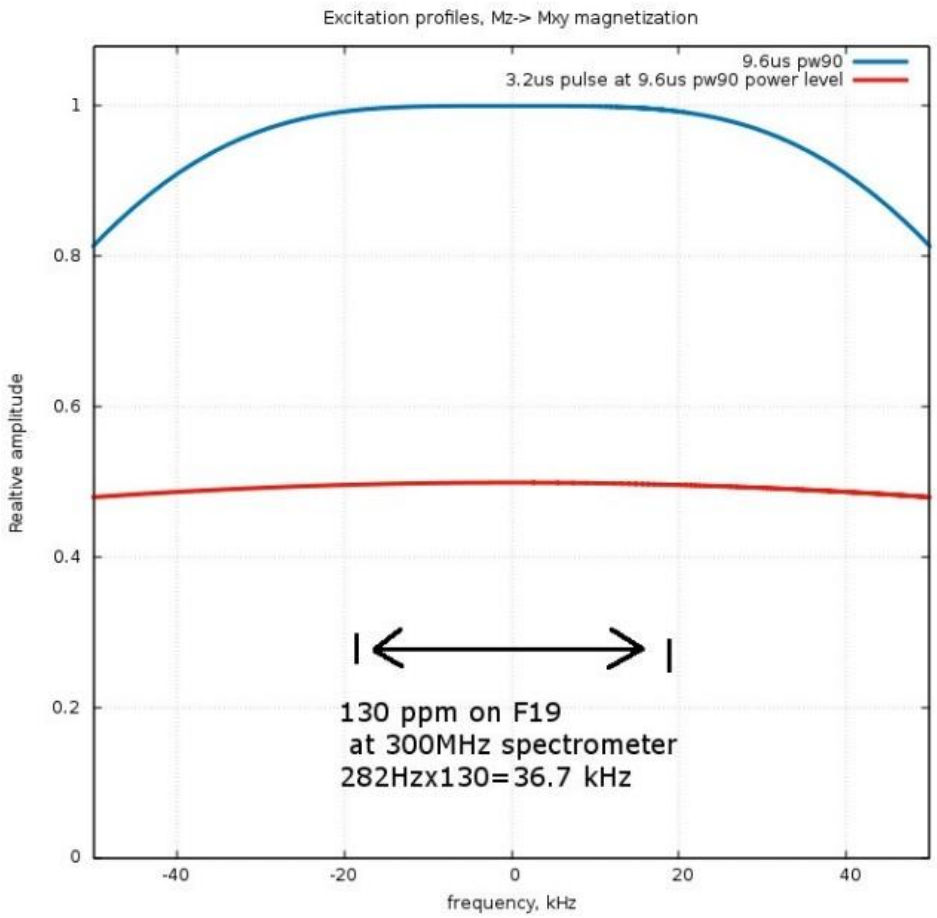


**Figure 4. Simulated Excitation Profiles**

Simulated excitation profiles of a 90° tip angle (9.6 µs pulse, top, blue) and a 30° tip angle (3.2 µs pulse, bottom, red) The maximum spectral sweep width resulting in uniform signal excitation for a 90° tip angle is 36.7 kHz (130 ppm for $^{19}F$ at 300 MHz) while a 30° tip results in 56.4 kHz (200 ppm for $^{19}F$ at 300 MHz)

### *3.4.4 Acquiring Quantitative $^{19}F$ NMR Spectra - Excitation Bandwidth*

The excitation profile of a nominal 90-degree square pulse is shown in Figure 4 on top in blue. The width of the excitation window is proportional to the intensity of the radiofrequency field $\gamma B_1$ during that pulse (or inversely proportional to a nominal 90-degree pulse width). For quantitative applications, all resonances in the spectrum must be excited uniformly; therefore a broad excitation profile is required for accurate results. In the case of $^{1}H$ NMR, pulse widths are typically in the 5 – 15 µs range affording a useful excitation window on the order of 30 KHz.

This is more than adequate for uniform $^{1}H$ signal excitation. However, for $^{19}F$ NMR the spectral window can be in excess of 200 ppm or ~100 kHz on an 11.7 T spectrometer (i.e., a proton frequency of 500 MHz). The power handling limitations of an NMR probe typically do not allow a uniform excitation of such large bandwidths using a square pulse.

Four methods can be employed to overcome this limitation. First, when the peaks of interest are located in close proximity to one another, the transmitter can simply be set close to the peaks of interest. Second, multiple spectra can be collected where the transmitter is located near the peaks of interest; however, this results in increased total experimental time due to multiple acquisitions, increased data storage and manipulation, as well as potential instrument and data interpretation errors. Third, a shorter excitation pulse at the same power level can be used resulting in a broader excitation window, albeit with a sacrifice in S:N per transient (seen in Figure 4). Fourth, a shaped radio frequency pulse can be employed to increase the excitation bandwidth without increasing the power handling demands on the hardware. This approach was elegantly demonstrated by Power, et. al.[77] wherein the use of a shaped pulse sequence dubbed CHORUS (CHirped, ORdered pulses for Ultra-broadband Spectroscopy) provided nearly perfect excitation over a very large bandwidth through the use of multiple CHIRP pulses.[78] The use of a CHORUS pulse for excitation is limited to cases where there is not a strong $J_{FF}$ coupling due to perturbations in lineshape under this condition.

### *3.4.5 Acquiring Quantitative $^{19}F$ NMR Spectra - Signal to Noise*

It is clear that the uncertainty in measuring the amplitude of a signal increases as the S:N of the data decreases. A report of the parameters critical for qNMR validation has confirmed this, demonstrating that the S:N ratio of the NMR resonance(s) must be greater than 150:1 to obtain

<1% uncertainty in the measurement.[79] The effect of S:N on accuracy was also observed during this absolute intensity method development, as seen below in Figure 5.

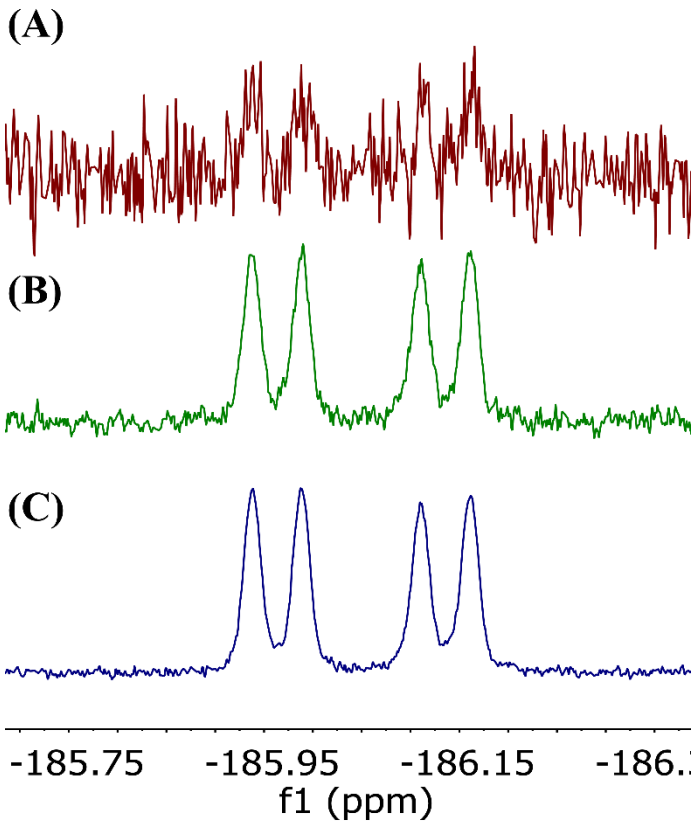


**Figure 5. Correlation of S:N and Experimental Error.**
$^{19}F$ ($^{1}H$ coupled) spectra of a fluconazole signal showing direct correlation between increasing concentration, increasing S:N and decreased experimental error: A: top (red) is a sample at 0.5 mmol/L (0.1 mg/mL), S:N 7, Error: N/A, B: middle (green) is a sample at 4 mmol/L (1 mg/mL), S:N 46, Error: 10%, and C: bottom (blue) is a sample at 10 mmol/L (2mg/mL), S:N 112, Error: 3%. Errors were calculated relative to gravimetrically determined concentrations.

### *3.4.6 Acquiring Quantitative $^{19}F$ NMR Spectra - Number of Transients*

There is no direct impact on the quality of a qNMR result that can be related to the number of transients used to collect the data. However, there are two competing trends that must

be considered. Relaxation errors are often a significant part of the uncertainty in a qNMR measurement. By collecting data with a single transient, errors induced by relaxation are avoided. In contrast, summing multiple transients increases the S:N of the aggregated data as a function of $2^n$ with respect to the number of transients collected, and it averages scan-to-scan variations due to environmental issues such as vibration.

### *3.4.7 Processing Quantitative $^{19}F$ NMR Spectra - Apodization*

Apodization refers to the practice of applying a weighting function to the time-domain data before the Fourier transformation is applied. Apodization can be used to enhance the data in numerous ways, but for qNMR methods the primary objective is to reduce the noise in the data and smooth the resulting spectrum. This results in increasing the effective S:N ratio. The average line width for most small molecules will be 0.4 – 0.6 Hz at half-height. Therefore, application of an exponential weighing function of about 0.5 Hz is useful to suppress noise without significantly broadening the lines of interest.

### *3.4.8 Processing Quantitative $^{19}F$ NMR Spectra - Fourier Number*

More digital data points in a FID result in better digital resolution of the spectrum. Accordingly, one might be tempted set the number of points collected to a very large number. This approach is too simplistic and when taken to an extreme, it degrades the quality of the resulting data. There is a linear relationship between the number of points collected in the FID and the acquisition time. As noted above, the acquisition time is best set to match the reciprocal of the narrowest line in the FID. Collecting more data points than required to meet this condition

leads to a decrease in S:N (i.e., collecting only noise after the signal has decayed). As seen in Figure 6, digital resolution critically impacts the error in the measurement.

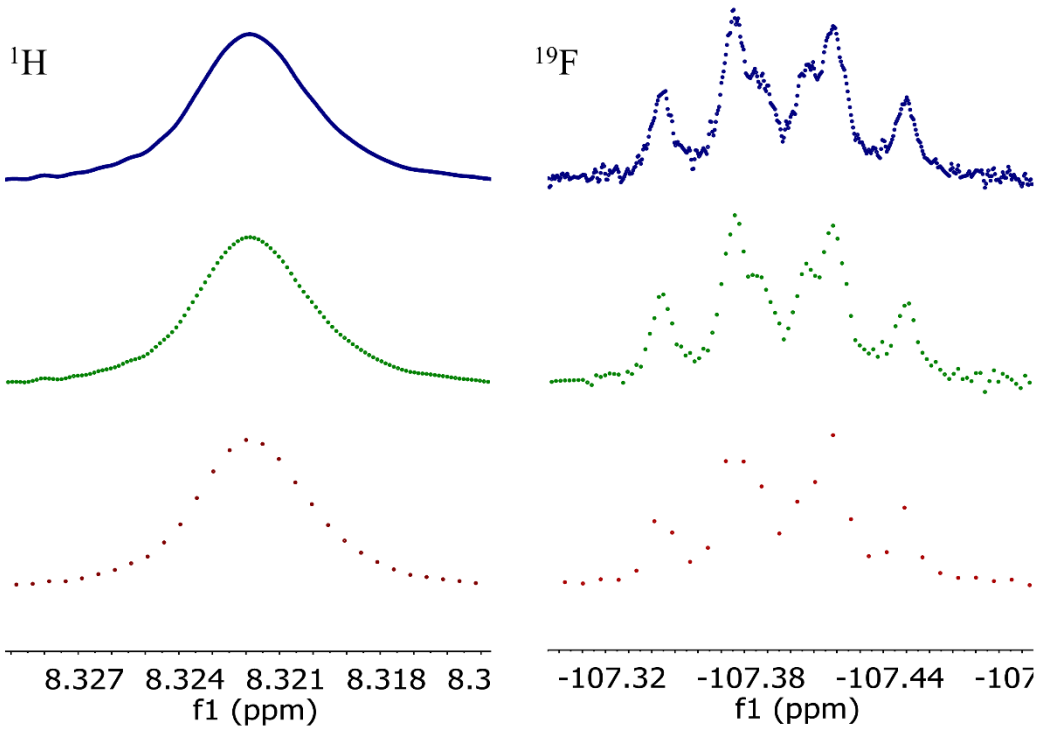


**Figure 6. Digital Resolution Comparisons**
Digital resolution comparisons between 512k (top, blue), 128k (middle, green) and 32k data sets of $^{1}$H and $^{19}$F spectra. The wide sweep width of $^{19}$F relative to $^{1}$H yields fewer data points and increased error in quantitation which can be compensated for through zero filling.

For the case of $^{1}$H NMR spectra, the spectral window is limited and the resolution afforded by setting the number of points based on the half-height relationship is reasonable at average field strengths (e.g., 14T). However the spectral bandwidth for $^{19}$F is much larger. To overcome the problems associated with unacceptably long acquisition times, a technique known as zero filling is used. Zero filling is the act of adding zeros to the back of the FID until an

acceptable total number of data points are reached. The total number of points is known as the Fourier number, which is the number of points used in the Fourier transform. The result is essentially the same as collecting more data points without an increase in noise due to addition of zeros to the decayed potion of the FID. Other than increased computational effort, there is no detriment to increasing the Fourier number.

### *3.4.9 Processing Quantitative $^{19}F$ NMR Spectra - Data Reduction*

Measuring the highest quality data requires care and attention to experimental parameters, but the boundaries for these tasks are generally well defined by physics and mathematics.[80] Once data are collected and transformed into a spectrum, the next step is data reduction to generate interpretable results. Some parts of data reduction are well defined by theory while others are more subjective. One published study involving 33 different facilities found 4% uncertainty between qNMR results despite following a strict protocol.[14] A portion of this variability could be attributed to manual phasing and baseline correction, which are often influenced by human factors.

### *3.4.10 Processing Quantitative $^{19}F$ NMR Spectra - Extracting Peak Intensities*

Measuring peak intensity can be done using several methods. The traditional approach is to choose appropriate break points for an integral region and calculating the area under the curve between them. Setting the correct location of the integral break points should be done based on line width. For example, assuming a pseudo-Lorentzian lineshape, the integral should extend for a distance equal to +/- 32× the half height to include 99% of the signal intensity.[81] To achieve an integration of 99.9% of a signal's intensity, the break points must be extended to 72× the half

height. Typically, an acceptable signal from a small molecule is ~0.5 Hz wide which yields an area integral of 86.4 Hz. This limitation should be easier to satisfy for $^{19}F$ than $^{1}H$, but there will be cases where integration without interference from other resonances will be problematic. For these reasons, a quantitative deconvolution method can be employed to good effect when spectral crowding precludes peak area integration.

Signal deconvolution is accomplished by using mathematical methods to fit each line in the data set to the models that represents the single resonance peak.[82] The models are accurately calculated and the sum of integrals provide an amplitude for the resonances under investigation. This method avoids the uncertainties in integration that arise from overlap and baseline errors, but suffers from reliance on near-perfect lineshape for the highest quality results. Schoenberger and co-workers[83] have demonstrated that a combination of integration with Global Signal Deconvolution[84] can be used to accurately extract the true amplitude of a desired peak by integrating the area containing the signal of interest, then correcting the size of that integral value by subtracting the deconvoluted intensities of interfering signals.

### *3.4.11 Conversion of Signal Intensity to Concentration - Internal Standard Versus Absolute Intensity*

The linearity and reproducibility of modern NMR systems can be leveraged to provide quantitative NMR results that do not require the addition of an internal standard.[85] Modern spectrometers are stable, linear, and highly reproducible, allowing a single point calibration to be used as a reference for subsequent data ($S=kN$: $S$ is signal, $N$ is number of nuclides, and $k$ is a proportionality constant[86]). While this can be manually calculated, it can be time consuming and obscure to the typical NMR user.

The software provided with both Agilent and Bruker spectrometers have the built-in capability to perform quantitative calculations. The Agilent method is predicated on a calibration stored in the probe file, while the Bruker method requires a second data set collected on a standard sample.

A commercially available software tool in Mnova NMR data processing package from Mestrelab uses a method analogous to that in the Agilent system. It will automatically compute the quantitative results relative to a calibration file (Mnova termed calfile) to provide users a simple-to-implement $^{19}$F qNMR method for routine pharmaceutical analyses.

To perform experiments in the absence of an internal standard using the Mnova tool, a sample of known purity and concentration is first measured to calibrate the response of the system to the standard sample (Mnova termed concentration conversion factor, CCF). The CCF is saved along with the data acquisition parameters used to collect the calibration spectrum in the calfile. Once this calibration factor is available, it can be used to scale the integrals of any subsequent data set to yield sample concentration. The software can accommodate for differences in the number of transients, the value of the receiver gain, and the tip angle used to collect the reference spectrum and the analyte spectrum since these parameters all affect the intensity of the spectrum in a predictable, mathematical way.[80]

### *3.3.12 Implementation of Absolute $^{19}$F qNMR Method*

For the current study, all NMR data were collected on a 300 MHz broadband NMR spectrometer unless otherwise noted. A 30 degree tip angle (3.2 µs excitation pulse) was used to yield over 60 KHz (200 ppm) of excitation bandwidth. A total delay of 10 s (~ 9 x T1) was used: 1.75 s acquisition time equaling 0.57 Hz resolution and 8.25 s relaxation delay (d1). One

hundred and twenty eight transients were recorded and the resulting data were processed using 0.3 Hz exponential apodization and zero filled from 128k to 512k data points. Total time for each experiment was less than 25 minutes.

Samples of fluconazole, flumethasone pivalate, and GDC-0339 were prepared in DMSO across a concentration range of 0.9834 mM to 91.96 mM, 0.8141 mM to 76.12 mM, and 0.1815 mM to 23.99 mM, respectively. The 9.188 mM fluconazole sample was used as the calibration standard for the absolute intensity method. Of the two fluconazole fluorine signals, the signal at -111.4 ppm was used to generate the Mnova calfile.

The calfile was created by acquiring a quality spectrum of the 9.188 mM fluconazole sample. Next, the signal at 111.4 ppm was analyzed with the multiplet global signal deconvolution tool. In the quantitation tab of the Mnova ribbon, the concentration window was opened and the concentration, signal, and number of nuclides updated in the settings. The calculated CCF settings were saved as the fluconazole calfile.

The calfile was referenced to compute the remaining fluconazole sample concentrations ($n$ = 7) and compared to the gravimetrically calculated concentrations to confirm linearity. The resultant $R^2$ value was 0.9999. Robustness was determined by referencing this fluconazole calfile to determine the concentration of flumethasone pivalate ($n$ = 8) and GDC-0339 ($n$ = 6). The resultant $R^2$ values were 0.9969 and 0.9996, respectively (see Figure 7). The average percent error at the low concentrations was 2.9% (flumethasone), 3.5% (fluconazole), and 3.8% (GDC-0339).

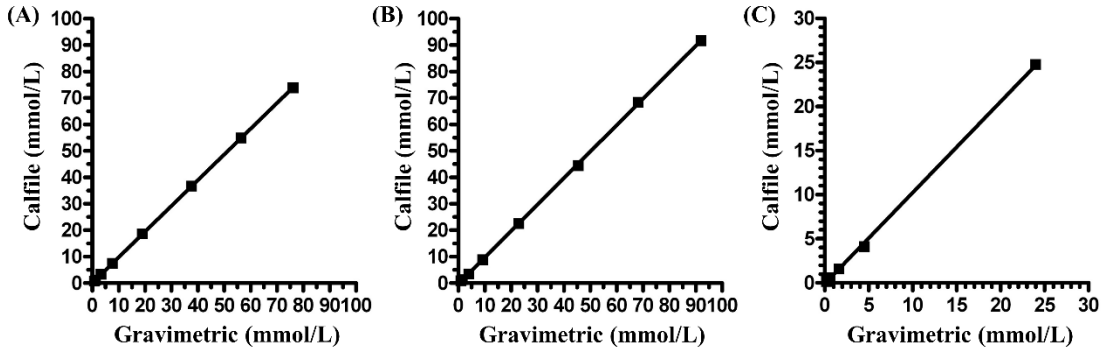


**Figure 7. Method Linearity**
Linearity was confirmed when comparing absolute intensity extrapolated at qNMR concentration from MNova software (Calfile, y axis) versus gravimetric concentrations (x axis). A. Flumethasone pivalated exhibited an $R^2$ value of 1.0000, a slope of 0.972 ± 0.002 and an average percent error of 2.9% (range ~0.81-76.1 mmol/L), B, Fluconazole exhibited an R2 value of 0.9999, a slope of 1.001 ± 0.004, and an average percent error of 3.5% (range ~0.98-92.0 mmol/L), and C, GDC-0339 exhibited an R2 value of 0.9996, a slope of 1.03 ± 0.01, and an average percent error of 3.8% (range ~0.18-24.0 mmol/L)

The same fluconazole and flumethasone pivalate samples were run in repetition to determine the standard percent deviation introduced by the instrument itself. It was found to be 2.8% and 2.6% for fluconazole and flumethasone pivalate, respectively, suggesting a significant contribution of the error occurred from the spectrometer and environment rather than the method.

Another test of robustness important to this method is how well it transfers to other instruments. Using the experimental parameters described above, data were acquired on varied fluconazole ($n$ = 5, 0.4917 – 45.42 mM) and flumethasone pivalate ($n$ = 5, 0.4071 – 37.59 mM) samples using a 400 (376.49 MHz) MHz broadband NMR. A new Mnova calfile was generated relative to the 9.188 mM fluconazole spectrum. The average error associated with the fluconazole concentrations was reduced to 2.8% and the flumethasone pivalate concentration error was reduced to 2.3%. Duplicate sample analyses revealed a similar average error to the spectrometer and environment.

The mean average errors were determined relative to traditional internal standard measurements and assumed no error in their weight measurements. Overall, all mean average errors using the absolute intensity method were less than 4%, which included S:N levels as low as 50:1. These results suggested that the experimental methods and analysis tools (i.e., Mnova qNMR software) provide acceptable results for $^{19}F$ qNMR analysis.

### 3.4 Conclusions

There are advantages to both the traditional and the absolute intensity qNMR methods. Using the traditional approach requires that a suitable reference standard of known purity and appropriate stability is available. The reference standard must be soluble in the same solvent as the analyte, it must be non-reactive in the test sample, it must provide suitable resonances for analysis that are non-interfering with the spectrum of the analyte, and it must be readily available and affordable. Obviously, it can be difficult to find such compounds for all situations. Experimentally, the traditional approach requires that two samples, the analyte and the reference material, each be weighed with appropriate accuracy. Given the constraints on sample size and volume for NMR analysis, it is not unexpected that weighing errors represent the most significant source of uncertainty for qNMR results.

While the absolute intensity method essentially circumvents these limitations, it too suffers from shortcomings. This technique is predicated on the idea that the volume of sample interrogated by the NMR coil is constant for both the calibration and the experimental measurement. In practice, an NMR coil observes signals from the region outside the physical dimensions of the coil itself and care must be taken to assure that the calibration sample and the experimental sample are long enough to represent an infinite column. Additionally, the solvent

used between the two samples should be the same to limit error in the measurement. The console of an NMR system is not in a temperature controlled cabinet and anecdotal evidence suggests that the temperature of the electronic components, particularly those components that mix or filter frequencies, affects their performance. As such, the calibration analysis should be made at the same room temperature as the experimental analysis. This condition is easily achieved by using a run-time calibration at the cost of extra work and spectrometer time for every study. Finally, the Q of the NMR coil must be the same when collecting data for the calibration standard and the analyte. Therefore, each sample must be tuned equally well. The sample-to-sample variation in the Q of the coil will be strongly dependent on the probe architecture, with greatest susceptibility to dielectric changes occurring when acquisition is performed on the inner coil of an Alderman-Grant style probe.

In conclusion, a general guide for the application of $^{19}F$ qNMR measurements to pharmaceutical samples has been presented. Implementation of the absolute intensity qNMR methodology enables organic and analytical chemists to collect their own qNMR measurements to evaluate the purity of fluorine-containing compounds without the addition of time and labor required to incorporate internal standards.

# Chapter 4: Isolation of Asteltoxin Derivative

## 4.1 Abstract

In this project, a fungal extract screening program was initiated on cells grown in monolayer looking for compounds with selective toxicity that killed MIA PaCa-2 and Panc-1 pancreatic cancer cell lines while remaining safe to NIH/3T3 normal mouse fibroblasts and hTERT-HPNE normal pancreas ductal cells. One extract out of 3,588 showed the desired characteristics. That extract had been prepared from a fungus isolated from a soil sample collected from a forest near Mt. Hood, Oregon and later identified as *Pochonia suchlasporia*. The fungal extract was subjected to bioassay-guided fractionation, which yielded a new asteltoxin derivative, named here as asteltoxin G, as well as two other polyenic alpha-pyrones: asteltoxin and AB5529. Two known compounds from other classes were also isolated, sclerotinin A, and (-)-terpestacin. To further examine the *in vivo* applicability of this set of compounds a three-dimensional spheroid assay was developed using the Perkin Elmer Operetta High Content Imaging System. Asteltoxin G caused a more than five-fold reduction in MIA PaCa-2 tumor spheroid volume in doses as low as 6.25 µM, while NIH/3T3 fibroblast spheroids and hTERT-HPNE E6/E7 spheroids were unaffected at the highest concentration tested of 50 µM. A selectivity index of >15 was found for the MIA PaCa-2 spheroids compared to the normal cell line spheroids.

## 4.2 Acknowledgements

The organism was originally isolated by the “chemical zoo” team, specifically Sara Helff, and Carolyn Le. Jarrod King researched, initiated and performed assays. NMR was completed on instruments maintained by Susan Nimmo in the OU NMR lab. Natural product purification and

chemical analyses were performed by Allison Mattes. Data were analyzed and reported by Allison Mattes, Jarrod King, and Robert Cichewicz.

## 4.3 Introduction

Pancreatic cancer is projected to become a leading cause of cancer-related death by 2030.[87] It has a poor survival rate of only 7.7% after 5 years,[88] and has had little progress in treatment since gemcitabine became the lead treatment in 1997.[89] Most advances since its discovery have been combination therapies with gemcitabine, but with only modest success (i.e., prolonging life by an average of only 4 months).[89] The difficulty in treating pancreatic cancer arises from many factors such as late detection of the disease, tumor heterogeneity, early recurrence, and high incidence of resistance even when the cancer is caught early.[90]

There is a dire need to explore new chemical space to find compounds to address the need for new therapies, but the identification of a potential pancreatic cancer drug relies heavily on the use of limited assay systems. One of the first limits of assays are the source of the cells. There are two types of cells that can be used: primary (directly taken from the parent source with a finite lifespan) or immortalized cell lines (genetically manipulated primary cells). While primary cells may more closely mimic the disease state as they are not genetically mutated, they are problematic as they are slow growing with a finite lifespan.[61] Additionally, samples may have high genetic variability, even of the same class of disease, causing reproducibility issues.[61] Alternatively, immortalized cell lines have genetic alterations that can cause changes in hormone signaling pathways that may not be easily identifiable due to the complexity of cells and current biochemical knowledge, and they may further experience genetic drift upon repeated culturing that may further alter the cells from the primary cells and disease state.[61] Contamination is also a

problem with cell lines, both in the cases where a fast-growing contaminate cell, like the HeLa cells, can overtake a culture in a few generations, or in the case of mycoplasms, that are found in up to 15-35% of cell lines.[61] We decided to use well known cell lines due to the reproducibility and large quantity needed for high-throughput screening, as primary cell lines would be too impractical. Contamination issues were negated by periodically testing the cell lines for genetic purity.[91]

While cancer is an extremely heterogeneous classification, most cancer cells do share common hallmarks, such as resistances to cell death, dysregulation of cellular energetics, sustained proliferative signaling, evasion of growth suppressors, avoidance of immune destruction, enabled replicative immortality, tumor-promoting inflammation, activation of invasion and metastasis, inducing angiogenesis, and genome instability and mutation,[92] which indicates that theoretically druggable targets do exist. This technique of targeting hallmarks of all cancers is utilized by many of the current anticancer pharmaceutical agents. Since a shared attribute among cancers is the high rate of replication, (e.g., the result of sustaining proliferative signaling) certain anticancer compounds that arrest essential steps in mitosis, such as the tubulin binding ability of paclitaxel, have been successful.[93] We hypothesized that compounds could be identified to specifically target the common mutations found in pancreatic cancer, while sparing normal cells.[94]

Another criticism of traditional monolayer assays has historically been that they do not properly mimic the 3-D environment of a tumor. This is important because cells display complex signaling pathways that are often dependent on receptors interacting with adjacent cells.[92] In fact, one of the hallmarks of cancer cells, is that they often reduce the signaling of these receptors allowing them to grow and replicate.[92] In addition, the 3D environment brings a different

challenge to the penetration ability of a compound because it tests a compounds ability not just to penetrate one layer of cells, but it also requires penetration between multiple cells and/or through the lipophilic environment between two adjacent cells.[95] To counter this, cytotoxicity testing using 3-D cancer spheroids was developed. Spheroids have been shown to more closely replicate the *in vivo* effects of drugs due to increased cell-cell interactions and signaling, increased hypoxia in the interior of the spheroid, as well as the physical size and multiple layers of cells that must be penetrated by a drug.[96] Spheroid assays can be applied either to crude extracts or pure compounds as an important step between *in vitro* and *in vivo* assays. As part of our research into implementing a spheroid assay, we began to use it in screening extracts and pure compounds (Figure 8).

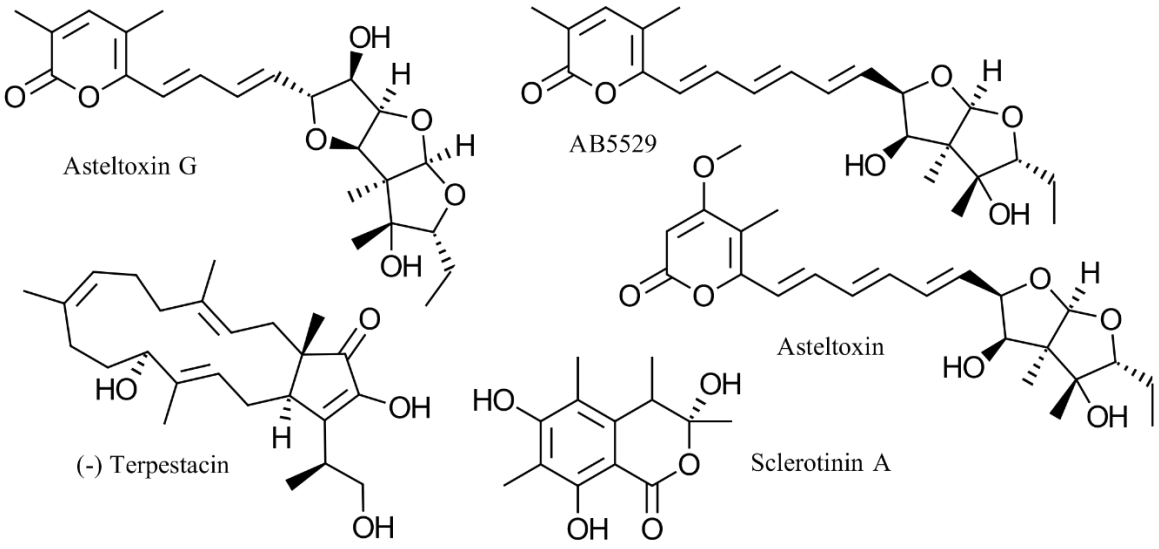


**Figure 8. Compounds Isolated from *Pochonia suchlasporia***
These isolated compounds were then analyzed first in the monolayer and then in the spheroid assays.

## 4.4 Results and Discussion:

### *4.4.1 Screenings*

Extracts were initially tested on MIA PaCa-2 pancreatic ductal adenocarcinoma and NIH/3T3 normal mouse fibroblast cells in monolayer assay. To further examine the specificity of our hit, extracts were further tested against Panc-1 pancreatic ductal adenocarcinoma and hTERT-HPNE normal pancreatic duct cells immortalized with telomerase. MIA PaCa-2 and Panc-1 are well-studied pancreatic tumor lines that bear many of the mutations that are typically found to be altered in pancreatic tumors *in vivo* such as KRAS, TP53, and CDKN2A/p16 (100%, 50%, and 98% of tumors, respectively).[97] The cell lines also possess robust growth rates, low adherence to extracellular matrices (resulting in higher instances of metastasis), and higher quantities of pro-angiogenisis (artery/vein forming) factors.[97] For counter-screening, the NIH/3T3 mouse fibroblast line was chosen due to its normal cellular phenotype and non-tumorigenicity.[7] In addition, and in contrast to human cells, mouse cells will spontaneously immortalize with ease in culture due to the presence of inherent telomerase activity.[98] We hypothesized that this natural tendency to immortalize in cell culture would yield cells with low background mutation rates.[99,100] The hTERT-HPNE line was chosen as the second normal line due to its human origin, lack of tumorigenicity, and its close similarity to normal pancreatic ductal cells, as reported in the literature.[101] Unlike the tumor-forming lines chosen, the hTERT-HPNE line expresses normal KRAS, TP53, and CDKN2A/p16 gene products. Another positive attribute of using the cell lines that were chosen was that all four lines could be grown in RPMI medium (supplemented with EGF in the case of hTERT-HPNE), removing media differences as a variable from comparisons between lines.

Based on its inhibiting activity in monolayer selectivity assays, a promising fungal extract was selected and the fungus regrown. Based on ITS sequence data, the fungus was found to be *Pochonia suchlasporia.* While there have been anticancer compounds (pochonins)[102] reported from this fungus, these compounds were not observable via LCMS dereplication. Therefore, the extract was deemed suitable for compound identification and assays.

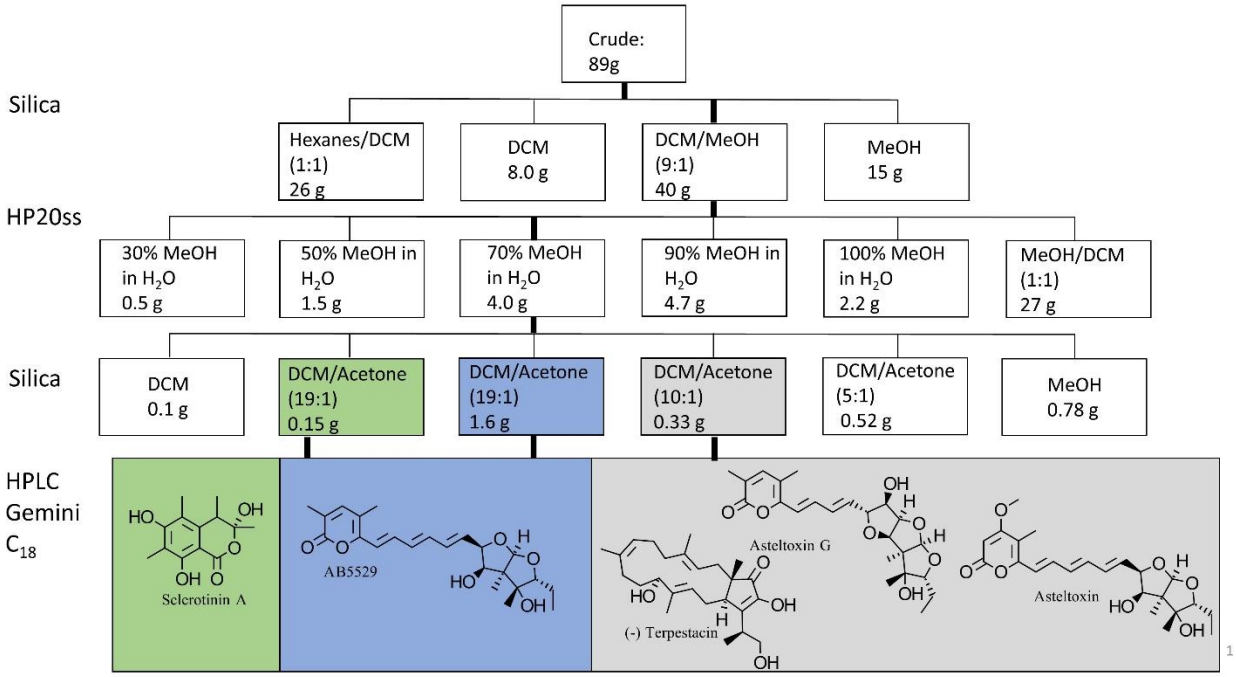


**Figure 9. Isolation Scheme of Compounds from *Pochonia suchlasporia*.** Bioassay guided fractionation singled out three sub-fractions which yielded five compounds that were subjected to both monolayer and spheroid assays.

### *4.4.2 Compound Identification and Structure Elucidation*

The *Pochonia suchlosporia* was grown Cheerios,™ and after 4 weeks, the fungus was homogenized and extracted with ethyl acetate to yield 89 g of crude extract. A stepwise gradient consisting of hexanes, dichloromethane, and methanol on a silica column afforded 40 g of an active fraction from the 9:1 dichloromethane:methanol elution step. This fraction was further

separated using a stepwise gradient of methanol and water on an HP20ss column affording 4.0 g of an active fraction from 70% methanol in water. This subfraction was further subjected to separation via silica gel and monitored by TLC using a solvent system of dichloromethane and acetone. The major compounds were purified using reverse phase ($C_{18}$) by HPLC with 0.1% formic acid in water and acetonitrile or water and methanol (Figure 9). Bond-line structures were determined through $^{1}$H, HSQC, HMBC, and COSY NMR and accurate mass data were obtained.

A *m/z* 251 compound $[M - H]^-$ was purified from the DCM/acetone (19:1) fraction via semipreparative chromatography over Gemeni C18 at 60% MeOH in $H_2O$ and was consistent with the molecular formula $C_{13}H_{16}O_5$. $^{1}$HNMR in deuterated methanol revealed only five resonances. One quartet integrated to a 1H, 3 singlets each integrated to 3H, and one doublet also integrated to 3H. The quartet was the farthest shift downfield at δ3.5, suggesting the presence of an electron withdrawing group and split by the doublet methyl. The singlet methyls had no neighboring protons. A $^{13}$C NMR spectrum was not collected, however, HMBC data were collected and showed $^{13}$C shifts of δ159.9, δ141.5, and δ110.2 ppm representing $sp^2$ carbons that were consistent with a substituted aromatic ring with the resonance effects of oxygen π donation causing the oxygen substituted carbons to shift further up field and the methyl substituted carbons to shift downfield. The substituted aromatic ring system accounted for 4 units of unsaturation and 6 carbons, leaving 2 units of unsaturation and 3 carbons unassigned to methyls. During the dereplication of the remaining proton shifts, the two methyls upfield of δ1.7 ppm suggested a double bond was unlikely; therefore, the most likely functional groups would be a carbonyl and another ring. Due to the number of oxygens, an ester functionality was proposed, and if the quartet hydrogen was adjacent to the oxygen of the ester it's shift would be closer to

δ5.0 ppm. The proposed structure was confirmed to be sclerotinin A by a comparison to literature values.[103] (-)Terpestacin was also dreplicated according to literature.[104]

A *m/z* 419.2055 compound $[M + H]^+$ was isolated from a DCM/Acetone (10:1) fraction *via* preparative HPLC (Gemini C18) at 55% MeOH in $H_2O$ for 4 minutes followed by a gradient of 55-80% over 16 minutes and a wash of 80-100% over 1 minute. The mass data were consistent with a molecular formula of $C_{23}H_{30}O_7$ and had an unsaturation number of 9. Asteltoxin was dereplicated via literature by comparing $^1H$ NMR and $^{13}C$ NMR values.[105]

A *m/z* 403.2109 compound $[M + H]^+$ was isolated from a DCM/Acetone (19:1) fraction *via* preparative HPLC (Gemini C18) at 55% MeOH in $H_2O$ for 4 minutes followed by a gradient of 55-80% over 16 minutes and a wash of 80-100% over 1 minute. The mass data were consistent with a molecular formula of $C_{23}H_{30}O_6$ and an unsaturation number of 9. AB5529 was dereplicated according to literature.[106]

A *m/z* 425.2671 compound $[M + Na]^+$ was isolated from the DCM/acetone (19:1) fraction via semipreparative chromatography over Gemeni C18 at 55% MeOH in $H_2O$ for 4 min followed by a gradient of 55-80% over 16 minutes, and was consistent with the molecular formula $C_{23}H_{30}O_6$ and was not consistent with any structure in the literature. From the molecular formula, an unsaturation number of 9 was calculated. The structure was elucidated using a combination of $^1H$ NMR, $^{13}C$ NMR, COSY, HSQC, and HMBC. A shift of 162.2 ppm (C-1) suggested a carbonyl was present. There was a HMBC correlation between the carbonyl (C-1) and a proton singlet integrating to 1 at 7.23 ppm, which was determined to be an aromatic proton (H-3). Proton H-3, had HMBC correlations to two singlet methyls at 12.0 ppm and 16.8 ppm (C-22 and C-23) as well as a quaternary carbon at 152.3 ppm (C-5). HMBC correlations between the protons of two methyls (H-22 and H-23), indicated two more quaternary carbons at 123.7 ppm

and 113.4 ppm (C-2 and C-4), which afforded a substructure of a dimethylated pyrone. There was an additional HMBC correlation from C-5 in the substituted pyrone unit with a doublet proton, integrating to 1 at 6.57 ppm (H-6). HSQC of the H-6 to 121.7 ppm (C-6) suggested an olefin, and a *J* coupling of 15.0 Hz from $^{1}$H NMR suggested a *trans* olefin. Using COSY and *J* couplings of the associated protons (H-7 to H-9, 15.1 to 15.3 Hz), carbons C7-C9 were determined to be a dienyl moiety in the *trans* configuration for both olefins. COSY correlations further connected H-9/H-10, H-10/H-11, H-11/H-12, and H-12/H-13, such as was seen in both asteltoxin and AB5529, however, C-10 had a $^{13}$C shift of 81.0 ppm instead of 132.5 ppm signifying the reduction of the $sp^2$ carbon to $sp^3$. The two possible substitutions would be either an epoxide, or a furan ring via ether connection between C-10 and C-13. The carbon shifts of C-10 and C-11 (81.0 ppm and 77.3 ppm respectively) were more consistent with a furan ring system than an epoxide (expected shifts 40-65 ppm), similar to what was determined in the revision of asteltoxin B.[105] The remaining $^{13}$C NMR and $^{1}$H NMR shifts corresponded closely to the literature shifts of the bicyclic ring system of asteltoxin and AB5529 as well the literature shifts of the tricyclic ring system for asteltoxin D.[105,106]

**Table 1. NMR Spectroscopic Data (600 MHz, DMSO-$d_6$) for Asteltoxin and Derivatives**

| | AB5529 | | Asteltoxin | | Asteltoxin G | |
|---|---|---|---|---|---|---|
| Position | $^{13}$C | $^{1}$H (*J* in Hz) | $^{13}$C | $^{1}$H (*J* in Hz) | $^{13}$C | $^{1}$H (*J* in Hz) |
| 1 | 162.2 | | 170.5 | | 162.2 | |
| 2 | 123.4 | | 89.2 | 5.58, s | 123.7 | |
| 3 | 145.4 | 7.22, 2 | 162.4 | | 145.7 | 7.23, s |
| 4 | 113.3 | | 108.4 | | 113.4 | |
| 5 | 152.5 | | 154.0 | | 152.3 | |
| 6 | 120.5 | 6.5, d (*J*=15.0) | 120.6 | 6.63, d (*J*=14.9, 10.9) | 121.7 | 6.57, d (*J*=15.0) |
| 7 | 133.9 | 6.89, dd (*J*=15.0, 11.1) | 135.3 | 6.96, dd (*J*=15.0, 11.2) | 132.6 | 6.83, dd (*J*=15.1, 10.8) |
| 8 | 132.2 | 6.45, dd (*J*=14.9, 10.8) | 132.0 | 6.47, dd (*J*=14.9, 10.9) | 131.9 | 6.42, dd (*J*=15.2, 7.1) |
| 9 | 137.1 | 6.59, dd (*J*=14.9, 10.8) | 137.8 | 6.63, dd (*J*=14.9, 10.9) | 137.2 | 5.99, dd (*J*=15.2, 7.1) |
| 10 | 132.5 | 6.32, dd (*J*=15.3, 10.7) | 132.5 | 6.33, dd (*J*=15.3, 7.2) | 81.0 | 4.2, t (*J*=8.1) |
| 11 | 132.7 | 5.94, dd (*J*=15.3, 7.4) | 134.5 | 5.96, dd (*J*=15.3, 7.2) | 77.3 | 3.67, dd (*J*=9.3, 4.0) |
| 12 | 78.7 | 4.47, dd (*J*=7.6, 3.2) | 84.4 | 4.48, dd (*J*=7.2, 3.0) | 86.6 | 4.57, t (*J*=3.8) |
| 13 | 84.6 | 4.12, dd (*J*=9.5, 3.9) | 78.8 | 3.56, s | 87.1 | 4.11, d (*J*=3.5) |
| 14 | 61.7 | | 61.7 | | 62.1 | |
| 15 | 79.8 | | 79.8 | | 79.2 | |
| 16 | 89.4 | 3.55, dd (*J*=6.1, 3.3) | 89.3 | 4.12, dd (*J*=9.1, 3.6) | 91.3 | 3.85, dd (*J*=9.0, 4.0) |
| 17 | 21.9 | 1.27-1.48, m | 21.9 | 1.31-1.43, m | 22.6 | 1.32-1.45, m |
| 18 | 11.8 | 0.86, t (*J*=7.2) | 11.8 | 0.86, m | 12.1 | 0.88, t (*J*=7.4) |
| 19 | 111.6 | 5.00, s | 111.9 | 5.00, s | 113.7 | 5.22, s |
| 20 | 18.2 | 1.16, s | 18.2 | 1.15, s | 19.1 | 1.16, s |
| 21 | 16.4 | 0.99, s | 16.4 | 0.99, s | 15.3 | 0.9, s |
| 22 | 18.2 | 1.99, s | 9.1 | 1.89, s | 15.0 | 2.00, s |
| 23 | 14.9 | 1.93, s | 57.1 | 3.79, s | 16.8 | 1.94, s |
| 15OH | | 5.1, d (*J*=6.1) | | 5.11, d (*J*=6.1) | | 5.12, s |
| 13OH | | 4.23, s | | 4.23, s | | |
| 11OH | | | | | | 4.49 |

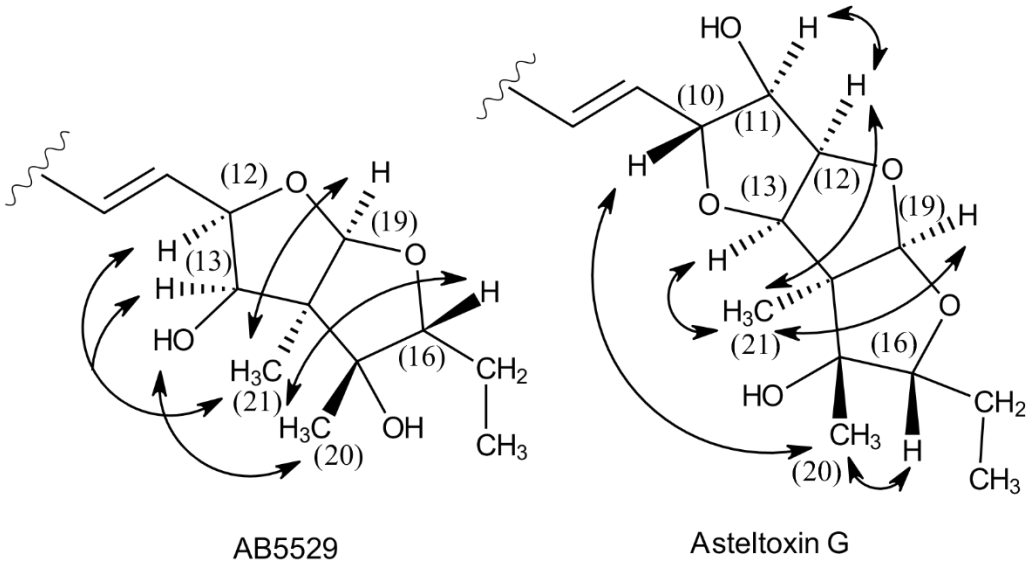


**Figure 10. ROESY Correlations of AB5529 and New Derivative Asteltoxin G.** Atom labels shown in parentheses.

Since only the planar structure of AB5529 was present in the literature, ROESY was used to determine the relative configuration of both AB5529 and asteltoxin G. AB5529 was found to have the same relative configuration of asteltoxin based on the ROSEY correlations of H-12, H-13 and H-19 to the H-21. On the opposite face of the molecule, H-16 and the hydroxyl on C-13 correlated to H-20. For the new compound, asteltoxin G, the H-21 proton was correlated to the H-12, H-13, and H-19 (Figure 10). A correlation between H-11 and H-12 gave the relative configuration of the hydroxyl on C-11. On the opposite face of the molecule, H-20 was correlated to the H-10 and H-16. The seemingly long-range correlation between H-20 and H-10 was possible due to the concave nature of fused furan rings (Figure 11). These correlations also matched what was seen for asteltoxin B in a previous report.[105]

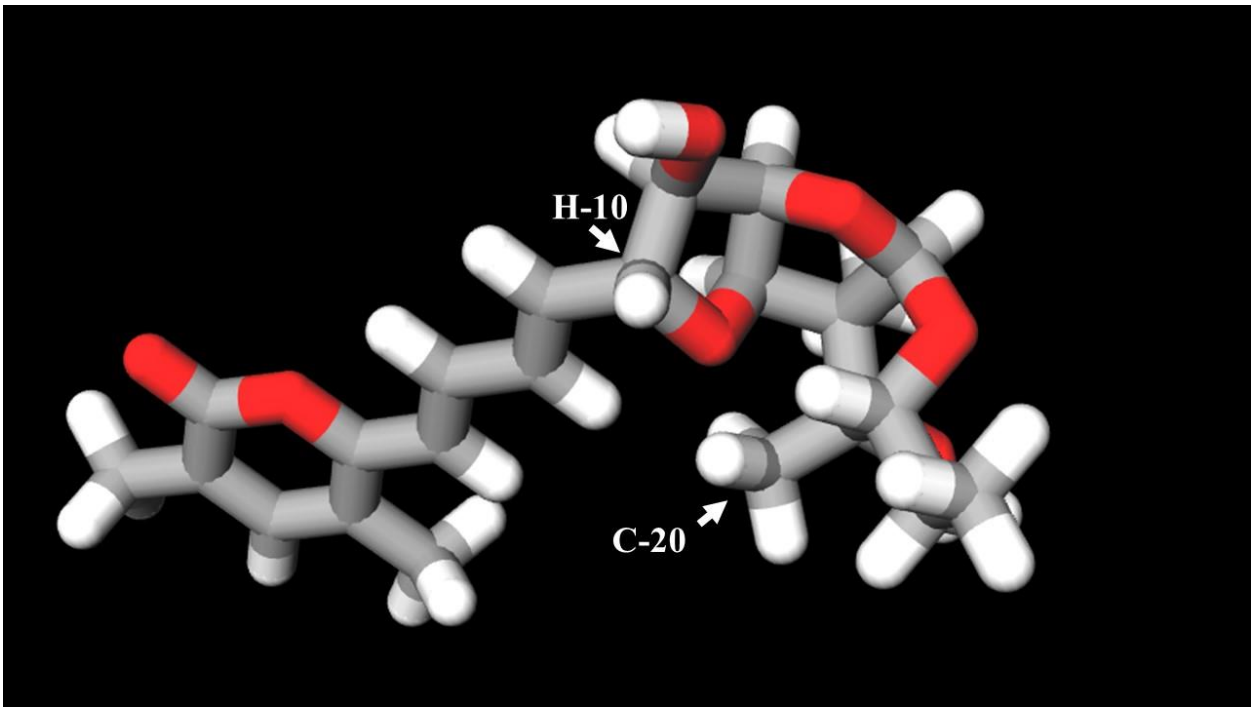


**Figure 11: 3D Rendition of Asteltoxin G.** The image is centered on the H-10 which is facing out from the plane of the page. Directly below it, is the methyl C-20.

Since the only differences between AB5529 and asteltoxin involved the C-2 and C-3 $sp^2$ carbons on the pyrone ring, and the relative configurations were the same, the optical rotation values could be compared between the two. This is because circular light, a photon with its own electromagnetic field, can be affected by the electromagnetic field of each atom/bond within a molecule. Therefore, differences in electron density of chiral centers can have different effects on circular light. Since $sp^2$ carbons are planar, there is no potential chirality therefore there is no difference in electron density that would change the angle. Both AB5529 and asteltoxin had positive optical rotations ([α] +28 and [α] +20), therefore AB5529 is predicted to have the same absolute configuration. Asteltoxin G, however, had extra chiral centers meaning that the optical rotation could not be directly correlated. Calculated optical rotations were determined using DFT b3lyp/3-21g in Gaussian 09 and resulted in -269 degrees for 1a, +120 degrees for 1b. The

experimental optical rotation of asteltoxin G was found to be [α] +48 (c 0.1, MeOH), suggesting that the absolute configuration of asteltoxin G is as show in 1b (Figure 12). This correlates with the absolute configuration of the two furanose rings on asteltoxin and AB5529. It is important to note that large differences in the magnitude of specific rotations between DFT and experimental calculations are expected as discussed in published evaluations of DFT.[107] Differences in magnitudes can occasionally be affected by the quality of the basis set used, but as molecules get more complex with more degrees of freedom, either exponential time or smaller basis sets are necessary to calculate specific rotation.

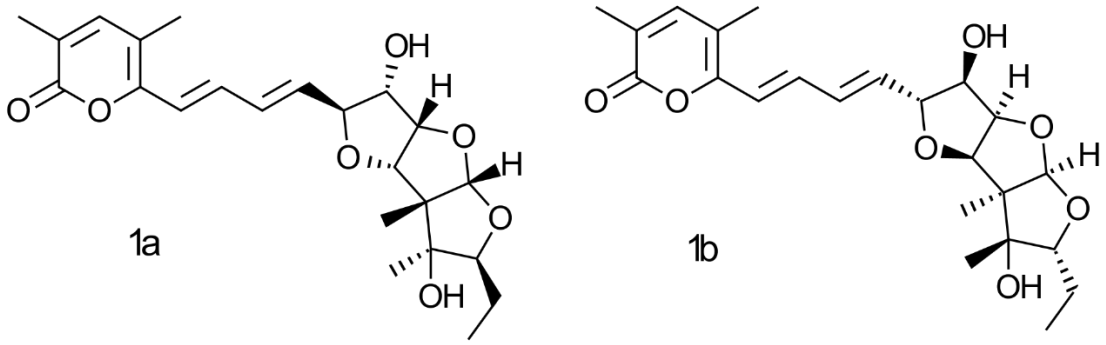


**Figure 12. Possible Configurations of Asteltoxin G.** Each enantiomer was examined via computational analysis to determine the absolute configuration of the isolated compound asteltoxin G.

Mosher analysis was unsuccessful due to the addition of base causing compound degradation. CD (circular dichroism) analysis was also unsuccessful. Like optical rotation, CD is dependent on the molecule influencing light, however CD uses the difference in right-handed and left-handed circularly polarized light while polarimetry utilizes linearly polarized light.[108] For CD to be easily detected, a chiral center needs to be sufficiently near a source of absorption such as a chromophore (eg., a $\pi \rightarrow \pi^*$).[108] When not sufficiently near a chromophore, as was the case in these molecules, the electronic transmission of other functional groups may be hidden.[108]

An alternative support for the absolute configuration of asteltoxin G can use biosynthesis information. While there is precedent in the literature for fungi producing enantiomers of natural products, this combined with DFT calculations makes the proposed absolute configuration of 1b (Figure 12) for asteltoxin G more likely. Asteltoxin, and therefore its analogs, are formed by polyketide synthetase. $^{13}C$ studies have determined that the carbon source of asteltoxin is from acetate and the methylation is theorized to be from methionine. The biosynthesis (Figures 13-14) is hypothesized to occur when acetate is formed into to acetyl CoA or propionyl-CoA,[109,110] modified into malonyl CoA via acetyl CoA carboxylase, elongated by the Claisen condensation and then depending on the location on the molecule, is reduced first by a ketoreductase followed by a dehydrase to form the olefins with the proper *E/Z* conformation to give the $C_{18}$ polyketide seen in Figure 14.[111,112] The pyrone is formed by a nucleophilic attack on the enol thioester attaching the polyketide to the enzyme to release it.[111] Epoxides are formed by mono-oxygenases followed by nucleophilic attack of water to afford the compounds.[111] It is reasonable to assume that asteltoxin G can be formed by the mono-oxygenase epoxidizing the next olefin so that as the compound is undergoing cyclization for form the bicyclic furan ring, it cyclizes and additional time to afford a tricyclic furan ring system.

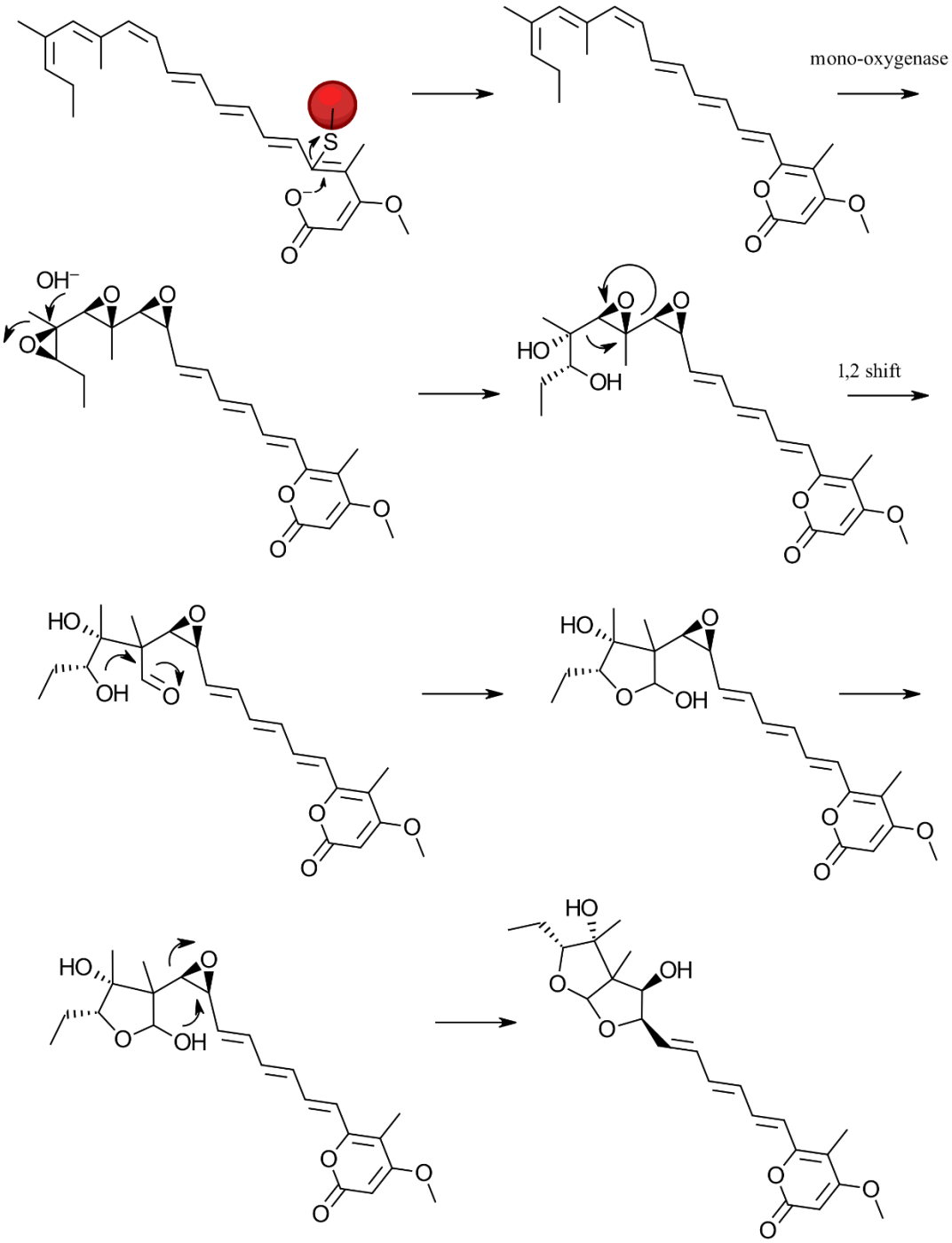


**Figure 13: Proposed Asteltoxin Biosynthetic Mechanism.** Following polyketide backbone formation, a mono-oxygenase epoxidizes key olefins which is then nucleophilically attacked by water to initiate cyclization of the furan ring system.

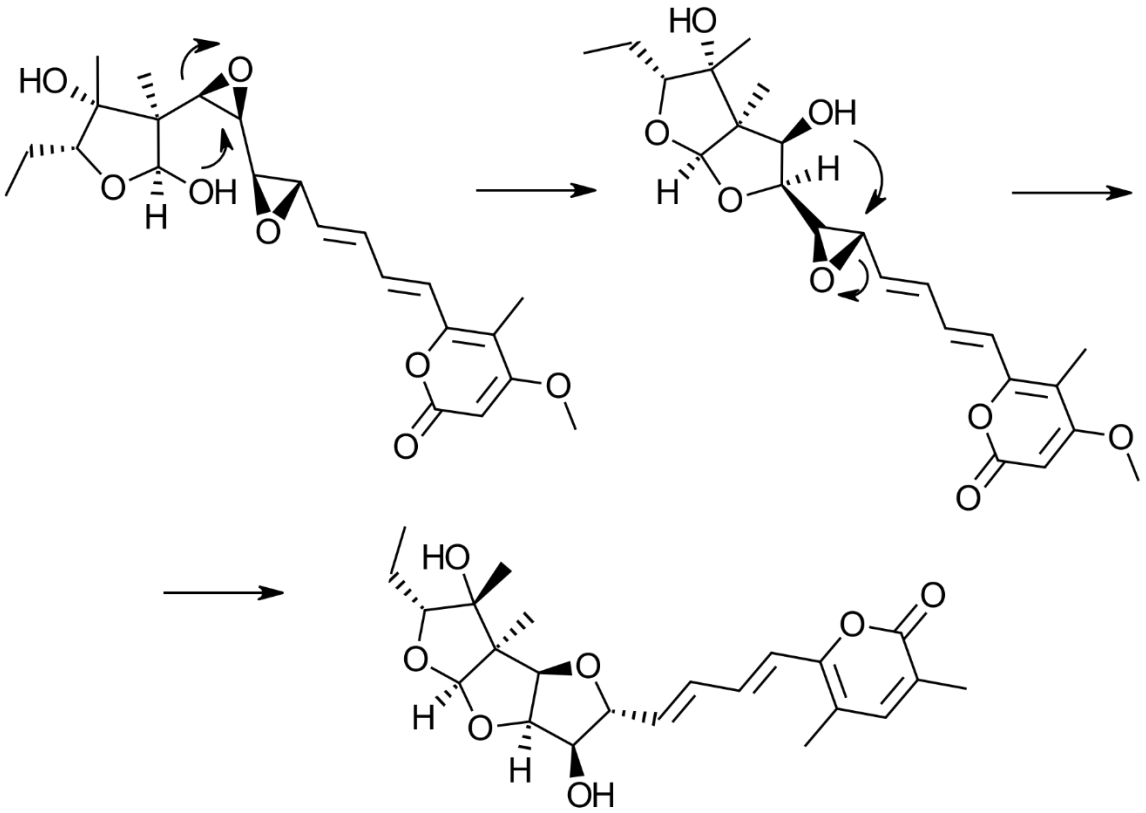


**Figure** 14**. Proposed Biosynthetic Mechanism for Asteltoxin G.** During the epoxidation by mono-oxygenase, an additional olefin is epoxidized so that during the during the furan cyclization, a tricyclic ring is formed instead of a bicyclic ring.

### *4.4.3 Pure Compound Assays*

Initial monolayer assays determined that sclerotinin A did not have enough cytotoxic activity to warrant further interest (>50 µM against 3T3 mouse fibroblasts, and >50 µM against Panc-1 cells). (-)-Terpestacin, had slight selectivity against Panc-1 cells compared to the 3T3 mouse fibroblasts ($LC_{50}$ values of 28.5 µM and 39 µM, respectively), but it had been investigated by others so was not chosen for further study.[24]

The selectivity indices of the three asteltoxin compounds were calculated (Table 5) by dividing the $LC_{50}$ of normal cell lines by the $LC_{50}$ of cancerous cells lines to create a value that can be used to easily compare the cytotoxicity of the compounds while taking into account

potential cytotoxicity to normal cell lines.[113] For these indices, the larger the number, the more potent the compound was at targeting the cancer cells versus the normal cells. Asteltoxin was shown to have no selectivity with regard to NIH/3T3 cells and Panc-1 cells. On the other hand, the $LC_{50}$ values and selectivity of asteltoxin G against Panc-1 and MIA PaCa-2 monolayer assays were quite promising, showing potency in the pancreatic tumor lines and relative safety in the mouse fibroblast and normal pancreas lines (Figures 15-18, Table 3). Most notable was the fact that the normal lines retained their characteristic shape even at high doses of the compounds, a feature not shared by the tumor lines, which swelled and proceeded to die. This was a rare occurrence in our screen, with most normal lines dying or becoming damaged in similar ways to the tumor lines when treated with other compounds or extracts, and made the compounds better candidates for lead compounds.

The compounds were tested further in the newly developed spheroid assay. Previous comparisons of the two assays in our lab have shown that a higher concentration, (~10x), is required to attain similar cytotoxicity in the spheroid assay compared to the monolayer assay. $LC_{50}$ values were significantly increased for all of the compounds tested except asteltoxin G in the MIA PaCa-2 spheroid assay (Figures 19-22, Table 4). Asteltoxin G showed an increase in potency in the tumor spheroid assay compared to the monolayer with a selectivity values of >15.6 for both the Spheroid NIH 3T3 and the hTERT-HPNE MIA PaCa-2 versus 2 to >8.3 in the monolayer assays, (Table 5), a result we had not previously encountered. No toxicity to the normal mouse NIH/3T3 fibroblast spheroids and the hTERT-HPNE spheroids was seen even at the highest concentration tested of 50 µM. The MIA PaCa-2 spheroids treated with 6.25 µM of asteltoxin G for three days were one-third the size of DMSO control spheroids based on cell area. Data reveals that spheroids treated with asteltoxin G had five-fold reduction in spheroid

size compared to DMSO control at 6.25 µM. This showed that asteltoxin G was the most prominent drug lead of the isolated compounds as it might selectively target spheroid cells.

**Table 3. Cytotoxicity Values for Monolayer Assays**. Normal cell lines are labeled in green, tumor in red. NT = not tested

| Compound | Monolayer NIH/3T3 ($LC_{50}$ in µM) | Monolayer hTERT-HPNE ($LC_{50}$ in µM) | Monolayer Panc-1 ($LC_{50}$ in µM) | Monolayer MIA PaCa-2 ($LC_{50}$ in µM) |
|---|---|---|---|---|
| Sclerotinin A | **>50** | **NT** | **>50** | **NT** |
| (-) Terpestacin | **39** | **NT** | **29** | **NT** |
| AB5529 | **>50** | **>50** | **>50** | **32** |
| Asteltoxin | **4** | **>50** | **6.25** | **40** |
| Asteltoxin G | **30** | **>50** | **15** | **6** |

**Table 4. Cytotoxicity Values for Spheroid Assays.** Normal cell lines are labeled in green, tumor in red. NT = not tested

| Compound | Spheroid NIH/3T3 ($LC_{50}$ in µM) | Spheroid hTERT-HPNE ($LC_{50}$ in µM) | Spheroid Panc-1 ($LC_{50}$ in µM) | Spheroid MIA PaCa-2 ($LC_{50}$ in µM) |
|---|---|---|---|---|
| Sclerotinin A | **>50** | **>50** | **>50** | **NT** |
| (-) Terpestacin | **>50** | **>50** | **36** | **NT** |
| AB5529 | **>50** | **>50** | **>50** | **32** |
| Asteltoxin | **>50** | **>50** | **>50** | **42** |
| Asteltoxin G | **>50** | **>50** | **>50** | **3.2** |

**Table 5. Selectivity Indices of Asteltoxin and Derivatives.** NA= not applicable

| Selectivity | AB5529 | Asteltoxin | Asteltoxin G |
|---|---|---|---|
| Monolayer NIH 3T3/Panc-1 | **NA** | **0.6** | **2** |
| Monolayer NIH 3T3/MIA PaCa-2 | **>1.6** | **0.1** | **5** |
| Monolayer hTERT-HPNE/Panc-1 | **NA** | **>8** | **>3.3** |
| Monolayer hTERT-HPNE/MIA PaCa-2 | **>1.6** | **>1.3** | **>8.3** |
| Spheroid NIH 3T3/Panc-1 | **NA** | **NA** | **NA** |
| Spheroid NIH 3T3/MIA PaCa-2 | **>1.6** | **>1.2** | **>15.6** |
| Spheroid hTERT-HPNE/Panc-1 | **NA** | **NA** | **NA** |
| Spheroid hTERT-HPNE/MIA PaCa-2 | **>1.6** | **>1.2** | **>15.6** |

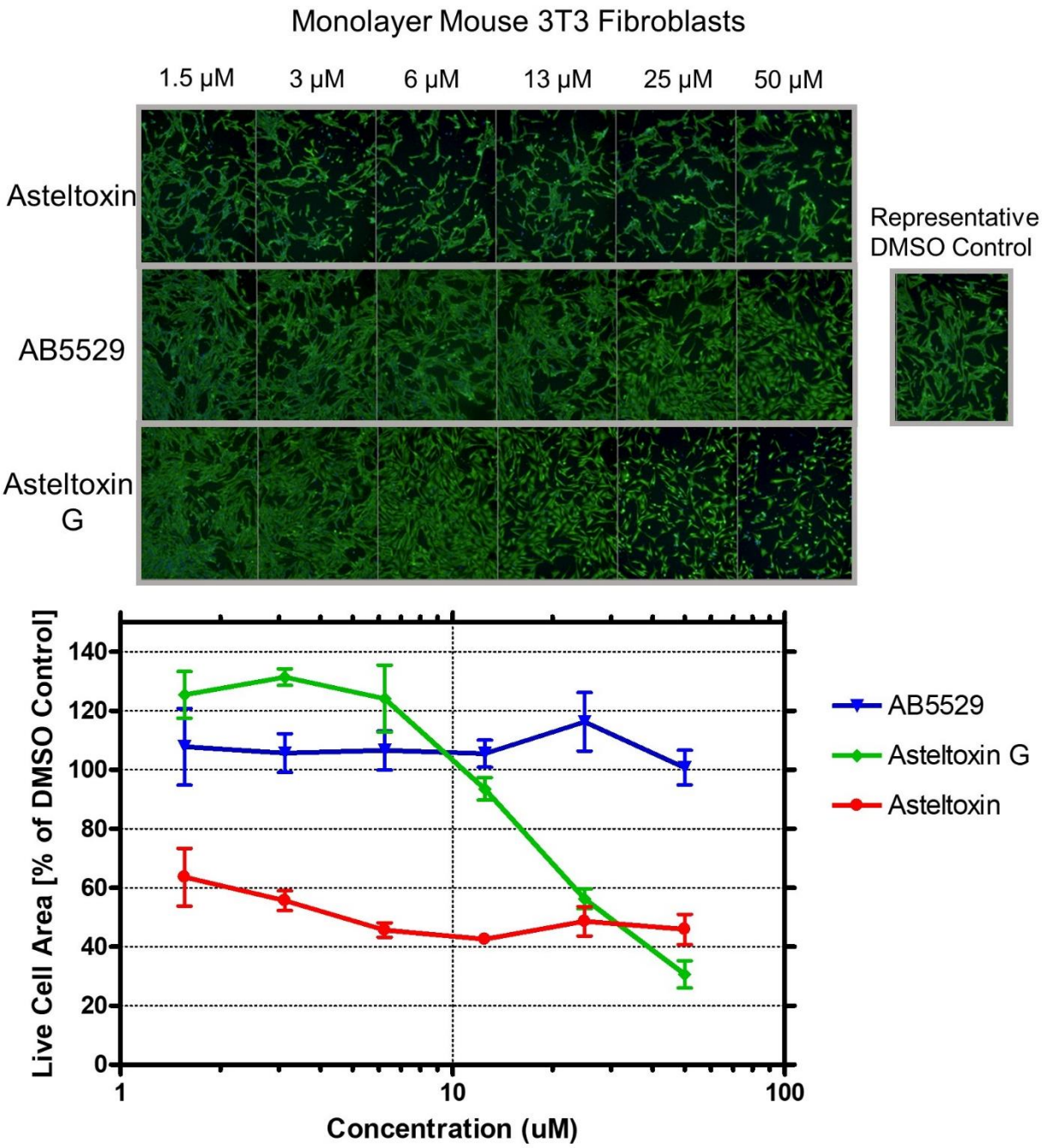


**Figure 15. Cytotoxicity Assays for the Asteltoxin Class Compounds in Monolayer Mouse 3T3 Fibroblast Cells.** Cellular density is show in green fluorescence. Asteltoxin shows consistent cytotoxicity up to 50 µM, AB5529 only showed slight cellular toxicity at 50 µM, and asteltoxin G showed increasing cytotoxicity over the range tested as well as reduced cellular size.

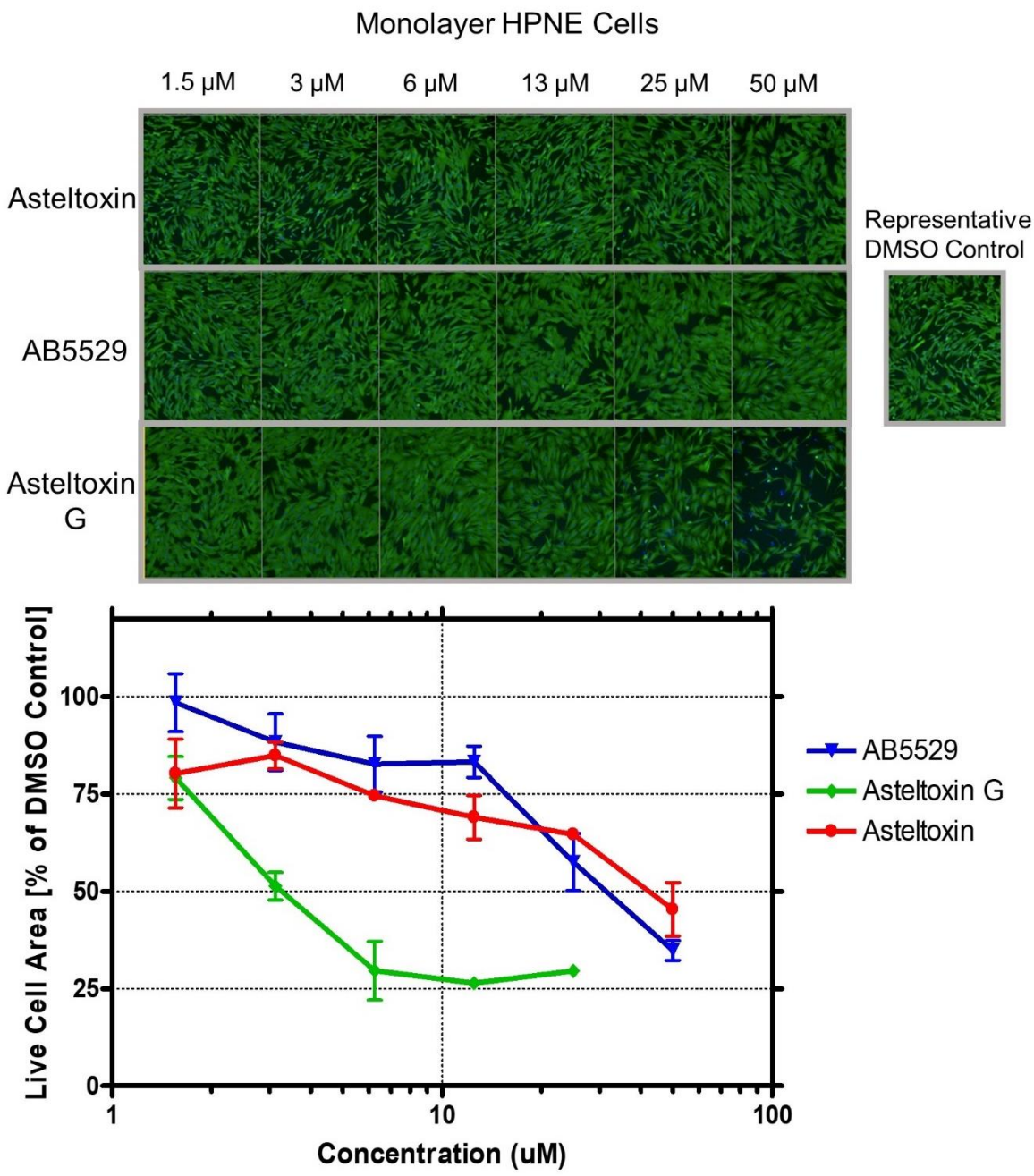


**Figure 16**. **Cytotoxicity Assays for the Asteltoxin Class Compounds in Monolayer HPNE Cells.** Cellular density is show in green fluorescence. Cytotoxicity was only noticed at the highest 50 µM with the asteltoxin G.

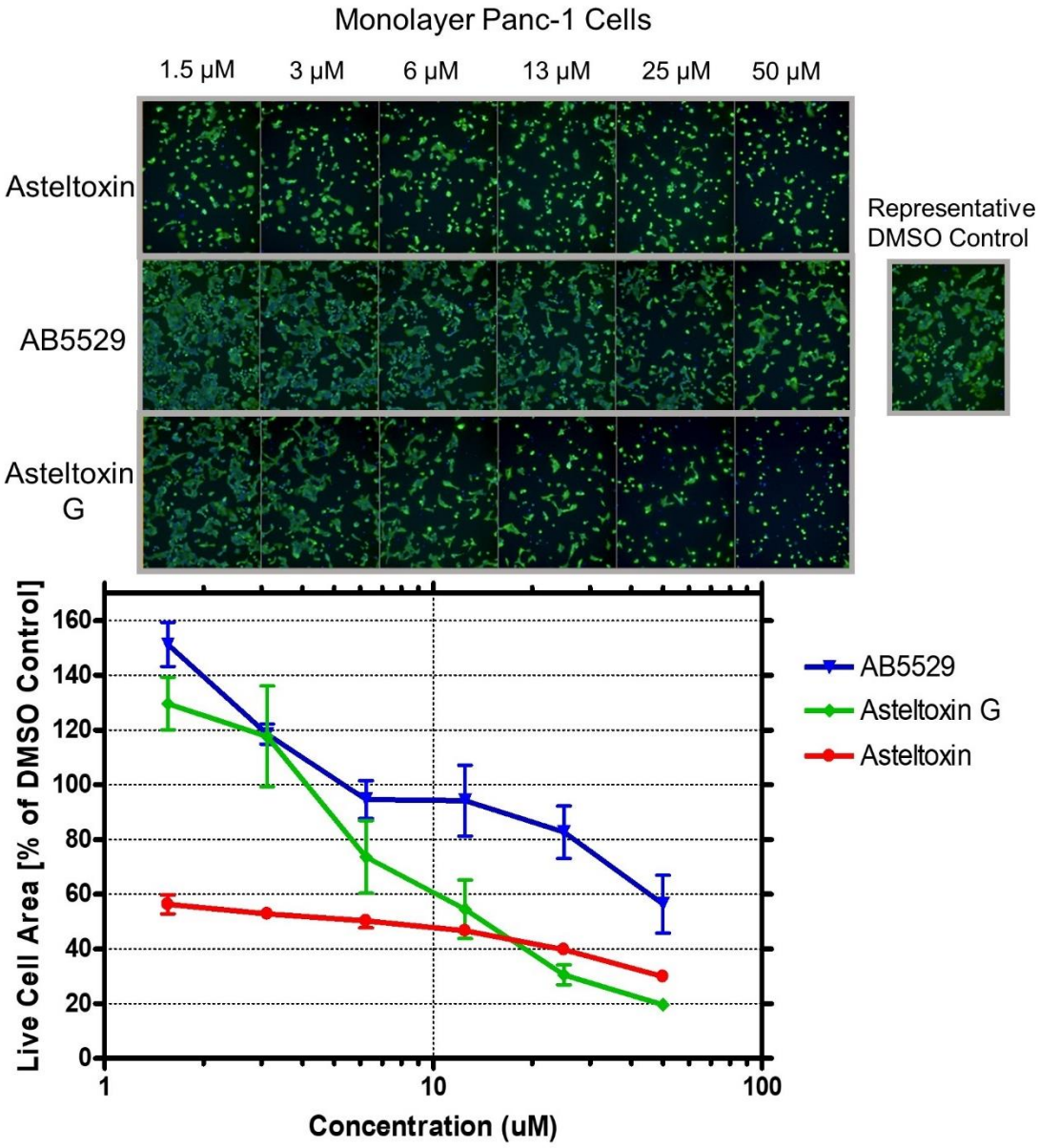


**Figure 17. Cytotoxicity Assays for the Asteltoxin Class Compounds in Monolayer Panc-1 Cells.** Cellular density shown by green fluorescence; nuclei located by blue fluorescent. Asteltoxin shows decreased cellular density across all concentration ranges, while AB5529 shows no decrease until 50 µM. Asteltoxin G caused decreased cellular density over the tested range.

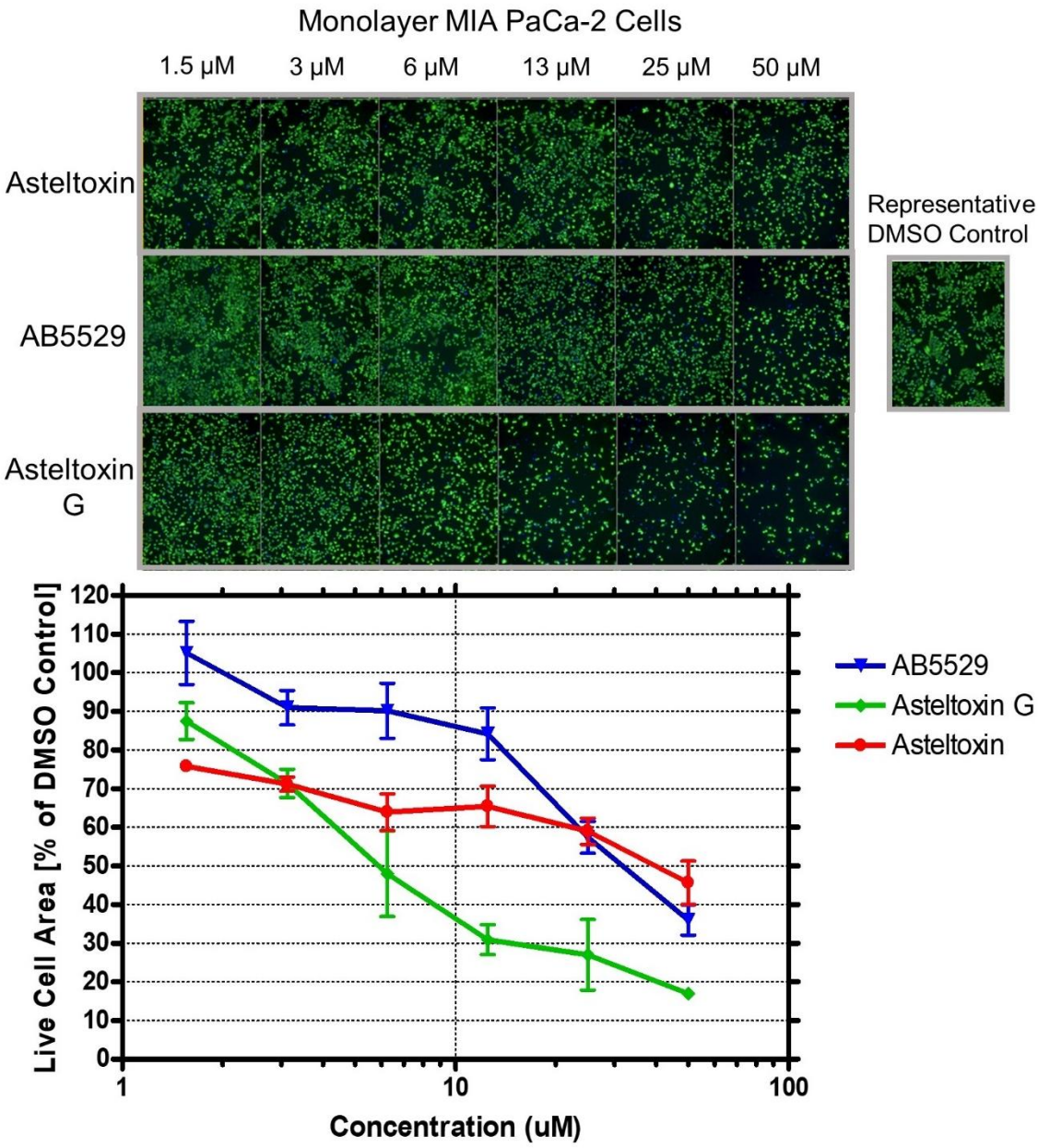


**Figure 18. Cytotoxicity Assays for the Asteltoxin Class Compounds in Monolayer MIA PaCa-2 Cells.** Cellular density is show in green fluorescence. Asteltoxin shows consistent cytotoxicity up to 50 µM, AB5529 started showing cellular toxicity beginning at 25 µM, and asteltoxin G showed increasing cytotoxicity over the range with almost complete cell death at 50 µM.

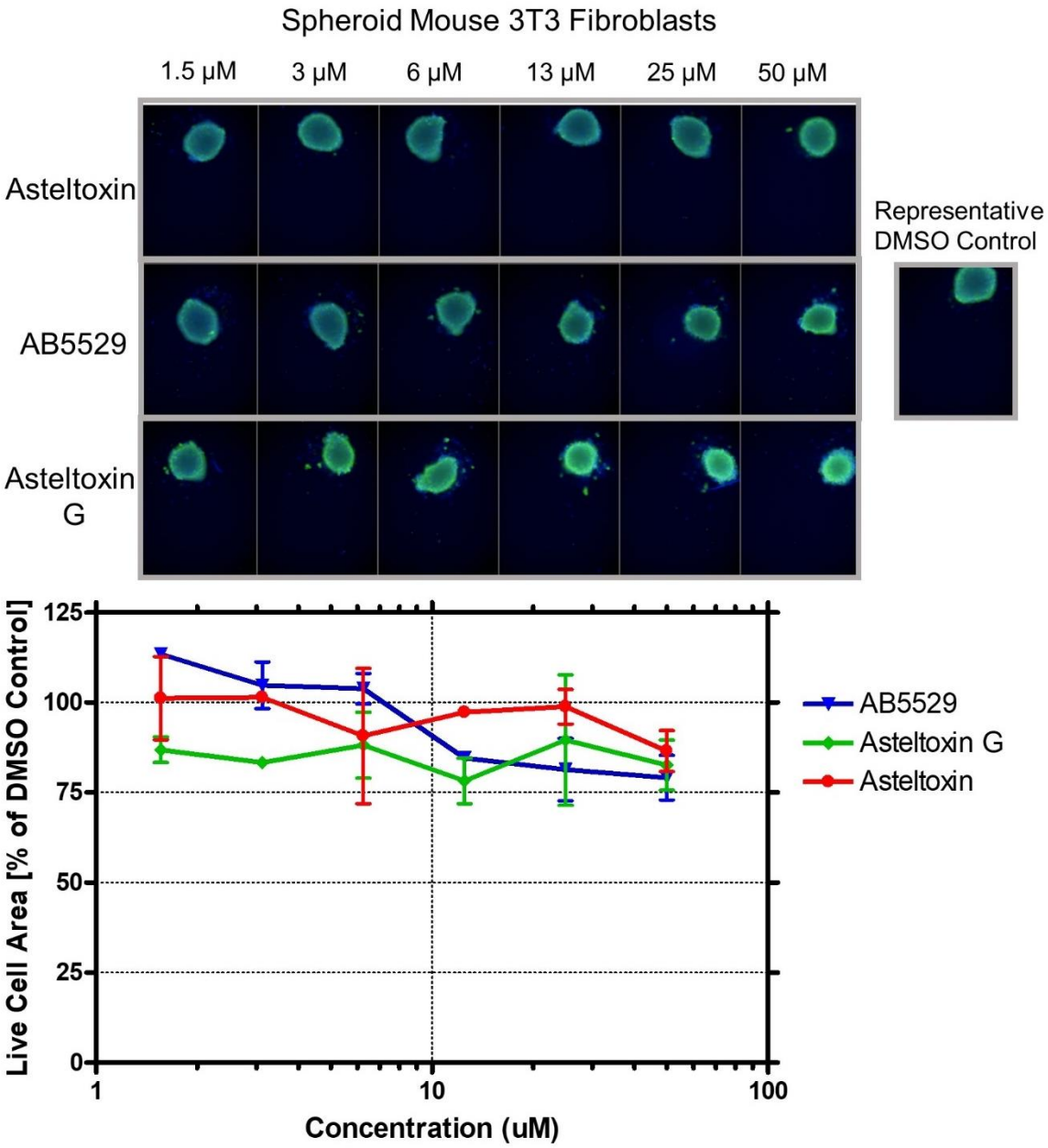


**Figure 19. Cytotoxicity Assays for the Asteltoxin Class Compounds in Spheroid Mouse 3T3 Fibroblast Cells.** Cellular density shown by green fluorescence; nuclei located by blue fluorescent. All compounds showed no significant decrease across any of the tested concentrations.

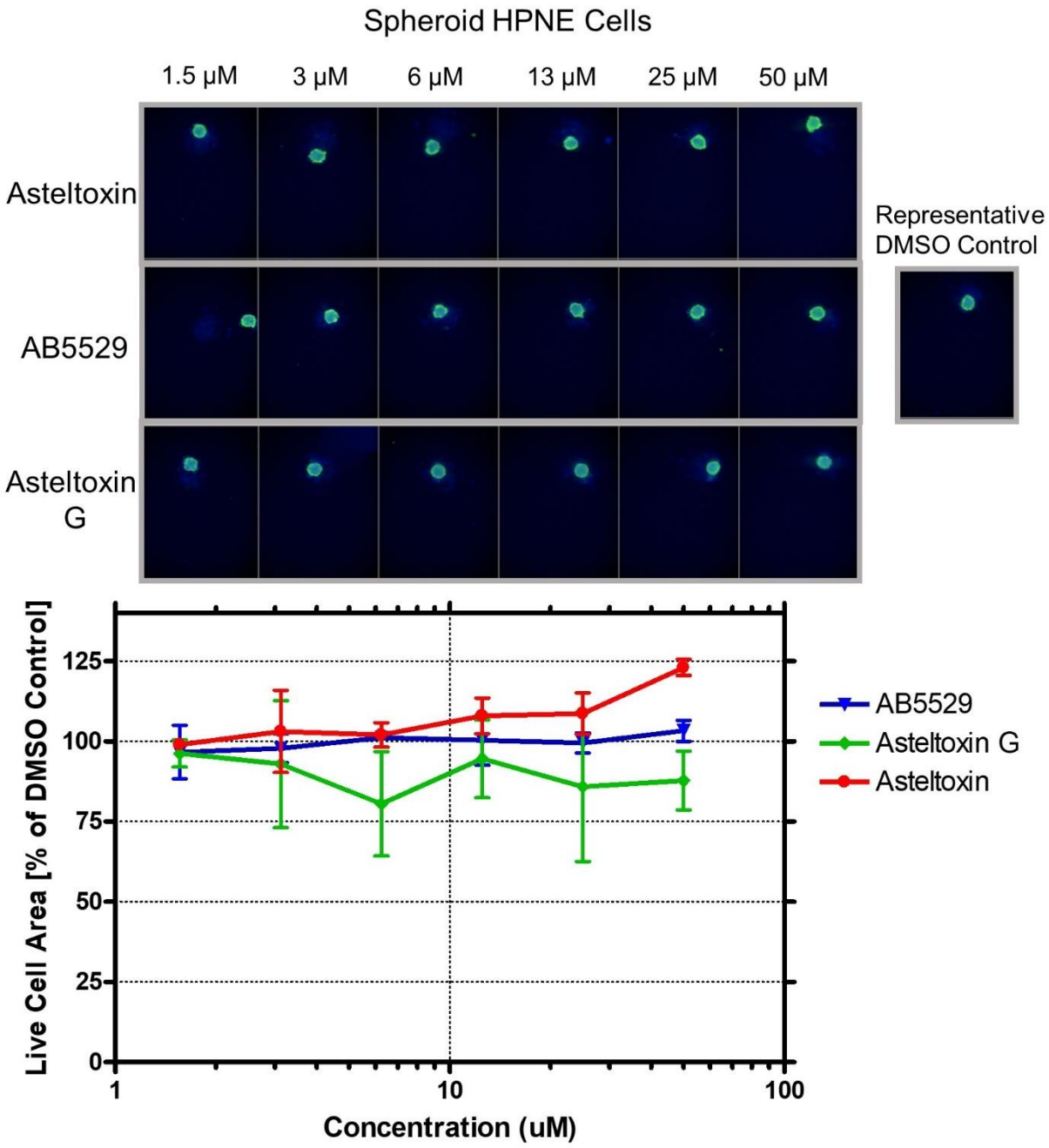


**Figure 20. Cytotoxicity Assays for the Asteltoxin Class Compounds in Spheroid HPNE Cells.** Cellular density shown by green fluorescence; nuclei located by blue fluorescent. All compounds showed no significant decrease across any of the tested concentrations.

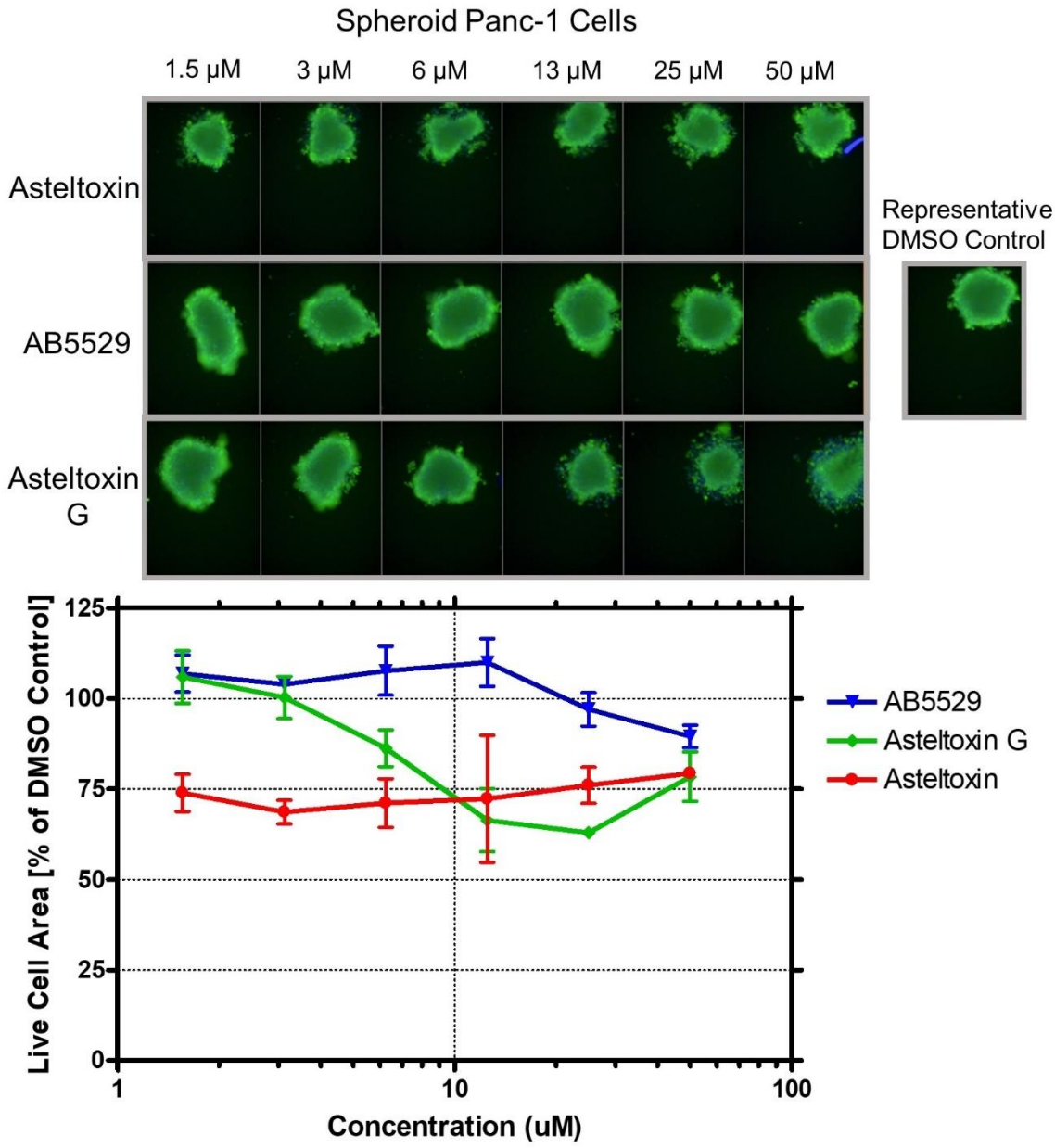


**Figure 21**. **Cytotoxicity Assays for the Asteltoxin Class Compounds in Spheroid Panc-1 Cells.** Cellular density shown by green fluorescence. Asteltoxin showed cytostatic activity, while AB5529 showed no noticeable cytotoxicity. Asteltoxin G showed decreased cellular density over the tested range.

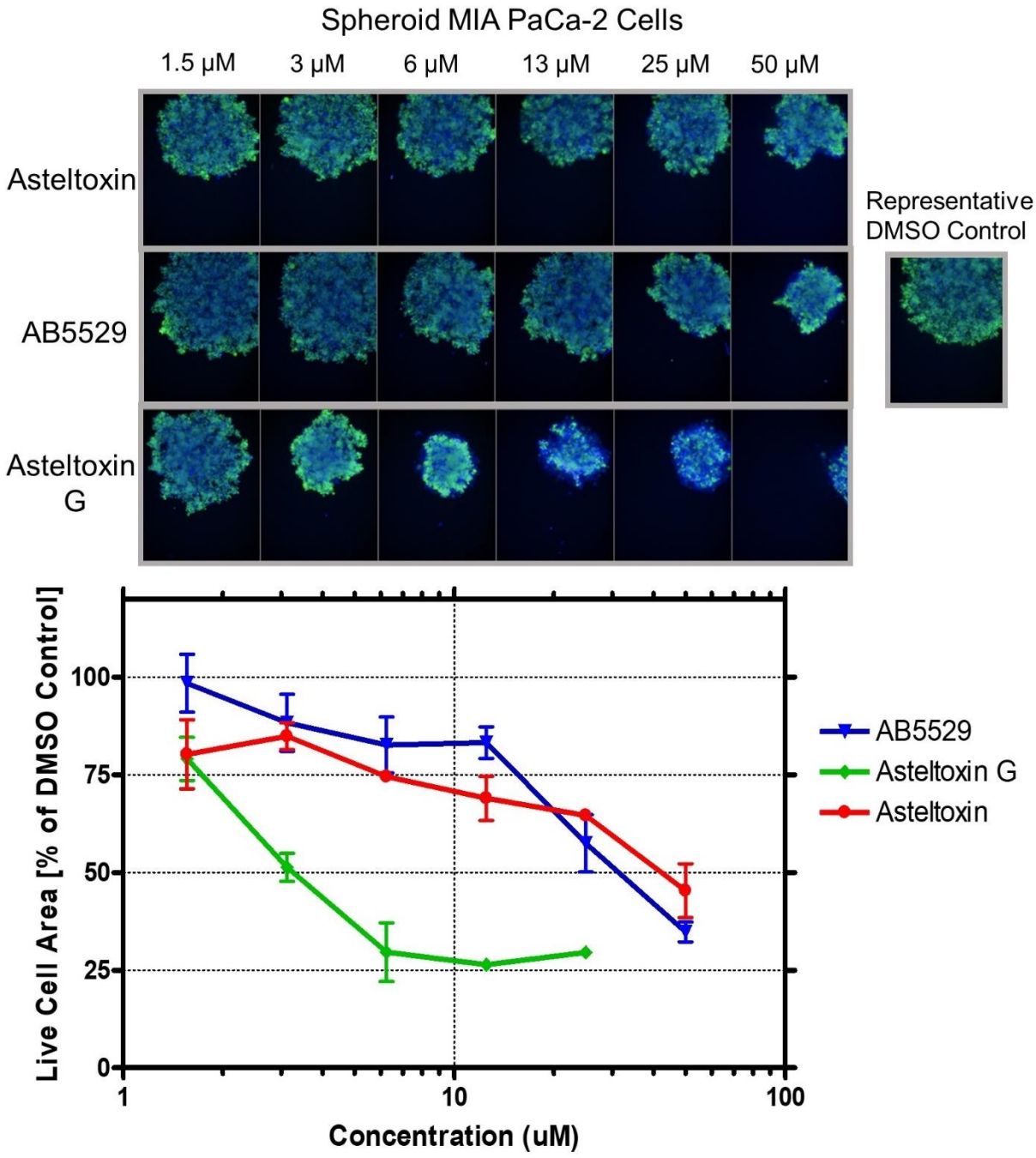


**Figure 22. Cytotoxicity Assays for the Asteltoxin Class Compounds in Spheroid MIA PaCa-2 Cells.** Cellular density shown by green fluorescence; nuclei located by blue fluorescent. Cellular density decreased with all three compounds. Asteltoxin G was the most potent causing nearly complete spheroid death at 50 µM.

### *4.4.4 Stability of Compounds and Their Activity*

Compound degradation and loss of activity has been noted for other polyenic alpha pyrones such as citreoviridin.[114] A *cis-trans* conversion of citreoviridin to isocitreoviridin, after as little as 30 minutes light exposure, resulting in a significant decrease in their anticancer activity.[114] The polyenic motif itself is known to degrade in light, as is also seen in beta-carotene,[115] first through a *cis-trans* isomerization followed by a singlet diradical[116] which then degrades into other compounds. Since, the location of the initial isomerization of the degradation of beta-carotene is theorized to be non-specific along the polyenic chain,[116] it can be logically construed that a longer polyenic chain affords more opportunities for the initiation of degradation. Since asteltoxin G has fewer olefins and more steric hindrance for a *cis-trans* isomerization, it was hypothesized that the degradation of asteltoxin should therefore be inhibited.

Bioassays were repeated to confirm the activity of the metabolites; however it is possible that rearrangements could occur during the assay itself. To test the relative stability of asteltoxin, AB5529 and asteltoxin G, the compounds were dissolved in DMSO at 0.1 mg/mL and placed in front of a 60w GE tungsten lightbulb for 0 to 600 minutes.[117] Samples were then analyzed by LC-MS to determine the relative purity. Asteltoxin began degrading within 5 minutes, while asteltoxin G only showed slight degradation even when exposed for up to 600 minutes (Appendix Figure A24). Since AB5529, which shared the same pyrone motif as asteltoxin G and the polycyclic furanose group as asteltoxin, also degraded rather quickly, the increased stability of asteltoxin G may be able to be attributed to the tricyclic furanose ring, possibly due to either steric hindrances to decrease the frequency of the *cis-trans* isomerization.

While degradation rate could explain the increased activity of asteltoxin G in a spheroid, it is not the only possible explanation. Alternative hypothesis could include different molecular targets between asteltoxin and asteltoxin G, spheroid permeability, cell permeability, or increased uptake.[118] Additionally, the increased *in vivo* like state , the cell-cell interactions, and signaling of the cells within the spheroid assay may make a completely different mechanism responsible for the observed results.[118]

## 4.5 Conclusion:

In summary, asteltoxin analogs as well as a benzophenone and (-) terpestacin were isolated form the fungus *Pochonia suchlasporia* after its crude extract was found to have selectivity towards MIA PaCa-2 and Panc-1 pancreatic ductal adenocarcinoma cell lines over NIH/3T3 normal mouse fibroblasts and hTERT-HPNE cell lines. The benzophenone, sclerotinin A was found to be inactive at the concentrations tested, and the (-) terpestacin had activity consistent with a literature report.[104] Among the three asteltoxin analogs, AB5529 only achieved and $LC_{50}$ of below 50 μM for one cell line (MIA PaCa-2), while both asteltoxin and asteltoxin G had $LC_{50}$ values below 50 μM for 3 out of 4 of the cell lines. The selectivity indices for asteltoxin, asteltoxin G, and AB5529 were calculated and asteltoxin was found to have monolayer selectivity indices lower than 1 for the NIH 3T3 cells compared to both the Panc-1 and the MIA PaCa-2 cell lines, which means that it was more cytotoxic to the non-cancerous cell line than the cancerous cell lines. The monolayer selectivity indices of asteltoxin were greater than 1 for the hTERT-HPNE cells line versus the both the Panc-1 and MIA PaCa-2 cell lines, which means it was less cytotoxic to the non-cancerous cells. Asteltoxin G, however, had monolayer specificity indices greater than 1 in all cases indicating that it was selective for the

cancer lines over the non-cancer lines in all cases. The pure compounds were also subjected to a 3-D spheroid assay which better mimics the *in vivo* conditions of pancreatic cancer tumors. Two compounds retained their selectivity within the spheroid assay, (-) terpestacin and the new analogue asteltoxin G with values of >1.3 and >15.6, respectively.

## 4.6 Experimental:

### *4.6.1 Small Scale Screening of Soil Samples*

Soil samples were briefly washed, diluted with water and plated on a variety of media and growth conditions.[119] Purified fungal isolates were grown in small scale solid-state conditions with a medium composed of three autoclaved Cheerios™ in a test tube and 1800 µL of a sterile sucrose water (2 g/L) with 0.05 mg/L of chloramphenicol. After growing for four weeks, test tubes were partitioned twice with 2 mL of ethyl acetate using a liquid partitioning robot. Ethyl acetate partitions were evaporated under vacuum, dissolved in 500 µL DMSO and submitted for assay. A total of 3,588 fungal extracts were tested by using a 0.5 µL pin tool and tested in both tumor and normal cell lines at a concentration of 10 µg/mL. Cell viability was determined by MTT assay when the project began but evolved later to use live cell area determination using the Operetta, which we found to correlate well with MTT values ($r^2$=0.9, data not shown). Follow-up screening regrows for confirmation of activity were done in 250 mL Erlenmeyer flasks and grown for the same period of time prior to extraction.

### *4.6.2 Large Scale Regrow of Small Scale Hit*

Once the activity was confirmed, a large scale grow-up was initiated in three large mycobags (Unicorn Bags, Plano, TX) with a combined total area of 5,565 $cm^2$, the equivalent of

fifty 1 L Erlenmeyer flasks. 850mL of 9.52 g/L sucrose water with 0.15 g/L chloramphenicol were added to 500 mL autoclaved Cheerios™ in each bag. The fungi were grown for 4 weeks and extracted with ethyl acetate three times overnight to get the initial crude extract.

### *4.6.3 Fungal Isolation and Identification*

The fungus studied here was isolated from Gelzan Czapek agar and named internally "Mt. Hood-5 Gelzan-5." The fungus was discovered in a soil sample obtained near Mount Hood, Oregon. PCR was performed with the ITS1 and ITS4 primers and products sent to the Biology Core Molecular Lab at OU for ITS sequencing. The results indicated a 99% max identity to *Pochonia suchlasporia*, when compared to NCBI BLAST.

### *4.6.4 Compound Isolation*

The crude extract (89g) was initially fractionated by a stepwise gradient consisting of hexanes, dichloromethane, and methanol over a silica column. The active fraction, 4.0 g, from a 9:1 dichloromethane:methanol condition, was further subjected to chromatography using a stepwise gradient of methanol and water over a HP20ss column. The 70% methanol in water subfraction was selected for further separation over silica based on conditions selected by TLC. A solvent system of dichloromethane and acetone over silica was chosen as it had the best resolution, and the separation was monitored by TLC. Further fractionation was carried out using preparative HPLC (Shimadzu, Gemini $C_{18}$ column - 250 mm x 10.1mm, 5µm, Phenomenex) with a gradient of MeOH and $H_2O$ and a semi-preparative HPLC (Waters, Gemini $C_{18}$ column - 250 mm x 21.2 mm, 5µm, Phenomenex) using either isocratic or gradient conditions (see Appendix Section A.1.2). Each fraction was analyzed using LC-MS, (Shimadzu, Kinetex C18

column – 3.0 mm x 75 mm, 2.6 µm, Phenomenex) with a 0.1% formic acid in water to acetonitrile gradient (10:90 to 100). Planar structures were determined through $^{1}$H, HSQC, HMBC, and COSY NMR (Varian Unity Inova 600 MHz) and mass data were on a HRESIMS (Agilent 6538 high mass resolution QTOF MS and Agilent 1290 HPLC). Optical rotation values were determined using an AUTOPOL III automatic polarimeter. When applicable, NMR data and optical rotation were compared to literature values. ROSEY NMR was used for relative configuration.

### *4.6.5 Calculation for Absolute Configuration of Asteltoxin G*

Structure confirmations were minimized using DFT calculations using aug-cc-pVDZ basis set in MeOH solvent conditions. The resulting minimized structures were subjected to polar=optrot command using b3lyp/3-21g basis set in Gaussian 09..

### *4.6.7 Monolayer Cytotoxicity and Selectivity Assays*

Monolayer mammalian cell assays were performed as described previously[120] and viability determined by MTT assay[121] or by a Calcein AM and Hoechst 33342 live cell area assay on the Perkin Elmer Operetta using the 10x objective. This assay was performed by adding to each well 5 µL of a 1:5 dilution in PBS of a 40 µM calcein AM and 160 µM Hoechst 33342 DMSO stock, incubating the plate for 30 minutes at 37°C and recording data from the Operetta. Harmony software was used to calculate the live cell area by finding all Hoechst-labeled nuclei and then assigns live or dead assessments to each cell based on a predetermined threshold of green fluorescence. Live cells are those with esterases still capable of cleaving the AM group from calcein AM causing them to glow bright green.

### *4.6.8 Spheroid Cytotoxicity and Selectivity Assays*

Spheroid cytotoxicity assays were performed using a modification of the published protocol from the Eccles group.[122] Cell lines were trypsinized and seeded at 1,000 cells per well (250 cells per well in MIA PaCa-2 due to more rapid growth in this cell line that would overgrow the field of view) in 100 µL of the appropriate cell media into Ultra Low Attachment 96-well plates (Corning Cat. # 7007). Spheroids were grown for four days in a humidified 37 ºC 5% $CO_2$ incubator. At day four, cells were treated with compounds dissolved in DMSO. Final DMSO concentration in the well was 0.5%. The spheroids were grown for an additional three days in the incubator, then analyzed using the same calcein AM and Hoechst assay used in the monolayer assay, and all images were recorded on the Operetta using the 10x objective. Harmony software was used to calculate the live cell area for each spheroid.

### *4.6.9 Compound Degradations Study*

A lamp fitted with a 60w GE tungsten filament lightbulb was placed 6 inches from 3 vials each containing 100 µL of 0.1 mg/mL of either asteltoxin, AB5529, or asteltoxin G. The samples were analyzed by LCMS after the total light exposure times of 0, 5, 15, 30, 60, 180, and 600 minutes. PDA chromatogram data at 254 nm was exported and analyzed with GraphPad Prism software.

# Chapter 5: Antifungal Cyclic Peptide from *Sphaceloma corylii*

## 5.1 Abstract

A leaf is composed of more than just plant cells. There are also microorganisms inhabiting the intercellular tissues. that can be either benign or pathogenic to the host plant. The benign microorganisms, called endophytes, can work in an symbiotic fashion providing secondary metabolites used by the host plants for nutrients or defense against other pathogenetic microorganisms.[53–55] Due to the defensive nature of some of these endophytes, we theorized that they might contain new antifungal secondary metabolites that would be safe to use agriculturally.

Isolating endophytes from other organisms that reside within the host plant can be a difficult and time-consuming process. To incorporate this process into a high throughput environment, a modified laser device was created to cut squares from pre-sterilized poplar leaves. These squares were released into a 96-deep-well plate with agar and the resulting colonies were isolated on small Petri plates.

One isolate was noted for a unique morphology and fungicidal activity and was therefore chosen for further analysis. Subsequent ITS sequencing and morphological analyses determined the organism was a *Sphaceloma coryli*, a species previously noted only in relation to a hazelnut blight,[123] however its teleomorph of the *Elsinoë* genus has been known to be pathogenic to other hosts such as mangos and avocados.[124] Using bioassay guided fractionation, 3 nine-residue peptides were isolated and named persephacins A-C. Also isolated were 3 elsinochromes, A, D and a new analogue E, which were found not to be responsible for the bioactivity. The bioactive persephacins were tested for their suitability as an agriculture antifungal through infiltration, systemicity, and antifungal assays.

## 5.2 Acknowledgements

The isolation, purification, and identification of *Sphecaloma* were completed by the endophyte team led by Dr. Shikha Srivastava and the initial chemical extraction of the fungus, initial isolation of the elsinochromes and the isolation of persephacin A were completed by Dr. Saiket Haldar. Structure elucidation was completed by Allison Mattes in conjunction with both Dr. Saiket Haldar and Dr. Lin Du. Both *in vitro* and *in vivo* assays reported here were completed by Dr. Shikha Srivastava. Assay quantification and media optimization experiments were performed by Allison Mattes.

## 5.3 Introduction

Within a leaf, there is much more than just plant cells and nutrients. Residing among the "internal tissues of plants beneath the epidermal cell layer, where they colonize healthy and living tissue via quiescent infections"[52] are the cells of other organisms called endophytes. These quiescent infections do not necessarily extend to the for the entire duration of the organism's life and at some point they may turn pathogenic.[53–55] When in symbiosis, endophytes have been known to benefit plant growth by providing secondary metabolites that provide nutrients or signaling specific growth conditions.[53–55] Their largest noted effect, however, is the control of other pathogenic microorganisms.[51]

This noted effect of microbial defense has made endophytes an interest as a new frontier of natural products drug discovery.[48–51] Research into endophytes have already produced results including secondary metabolites with antimicrobial activities that have spanned across a broad range of classes, from terpenoids to peptides.[51] In this chapter, we decided to use the defensive nature of these endophytes to explore a different avenue. We theorized, that due to the defensive

nature of some of these endophytes, they might serve as a source of secondary metabolites with antimicrobial applications that would be safe to use agriculturally.

Why are antimicrobial agricultural compounds an important area of research? While not the most prestigious target of anti-microbial compounds, diseases to agricultural plants account for approximately 16% of losses[125] translating into an approximate global financial loss of $540 billion.[126] In addition, noted agricultural resistances mechanisms have been theorized to either forecast or induce drug resistances in the clinical setting. This is being questioned, especially in Europe, where the key agricultural antifungal is azole based and there has been an increased occurrence of azole-resistant microorganisms appearing as human pathogens.[127] This theory is founded on the concept that, the selective elimination of species at the agricultural level allow those that have resistance to dominate the landscape.[127] As the antibiotic resistant organisms begin to comprise the majority of microbes in the treated soils, the chance of a resistant pathogenic species infecting a human host increases.[127] For this reason, it is important that antimicrobials with different modes of action be applied at varying times to agricultural crops, and therefore it is important to isolate new compounds with these new modes of action.

One of the important classes of compounds being considered as agricultural antimicrobial compounds are peptides due to their potential for reducing toxicity and having minimal environmental impact that can meet newly strengthened regulations imposed by European and US governments.[125] To date, over 900 antimicriobial peptides have been identified.[125] Those that are produced non-ribosomally can have a variety of alterations, including non-proteogenic amino acids, *N*-methyllation, and cyclization, all of which can prevent proteolysis.[125]

One peptide known for antimicrobial, specifically antifungal, activity is aureobasidin A. It is a cyclic depsipeptide with 8 amino acids and a hydroxy acid. [128] The activity of

aureobasidin A is theorized to target growing cells by causing unusual actin distributions and preventing mitosis.[128] While useful in laboratory experiments, this antifungal has not seen clinical applications currently due to resistance genes already found, [128] however further analysis has found that the aromatic phenylalanine in the aureobasidin is a target for an efflux pump in the resistance mechanism.[129]

Assay-guided fractionation of an extract from the *Spaceloma* endophyte discussed in this chapter resulted in the compound isolation and structure elucidation of three new peptides (Figure 23), similar to aureobasidin, but in place of the phenylalanine, a new aliphatic amino acid was found. These new peptides have the potential for antifungal activity that evades resistance mechanisms. We analyzed these compounds for applicability as an agricultural antifungal via infiltration assays.

## 5.4 Results and Discussion

### *5.4.1 Selection and Identification of Isolate*

Under the premise that endophytic fungi might be an excellent source of new antifungal compounds for use in agriculture systems,[48–51] a way to efficiently isolate endophytes without contaminating the isolates with surface-dwelling fungi was explored. The greatest source of contamination can occur from the cutting implements used to prepare leaf samples, therefore a cutting apparatus that minimizes transfer contaminiation in a high throughput manner was a primary advancement. Since commercially available lasers of higher power have become increasingly more available for the common consumer, we thought they might be advantageous for using as sterile incisions on leaves. Externally sterilized leaves were arrayed over a 96 well plate filed with agar, small squares were cut via the laser, and fungi were allowed to grow before

the isolates were purified. During purification, an inhibition ring between two fungi. The inhibiting fungus was isolated and grown in PDB broth and extracted in ethyl acetate. The resulting extract was tested against *Peyronellaea glomerate* and showed 80% inhibition at 0.5 mg/mL

The inhibiting fungus was identified through morphologically means and later confirmed by ITS sequencing as *Sphaceloma coryli,* a telemorph of *Elsinoe*.[123] The general morphology formed irregular, strongly folded, compact and elastic colonies, however, it varied in appearance depending on the medium used. On MEA (malt extract agar), colonies were yellow to deep orange with a light color margin, wrinkled, raised on the sides with a mostly hollow (concave) center. However, on PDA (potato dextrose agar), colonies appeared purplish-red/brown with a yellow ochre margin. The colonies were raised, wrinkled surface and elastic on the reverse side of the plate.

### *5.4.2 Compound Isolation and Structure Determination*

Few compounds have been purified from the genus *Sphaceloma*: elsinochrome C1, a dithiofatty acid, and a steroidal compound; none of which have noted antifungal activity.[130] Therefore, this isolate showed exceptional promise to yield new natural products

The initial extraction was completed using the fungus grown in 15 flasks of PDB media. An extract was prepared by ethyl acetate partitioning followed by bioassay guided fractionation. Initial prefractionation occurred by VLC column chromatography on HP20ss with MeOH and $H_2O$ in a stepwise gradient. Afterwards, HPLC using both C18 and biphenyl columns was used to purify three rich red colored compounds, which were determined to be elsinochromes. Elsinochrome A and D (see Appendix sections A.2.5 and A.2.6) were confirmed by comparing

NMR data with the literature values, however, elsinochrome D did not have a designated relative configuration.[131,132] The new analogue, elsinochrome E showed similarities to the planar structure of elsinochrome D, except with one of the secondary hydroxyls was oxidized to a ketone. Relative configuration was not determined on this compound as it was not biologically active.

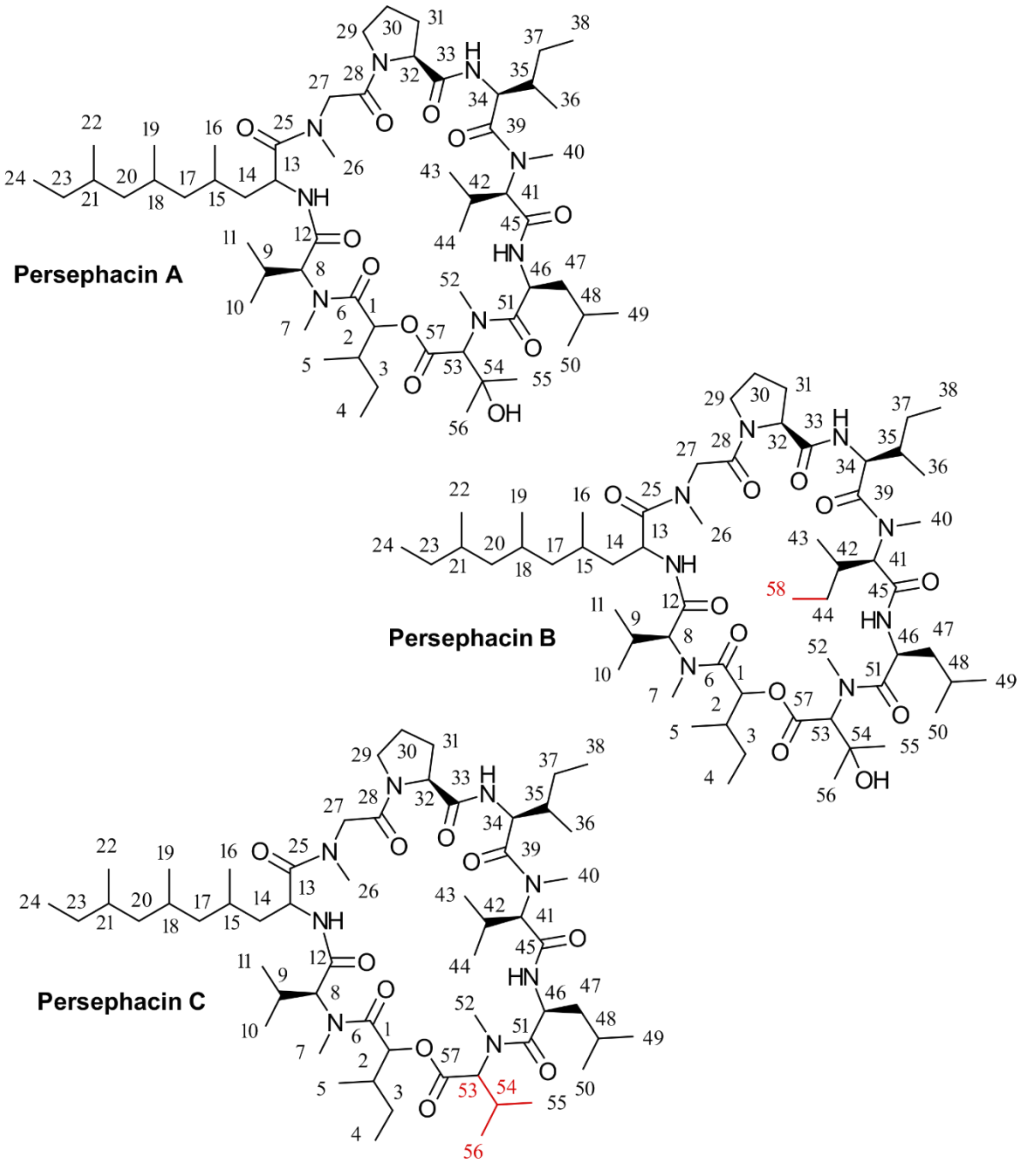


**Figure 23: Structure of Persephacins A-C.** The differences between each molecule are noted in red.

The bioactive compound was found to not be an elsinochrome. Accurate mass was carried out on the major active compound yielding an ion at *m/z* 1097.7586 $[M + Na]^+$, which gave a molecular formula of $C_{57}H_{102}N_8O_{11}$. To elucidate the structure, $^1H$, $^{13}C$, HSQC, HMBC, and COSY NMR were completed on the compound (Table 5). The $^1H$ NMR revealed three doublets between 8.0 and 9.0 ppm suggesting amide protons and 4 singlets integrating to 3 between 3.0 and 3.5 ppm reminiscent of methylated amides. There were also 9 carbonyl shifts according to the $^{13}C$ NMR. Between the mass data, the number of carbonyls, and the number of amide/methylated amides, it was determined that the compound was likely a peptide with 7-9 residues. A key feature of peptides is that each residue is isolated in a spin system by the carbonyls, and there is an NMR experiment called TOCSY which can correlate all protons within a spin system. To determine the confirm the presence of a peptide as well as the number of residues, a TOCSY was run on the sample in addition to the other NMR experiments. The TOCSY results showed 9 distinct spin systems further confirming the identity of the compound as a peptide and the number of residues.

**Table 1. NMR Shifts of Persephacins A,B,C**

| | Persephacin A | | Persephacin B | | Persephacin C | |
|---|---|---|---|---|---|---|
| **Position** | **$^{13}C$** | **$^1H$** | **$^{13}C$** | **$^1H$** | **$^{13}C$** | **$^1H$** |
| **OH-ILE** | | | | | | |
| **1** | **73.13** | **5.73** | **74.31** | **5.73** | **73.46** | **5.66** |
| **2** | **36.48** | **1.92** | **37.62** | **1.92** | **36.31** | **1.92** |
| **3** | **22.99** | **1.14,1.57** | **23.97** | **1.14, 1.57** | **23.00** | **1.15, 1.58** |
| **4** | **10.35** | **0.85** | **11.53** | **0.86** | **10.39** | **0.84** |
| **5** | **14.91** | **1.06** | **15.95** | **1.06** | **14.83** | **1.06** |
| **6** | **169.20** | | **169.20** | | **169.47** | |
| **N-Me-Val** | | | | | | |
| **7** | **29.90** | **3.28** | **30.99** | **3.27** | **29.91** | **3.28** |

| | | | | | | |
|---|---|---|---|---|---|---|
| **8** | **61.58** | **5.02** | **62.66** | **5.00** | **61.42** | **5.05** |
| **9** | **27.66** | **2.21** | **28.77** | **2.20** | **27.84** | **2.21** |
| **10** | **10.21** | **0.85** | **19.73** | **0.82** | **10.26** | **0.85** |
| **11** | **19.02** | **1.01** | **20.11** | **1.00** | **19.23** | **1.00** |
| **12** | **169.85** | | **169.86** | | **170.03** | |
| **Per** | | | | | | |
| **NH** | | **8.49** | | **8.49** | | **8.48** |
| **13** | **45.56** | **5.28** | **46.61** | **5.27** | **45.45** | **5.29** |
| **14** | **38.99** | **1.26, 1.98** | **40.03** | **1.26, 1.98** | **38.77** | **1.25, 2.03** |
| **15** | **22.39** | **1.33** | **22.39** | **1.33** | **20.35** | **1.09** |
| **16** | **19.58** | **0.91** | **20.59** | **0.91** | **19.47** | **0.93** |
| **17** | **45.94** | **0.93, 1.24** | **47.03** | **0.93, 1.24** | **46.05** | **0.95, 1.24** |
| **18** | **27.08** | **1.60** | **28.26** | **1.60** | **19.19** | **0.85** |
| **19** | **18.85** | **0.85** | **20.22** | **0.86** | **19.16** | **0.86** |
| **20** | **44.83** | **0.87, 1.24** | **45.90** | **0.87, 1.24** | **44.95** | **0.89, 1.24** |
| **21** | **31.47** | **1.42** | **32.59** | **1.42** | **31.47** | **1.42** |
| **22** | **19.95** | **0.84** | **21.02** | **0.84** | **19.70** | **0.84** |
| **23** | **25.14** | **1.11.12,1.462** | **27.41** | **0.94, 1.02** | **24.96** | **1.11, 1.43** |
| **24** | **11.53** | **0.97** | **12.51** | **0.97** | **11.43** | **0.97** |
| **25** | **172.15** | | **172.15** | | **172.15** | |
| **N-Me-Gly** | | | | | | |
| **26** | **37.95** | **3.39** | **39.07** | **3.38** | **37.95** | **3.39** |
| **27** | **51.40** | **3.40, 4.48** | **52.46** | **3.40, 4.48** | **51.40** | **3.40, 4.48** |
| **28** | **169.09** | | **169.09** | | **169.09** | |
| **Pro** | | | | | | |
| **29** | **23.31** | **1.94, 2.07** | **24.41** | **1.94, 2.07** | **23.31** | **1.94, 2.07** |
| **30** | **29.58** | **2.15** | **30.64** | **2.15** | **29.58** | **2.15** |
| **31** | **46.50** | **3.66, 3.99** | **47.60** | **3.66, 3.99** | **46.50** | **3.66, 3.99** |
| **32** | **59.89** | **4.60** | **61.09** | **4.60** | **59.95** | **4.59** |
| **33** | **172.39** | | **172.39** | | **172.34** | |
| **Ile** | | | | | | |
| **NH** | | **8.00** | | **8.00** | | **8.00** |
| **34** | **54.32** | **4.68** | **55.34** | **4.67** | **54.33** | **4.65** |
| **35** | **36.91** | **2.29** | **38.04** | **2.29** | **36.90** | **2.29** |
| **36** | **14.82** | **1.01** | **15.90** | **1.00** | **14.90** | **1.00** |
| **37** | **28.65** | **1.08** | **29.90** | **1.08, 1.39** | **28.79** | **1.08, 1.39** |
| **38** | **27.02** | **1.44** | **28.18** | **1.44** | **20.70** | **1.04** |

| | | | | | | |
|---|---|---|---|---|---|---|
| **39 N-Me-Val** | **172.64** | | **172.64** | | **172.69** | |
| **40** | **30.00** | **3.22** | **31.06** | **3.21** | **29.91** | **3.23** |
| **41** | **61.48** | **5.28** | **61.83** | **5.31** | **61.38** | **5.24** |
| **42** | **25.47** | **2.25** | **33.50** | **1.97** | **25.44** | **2.25** |
| **43** | **17.50** | **0.81** | **14.81** | **0.78** | **17.66** | **0.81** |
| **44** | **18.51** | **0.94** | **25.92** | **0.99, 1.11** | **18.36** | **0.93** |
| **45** | **170.50** | | **170.50** | | **170.23** | |
| **58 Leu** | | | **12.01** | **0.92** | | |
| **NH** | | **8.06** | | **8.06** | | **8.07** |
| **46** | **47.52** | **4.94** | **48.57** | **4.94** | **47.55** | **4.87** |
| **47** | **42.27** | **1.36, 1.69** | **43.51** | **1.36, 1.69** | **41.69** | **1.29, 1.71** |
| **48** | **24.84** | **1.53** | **25.93** | **1.52** | **24.93** | **1.49** |
| **49** | **22.32** | **0.96** | **23.53** | **0.95** | **22.63** | **0.94** |
| **50** | **21.00** | **0.99** | **22.21** | **0.98** | **20.77** | **0.97** |
| **51 N-Me-3-OH-Val** | **172.37** | | **172.37** | | **170.23** | |
| **52** | **39.57** | **3.34** | **40.76** | **3.34** | **39.09** | **3.30** |
| **53** | **71.65** | **3.80** | **72.79** | **3.80** | **30.08** | **2.86** |
| **54** | **72.95** | | **72.95** | | **27.09** | **2.65** |
| **55** | **27.04** | **1.30** | **28.21** | **1.30** | **27.21** | **1.61** |
| **56** | **26.23** | **1.36** | **27.31** | **1.36** | **18.69** | **0.99** |
| **57 OH** | **166.96** | | **166.96** | | **168.87** | |

Before identifying each residue, there were a few things to note. There were no shifts in the aromatic region for either the $^{1}H$ or the $^{13}C$ spectrum, eliminating the presence of any tryptophan, tyrosine, histidine, and phenylalanine residues. Additionally, there were only 7 amide/methylated amide shifts detected in the $^{1}H$ NMR, while it was determined there were a total of 9 residues. Therefore, two residues would likely be some combinations of prolines and depsi-bonds to account for the lack of amide protons or methyls.

The proton peak at 5.73ppm, showed strong TOCSY (Figure 24) correlations to 1.92 ppm and 1.06 ppm. HSQC correlations of these to peak signify carbon shifts at (C-2) 36.48 and (C-3) 22.99 ppm respectively which were in opposite phases and allowed the determination of the C-2 as a methine and C-3 as a methylene. These shifts would signify the residue as either an isoleucine or a leucine. Because C-2 was further downfield than C-3, it was determined to be the β-carbon of the amino acid, which would make the residue an isoleucine. HMBC correlations confirmed the remaining methyl shifts, however there was no correlations seen to either a protonated or methylated amine. It was concluded that this could possibly be a depsi-bond instead.

For the second residue, there were TOCSY correlations of 2.21, 1.01, and 0.85 ppm. From HSQC, these residues all had the same phase and in combination with $^{1}$H NMR were determined to be a methine and two methyls respectively. The residue was identified as a valine.

A third residue showed at least 4 TOCSY correlations with the amide proton at 8.49 ppm. According to HSQC phase data, these correlated to two methines, one methylene, and one methyl. These shifts did not suggest any of the proteogenic amino acids. For the time being it was assigned as an unknown amino acid.

The fourth residue was determined to be glycine. It had no TOCSY correlations, but the α-carbon, which was determined by the carbon shift of 51.50 ppm, was a methylene as determined by both $^{1}$H NMR integration and HSQC phase.

The fifth residue determined had 5 TOCSY signals correlating to 4.60 ppm α-proton, all between 1.94 and 3.99 ppm. HSQC phase determination of the shifts showed that they belonged to 3 methylenes two of which had *J* couplings of 8 Hz. Both the $^{1}$H NMR and the $^{13}$C NMR shifts of each atom were consistent with a proline.

For the sixth residue, there were 3 easily apparently TOCSY correlations to the 4.68 ppm α-proton, and one weaker correlation at 1.44 ppm. HMBC correlations confirmed the weaker correlation. According toe HSQC phase data, there were 3 methines/methyls and 1 methylene, which suggested either a leucine or an isoleucine. The 2.29 ppm methine (H-35) had the $^{13}C$ shift furthest downfield making it the β-carbon of the amino acid and therefore an isoleucine.

The seventh residue identified had 3 TOCSY correlations to the 5.28 α-proton. HSQC phase data showed that all 3 atoms were methine/methyls. The residue was therefore determined to be a valine.

The eighth residue identified had 5 strong TOCSY correlations to the 8.06 ppm amide proton. An additional TOCSY correlation was seen between the 4.94 ppm α-proton and 1.53 ppm (H-48). The 1.36 and 1.69 ppm methylene (H-47) had the $^{13}C$ shift furthest downfield making it the β-carbon of the amino acid and therefore a leucine.

The ninth residue identified had two strong TOCSY correlations at 1.30 and 1.36 ppm. Upon investigation with HMBC, correlations were observed between the 3.80 ppm α-proton and a $^{13}C$ signal at 72.95 ppm (C-54). The 72.95 ppm signal had no corresponding HSQC signal suggesting a quaternary carbon. These signals were not consistent with any of the 20 proteogenic amino acids, however hydroxy substitutions on quaternary hydrocarbons typically cause $^{13}C$ shift of around 70-80 ppm. Therefore, the amino acid was determined to be the N-Me-hydroxy-valine. configuration of the common amino acids N-Me-Val, Ile, and Leu as N-Me-L-Val, L-Ile, and L-Leu (Appendix Figures A61-A62). HMBC correlations were used to assemble the backbone of the peptide by correlating the shifts of alpha carbons, amide protons, and methylated amides to their nearby carbonyls. One alpha proton, showed correlations to two carbonyls, but one of these carbonyls did not show correlations to any amide protons or methylated amides. The alpha

carbon was determined to belong to an isoleucine residue (C-1), however its carbon shift was further downfield than one would expect: being at 73.13 ppm. In comparison, there was another isoleucine residue in the same molecule and the alpha carbon had a $^{13}C$ chemical shift of 54.32 ppm. This suggested that the more shielding ester moiety was present instead of an amide, which would make the compound a depsipeptide and accounted for the lack of the second amide proton.

In summary, TOCSY, HMBC, and HSQC analysis confirmed the presence of two N-Me-valine residues, a N-Me-glycine residue, a leucine residue, an isoleucine residue, and the unusual N-Me-3-OH-valine residue. Using HMBC correlations of the α-atom to either the amide proton/methyl yielded the following order: OH-Ile-N-Me-Val-unknown residue-N-Me-Gly-Pro-Ile-N-Me-Val-Leu-N-Me-3-OH-Val. Marfey's analysis was used to determine the absolute configuration of the common amino acids N-Me-Val, Ile, and Leu as N-Me-L-Val, L-Ile, and L-Leu (Appendix Figures A61-A62).

The scaffold described above accounted for 46 C, 79 H, 8 N, and 11 O. This meant the remaining residue consisted of 11 C and 23 H according to the molecular formula $C_{57}H_{102}N_8O_{11}$. Using the phase sensitive nature of HSQC, it was determined that there were 4 methyls, 4 methylenes, and 3 methines remaining. The proton on the alpha carbon showed as a triplet meaning the adjacent carbon was a methylene, however the splitting patterns and coupling constants for other protons were unable to be distinguished. Using the HMBC correlations shown in Figure 25, the new residue, we propose calling persephanine, had its planar structure determined.

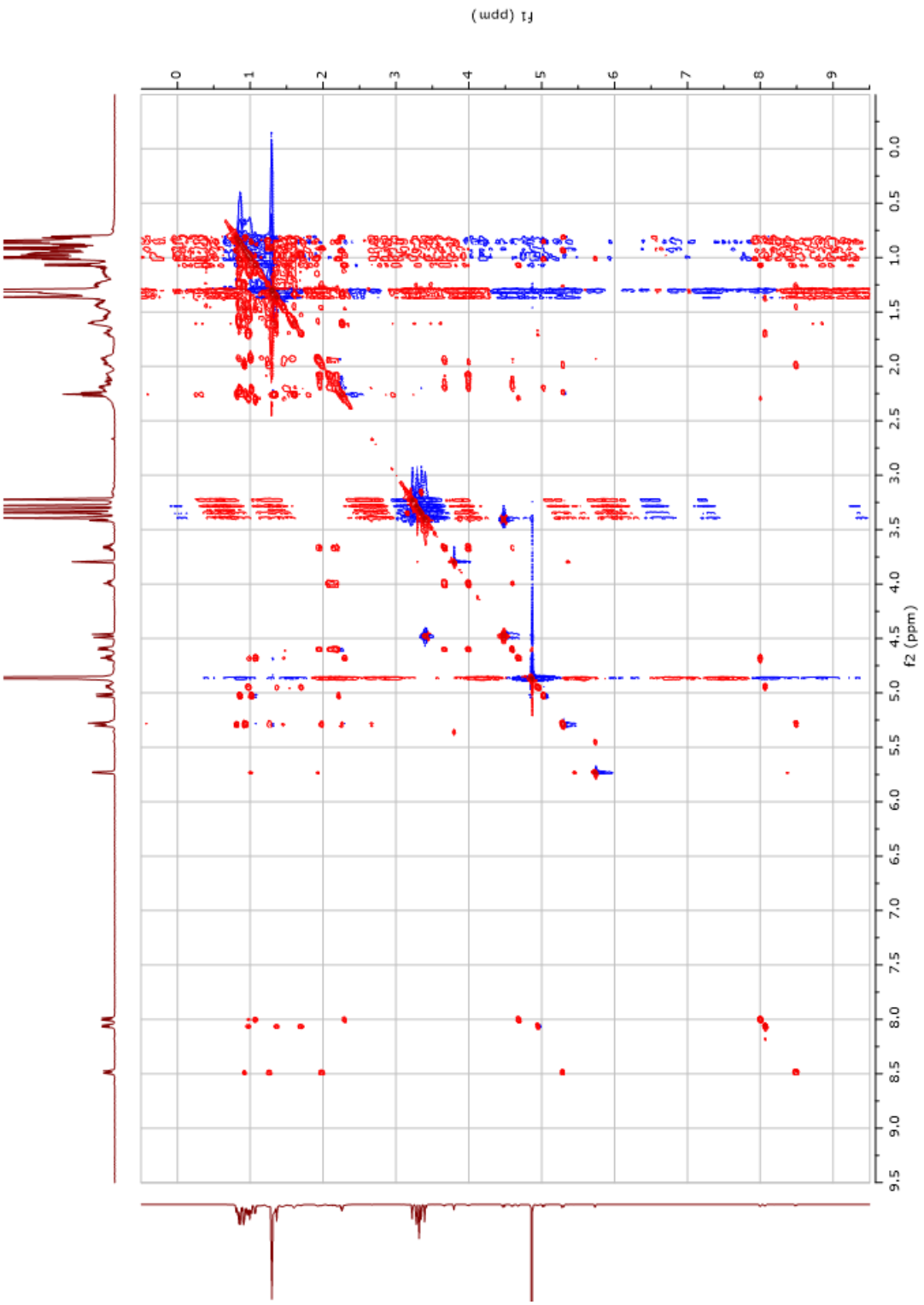


**Figure 24: TOCSY of Persephacin A.** TOCSY shows correlations within a spin system.

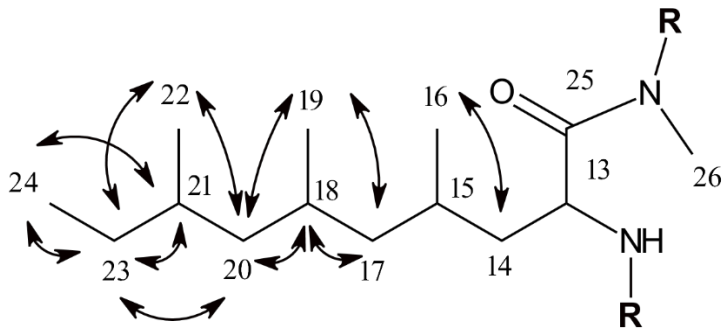


**Figure 25: HMBC Correlations of the New Amino Acid Residue, Persephanine.**

While optimizing growth conditions, two analogues of persephacin were isolated in relatively minor amounts (Appendix Figure A26 for isolation scheme), 1.5 mg for persephacin B and 8 mg for persephacin C. The planar structure of persephacin B was very similar to persephacin A. When comparing the HSQC, three distinct differences can be observed: the loss of a signal at 0.94 ($^{1}$H) and 18.51 ($^{13}$C) ppm corresponding to the C-44 carbon of the valine residue, the presence of signals at 25.92($^{13}$C) and 0.99 ($^{1}$H) and 1.11 ($^{1}$H) ppm corresponding to a methylene, and new signals at 12.01 ($^{13}$C) and 0.82 ($^{1}$H) ppm corresponding to a methyl. The mass was determined to have 14 amu units higher than persephacin A. Therefore, persephacin B had a substitution of either an isoleucine or a leucine. The alpha proton (H-41) of the altered valine residue, remained as a doublet (Figure 26B), which suggested an isoleucine rather than a leucine. It has been noted with aureobasidin that the important residue used for exportation was the phenylalanine and the important residue for activity was the alpha-hydroxy, therefore it is unlikely that the substitution of an isoleucine for a valine would cause a significant effect on bioactivity.[133] Marfey's analysis was used to determine the absolute configuration of the common amino acids N-Me-Val, Ile, N-Me-Ile, and Leu as N-Me-L-Val, L-Ile, and L-Leu (Appendix Figures A61-A62).

The third analog, persephacin C, was much more hydrophobic than either persephacin A or B. While a preparatory HPLC column at 95% acetonitrile caused both persephacin A and B to elute within 35 minutes, persephacin C required an extra 20 minutes to elute from the column. Upon analysis of the mass spectrum, it was noted that the mass was *m/z* 16 less than persephacin A, suggesting the loss of an oxygen atom. As can be seen from the $^{1}$H NMR spectrum, the two methyls of the N-Me-3-OH-Val shifted as singlets at 1.30 and 1.36 ppm to unidentifiable splitting at 0.99 ppm and 1.61 ppm (Figure 26). The proton peak of C-53 was shifted upfield from 3.80 to 2.86 ppm, which one might expect with the loss of a nearby hydroxy group. In addition, a new multiplet appeared at 2.65 ppm which was assigned to C-54, the previously quaternary carbon on the N-Me-3-OH-Val residue. Therefore, persephacin C was determined to have a substitution of a N-Me-Val in place of the N-Me-3-OH-Val residue. Marfey's analysis was used to determine the absolute configuration of the common amino acids N-Me-Val, Ile, and Leu as N-Me-L-Val, L-Ile, and L-Leu (Appendix Figures A61-A62).

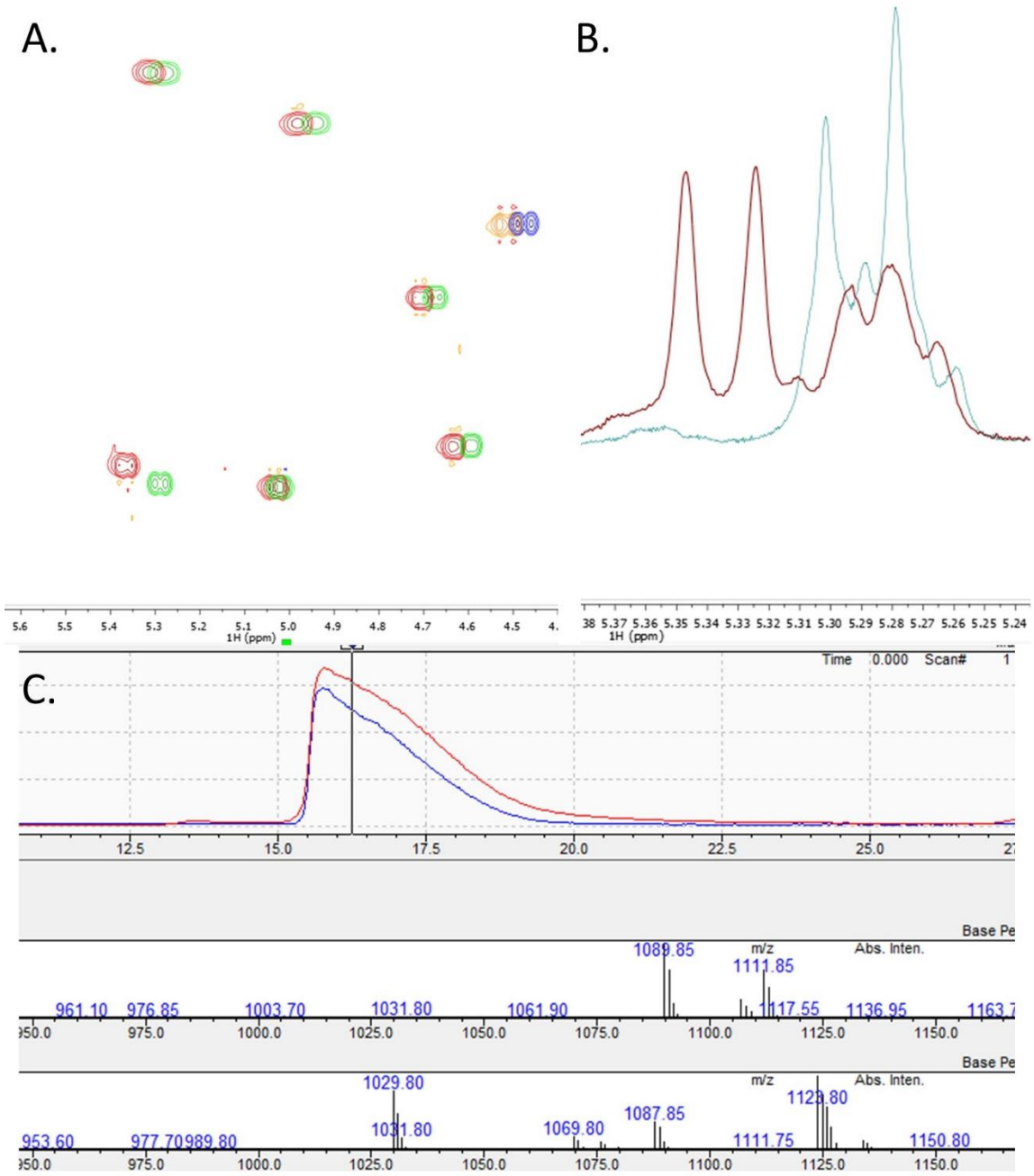


**Figure 26: Determination of Persephacin B.** The new analog of persephacin B, shifts designated in red/yellow in HSQC (A) and red in $^{1}$H NMR (B), the signal of the alpha carbon which was followed by TOCSY to identify the residue. (C) LCMS shows an increase of 14 amu indicating the addition of a methylene.

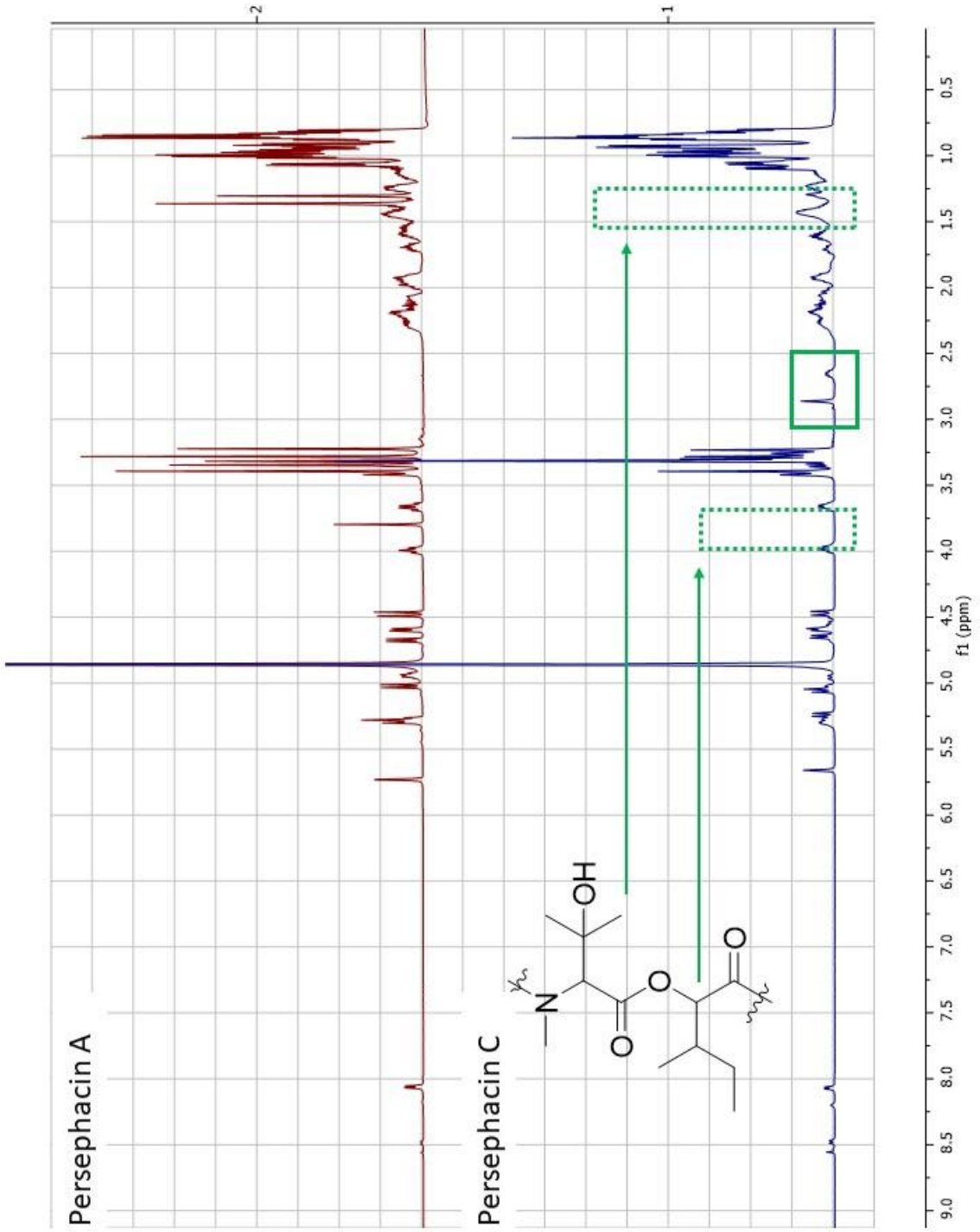


**Figure 27 $^{1}$H NMR Comparison of Persephacin A and Persephacin C.** The dotted regions show where the designated peaks appear in persephacin A and the solid green region is where the peaks appear for persephacin C.

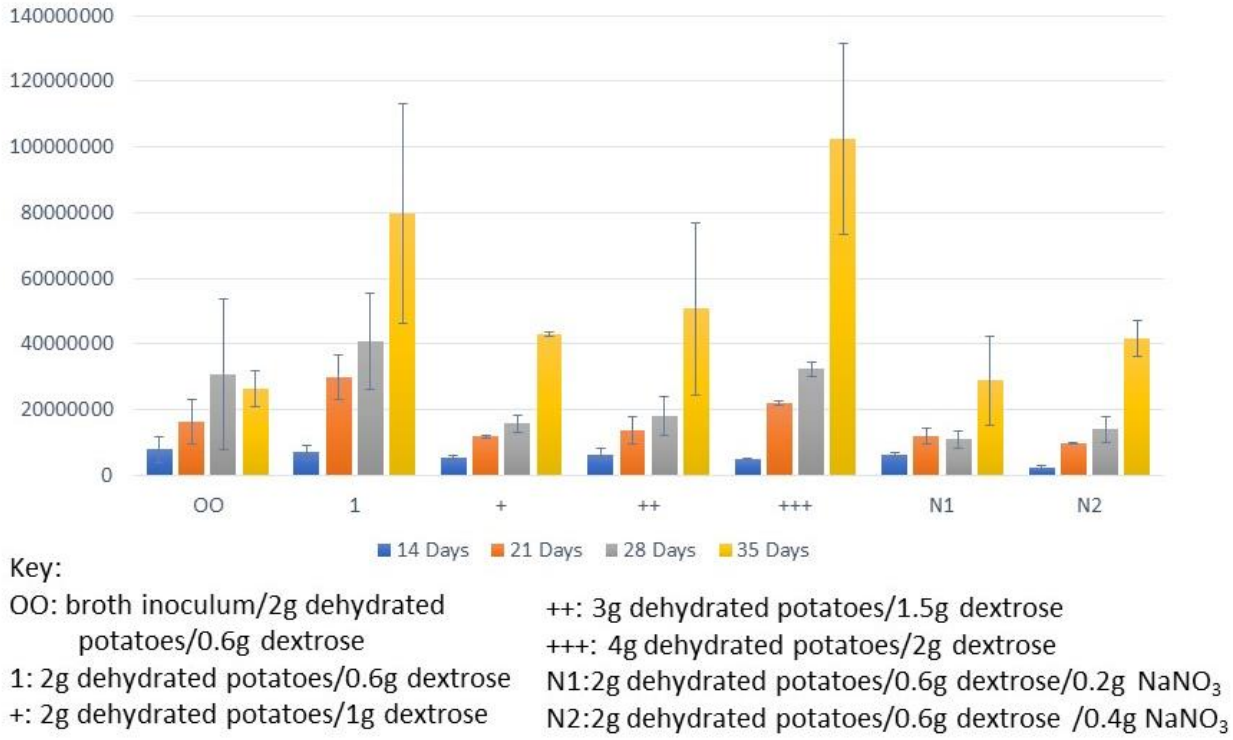


**Figure 28: Productions of Persephacin.** Quantification of persephacin over time in different media. While less persephacin was produced at 14 days with the higher concentration of dehydrated potatoes and dextrose, at 35 days the yields were the highest. Sodium nitrate caused a decrease in persephacin production.

### *5.4.3 Media Optimization and Optimized Isolation*

Due to the slow growing nature of the fungus, media optimization was attempted. A concentration curve was generated according to LCMS conditions that could quantify crude extracts from each medium. The different media compositions (Figure 28) included increased ratios of dehydrated potatoes to dextrose either in a 2:0.6 ratio or a 2:1 ratio. The second parameter tested was an increase in the concentration of media components (at a 2:1 ratio), and the third parameter tested an additional nitrogen source, $NaNO_3$, would be beneficial to the production of persephacin. A final parameter, the type of inoculum used, was tested. Broth

inoculum was taken from a shaken liquid aged 2 weeks in PDB media of 2 g dehydrated potatoes with 0.6 g dextrose, and agar inoculum was taken from YM plates. On days 14, 21, 28, and 35, a sample of 5 mL was taken aseptically from each condition and extracted with 5 mL ethyl acetate 3 times. Samples were dissolved in 200 µL before being subjected to chromatography for quantification and assessed for metabolite complexity on the LCMS in identical conditions to the concentration curve. It was determined that persephacin concentration increased in all media over time, suggesting that the fungus does not degrade persephacin after a certain point in the time range tested. The inclusion of $NaNO_3$ showed a retardation of growth at all conditions and time points. The ratio and the quantity of dehydrated potatoes and dextrose did have a noticeable difference on the production of persephacin A. With the same quantity of dehydrated potatoes, the ratio of 2:0.6 had increased production over the 2:1 over all time peroids, however after 35 days, the increased PDB, at 4g dehydrated potatoes and 2g dextrose, surpassed the persephacin A concentration of the 2:0.6 ratio. It was determined that PDB +++, 4g dehydrated potatoes and 2g dextrose, was determined to yield the greatest amount and that the fungi should be grown for about 35 days prior to extraction. Even with the optimized PDB conditions, the yield of persephacin A was still low in the shaken flasks. Since endophytes grow among plant tissues, we hypothesized that a change in the flask might cause a change in both the surface area and oxygen content of the fungal cultures which has been known to influence fungal growth.[134,135] Both roller bottles and baffled flasks with different volumes were explored.

**Figure 29. Photo of Roller Bottles.** A device that slowly rotates bottles, potentially allowing greater surface adhesion of growing organisms.

A roller bottle fermentation (Figure 29) slowly rotates a bottle on its side in an attempt to provide a large surface area for cells to adhere to while allowing continual moisture and nutrients to reach the cells. Roller bottles with a variety of media (PDB +++ with agar, avocado, PDB+++, PDB, PDB+++ with vermiculite, HR-01, and Etched glass with PDB medium) were inoculated with equivalent amounts of fungi and grown for 4 weeks. Avocado was chosen as a media additive because *Spaceloma corylii*, has been known to be a pathogenic species of avocado,[136] therefore avocado might provide some nutrients the fungus that were missing in PDB. While substantial growth was noticed in the avocado medium, in smaller and more uniform colonies

than the other media, there was no red color and a not as much persephacin production as the PDB media which produced the most persephacin A in the 200 mL condition. The PDB+++ medium had inconsistent growth between the two flasks, one producing the red pigmentation while the other did not. This suggested that persephacin A production is correlated with the red pigmentation of the elsinochromes. The fungi grown in the etched flasks, which was a PDB+++ media, had increased growth in the 200 mL condition. Ultimately, roller bottles were deemed not to be the best conditions for large scale production due to their inconsistencies and not substantial increased persephacin production to mitigate the labor involved in prepping and cleaning glassware.

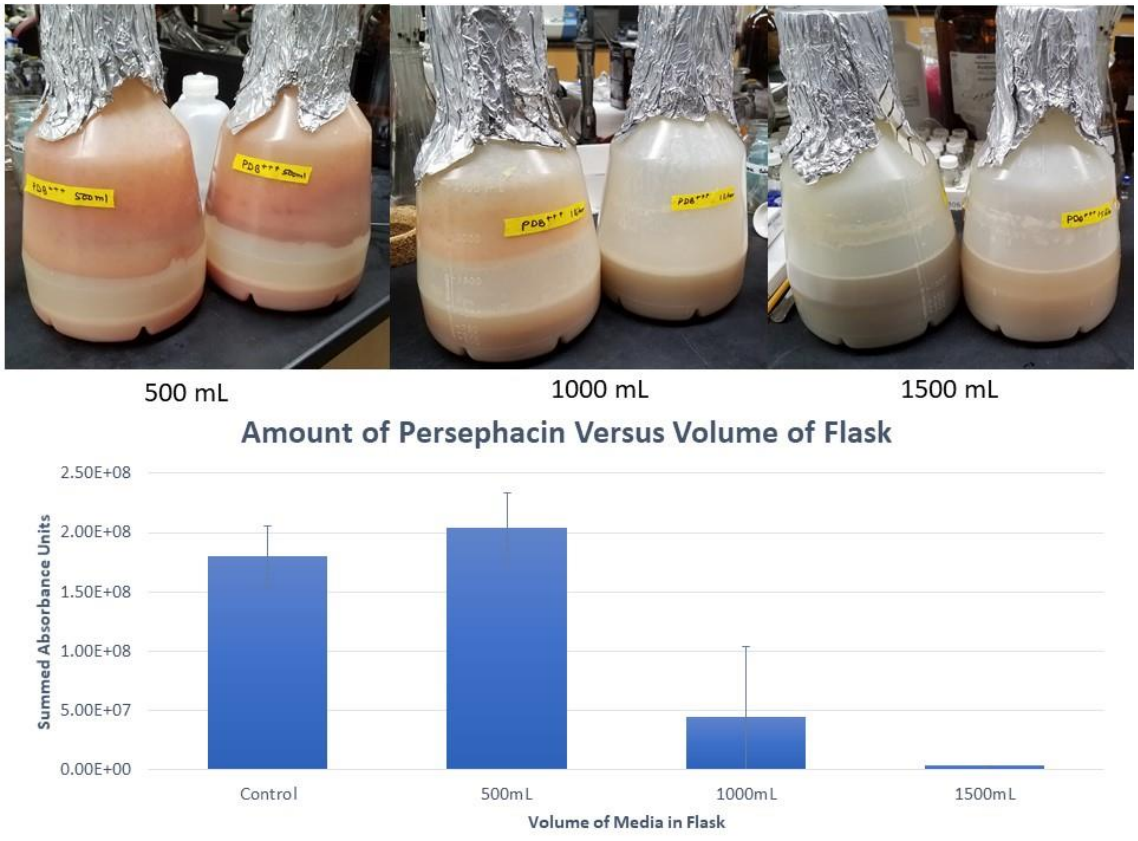


**Figure 30. Comparative Yield of Persephacin A Respective of Volume.** Using baffled flasks, different volumes were tested for persephacin production. The 500 mL baffled flask had a greatest yield.

Baffled flasks are large plastic flasks with divots in the bottom to increase aeration and circulation while mixing (Figure 30). Three different volumes (500mL, 1000mL and 1500mL) were tested with proportional inoculum in PDB +++ media were grown for 4 weeks on a shaker before being extracted with proportional volumes of ethyl acetate. Persephacin A yields were quantified *via* a calibration curve on the LCMS and were found to be inversely correlated with the volume in the flask, which is consistent with the theory that greater amounts of oxygen and/or surface area was necessary for the increased production of persephacin A. Since baffled flasks did not show a significant increase in persephacin A production, baffled flasks would not cause a significant improvement in the fermentation process.


**Figure 31: Bioreactor of *Spaceloma corylii.*** A large quantity of medium, 10L, was able to be inoculated and grown in a single container with increased air flow.

One of the largest limiting factors in the fermentation of persephacin A is the quantity of flasks necessary to get a large enough yield of persephacin A, a bioreactor was explored using 10 L of PDB+++ media and inoculated with 200 mL of a 2 week old *Spaceloma corylii* culture (Figure 31). The bioreactor was covered with aluminum foil to remove light as a variable. A bioreactor culture was grown for 4 weeks, and each week 1 L of autoclaved distilled water was added to mitigate the loss due to evaporation. Upon extraction, and analysis via LCMS, it an esimated yield of 89 mg of persephacin A was expected to be obtained from the single bioreactor. A bioreactor of PDB+++ media, with a 4 week growth time was the optimized growth conditions for the production of persephacin A.

### *5.4.4 Bioactivity*

Persephacin A-C were tested against a panel of fungal species that are known to be plant pathogens using fludioxonil,[137] a non-systematic fungicide used for agriculture purposes, as a positive control. The MIC, minimum inhibitory concentration or the amount required to reduced 75% of growth, and the MFC, minimum fungicidal concentration or the amount required to reduce 100% of growth, were determined against the 8 different isolates: *Alternaria brassicicola, Alternaria brassicae, Alternaria Tennuissiema, Fusarium oxysporum, Fusarium tricinctum, Mycosphaerella populorum, Nodulosporium spp,* and *Pfaffia gloerata*. In all cases, persephacin C did not achieve complete or even 75% inhibition in the tested ranges of 0.32 µM to 10 µM. This is consistent with published data on aureobasidins, a similar cyclic peptide also with a 3-OH valine, that lost activity after synthetic modifications attached long chain aliphatic residues.[133] Percephacin B had lower MIC values than persephacin A for all fungi except the *M. populorium* and *P. glomerate* in which persephacin A had a lower MIC value and *Nodulosporium* where

neither compound showed MIC or MFC activity in the designated range. The fludioxonil was more potent than the peptides, with lower MIC except in the cases of *F. oxysporum* where it matched persephacin A and persephacin B had a lower MIC (1.25 µM versus 5 µM), and *P. glomerata* where fludioxonil had no activity in the range tested whereas both persephacin A and B had low MIC (0.625, 1.25) and MFC (1.25, 5) values.

**Table 2: MIC and MFC Values of Persephacin A-C and Fluidioxonil Against Possible Phytopathogenic (Endophytic) Fungi.** MIC is the minimum inhibitory concentration or the amount required to reduced 75% of growth, and MFC is the minimum fungicidal concentration or the amount required to reduce 100% of growth.

| | *Persephacin A* | | *Persephacin B* | | *Persephacin C* | | *Fludioxonil* | |
|---|---|---|---|---|---|---|---|---|
| *Test Fungus* | MIC (µM) | MFC (µM) | MIC (µM) | MFC (µM) | MIC (µM) | MFC (µM) | MIC (µM) | MFC (µM) |
| *A. brassicicola* | 5 | 20 | 2.5 | ≥20 | ≥20 | ≥20 | 1.25 | ≥20 |
| *A. brassicae* | 1.25 | 2.5 | 0.625 | 1.25 | ≥20 | ≥20 | 0.625 | 2.5 |
| *A. tennuissiema* | 10 | 10 | 2.5 | 2.5 | ≥20 | ≥20 | 1.25 | 1.25 |
| *Fusarium oxysporum* | 5 | 20 | 1.25 | 20 | ≥20 | ≥20 | 5 | ≥20 |
| *F. tricinctum* | 5 | 10 | 2.5 | ≥20 | ≥20 | ≥20 | 1.25 | ≥20 |
| *M. populorum* | 2.5 | 10 | 5 | ≥20 | ≥20 | ≥20 | 1.25 | ≥20 |
| *Nodulosporium spp.* | ≥20 | ≥20 | ≥20 | ≥20 | ≥20 | ≥20 | 0.625 | ≥20 |
| *P. glomerata* | 0.625 | 1.25 | 1.25 | 5 | ≥20 | ≥20 | ≥20 | ≥20 |

*5.4.5 Systemicity and Infiltration Studies*

The activity of persephacin A was evaluated in plants and its systemicity was also analyzed to determine if it was suitable for an agricultural fungicide and if so, what type of application might be necessary.[137] Depending on the mobility of a compound within a plant (i.e., xylem mobile, phloem mobile, and nonmobile) a fungicide can be applied to treat certain conditions. The xylem flow brings nutrition from the roots to the leaves and therefore would cause compounds to extend out from the point of contact. A spray application on the leaves, would not allow antifungal activity against root pathogens. For this, phloem mobility would be important which is typically used for transportation of sugars and works in a diffusion mediated fashion (Figure 32).

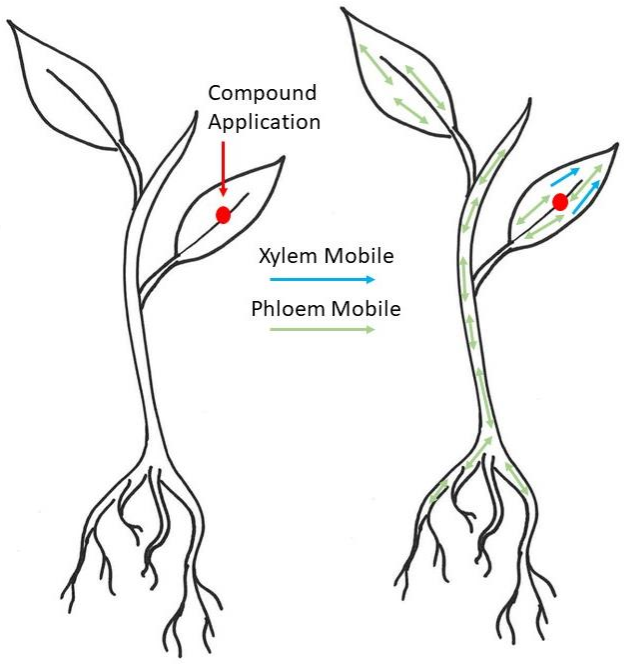


**Figure 32: Different Types of Compound Mobility** If a compound is xylem mobile it will move outward from the application location. If a compound is phloem mobile is will move both outwards and inwards and should therefore be seen everywhere in the plant. A non-mobile compound will be located only at the application location.

To test the mobility, an emulsifiable concentrate was created using DMSO as both the penetrant and solvent for mobility testing. While DMSO might not be applicable in the agricultural field due to its propensity for shuttling compounds through tissue in humans, using it in this instance would ensure penetration into plant tissues to measure general mobility.[138] Vehicle control and the xylem mobile compound azoxystrobin were used on two leaf stage cabbage plants.[139] The leaf on which the compound was applied was segmented into three different parts: distal, application zone, and inner. The rest of the plant was segmented into petiole of the leave with the compound applied, the new leaf, stem, and roots. After extraction with MeOH, compounds were analyzed by the LCMS with selected mass and had a detection limit of <1 μg/mL.

The azoxystrobin was seen in two of the segments: the application zone on the leaf and the distal end of the same leaf. As the azoxystrobin has been noted to be xylem mobile, this confirmed the assay as able to detect mobility. Persephacin A was only identified in the application zone of the original leaf and was therefore determined to be not mobile at detectable levels within the plant.

While working with the compound, it became insoluble at higher concentrations of water which might explain the lack of mobility within the plant, however, there was a noticeable inhibition zone around the major colony of *Sephacaloma corylii* as it grew on agar which suggested that there might be some ability of the compound to be mobile in the right media. With the currently tested emulsifiable concentrate, the compound would be best suited for preventative application against pathogens that affect the above-ground areas of the plant. Figure 33:

Infiltration Assay.

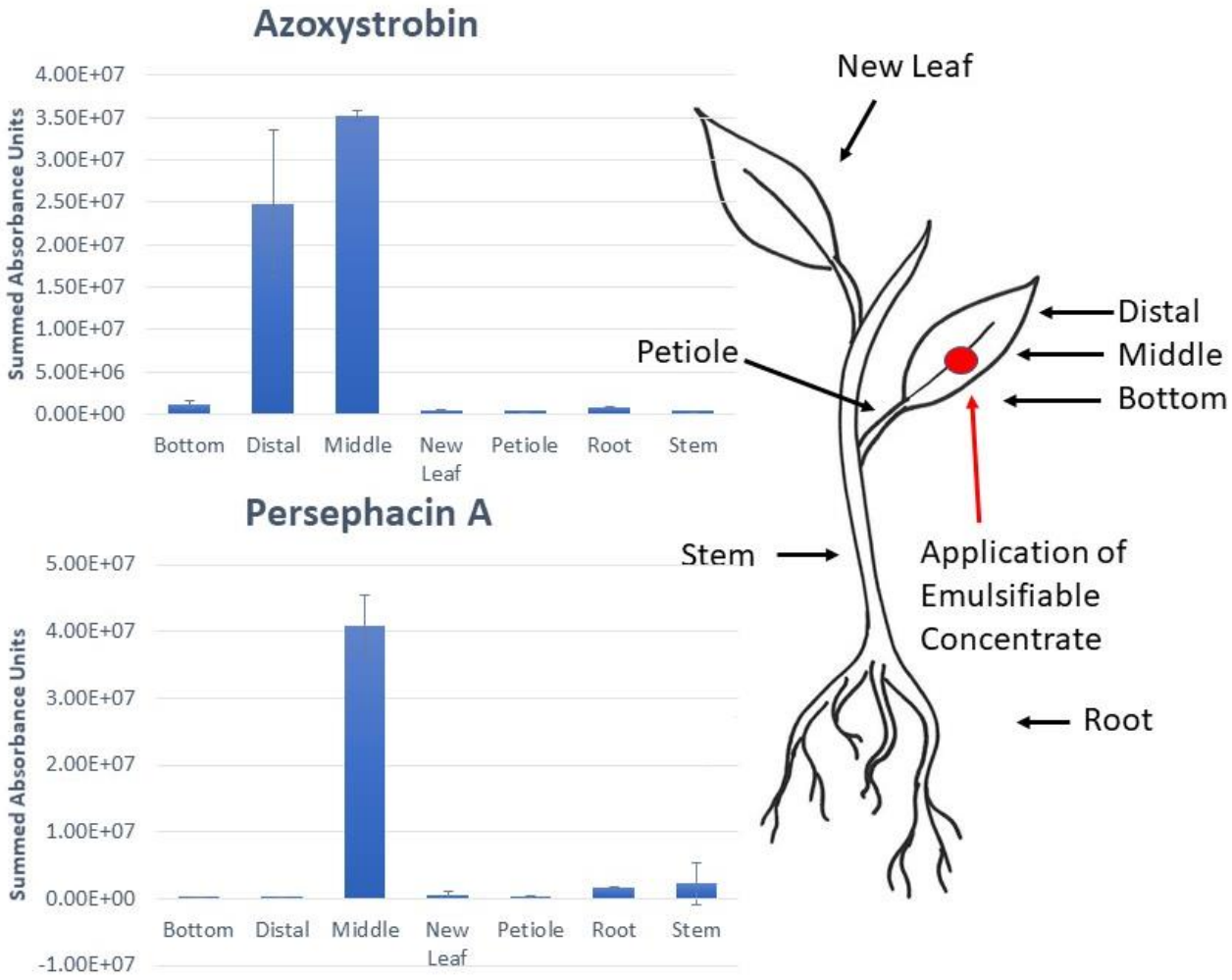


**Figure 33. Infiltration Assay of Emulsifiable Concentrate of Azoxystrobin Control and Persephacin A.**
After application of an emulsifiable concentrate(azoxystrobin control, persephacin A), different segments (Bottom, Middle and Distal of the leaf, petiole, new leaf, stem and roots) were extracted and analyzed via LC-MS. Azoxystrobin ions were observed in the distal and middle regions of the original leaf, while persephacin A ions were only observed in the middle region of the original leaf.

## 5.5 Conclusion

Two new bioactive compounds were isolated and termed persephacin A and B and a third inactive analogue termed persephacin C. These new compounds share structural similarities with the known class of cyclic peptides aureobasidins, however, in place of the phenylalanines of the aureobasidins, the persephacins have a new long aliphatic chain amino acid herein termed persephanine. This new aliphatic residue is thought to negate the efflux mechanism in fungi. Further research will need to be conducted to determine the susceptibility of compounds to such mechanisms.

These compounds were tested against 8 different suspected pathogens and had low μM MIC values against 7 of them. Mobility studies in cabbage plants suggested the compound does not exhibit systematic distribution and would therefore need to be applied as a topical agricultural fungicide. For a topical fungicide photodegradation studies would be necessary, but due to the absence of UV-sensitive moieties suggests the compound would likely have excellent photostability.

## 5.6 Experimental

### *5.6.1 Fungus Isolation and Identification*

The fungus was isolated from the heathy leaf of a poplar (*Populus nigra*) tree, collected in Oklahoma, USA. The plant samples were collected in zip-loc bags and stored at 4°C until processed. Leaf samples were thoroughly washed with mild soap and distilled water to clean the surface. Samples were then surface-disinfected by soaking in 95% Ethanol (Pharmco-AAPER, USA) for 10 seconds, in 10% bleach (Great Value, Wal-Mart, Inc., USA REF: 550655043) for 2 minutes, and then dried. Immediately before cutting, the samples were sprayed with 70% Ethanol

for 30 seconds and dried with sterilized paper towel before being processed for the isolation of endophytes by a laser into a 96-well plate containing CMAD (Corn Meal Agar + 1% Dextrose) media. The 96-well plate was incubated at ambient daylight and 22–24 °C for four weeks. The fungi were purified by single hyphal tip isolation onto CMAD small Petri plates and this was repeated three times. The pure culture was transferred to 20% glycerol for cryopreservation for further use. Finally, the fungus was identified using cultural characteristics, morphology and ITS sequencing (ITS1 primer: 5'- CTTGGTCATTTAGAGGAAGTAA-3' and ITS4 primer: 5'-TCCTCCGCTTATTGATATGC-3').

### *5.6.2 Compound Isolation*

The *Sphaceloma coryli* was grown in PDB media (2 g dehydrated potato flakes and 0.6g dextrose in 200 mL) in 15 shaken glass Erlenmeyer flasks. The slow-growing fungus was grown for 4 weeks and extracted with ethyl acetate to yield 1.3 g. The crude extract was subjected to bioassay guided fractionation on a VLC HP20ss column using a stepwise gradient of MeOH in $H_2O$ (30%, 50%, 70%, 90%, 100% and 50% MeOH in DCM). The resulting 90% MeOH in $H_2O$ fraction (240 mg) was subjected to a preparatory C18 HPLC column at 55% MeCN in $H_2O$ to give 21 mg of elsinochrome D. The 100% MeOH fraction (356mg) was further subjected to chromatography on C18 prep HPLC with a 40-100% MeCN in $H_2O$ with 0.1% formic acid as a gradient over 15 minutes to yield 8 fractions. Elsinochromes A (1.0 mg) and E (3.4 mg) were identified from these fractions and further purified using a semiprep biphenyl column at 40% MeCN in $H_2O$ with 0.1% formic acid. Persephacin A was also identified from the 8 fractions, but required an additional C18 Prep HPLC run at 100% MeCN followed by a semiprep HPLC at

95% MeCN in $H_2O$ and a biphenyl column (kinentex 5 µm biphenyl 100Å, 250x100mm) at 65% MeCN in $H_2O$ with 0.1% formic acid to yield 3 mg.

### *5.6.3 Media Optimization*

Due to the slow growing nature of the fungus, media optimization was attempted. A concentration curve (0.01 mg/mL to 1 mg/mL) and LCMS conditions (95% ACN and 5% 0.1% TFA in $H_2O$ isocratic,) were chosen to quantify crude extracts from each media analyzed. The different media compositions included increased ratios of dehydrated potatoes to dextrose either in a 2:0.6 ratio or a 2:1 ratio. The second parameters tested, was an increase in the concentration of media components (at a 2:1 ratio), and the third parameter tested was if the extra presence of a nitrogen source, $NaNO_3$, would be beneficial to the production of persephacin. A final parameter, the inoculum, was tested. Broth inoculum was taken from a shaken liquid aged 2 weeks in PDB media of 2 g dehydrated potatoes with 0.6g dextrose, and agar inoculum was taken from YM plates. On days 14, 21, 28, and 35, a sample of 5 mL was taken aseptically from each condition and extracted with 5mL ethyl acetate 3 times. Samples were dissolved in 200 µL before being subjected to chromatography for quantification and assessed for metabolite complexity on the LCMS in identical conditions to the concentration curve.

Baffled flask and roller bottles were each grown for 4 weeks prior to extraction with ethyl acetate and comparison of persephacin A in 20 mg/mL of crude extract in MeOH via LCMS and calibration curve. Media for baffled flasks was PDB +++, and media for the roller bottles were PDB +++, PDB +++ with 0.05% agar, PDB +++ with 6 g avocado per liter, PDB+++ on etched glass, PDB+++ with 1.5 g of vermiculite per 100mL media, and HR-01 media. Flasks were grown for 4 weeks before being extracted with 400 mL ethyl acetate and quantitated via LCMS.

For the bioreactor condition, 10L of PDB+++ media was inoculated with 200 mL of a 2 week of Spaceloma corylii culture and grown for 4 weeks. Every week, 1L distilled and autoclaved water was added to account for that lost due to the high air flow. Because the *Sphaceloma coryli* mycelium formed small hard balls that were unable to be properly homogenized, the mycelia were separated from the broth using linen and was extracted with methanol while the broth was partitioned using ethyl acetate. Both portions were combined, suspended at a concentration of 20 mg/mL, and quantified via LCMS. An estimated yield of 89 mg of Persephacin A was calculated from LCMS and the calibration curve.

### *5.6.4 Optimized Isolation*

Optimized growth conditions were chosen using an increase in the concentration of the mashed potato and sugar in the glass Erlenmeyer flasks (4g dehydrated potato flakes and 2 g dextrose per 200 mL). The broth was partitioned with ethyl acetate and the mycelium was filtered with linin and then extracted with methanol. When recombined, the extract yielded 25 g from 70 flasks. This extract was subjected to a step-gradient HP20ss VLC column with the 4 stepwise fractions: 70% MeOH in $H_2O$, 90% MeOH in $H_2O$, 100% MeOH in $H_2O$, and 50% MeOH in DCM. Both the 90% and 100% MeOH in $H_2O$ fractions (totaling 3.5 g) were applied to a Sephadex gravity column in MeOH with the fractions monitored by LCMS and yielded a total of ~500 mg in the active fraction (<50 mg eluted before the active fraction and ~3 g eluted after the active fraction). The fractions were then subjected to C18 preparatory HPLC (Shimadzu, Gemini $C_{18}$ column - 250 mm x 10.1mm, 5µm, Phenomenex) at 95% MeCN in $H_2O$. A final separation using a preparatory HPLC biphenyl column at 90% MeOH in $H_2O$ yielded as additional persephacin A. Alternative fractions from the C18 preparatory HPLC were further

separated using either preparatory or semi-preparatory biphenyl columns to yield persephacins B-C.

### *5.6.5 Structure Elucidation*

Bond-line structures were determined through $^{1}H$, HSQC, HMBC, TOCSY (NMRS 500 MHz with a triplet resonance indirect detect probe) and $^{13}C$ NMR (NMRS 400 MHz dual-broadband probe). Accurate mass data were acquired using Agilent 6538 high-mass-resolution QTOF mass spectrometer.

Absolute configurations of the proteogenic amino acids were determined by compound hydrolysis followed by Marfey's reaction.[140] Hydrolysis was completed on 1 mg of persephacin sample in 20% HCl at 100°C for 24 hours. Samples were then dried under nitrogen, and further dried *in vacuo* to remove any residual acid. 40 µl of 1 M $NaHCO_3$ was added to each vial followed by 200 µL of 1% FDAA (1-fluoro-2-4-dinitrophenyl-5-L-alanine amide) in acetone. The samples were heated for 1 hour at 70°C. Samples were dried under nitrogen, dissolved in 200 µL of 90% MeOH, and subjected to HPLC analysis (Shimadzu, Kinetex C18 column – 3.0 mm x 75 mm, 2.6 µm, Phenomenex).

### *5.6.6 Screening of Antagonistic Activity Against Peyronellaea glomerate (Bio-assay guided fractionation – see supplemental)*

Preliminary screening of test substance (crude, fractions and pure compound) inhibition was determined by using a method, described as a Poison Food Technique[141] and the inhibition to the mycelial growth of fungi was assayed. Briefly, mycelial disks of test fungi (5 mm in diameter) removed from the margins of a 7 day-old culture and were transferred to the center of 9 mm plate containing PDA media incorporating test compounds at noted concentrations.

Control plates containing media mixed with sterile water (10%, v/v) were included. Three replicates were used per treatment. For each concentration, inhibition of radial growth compared with the untreated control was calculated after 5 and 10 days of incubation at 23 °C, in the 12 hours dark phase. The percentage of growth inhibition (I) was calculated using the formula: I (%) =[(C-T)/C] X 100. Where C and T are the diameter of control fungus and test fungus respectively.

### *5.6.7 Peptide Infiltration Assay*

There are different application methods for agricultural antifungal compounds. The mobility of the compound within the plant tissues determines the appropriate application methodology.[142] A xylem and phloem mobile compound can be sprays anywhere on the plant and can easily treat current infections.[142] Compounds that are only xylem mobile need to be administered into the soil and compounds that are phloem mobile need to be administered on the leaves.[142] By using an infiltration assay, where the compound is forced into leaf tissues via osmotic pressure, mobility of persephacin A can be traced via LCMS. For this experiment cabbage (*Brassica olaracea*) plants were used. The upper surfaces of two leaves of each plant used for assay were marked by drawing lines across the leaf with a marker (Sharpie ultra fine point permanent marker). Two concentrations, 1 and 2 µL of persephacin C (2 mM stock DMSO) diluted in 98 µl of $H_2O$, were loaded into a syringe and pressed against the leaves at increased pressure to maximize compound penetration. Leaves were harvested after 24 hours and divided into 3 portions: the application zone, the petiole end, and the distal end. Each sample was crushed and extracted 3 times with 5 mL of MeOH. Samples were concentrated *in vacuo*, dissolved in 100 µL 9:1 MeOH/$H_2O$ and centrifuged to remove precipitates. Samples were run in

the LC-MS at 10-100% acetonitrile in 0.1% formic acid and the selected mass chromatogram was analyzed and compared to a calibration curve determined with stock persephacin A concentrations of 0.5, 1.0, 1.5 and 2.0 mg/mL

### *5.6.7 Determination of MIC and MFC Against Possible Pathogenic Fungi*

The MIC and MFC of persephacins A-C were determined against 8 phytophathogenic (endophytic) fungi. MIC analysis in 96 well plates with a 200 µL inoculum suspension in RPMI-1640 + MOPS with 4 µL of the tested compound at appropriate concentration. MIC concentrations ranged from 0.675 to 20 µM and incubated for 24 hours before being analyzed in the Operetta. Following analysis, 20 µL of MIC assay were plated on PDA plates to test MFC and allowed to incubate for 5 days.

## References


1. Williams, D. H., Stone, M. J., Hauck, P. R. & Rahman, S. K. Why Are Secondary Metabolites (Natural Products) Biosynthesized? *J. Nat. Prod.* **52**, 1189–1208 (1989). doi: 10.1002/hlca.19760590412
2. Geske, G. D., Wezeman, R. J., Siegel, A. P. & Blackwell, H. E. Small Molecule Inhibitors of Bacterial Quorum Sensing and Biofilm Formation. *J. Am. Chem. Soc.* **127**, 12762–12763 (2005). doi: 10.1002/hlca.19760590412
3. Veitch, G. E., Beckmann, E., Burke, B. A Relay Route for the Synthesis of Azadirachtin. *Angew. Chemie Int. Ed.* **46**, 7633–7635 (2007). doi: 10.1002/hlca.19760590412
4. Rüegger, A., Kuhn, M., Lichti, H., Loosli, H., Huguenin, R., Quiquerez, C. von Wartburg, A. Cyclosporin A, ein Immunsuppressiv Wirksamer Peptidmetabolit aus Trichoderma polysporum (L INK ex P ERS .) Rifai. *Helv. Chim. Acta* **59**, 1075–1092 (1976). doi: 10.1002/hlca.19760590412
5. Nibbs, A. E., Montgomery, T. D., Zhu, Y. & Rawal, V. H. Access to Spirocyclized Oxindoles and Indolenines via Palladium-Catalyzed Cascade Reactions of Propargyl Carbonates with 2-Oxotryptamines and Tryptamines. *J. Org. Chem.* **80**(10) 4928-4941 (2015). doi:10.1021/acs.joc.5b00277
6. Eloe-Fadrosh, E. A., Rasko, D. A. The Human Microbiome: From Symbiosis to Pathogenesis. *Annu. Rev. Med.* **64**, 145–163 (2013). doi: 10.1002/hlca.19760590412
7. Pearson, L.; Mihali, T.; Moffitt, M.; Kellmann, R.; Neilan, B. On the Chemistry, Toxicology and Genetics of the Cyanobacterial toxins, Microcystin, Nodularin, Saxitoxin and Cylindrospermopsin. *Marine Drugs* **8**(5) 1650-1680 (2010). doi:10.3390/md8051650
8. Brakhage, A. A., Schroeckh, V. Fungal Secondary Metabolites – Strategies to Activate

Silent Gene Clusters. *Fungal Genet. Biol.* **48**, 15–22 (2011). doi: 10.1016/j.fgb.2010.04.004

9. Teichert, I., Nowrousian, M., Pöggeler, S., Kück, U. The Filamentous Fungus Sordaria macrospora as a Genetic Model to Study Fruiting Body Development. *Advances in Genetics* (**87**) 199–244 (2014). doi:10.1016/B978-0-12-800149-3.00004-4
10. Spiteller, P. Chemical Ecology of Fungi. *Nat. Prod. Rep.* **32**, 971–993 (2015). doi: 10.1039/C4NP00166D
11. Riddle, J. M., Contraception and Abortion from the Ancient World to the Renaissance *Harvard University Press* (1994).
12. Buenz, E. J. Drug Discovery from Historic Herbal Texts. *Computer Applications in Pharmaceutical Research and Development* 103–120 (2006). doi:10.1002/0470037237.ch4
13. Amin, O. S. M. Coin from Cyrene Showing Silphium Plant. (2016). Unaltered. https://www.ancient.eu/image/5893/coin-from-cyrene-showing-silphium-plant/ License: https://creativecommons.org/licenses/by-nc-sa/3.0/legalcode
14. Baty, K. Cyrene Coin. *Celator* **9**, 6–8 (1995). access through wikimedia commons under fair use.
15. Ikeda, K., Arao, Y., Otsuka, H., Nomoto, S., Horiguchi, H., Kayama, F., Ikeda, K., Kato, S., Kayama, F., Kato, S. Terpenoids Found in the Umbelliferae Family Act as Agonists/Antagonists for ERα and ERβ: Differential Transcription Activity between Ferutinine-Liganded ERα and ERβ. *Biochem. Biophys. Res. Commun.* **291**, 354–360 (2002). doi: 10.1006/bbrc.2002.6446
16. Ciganda, C., Laborde, A. Herbal Infusions Used for Induced Abortion. *J. Toxicol. Clin.*

*Toxicol.* **41**, 235–239 (2003). doi: 10.1081/CLT-120021104

17. Trichopoulou, A. Traditional Mediterranean Diet and Longevity in the Elderly: a Review. *Public Health Nutr.* **7**, 943–947 (2004). doi: 10.1079/PHN2004558

18. Masarovičová, E., Kráľová, K. Medicinal Plants - Past, Nowadays, Future. *Acta Hortic.* ***749*** 19–27 (2007). doi:10.17660/ActaHortic.2007.749.1

19. Lavoisier, A. *Encyclopedia of Modern Europe: Europe 1789-1914: Encyclopedia of the Age of Industry and Empire*, Charles Scribner & Sons, **1**, 2006

20. Toledo-Pereyra, L. Medical Renaissance. *J. Investig. Surg.* **28**, 127–130 (2015).

21. Sneader, W. *Drug Discovery: The Evolution of Modern Medicines*. Wiley, **1** (1985).

22. Scheindlin, S. The Timeline: A Brief History of Pharmacology. *Mod. Drug Discov.* **4**, 87–88, 91 (2001).

23. Demain, A. L., Sanchez, S. Microbial Drug Discovery: 80 Years of Progress. *J. Antibiot. (Tokyo).* **62**, 5–16 (2009). doi: 10.1038/ja.2008.16

24. Tan, S. & Tatsumura, Y. Alexander Fleming (1881–1955): Discoverer of Penicillin. *Singapore Med. J.* **56**, 366–367 (2015). doi: 10.1038/ja.2008.16

25. Alexander Flemming, New World Encyclopedia, last modified 28 February 2019, http://www.newworldencyclopedia.org/entry/Alexander_Fleming accessed 02 July 2019

26. Lobanovska, M.; Giulia, P. Penicillin's Discovery and Antibiotic Resistance: Lessons for the Future? *Yale J. Biol. Med.* **90**, 135–145 (2017).

27. Ganesan, A. The Impact of Natural Products Upon Modern Drug Discovery. *Curr. Opin. Chem. Biol.* **12**, 306–317 (2008). doi: 10.1016/j.cbpa.2008.03.016

28. Singla, A. K., Garg, A., Aggarwal, D. Paclitaxel and its Formulations. *Int. J. Pharm.* **235**, 179–192 (2002). doi: 10.1016/S0378-5173(01)00986-3

29. Naidu, R. Semi-Synthetic Process for the Preparation of Taxane Derivatives. Patent US8299279B2 (2012).

30. Damen, E. W. P., Wiegerinch, P. H. G., Braamer, L., Sperling, D., de Vos, D., Scheeren, H. W. Paclitaxel Esters of Malic Acid as Prodrugs with Improved Water Solubility. *Bioorg. Med. Chem.* **8**, 427–432 (2000). doi: 10.1016/S0968-0896(99)00301-6

31. Feng, X.; Zhou, Z.; Cui, Y. Semisynthesis of Paclitaxel. Patent CN2013-10082108 (2013).

32. Gong, X.; Gao, J.; Zhou, L.; Yang, B.; Liang, P.; Lu, Y.; Wang, Q.; Yu, Q. Semi-synthetic Method for Preparation of Paclitaxel. Patent CH103450118 (2013).

33. Mountford, P. G. The Taxol® Story - Development of a Green Synthesis via Plant Cell Fermentation. *Green Chemistry in the Pharmaceutical Industry* Wley-VCH Verlag GmbH & Co. (2010). doi:10.1002/9783527629688.ch7

34. Presidential Green Chemistry Challenge: 2004 Greener Synthetic Pathways Award., EPA (2004) Accessed via https://www.epa.gov/greenchemistry/presidential-green-chemistry-challenge-2004-greener-synthetic-pathways-award on 02 July 2019

35. Webb, T. R. the Scope of the Role of Medicinal Chemists in Drug Discovery. *ACS Med. Chem. Lett.* **9** (12), 1153–1155 (2018). doi: 10.1021/acsmedchemlett.8b00548

36. Schenone, M., Wagner, B. K., Clemons, P. A., Program, B. Target Identification and Mechanism of Action in Chemical Biology and Drug Discovery. *Nat Chem Biol* **9**, 232–240 (2017). doi 10.1038/nchembio.1199.Target

37. Mehta, D., Jackson, R., Gaurav, P., Jiong, S., Sabbagh, M. Why Do Trials for Alzheimer's Disease Drugs Keep Failing? A Discontinued Drug Perspective for 2010-2015. *Expert Opin Investig Drugs.* **26**, 735–739 (2018). 10.1080/13543784.2017.1323868.Why

38. Itzhaki, R. F., Lathe, r., Balin, B., Ball, M., Bearer, E., Braak, H., Bullido, M., Carter, C.,

Clerici, M., Cosby, S., Del Tredici, K., Field, H., Fulop, T., Grassi, C., Griffin, W., Haas, J., Hudson, A., Kamer, A., Kell, D., Licastro, F., Letenneur, L., Loyheim, H., Mancuso, R., Miklossy, J., Otth, C., Palamara, A. T., Perry, G., Preston, C., Pretorius, E., Strandberg, T., Tabet, N., Taylor-robinson, S., Whittum-Hudson, J. Microbes and Alzheimer's Disease. *J. Alzheimer's Dis.* **51**, 979–984 (2016). doi: 10.3233/JAD-160152

39. Lapinski, C.; Lombardo, F.; Dominy, P.; Feeney, P. Experimental and Computational Approaches to Estimate Solubility and Permeability in Drug Discovery and Development Settings. *Adv. Drug Deliv. Rev.* **46**, 3–26 (2001).

40. Li, J.; Vederas, J. Drug Discovery and Natural Products: End of an Era or an Endless Frontier? *Science (80-. ).* **325**, 161–165 (2009).

41. Beutler, J. A. Natural Products as a Foundation for Drug Discovery. in *Current Protocols in Pharmacology* 1–30, John Wiley & Sons, Inc., (2009). doi:10.1002/0471141755.ph0911s46

42. Camp, D.; Davis, R.; Campitelli, M.; Ebdon, J.; Quinn, R. Drug-like Properties: Guiding Principles for the Design of Natural Product Libraries. *J. Nat. Prod.* **75** (1), 72–81 (2012).

43. Harvey, A.; Edrada-Ebel, R.; Quinn, R. The Re-Emergences of Natural Products for Drug Discovery in Genomics Era. *Discov, Nat Rev Drug* **14**, 111–129 (2015).

44. Barnes, E. C., Kumar, R. & Davis, R. A. The Use of Isolated Natural Products as Scaffolds for the Generation of Chemically Diverse Screening Libraries for Drug Discovery. *Nat. Prod. Rep.* **33**, 372–381 (2016). doi: 10.1039/C5NP00121H

45. Gerwick, B. C., Sparks, T. C. Natural Products for Pest Control: an Analysis of their Role, Value and Future. *Pest Manag. Sci.* **70**, 1169–1185 (2014). doi: 10.1002/ps.3744

46. Schueffler, A., Anke, T. Fungal Natural Products in Research and Development. *Nat.*

*Prod. Rep.* **31**, 1425–1448 (2014). doi: 10.1039/c4np00060a

47. Richards, T. A., Jones, M. D. M., Leonard, G. & Bass, D. Marine Fungi: Their Ecology and Molecular Diversity. *Ann. Rev. Mar. Sci.* **4**, 495–522 (2012). doi: 10.1146/annurev-marine-120710-100802

48. Li, G., Lou, H. X. Strategies to Diversify Natural Products for Drug Discovery. *Med. Res. Rev.* **38**, 1255–1294 (2018). doi: 10.1002/med.21474

49. Strobel, G., Daisy, B. Bioprospecting for Microbial Endophytes and their Natural Products. *Microbiol. Mol. Biol. Rev.* **67**, 491–502 (2003). 10.1128/MMBR.67.4.491–502.2003

50. Denning, D. W., Bromley, M. J. How to Bolster the Antifungal Pipeline. *Science.* **347**, 1414–1416 (2015). doi: 10.1126/science.aaa6097

51. Yu, H., Zhang, L., Li, L., Zeng, C., Guo, L., Li, W., Sun, P., Qin, L. Recent Developments and Future Prospects of Antimicrobial Metabolites Produced by Endophytes. *Microbiol. Res.* **165**, 437–449 (2010). doi: 10.1016/j.micres.2009.11.009

52. Ikeda, H., Fukuda, T., Yokoyama, J. Endophytic Fungi Associated with a Holoparasitic Plant, Balanophora japonica; (Balanophoraceae). *Am. J. Plant Sci.* **07**, 152–158 (2016). doi: 10.4236/ajps.2016.71016

53. Schulz, B., Boyle, C., Draeger, S., Römmert, A.-K., Krohn, K. Endophytic Fungi: a Source of Novel Biologically Active Secondary Metabolites. *Mycol. Res.* **106**, 996–1004 (2002). doi: 10.1017/S0953756202006342

54. Pedrosa, F. O., Monteiro, R. A., Wassem, R., Cruz, L., Ayub, R., Colauto, N., Fernandez, M. A., Fungaro, M., Grisard, E., Hungria, M., Madeira, H., Nodari, R., Osaku, C., Petzl-Erler, M., Terenzi, H., Vieira, L., Steffens, M., Weiss, V., Pereira, L., Almeida, M., Alves,

L., Marin, A., Araujo, L., Balsanelli, E., Baura, V., Chubatsu, L., Faoro, H., Favetti, A,. Friedermann, G., Glienke, C., Karp, S., Kava-Cordeiro, V., Raittz, R., Ramos, H., Ribeiro, E., Rigo, L., Rocha, S., Schwab, S., Silva, A., Souza, E., Tadrea-Sfeir, Torres, R., Dabul, A., Soares, M., Gasque, L., Gimenes, C., Valle, J., Ciferi, R., Corea, L., Murace, N., Pamphile, J., Patussi, E., Prioli, A., Prioli, S., Rocha, C., Arantes, O., Furlaneto, M., Godoy, L., Oliveria, C., Satori, D., Vilas-Boas, L., Watanabe, M., Dambros, B., Guerra, M., Mathioni, S., Santos, K., Steindel, M., Vernal, J., Barcellos, F., Campo, R., Chueire, L., Nicolas, M., Pereira-Ferrari, L, da Conceicao, S., Gioppo, N., Margarido, V., Menck-Soares, M., Pinto, F., Simao, R., Takahashi, E., Yates, M., Souza, E. Genome of Herbaspirillum Seropedicae Strain SmR1, a Specialized Diazotrophic Endophyte of Tropical Grasses. *PLoS Genet.* **7** (5), (2011). doi:10.1371/journal.pgen.1002064

55. Luo, S., Xu, T., Chen, L., Chen, J., Rao, C., Xiao, X., Wan, Y., Zeng, G., Long, F., Liu, C., Liu, Y. Endophyte-Assisted Promotion of Biomass Production and Metal-Uptake of Energy Crop Sweet Sorghum by Plant-Growth-Promoting Endophyte Bacillus sp. SLS18. *Appl. Microbiol. Biotechnol.* **93**, 1745–1753 (2012). doi: 10.1007/s00253-011-3483-0

56. Ye, Y., Takada, T., Buchwald, S. L. Palladium-Catalyzed Fluorination of Cyclic Vinyl Triflates: Effect of TESCF 3 as an Additive. *Angew. Chemie Int. Ed.* **55**, 15559–15563 (2016). doi: 10.1002/anie.201608927

57. Novel Drugs 2015 Summary. Acessed by: http://www.fda.gov/downloads/Drugs/DevelopmentApprovalProcess/DrugInnovation/UCM485053.pdf.

58. Mak, I. W., Evaniew, N., Ghert, M. Lost in Translation: Animal Models and Clinical Trials in Cancer Treatment. *Am. J. Transl. Res.* **6**, 114–8 (2014).

59. Combes, R., Berridge, T., Connelly, J., Eve, M., Garner, R., Toon, S., Wilcox, P. Early Microdose Drug Studies in Human Volunteers Can Minimise Animal Testing: Proceedings of a Workshop Organised by Volunteers in Research and Testing. *Eur. J. Pharm. Sci.* **19**, 1–11 (2003).

60. Hoffmann-La Roche Ltd. Growing Human Organs-on-a-Chip. (2019). Available at: https://www.roche.com/research_and_development/what_we_are_working_on/research_technologies/organs-on-a-chip-technology.htm.

61. Kaur, G. Dufour, J. M. Cell Lines. *Spermatogenesis* **2**, 1–5 (2012).

62. Begley, C. G., Ellis, L. M. Raise Standards for Preclinical Cancer Research. *Nature* **483**, 531–533 (2012).

63. Wang, B., Park, E., King, J., Mattes, A., Nimmo, S., Clendinen, C., Edison, A., Anklin, C., Cichewicz, R. Transferring Fungi to a Deuterium-Enriched Medium Results in Assorted, Conditional Changes in Secondary Metabolite Production. *J. Nat. Prod.* **78**, 1415–1421 (2015).

64. Asao, T., Buchi, G., Abdel-Kader, M., Chang, S., Wick, E., Wogan, G. The Structures of Aflatoxins B and G 1. *J. Am. Chem. Soc.* **87**, 882–886 (1965).

65. Eaton, D. L., Gallagher, E. P. Mechanisms of Aflatoxin Carcinogenesis. *Annu. Rev. Pharmacol. Toxicol.* **34**, 135–172 (1994).

66. Mattes, A. O., Russell, D., Tishchenko, E., Liu, Y., Cichewicz, R., Robinson, S. Application of 19 F Quantitative NMR to Pharmaceutical Analysis. *Concepts Magn. Reson. Part A* **45A**, e21422 (2016).

67. Pauli, G. F.; Jaki, B. U.; Lankin, D. C. Quantitative 1H NMR: Development and Potential of a Method for Natural Products Analysis. *J. Nat. Prod.* **68**, 133–149 (2005).

68. Bharti, S. K.; Roy, R. Quantitative 1H NMR Spectroscopy. *TrAC, Trends Anal. Chem* **35**, 5–26 (2012).

69. Griffiths, L. Assay by Nuclear Magnetic Resonance Spectroscopy: Quantification Limits. *Anal. (Cambridge, U. K.)* **123**, 1061–1068 (1998).

70. Dolbier, W. R. *Guide to Fluorine NMR for Organic Chemists*. John Wiley & Sons, Inc., 2009.

71. Barry, S. J., Pham, T. N., Borman, P. J., Edwards, A. J., Watson, S. A. A Risk-Based Statistical Investigation of the Quantification of Polymorphic Purity of a Pharmaceutical Candidate by Solid-State 19F NMR. *Anal. Chim. Acta* **712**, 30–36 (2012).

72. Do, N. M., Olivier, M. A., Salisbury, J. J., Wager, C. B. Application of Quantitative 19F and 1H NMR for Reaction Monitoring and In Situ Yield Determinations for an Early Stage Pharmaceutical Candidate. *Anal. Chem.* **83**, 8766–8771 (2011).

73. Mutlib, A., Espina, R., Atherton, J., Wang, J., Talaat, R., Scatina, J., Chandrasekaran, A. Alternate Strategies to Obtain Mass Balance without the Use of Radiolabeled Compounds: Application of Quantitative Fluorine (19F) Nuclear Magnetic Resonance (NMR) Spectroscopy in Metabolism Studies. *Chem. Res. Toxicol.* **83**, 8766–8771 (2012).

74. Wider, G., Dreier, L. Measuring Protein Concentrations by NMR Spectroscopy. *J. Am. Chem. Soc.* **128**, 2571–2576 (2006).

75. Dreier, L., Wider, G. Concentration Measurements by PULCON Using X-filtered or 2D NMR Spectra. *Magn. Reson. Chem.* **44**, S206–S212 (2006).

76. Traficante, D. D. Optimum Tip Angle and Relaxation Delay for Quantitative Analysis. *Concepts Magn. Reson.* **4**, 153–160 (1992).

77. Power, J. E., Foroozandeh, M., Adams, R. W., Nilsson, M., Coombes, S. R., Phillips, A.

R., Morris, G. A. Increasing the Quantitative Bandwidth of NMR Measurements. *Chem. Commun.* **52**, 2916–2919 (2016).

78. Boehlen, J. M., Burghardt, I., Rey, M., Bodenhausen, G. Frequency-Modulated 'Chirp' Pulses for Broadband Inversion Recovery in Magnetic Resonance. *J. Magn. Reson.* **90**, 183–91 (1990).

79. Malz, F., Jancke, H. Validation of Quantitative NMR. *J. Pharm. Biomed. Anal.* **38**, 813–823 (2005).

80. Keeler, J. *Understanding NMR Spectroscopy.* Wiley (2005)

81. Weiss, G. H., Ferretti, J. A. Accuracy and Precision in the Estimation of Peak Areas and NOE Factors. *J. Magn. Reson.* **55**, 397–407 (1983).

82. Laatikainen, R., Niemitz, M., Malaisse, W. J., Biesemans, M., Willem, R. A Computational Strategy for the Deconvolution of NMR Spectra with Multiplet Structures and Constraints: Analysis of Overlapping 13C-2H Multiplets of 13C Enriched Metabolites from Cell Suspensions Incubated in Deuterated Media. *Magn. Reson. Med.* **36**, 359–365 (1996).

83. Schoenberger, T., Menges, S., Bernstein, M. A., Perez, M., Seoane, F., Sykora, S., Cobas, C. Improving the Performance of High-Precision qNMR Measurements by a Double Integration Procedure in Practical Cases. *Anal. Chem* **88**, 3836–3843 (2016).

84. Cobas, C. S., Sykora, S. In Global Spectral Deconvolution (GSD) of 1D0NMR spectra. in *SMASH* (2008).

85. Sterling, C., Crouch, R., Russell, D. J., Calderon, A. I. 1H-NMR Quantification of Major Saccharides in Ac¸ai Raw Materials: a Comparison of the Internal Standard Methodology with the Absolute Intensity qNMR Method. *Phytochem. Anal.* **24**, 631–637 (2013).

86. Giraudeau, P. Challenges and Perspectives in Quantitative NMR. *Magn. Reson. Chem.* **55**, 61–69 (2017).

87. Rahib, L., Smith, B., Aizenberg, R., Rosenzweig, A., Fleshman, J., Matrisian, L. Projecting Cancer Incidence and Deaths to 2030: The Unexpected Burden of Thyroid, Liver, and Pancreas Cancers in the United States. *Cancer Res.* **74**, 2913–2921 (2014).

88. Howlader, N., Krapcho, M., Miller, D., Bishop, K., Altekruse, S., Kosary, C., Yu, M., Ruhl, J., Tatalovich, Z., Mariotto, A., Lewis, D., Chen, H., Feuer, E., Cronin, K. SEER Cancer Statistics Review, 1975-2013.

89. Chand, S., O'Hayer, K., Blanco, F. F., Winter, J. M., Brody, J. R. The Landscape of Pancreatic Cancer Therapeutic Resistance Mechanisms. *Int. J. Biol. Sci.* **12**, 273–282 (2016).

90. Mehlen, P., Puisieux, A. Metastasis: a Question of Life or Death. *Nat. Rev. Cancer* **6**, 449–458 (2006).

91. Carter, M.; Shieh, J. *Guide to Research Techniques in Neuroscience*. Elsevier (2015). doi:10.1016/C2013-0-06868-5

92. Hanahan, D., Weinberg, R. A. Hallmarks of Cancer: The Next Generation. *Cell* **144**, 646–674 (2011).

93. Weaver, B. A. How Taxol/Paclitaxel Kills Cancer Cells. *Mol. Biol. Cell* **25**, 2677–2681 (2014).

94. Shiau, A. K., Barstad, D., Loria, P., Cheng, L., Kushner, P., Agard, D., Greene, G. The Structural Basis of Estrogen Receptor/Coactivator Recognition and the Antagonism of this Interaction by Tamoxifen. *Cell* **95**, 927–937 (1998).

95. Duval, K., Grover, H., Han, L., Mou, Y., Pegoraro, A., Fredberg, J., Chen, Z. Modeling

Physiological Events in 2D vs. 3D Cell Culture. *Physiology* **32**, 266–277 (2017).

96. Zanoni, M., Piccinini, F., Arienti, C., Zamagni, A., Santi, S., Polico, R., Bevilacqua, A., Tesei, A. 3D tumor Spheroid Models for in vitro Therapeutic Screening: a Systematic Approach to Enhance the Biological Relevance of Data Obtained. *Sci. Rep.* **6**, 19103 (2016).

97. Deer, E. L., Gonzalez-Hernandez, J., Coursen, J., Shea, J., Ngatia, J., Scaife, C., Firpo, M., Mulvihill, S. Phenotype and Genotype of Pancreatic Cancer Cell Lines. *Pancreas* **39**, 425–435 (2010).

98. Prowse, K. R., Greider, C. W. Developmental and Tissue-Specific Regulation of Mouse Telomerase and Telomere Length. *Proc. Natl. Acad. Sci.* **92**, 4818–4822 (1995).

99. Hubbard, K., Ozer, H. L. Mechanism of Immortalization. *Age (Omaha).* **22**, 65–69 (1999).

100. Lorens, J. B. The Immortality Two-Step. *Cell Cycle* **14**, 798–798 (2015).

101. Lee, K., Nguyen, C., Ulrich, A., Pour, P., Ouellette, M. Immortalization with Telomerase of the Nestin-Positive Cells of the Human Pancreas. *Biochem. Biophys. Res. Commun.* **301**, 1038–1044 (2003).

102. Hellwig, V., Mayer-Bartschmid, A., Muller, H., Greif, G., Kleymann, G., Zitzmann, W., Tichy, H., Stadler, M. Pochonins A−F, New Antiviral and Antiparasitic Resorcylic Acid Lactones from Pochonia chlamydosporia var. c atenulata. *J. Nat. Prod.* **66**, 829–837 (2003).

103. Sassa, T., Aoki, H., Namiki, M., Munakata, K. Plant Growth-Promoting Metabolites of Sclerotinia sclerotiorum. I. Isolation and Structures of Sclerotinins A and B. *Agr. Biol. Chem.* **32**, 1432–9 (1968).

104. Chan, J., Jamison, T. F. Synthesis of (−)-Terpestacin via Catalytic, Stereoselective

Fragment Coupling: Siccanol Is Terpestacin, Not 11- e pi -Terpestacin. *J. Am. Chem. Soc.* **125**, 11514–11515 (2003).

105. Adachi, H., Doi, H., Kasahara, Y., Sawa, R., Nakajima, K., Kubota, Y., Hosokawa, N., Tateishi, K., Nomoto, A. Asteltoxins from the Entomopathogenic Fungus Pochonia bulbillosa 8-H-28. *J. Nat. Prod.* **78**, 1730–1734 (2015).

106. Maruyama, M., Osanawa, H., Sato, S., Sato, T., Takahashi, A., Takeuchi, T., Tamamura, T., Texuka, Y. JPH1112280A. (1997).

107. Stephens, P. J., Devlin, F. J., Cheeseman, J. R., Frisch, M. J. Calculation of Optical Rotation Using Density Functional Theory. *J. Phys. Chem. A* **105**, 5356–5371 (2001).

108. Berova, N., Bari, L., Pescitelli, G. Application of Electronic Circular Dichroism in Configurational and Conformational Analysis of Organic Compounds. *Chem. Soc. Rev.* **36**, 914 (2007).

109. Menendez, C., Bauer, Z., Huber, H., Gad'on, N., Steter, K., Fuchs, G. Presence of Acetyl Coenzyme A (CoA) Carboxylase and Propionyl-CoA Carboxylase in Autotrophic Crenarchaeota and Indication for Operation of a 3-Hydroxypropionate Cycle in Autotrophic Carbon Fixation. *J. Bacteriol.* **181**, 1088 LP-1098 (1999).

110. Steyn, P. S., Vleggaar, R. Biosynthesis of Asteltoxin by Cultures of Emericella Variecolor. The Role of Propionate in the Biosynthesis and Evidence for a 1,2-Bond Migration in the Formation of the Bistetrahydrofuran Moiety. *J. Chem. Soc. Chem. Commun.* 977 (1984). doi:10.1039/c39840000977

111. Vleggaar, R. Biosynthetic Studies on Some Polyene Mycotoxins. *Pure Appl. Chem.* **58**, 239–256 (1986).

112. Cummings, M., Breitling, R., Takano, E. Steps Towards the Synthetic Biology of

Polyketide Biosynthesis. *FEMS Microbiol. Lett.* **351**, 116–125 (2014).

113. Peña-Morán, O., Villarreal, M., Álvarez-Berber, L., Meneses-Acosta, A., Rodríguez-López, V. Cytotoxicity, Post-Treatment Recovery, and Selectivity Analysis of Naturally Occurring Podophyllotoxins from Bursera fagaroides var. fagaroides on Breast Cancer Cell Lines. *Molecules* **21**, 1013 (2016).

114. Sayood, S. F., Suh, H., Wilcox, C. S., Schuster, S. M. Effect of Citreoviridin and Isocitreoviridin on Beef Heart Mitochondrial ATPase. *Arch. Biochem. Biophys.* **270**, 714–721 (1989).

115. Scita, G. The Stability of β-Carotene Under Different Laboratory Conditions. *J. Nutr. Biochem.* **3**, 124–128 (1992).

116. Mordi, R. C. Mechanism of Beta-Carotene Degradation. *Biochem. J.* **292**, 310–2 (1993).

117. Genovese, S., Taddeo, V., Epifano, F., Fiorito, S., Bize, C., Rives, A., de Medina, P. Characterization of the Degradation Profile of Umbelliprenin, a Bioactive Prenylated Coumarin of a Ferulago Species. *J. Nat. Prod.* **80**, 2424–2431 (2017).

118. Ravi, M., Ramesh, A., Pattabhi, A. Contributions of 3D Cell Cultures for Cancer Research. *J. Cell. Physiol.* **232**, 2679–2697 (2017).

119. Warcup, J. H. Isolation of Fungi from Hyphæ present in Soil. *Nature* **175**, 953–954 (1955).

120. Du, L., King, J. B. & Cichewicz, R. H. Chlorinated Polyketide Obtained from a Daldinia sp. Treated with the Epigenetic Modifier Suberoylanilide Hydroxamic Acid. *J. Nat. Prod.* **77**, 2454–2458 (2014).

121. Hansen, M. B., Nielsen, S. E., Berg, K. Re-examination and Further Development of a Precise and Rapid Dye Method for Measuring Cell Growth/Cell Kill. *J. Immunol.*

*Methods* **119**, 203–210 (1989).

122. Vinci, M., Gowan, S., Boxall, F., Patterson, L., Zimmermann, M., Court, W., Lomas, C., Mendiola, M., Hardisson, D., Eccles, S. Advances in Establishment and Analysis of Three-Dimensional Tumor Spheroid-Based Functional Assays for Target Validation and Drug Evaluation. *BMC Biol.* **10**, 29 (2012).

123. Minutolo, M.; Nanni, B.; Scala, F.; Alioto, D. Sphaceloma coryli : A Reemerging Pathogen Causing Heavy Losses on Hazelnut in Southern Italy. *Plant Dis.* **100**, 548–554 (2016).

124. Fan, X. L., Barreto, R., Groenewald, J., Bezerra, J., Pereira, O., Cheewangkoon, R., Mostert, L., Tian, C., Crous, P. Phylogeny and Taxonomy of the Scab and Spot Anthracnose Fungus Elsinoë (Myriangiales, Dothideomycetes). *Stud. Mycol.* **87**, 1-41 (2017). doi:10.1016/j.simyco.2017.02.001

125. Montesinos, E., Bardají, E. Synthetic Antimicrobial Peptides as Agricultural Pesticides for Plant-Disease Control. *Chem. Biodivers.* **5**, 1225–1237 (2008).

126. Royal Botanic Gardens Kew. *State of the World's Plants 2017*. Accessed by http://stateoftheworldsplants.org/ (2018).

127. Azevedo, M. M., Faria-Ramos, I., Cruz, L. C., Pina-Vaz, C., Gonçalves Rodrigues, A. Genesis of Azole Antifungal Resistance from Agriculture to Clinical Settings. *J. Agric. Food Chem.* **63**, 7463–7468 (2015).

128. Hashida-Okado, T., Ogawa, A., Endo, M., Yasumoto, R., Takesako, K., Kato, I. AUR1, a Novel Gene Conferring Aureobasidin Resistance on Saccharomyces cersvisiae: A study of Defective Morphologies in Aur1p-Depleted Cells. *Mol. Gen. Genet.* **251**, 236–244 (1996).

129. Ogawa, A., Hashida-Okado, T., Endo, M., Yoshioka, H., Tsuruo, T., Takesako, K., Kato,

I. Role of ABC Transporters in Aureobasidin A Resistance. *Antimicrob. Agents Chemother.* **42**, 755–61 (1998).

130. Zhang, A., He, L., Gao, J., Xu, X., Li, S., Bai, M., Qin, J. Metabolites from an Endophytic Fungus Sphaceloma sp. LN-15 Isolated from the Leaves of Melia azedarach. *Lipids* **44**, 745–751 (2009).

131. Kurobane, I., Vining, L. C., McInnes, A. G., Smith, D. G., Walter, J. A. Biosynthesis of Elsinochromes C and D. Pattern of Acetate Incorporation Determined by 13 C and 2 H NMR. *Can. J. Chem.* **59**, 422–430 (1981).

132. Hu, J., Sarrami, F., Li, H., Zhang, G., Stubbs, K., Lacey, E., Stewart, S., Karton, A., Piggott, A., Chooi, Y. Heterologous Biosynthesis of Elsinochrome A Sheds Light on the Formation of the Photosensitive Perylenequinone System. *Chem. Sci.* **10**, 1457–1465 (2019).

133. Kurome, T.; Takesako, K.; Kato, O. Aureobasidins as New Inhibitors of P-Glycoprotein in Multidrug Resistant Tumor Cells. *J. Antibiot. (Tokyo).* **51**, 353–358 (1998).

134. Pansuriya, R. C., Singhal, R. S. Response Surface Methodology for Optimization of Production of Lovastatin by Solid State Fermentation. *Brazilian J. Microbiol.* **41**, 164–172 (2010).

135. Grahl, N., Shepardson, K. M., Chung, D., Cramer, R. A. Hypoxia and Fungal Pathogenesis: To Air or Not To Air? *Eukaryot. Cell* **11**, 560–570 (2012).

136. Hartill, W. F. T. Post-Harvest Diseases of Avocado Fruits in New Zealand. *New Zeal. J. Crop Hortic. Sci.* **19**, 297–304 (1991).

137. Klittich, C. J. R., Green, F. R., Ruiz, J. M., Weglarz, T., Blakeslee, B. A. Assessment of Fungicide Systemicity in Wheat Using LC-MS/MS. *Pest Manag. Sci.* **64**, (2008).

138. Barry, B. W. , Pham, T., Borman, P., Edwards, A., Watson, S. Mode of Action of Penetration Enhancers in Human Skin. *J. Control. Release* **6**, 85–97 (1987).

139. Klittich, C. J. R. Fungicide Mobility and the Influence of Physical Properties. in 95–109 (2014). doi:10.1021/bk-2014-1171.ch005

140. Bhushan, R., Bruckner, H. Marfey's Reagent for Chiral Amino Acid Analysis: A Review. *Amino Acids* **27**, 231–247 (2004).

141. Balouiri, M., Sadiki, M., Ibnsouda, S. K. Methods for in vitro Evaluating Antimicrobial Activity: A Review. *J. Pharm. Anal.* **6**, 71–79 (2016).

142. Güell, I., Micalo, L., Cano, L., Badosa, E., Ferre, R., Montesinos, E., Bardaji, L., Planas, Marta. Peptidotriazoles with Antimicrobial Activity Against Bacterial and Fungal Plant Pathogens. *Peptides* **33**, 9–17 (2012).

# Appendix A: Supplemental Information

## Appendix A.1: Chapter 4


**Figure A1: *Pochonia suchlasporia* Grown on Cheerios™** before being extracted for analysis.

### *A.1.1 Fungus Identification*

Sequence Determined by ITS and compared with NCBI Blast Genebank

CGTTNNNCNNCNGNNNNCGCNTCGCGCTCNNGNTTGCNANNNNNTGCTACTACGCANANGA

NGCCGCGACGAGGCCGCCAATTCATTTCGGGGGCGGCGGACGCACCGGGCACGCGCCCCGG

AGGGCGGGCTCGGGCGAGGTCGCCGGTCCCCAACACCAGGCCGCTGGGGCTTGAGGGTTGA

AATGACGCTCGAACAGGCATGCCCGCCAGAATACTGGCGGGCGCAATGTGCGTTCAAAGAT

TCGATGATTCACTGAATTCTGCAATTCACATTACTTATCGCATTTCGCTGCGTTCTTCATCGA

TGCCAGAACCAAGAGATCCGTTGTTGAAAGTTTTGATTCATTTGTTTATGATTCCACTCAGAC

ATGCTAGGTAAGAAAATACAAGAGTTTGGGTCCCCCGGCGGGCGCCTGGTTCCGGGGCGGC

TCCCTTTCGGGGGCCTTTCCGGGGCGTTAACCCGCCGAAGCAACGGTAAAGGTATAAGTTCA

CAGGNGTTTGGGAGTAGAAAACTCGGTAATGATCCCTCCGCAGGTTCACCTNCGGAN

*A.1.2 General Purification Methods*

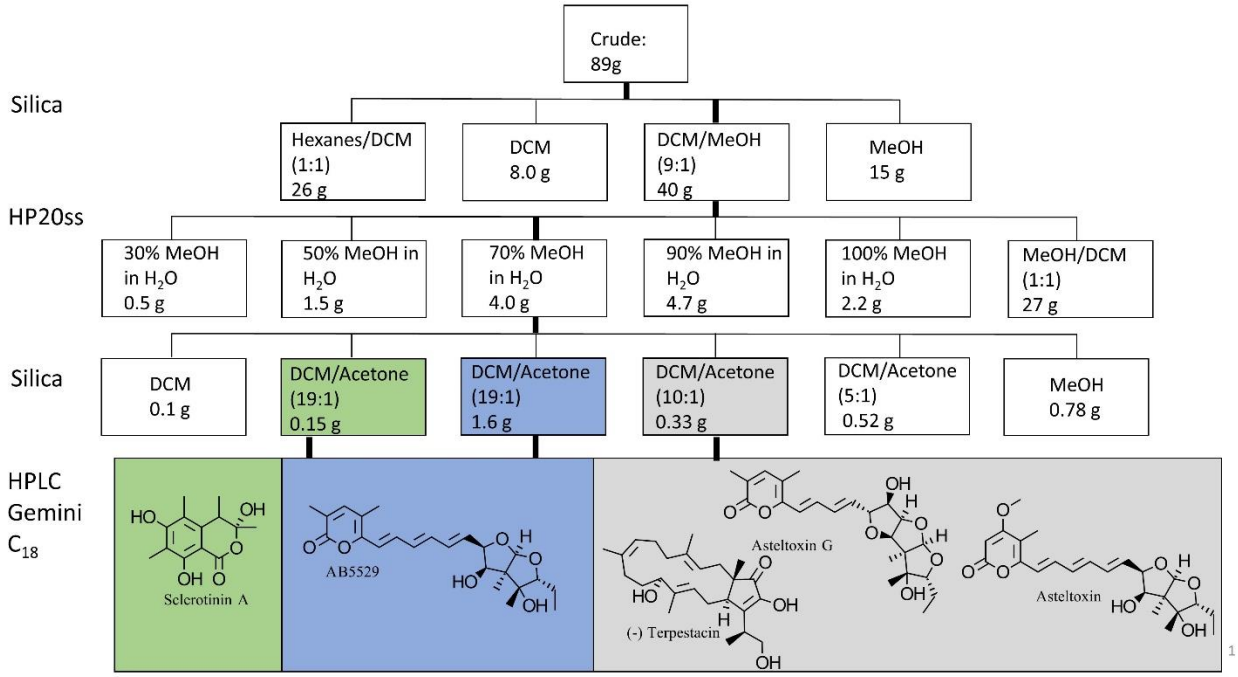


**Figure A2. Isolation Scheme of Compounds from *Pochonia suchlasporia.*** Bioassay guided fractionation singled out three sub-fractions which yielded five compounds that were subjected to both monolayer and spheroid assays.

Initial isolation was done as presented in the figure. HPLC conditions were optimized for purification of the following compounds. Asteltoxin was purified using preparative HPLC (Gemeni C18, 110 Å, 250 x 21.2 mm, 10 mL/min) at 55% MeOH for 4 minutes, followed by 55-80% over 16 minutes, and washed with 80 to 100% over 1 minute. AB5529 was purified using

preparative HPLC (Gemeni C18, 110 Å, 250 x 21.2 mm, 10 mL/min) at 40-80% over 20 minutes of MeOH/H2O. Asteltoxin G was purified by preparative HPLC (Gemeni C18, 110 Å, 250 x 21.2 mm, 10 mL/min) at 55% MeOH for 4 minutes, folowed by 55-80% over 16 minutes, and a wash of 80to100% over 1 minute. A second purification step was required using semipreparative HPLC (Gemeni C18, 110 Å, 250 x 21.2 mm, 4 mL/min) at 60% MeOH in isocratic conditions. Sclerotinin A was purified using preparative HPLC (Gemeni C18, 110 Å, 250 x 21.2 mm, 10 Ml/min) at 40-80% over 20 minutes in MeOH/H2O. (-)Terpestcin was purified by preparative HPLC (Gemeni C18, 110 Å, 250 x 21.2 mm, 10 mL/min) at 55% MeOH for 4 minutes, followed by 55-80% over 16 minutes, and washed with 80 to 100% over 1 minute.

*A.1.3 Spectroscopic Data for AB5529*

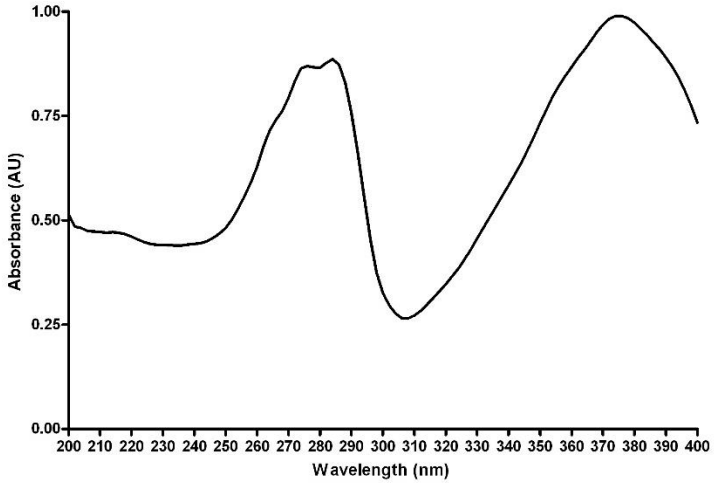


**Figure A3. UV/Vis for AB5529.** UV data was measured by Hewlett Packard 8452A diode array spectrophotometer.

Polaremetry Data/Optical Rotation measured on Rudolph Research Autopol III automatic polarimeter. AB5529 was an orange solid before dilution with MeOH. [α] +28 (c 0.1, MeOH);

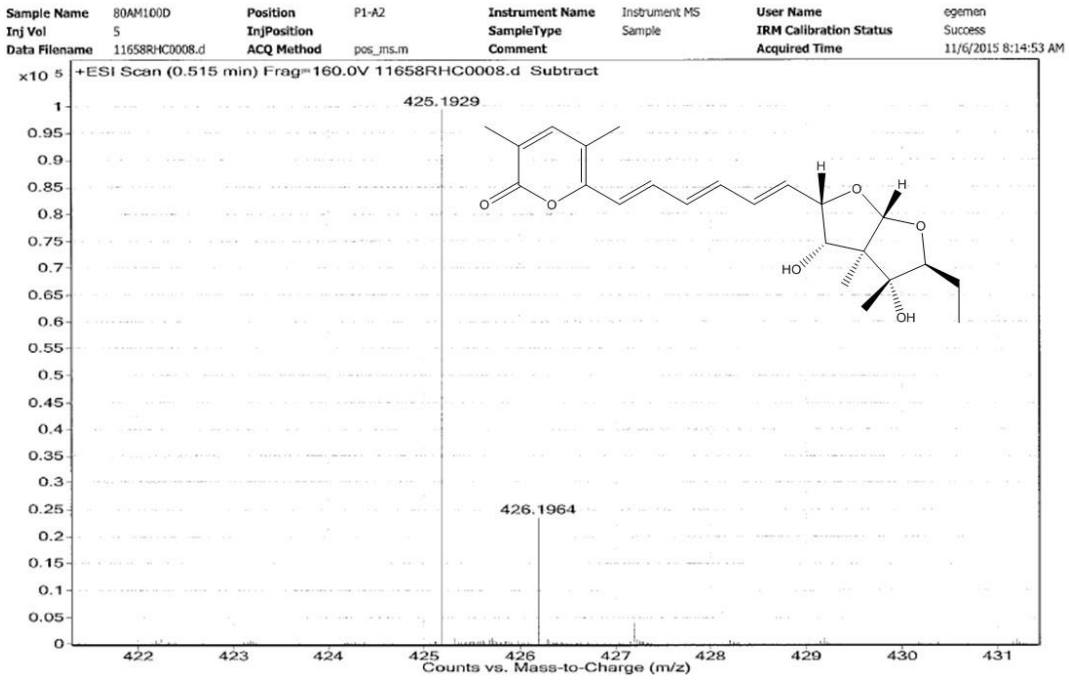


**Figure A4. HRESIMS of AB5529.** HRESIMS data was determined on Agilent 6538 QTOF and Agilent 1290 HPLC

HRESIMS *m/z* 403.2109 $[M + H]^+$ (calcd for $C_{23}H_{30}O_6$, 402.2042)

NMR data were recorded on "Varian VNMR spectrometers (400 and 500 MHz for $^{1}H$, 100 and 125 MHz for $^{13}C$) with broad band and triple resonance probes at 25 ±0.5 ˚C. Samples dissolved in DMSO-$d_6$.

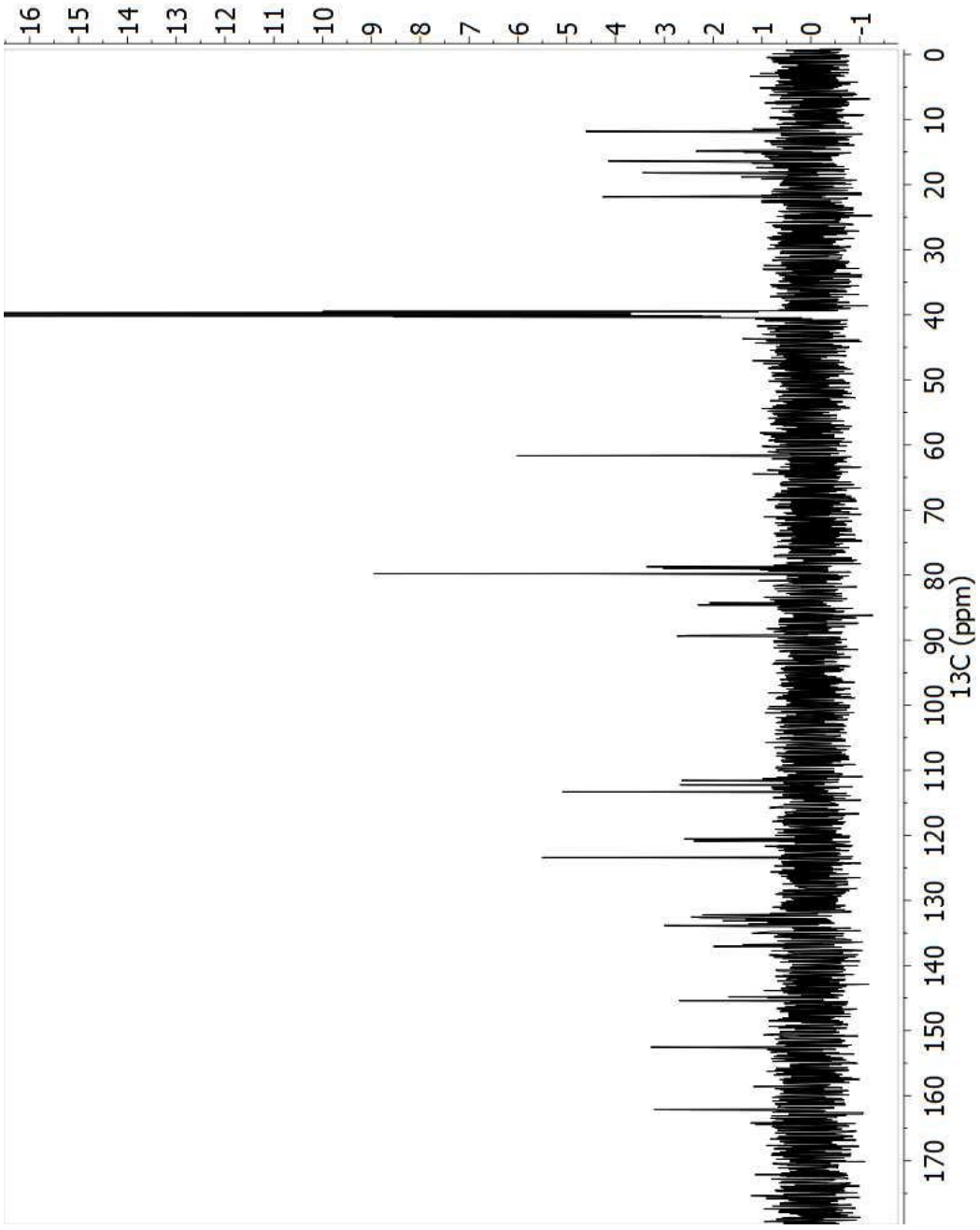


**Figure A5. $^{13}C$ NMR for AB5529**

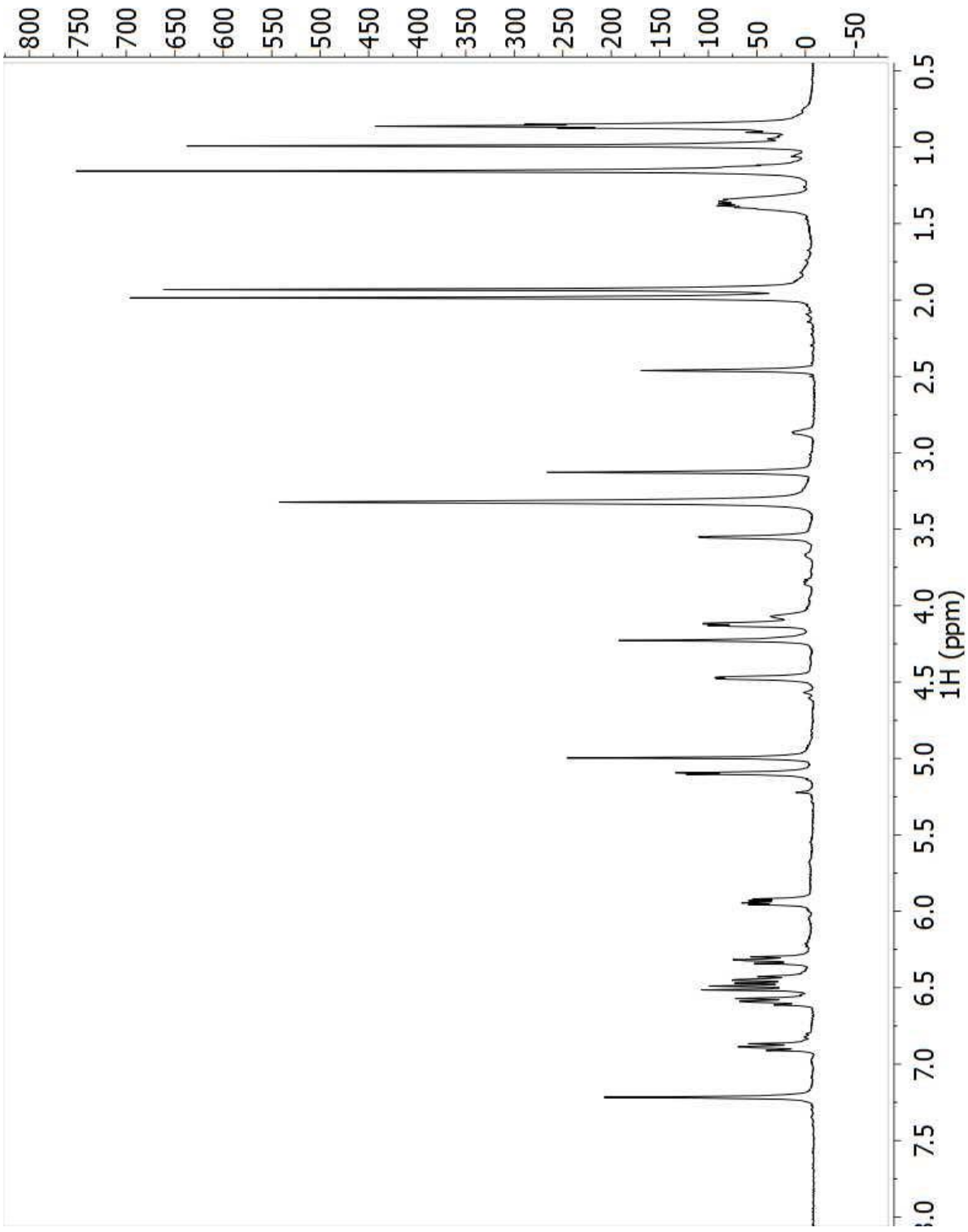


**Figure A6. $^{1}$H NMR for AB5529**

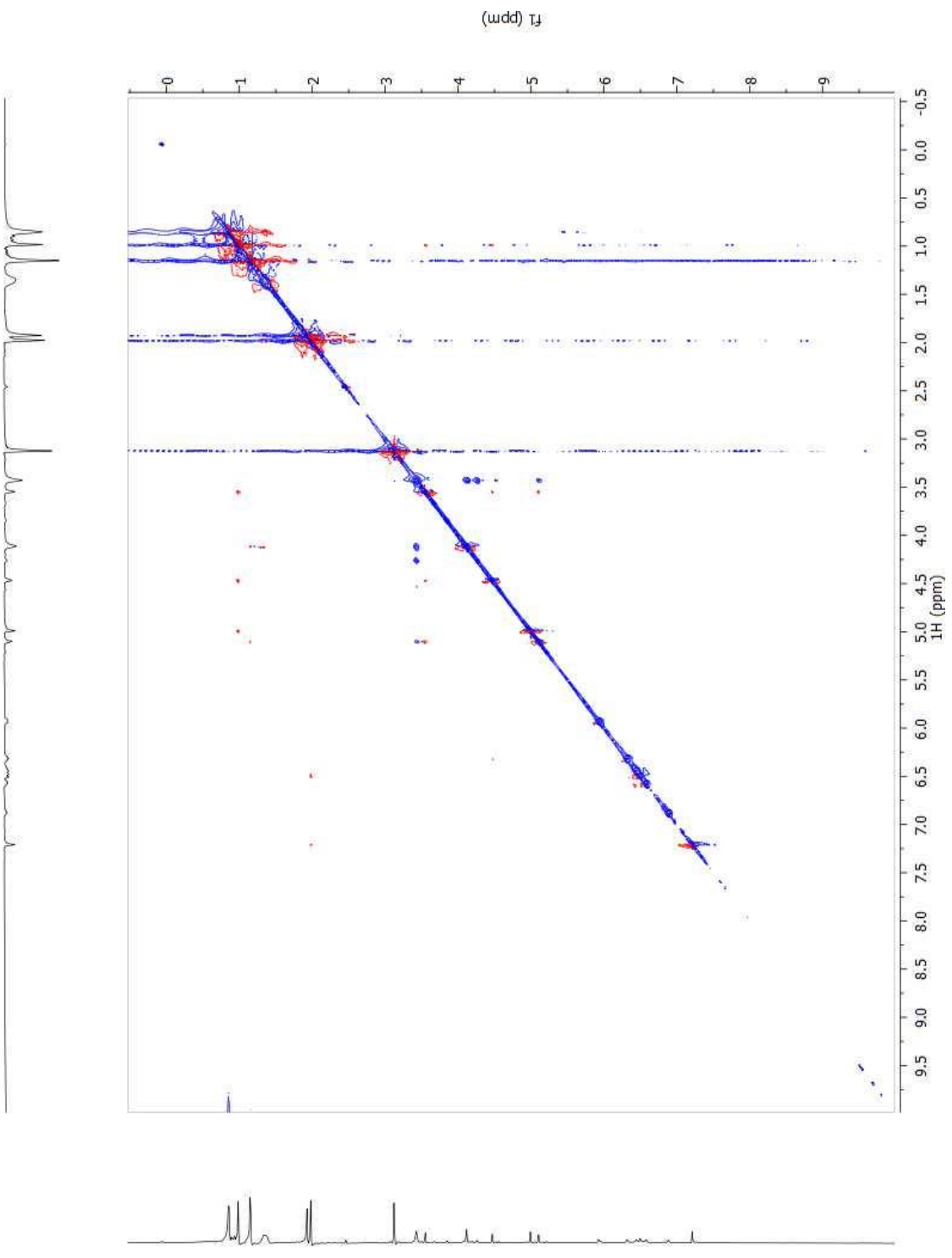


**Figure A7. HSQC for AB5529**

*A.1.4 Spectroscopic Data for Asteltoxin*

Asteltoxin: yellow solid; [α] +16 (c 0.1, MeOH); HRESIMS *m/z* 419.2055 $[M + H]^+$ (calcd for $C_{23}H_{30}O_7$, 418.1992)

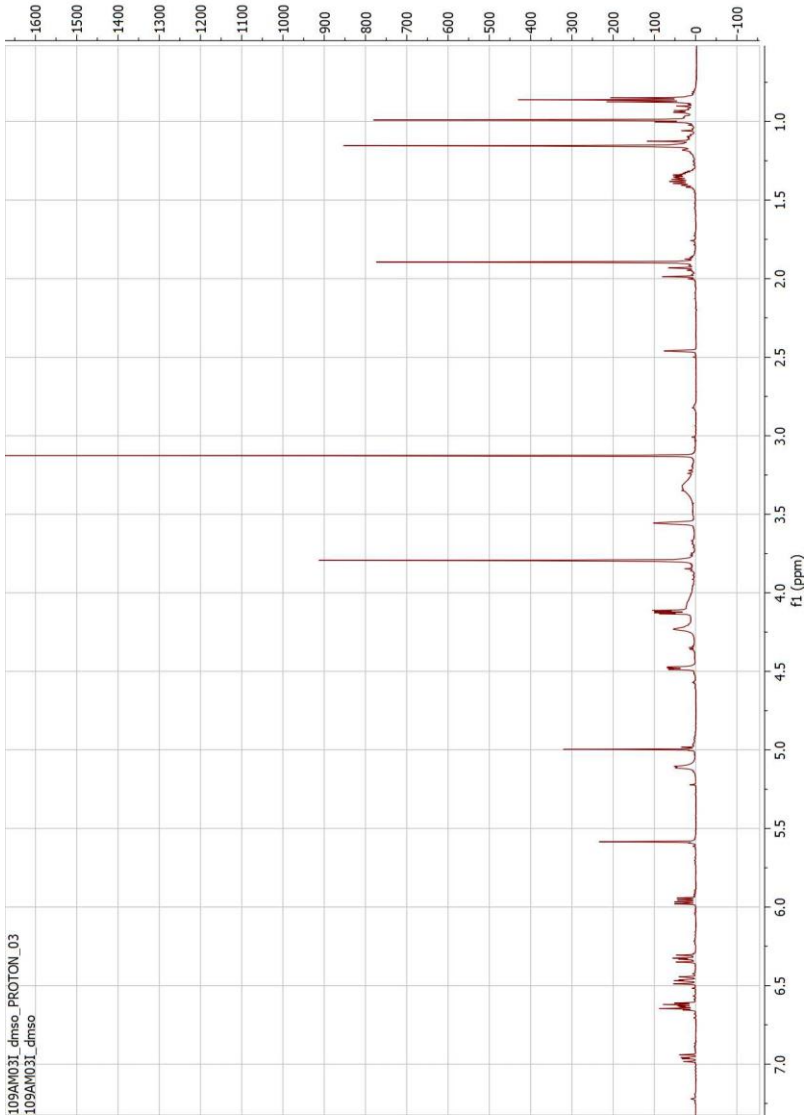


**Figure A8. $^1$H NMR of Asteltoxin**

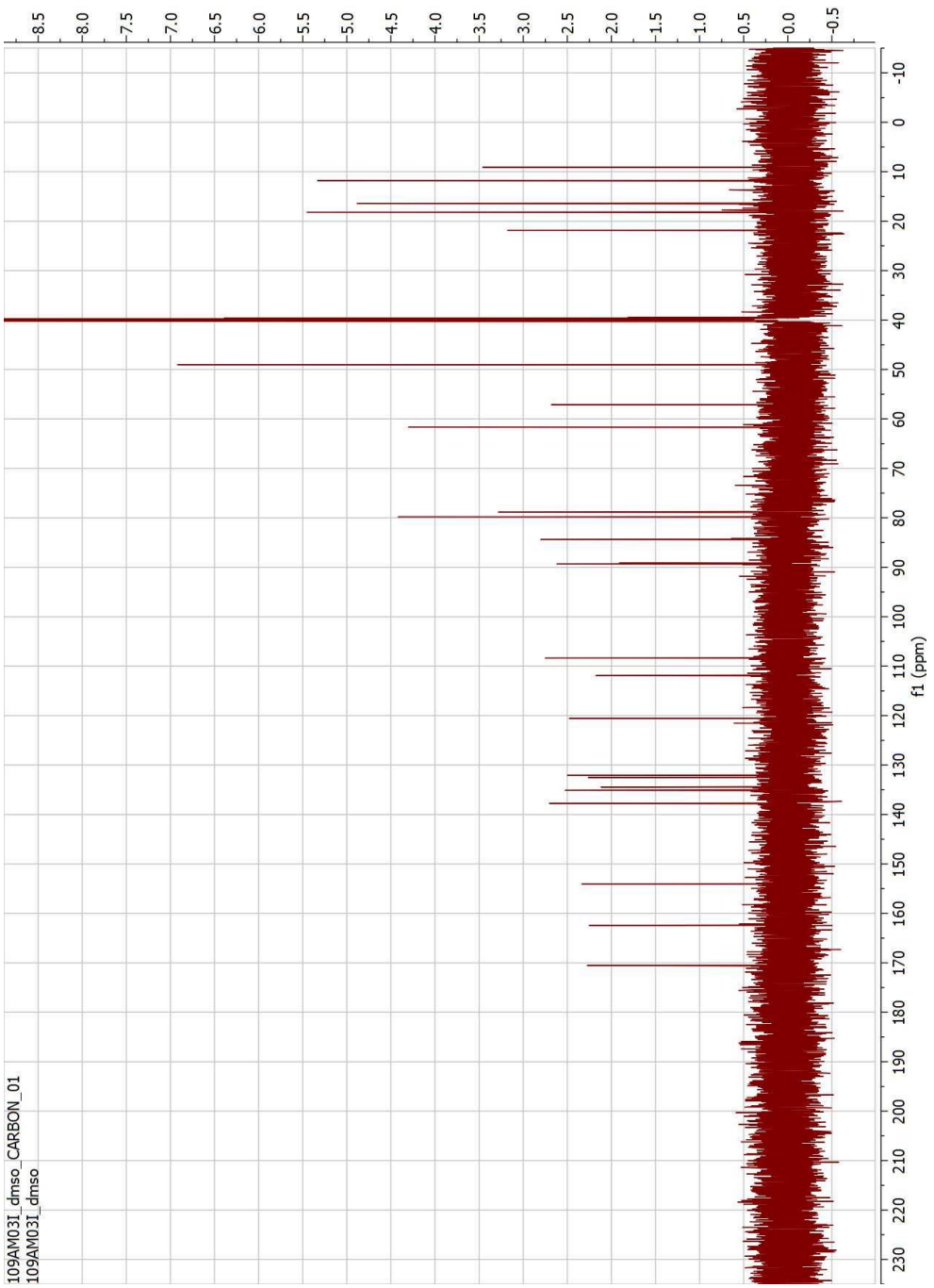


**Figure A9. $^{13}$C NMR of Asteltoxin**

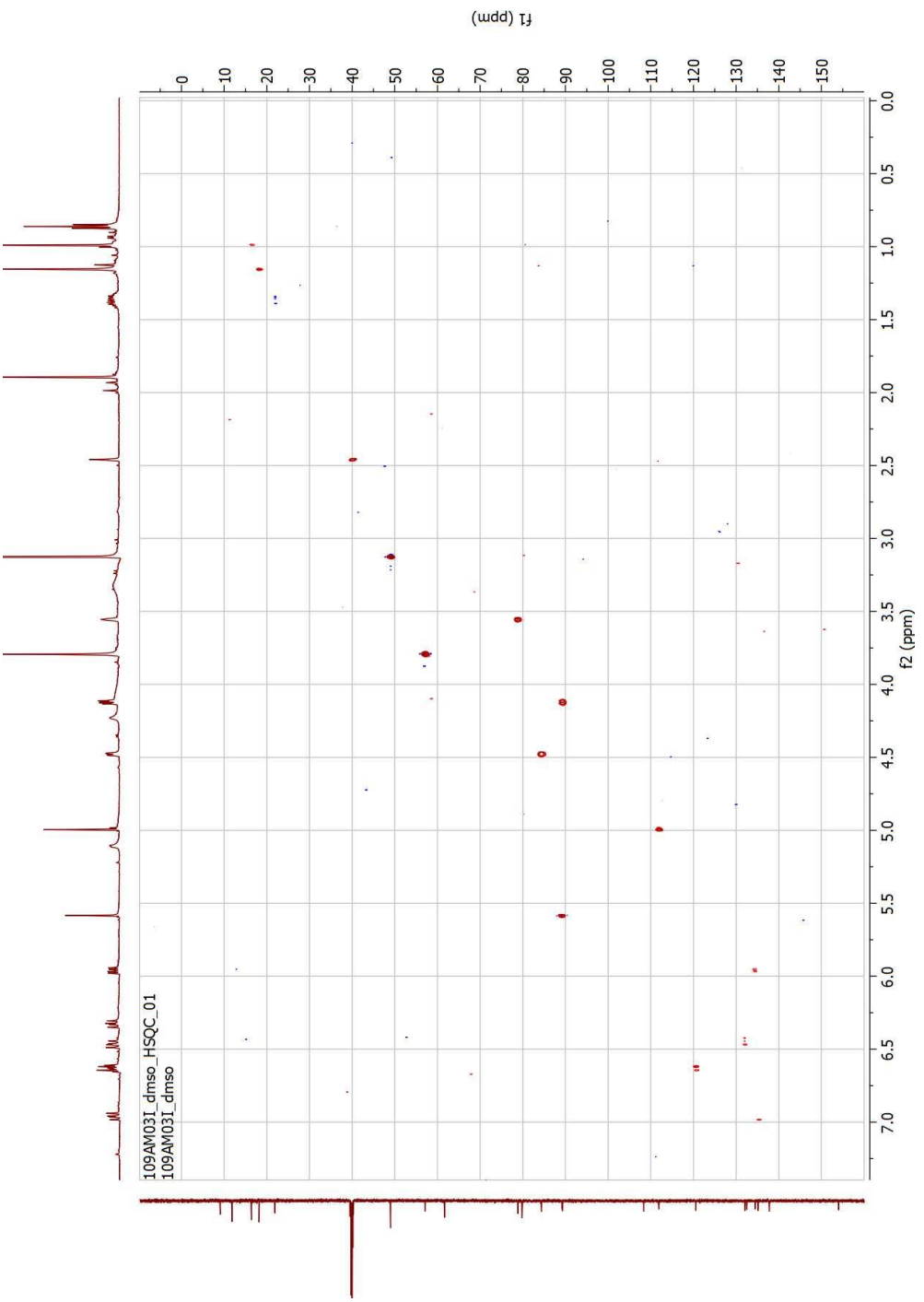


**Figure A10. HSQC for Asteltoxin**

*A.1.5 Spectroscopic Data for Asteltoxin G*

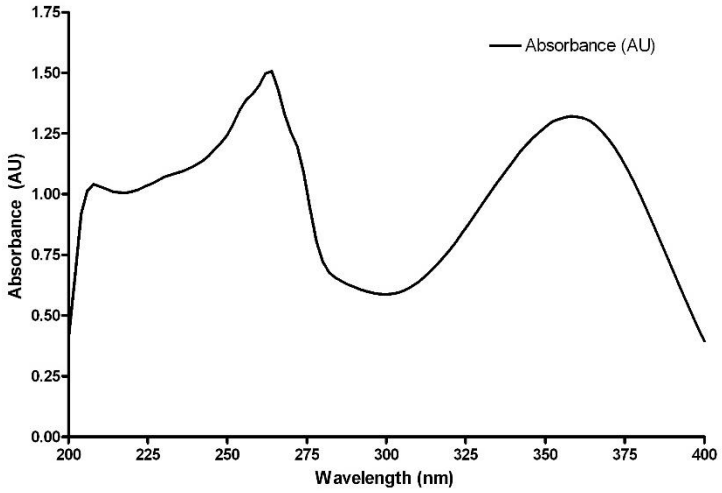


**Figure A11. UV/Vis for Asteltoxin G.** UV data was measured by Hewlett Packard 8452A diode array spectrophotometer.

Polaremetry Data/Optical Rotation measured on Rudolph Research Autopol III automatic polarimeter. Asteltoxin G was a yellow solid before dilution with MeOH. [α] +48 (c 0.1, MeOH);.

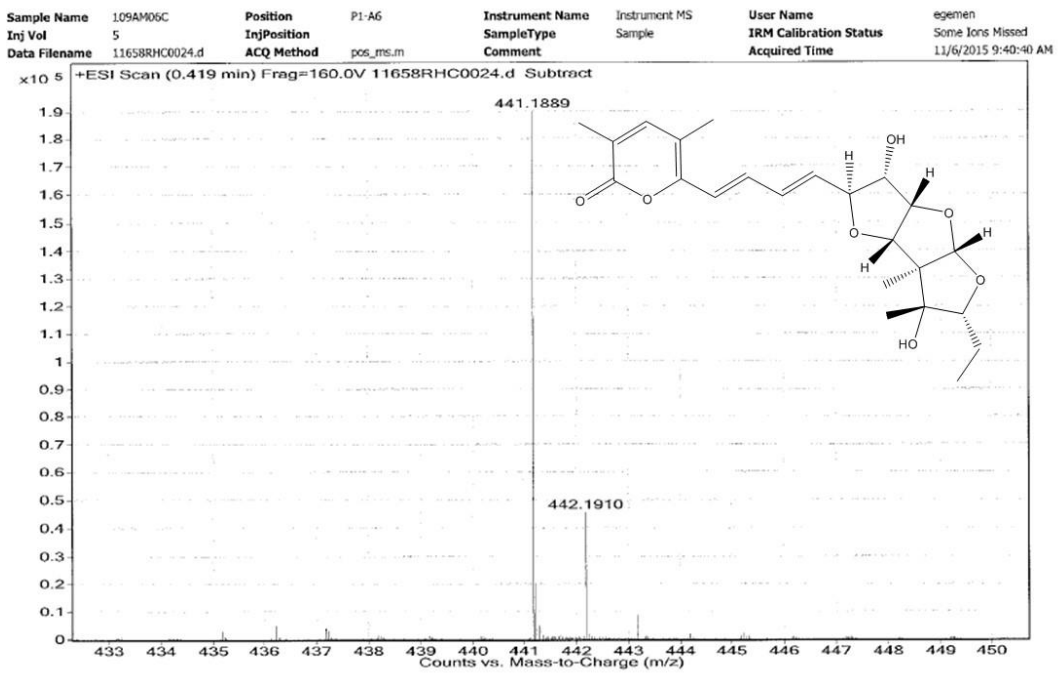


**Figure A12. HRESIMS of Asteltoxin G.** HRESIMS data was determined on Agilent 6538 QTOF and Agilent 1290 HPLC

HRESIMS *m/z* 441.1889 $[M + Na]^+$ (calcd for $C_{23}H_{30}O_7$, 418.1992)

NMR data were recorded on "Varian VNMR spectrometers (400 and 500 MHz for $^1H$, 100 and 125 MHz for $^{13}C$) with broad band and triple resonance probes at 25 ±0.5 ˚C. Samples dissolved in DMSO-$d_6$.

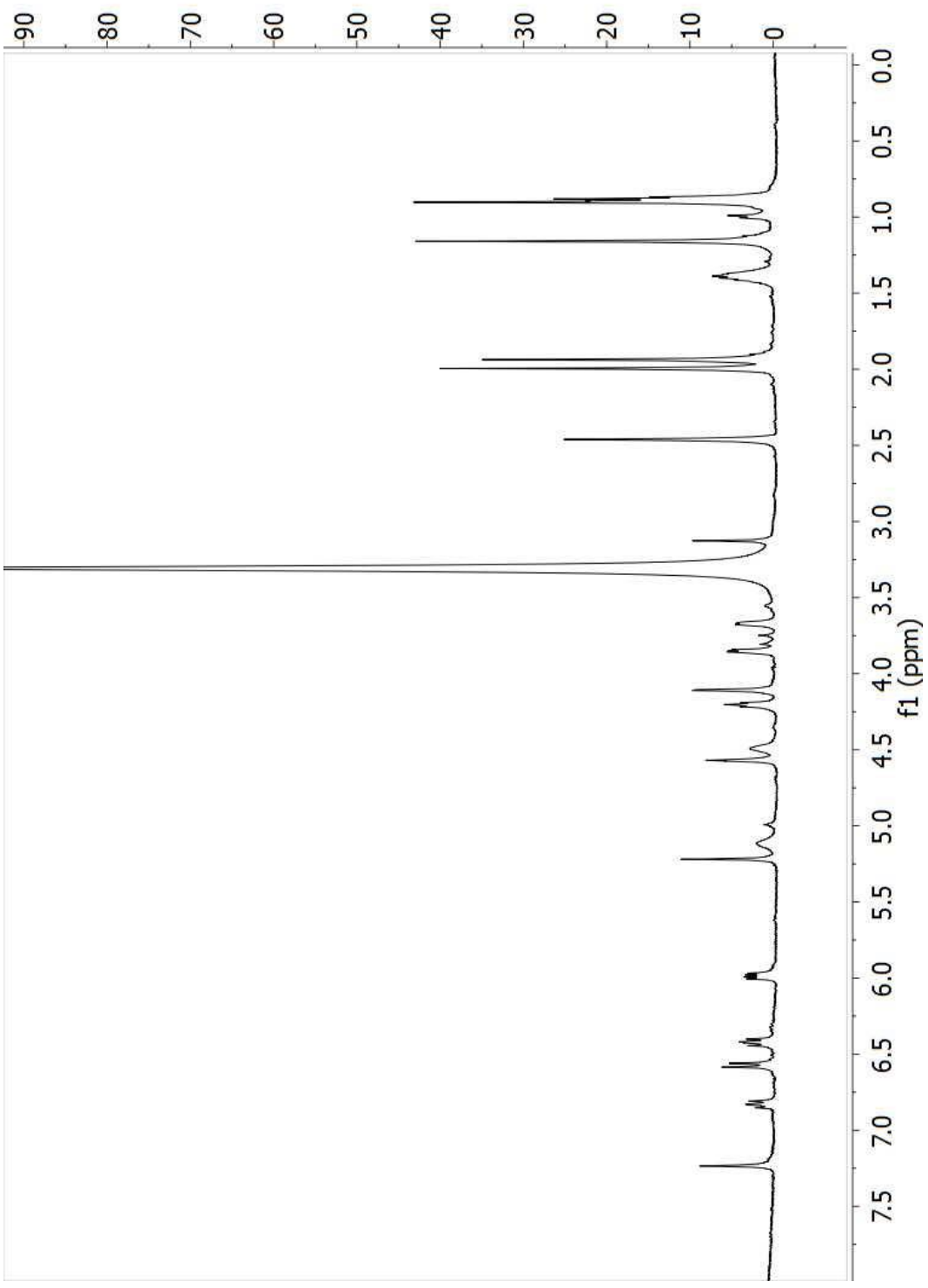


**Figure A13. $^{1}$H NMR for Asteltoxin G**

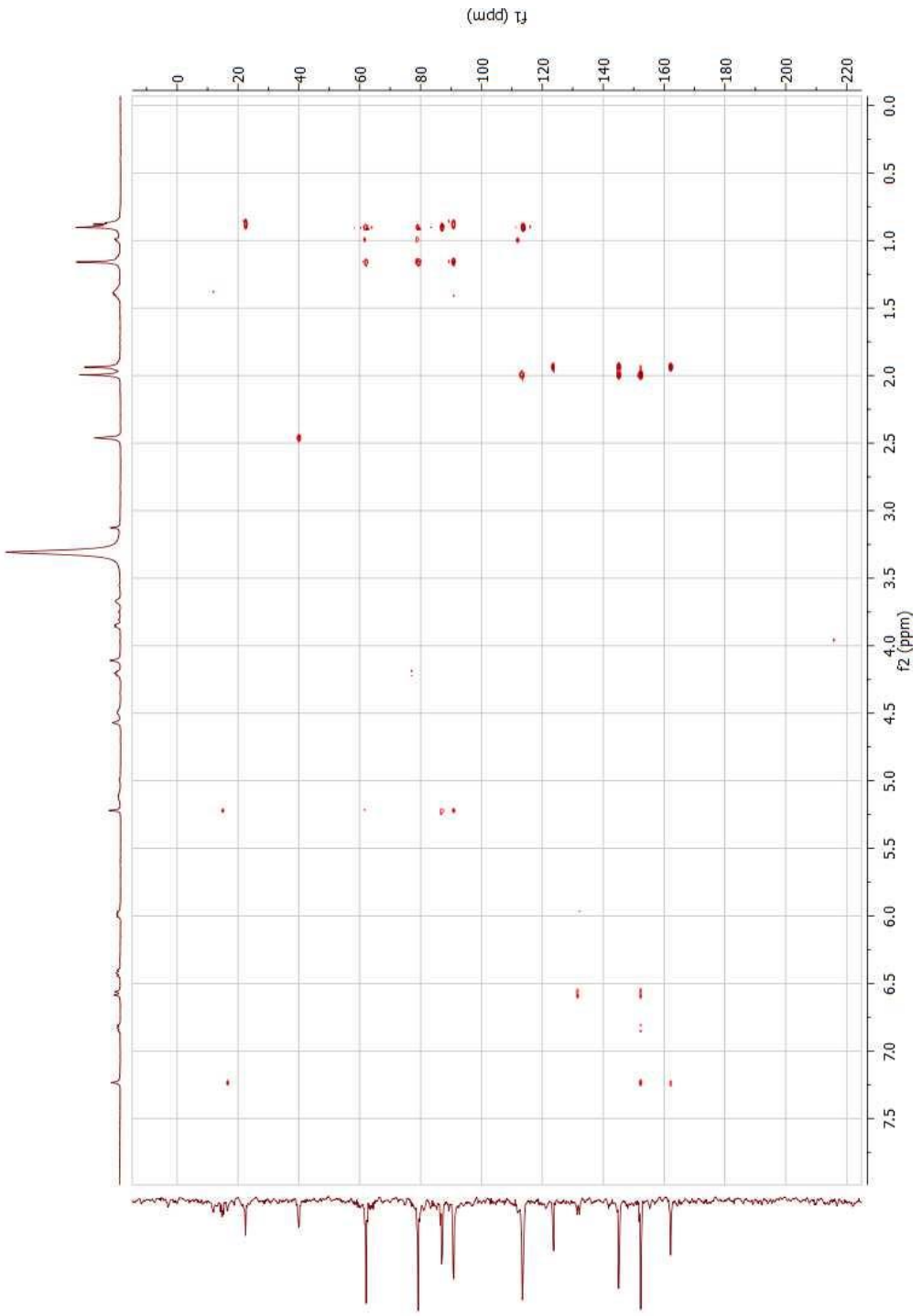


**Figure A14. HMBC for Asteltoxin G**

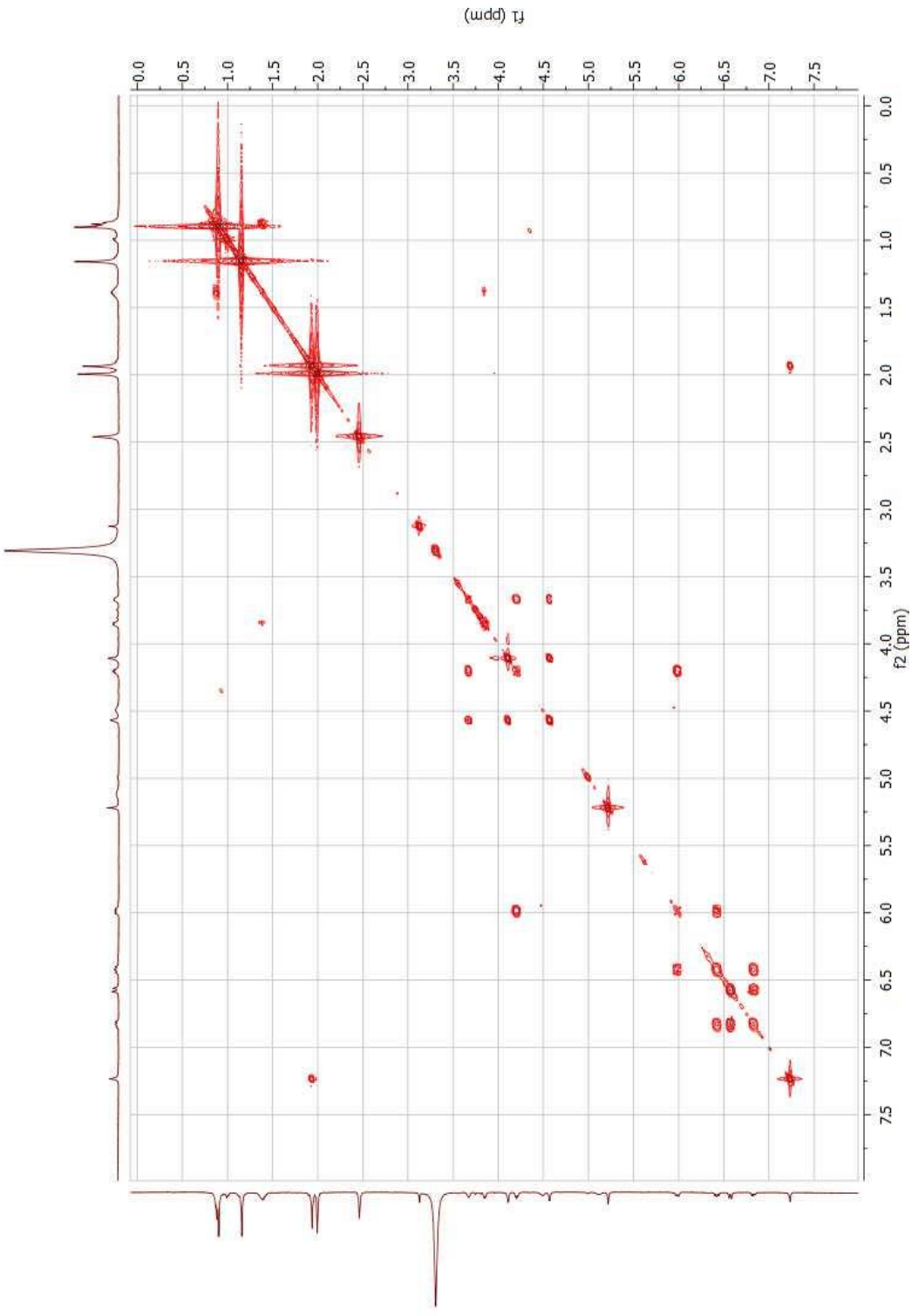


**Figure A15. COSY for Asteltoxin G**

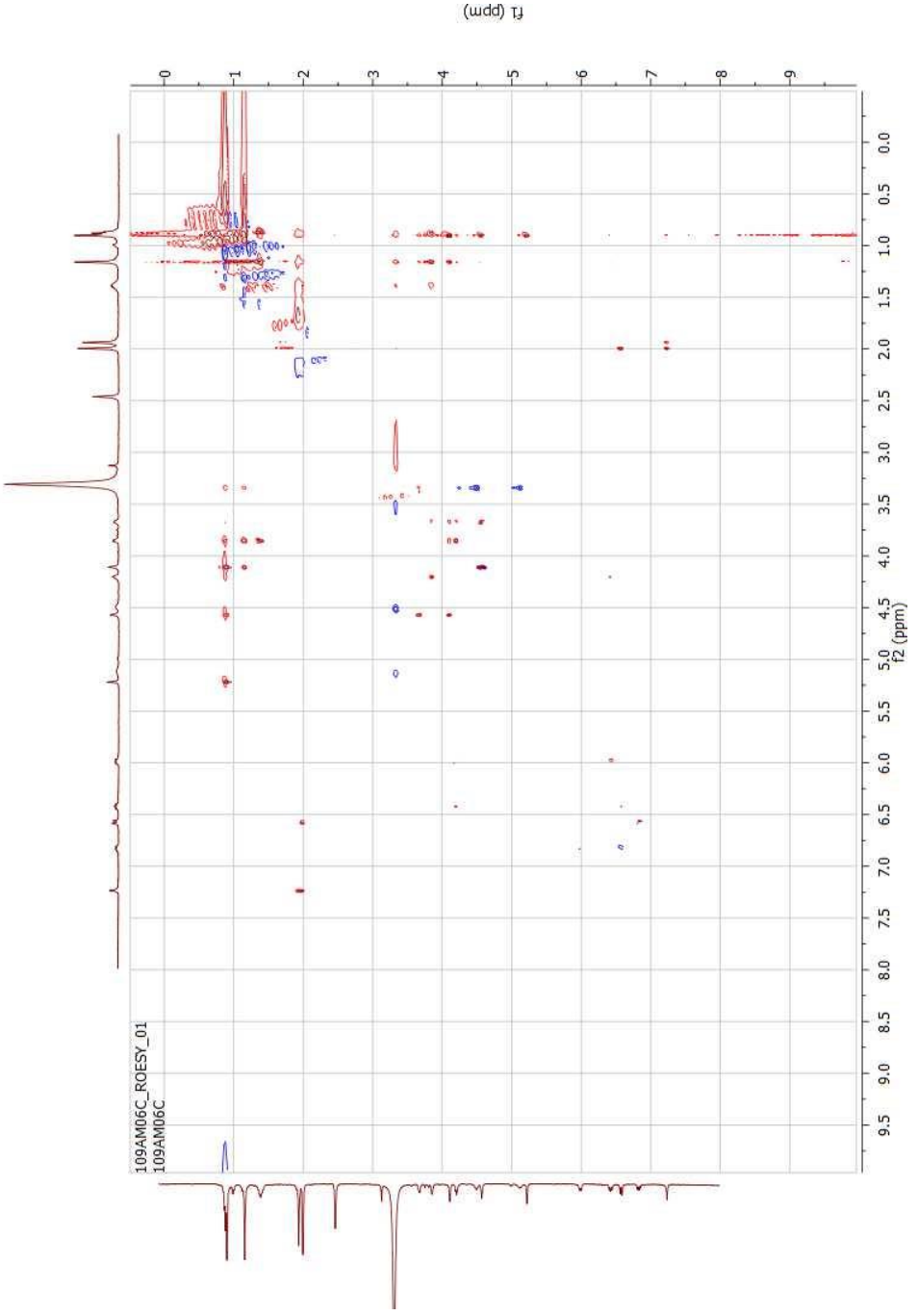


**Figure A16. ROSEY for Asteltoxin G.**

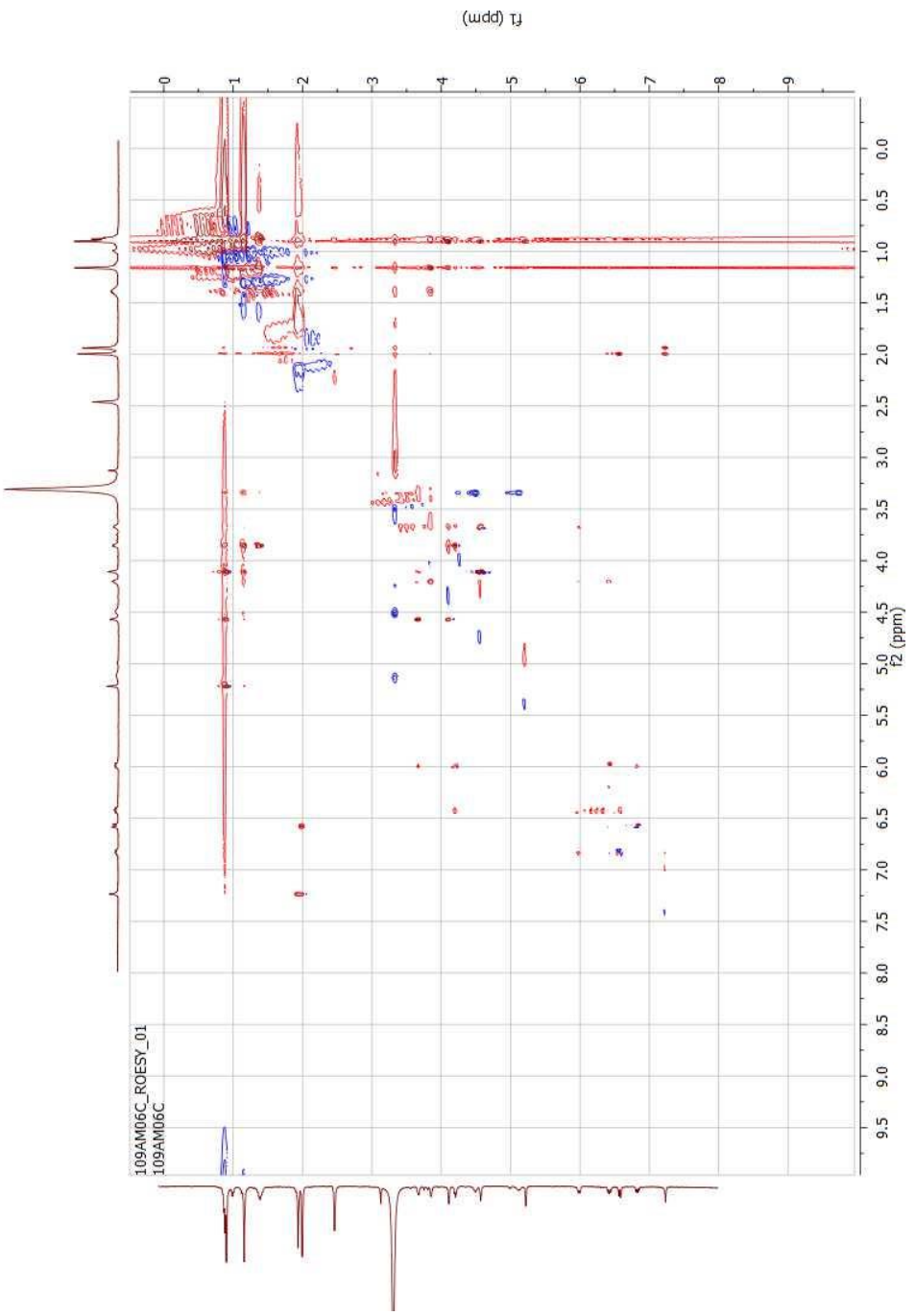


**Figure A17. ROSEY for Asteltoxin G.** Zoomed in to show additional correlations

*A.1.6 Spectroscopic Data for Sclerotinin A*

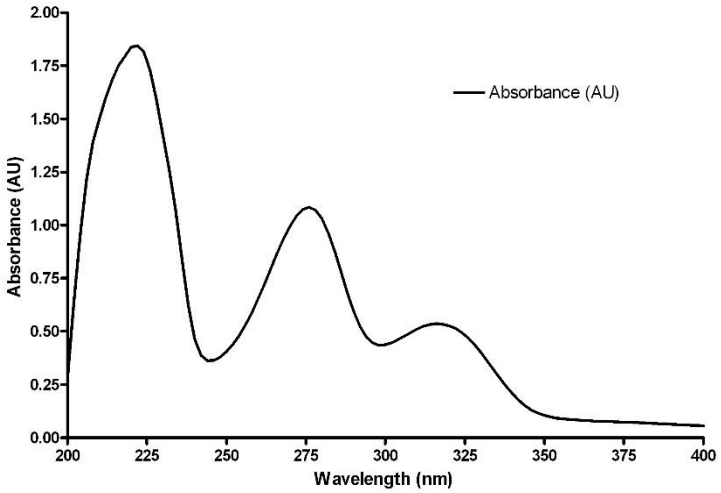


**Figure A18. UV/Vis of Sclerotinin A.** UV data was measured by Hewlett Packard 8452A diode array spectrophotometer

Polaremetry Data/Optical Rotation measured on Rudolph Research Autopol III automatic polarimeter. Asteltoxin G was a yellow solid before dilution with MeOH; [α] +32 (c 0.1, MeOH)

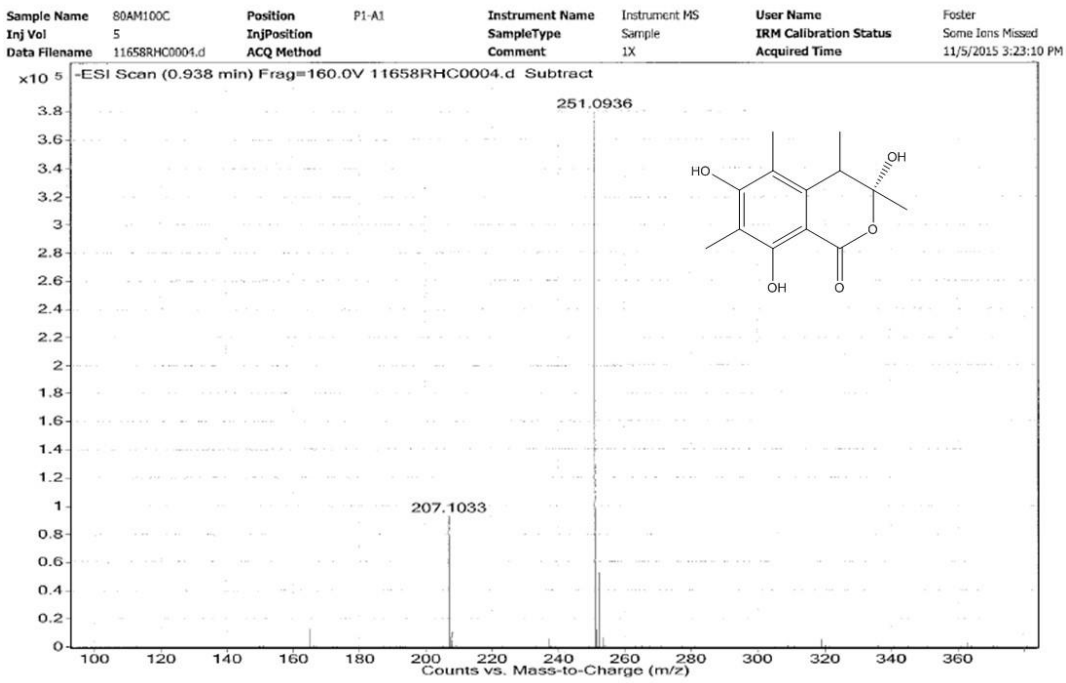


**Figure A19. HRESIMS Data for Sclerotinin A.** HRESIMS data was determined on Agilent 6538 QTOF and Agilent 1290 HPLC

HRESIMS *m/z* 251.0936 $[M - H]^-$ (calcd for $C_{13}H_{16}O_5$, 252.0998)

NMR data were recorded on "Varian VNMR spectrometers (400 and 500 MHz for $^1H$, 100 and 125 MHz for $^{13}C$) with broad band and triple resonance probes at 25 ±0.5 ˚C. Samples dissolved in dDMSO

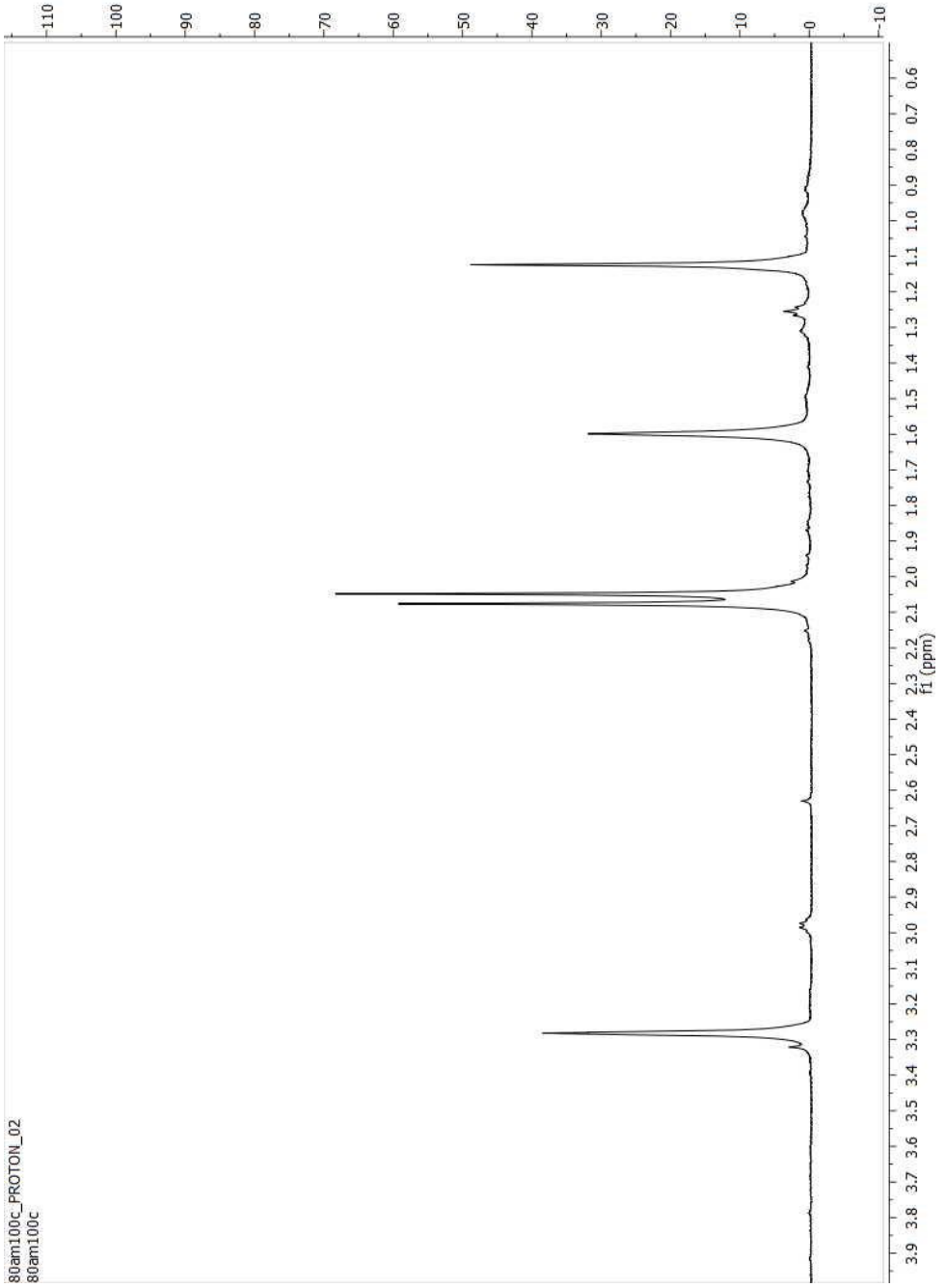


**Figure A20. $^{1}$H NMR for Sclerotinin A**

*A.1.7 Spectroscopic Data for (-)-terpestacin*

Polaremetry Data/Optical Rotation measured on Rudolph Research Autopol III automatic polarimeter. Asteltoxin G was an off-white solid before dilution with MeOH; [α] -36 (c 0.1, MeOH);

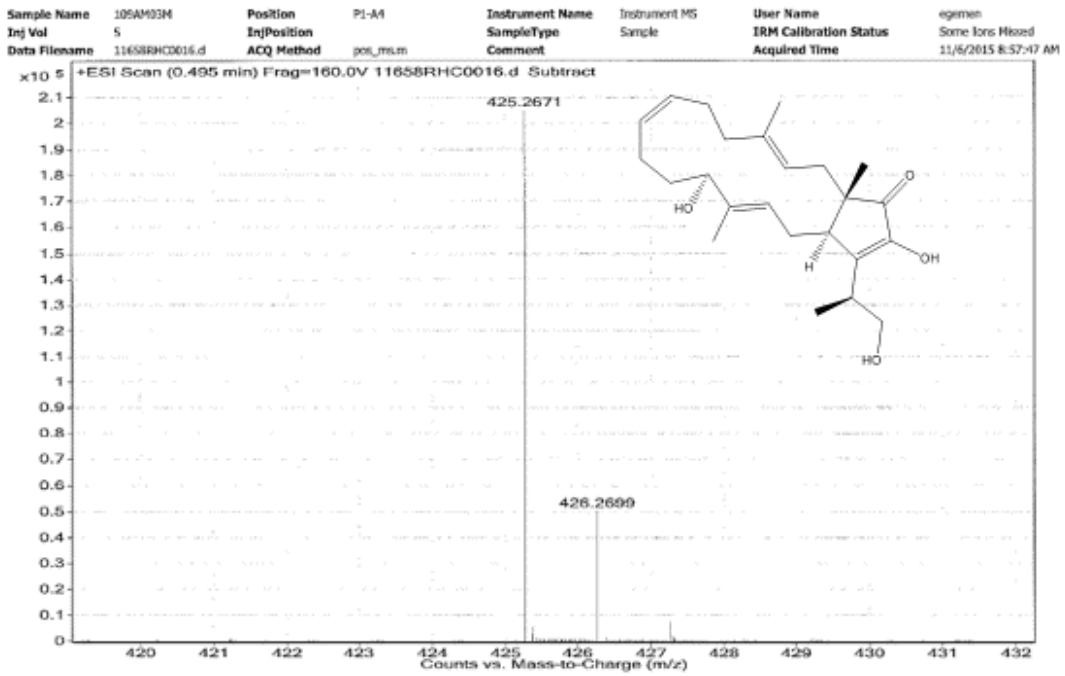


**Figure A21. HRESIMS data from (-)-terpestacin.** HRESIMS data was determined on Agilent 6538 QTOF and Agilent 1290 HPLC

HRESIMS m/z 425.2671 $[M + Na]^+$ (calcd for $C_{25}H_{38}O_4$, 402.2770)

NMR data were recorded on "Varian VNMR spectrometers (400 and 500 MHz for $^1H$, 100 and 125 MHz for $^{13}C$) with broad band and triple resonance probes at 25 ±0.5 ˚C. Samples dissolved in dDMSO

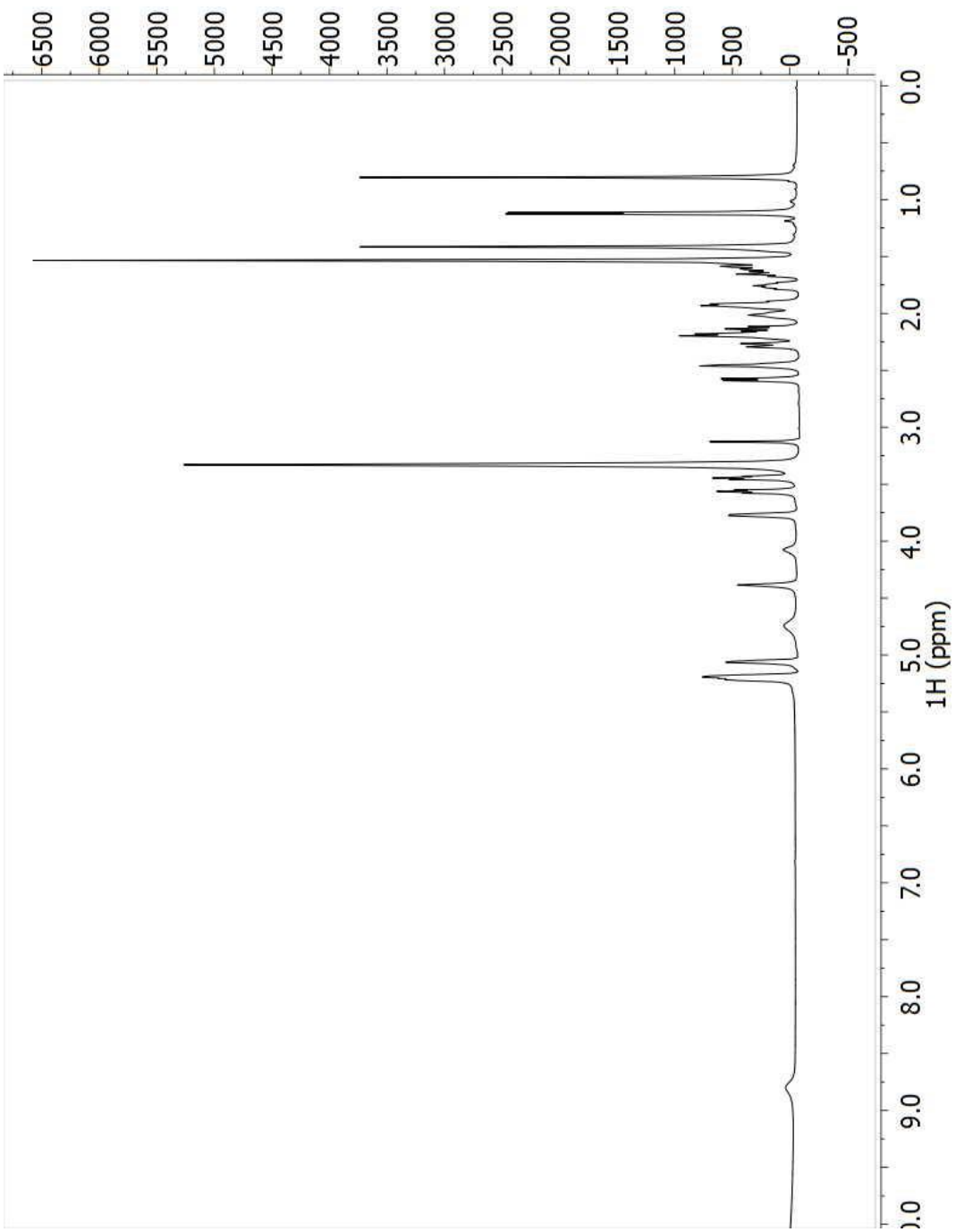


**Figure A22. $^{1}$H NMR for (-)-terpestacin**

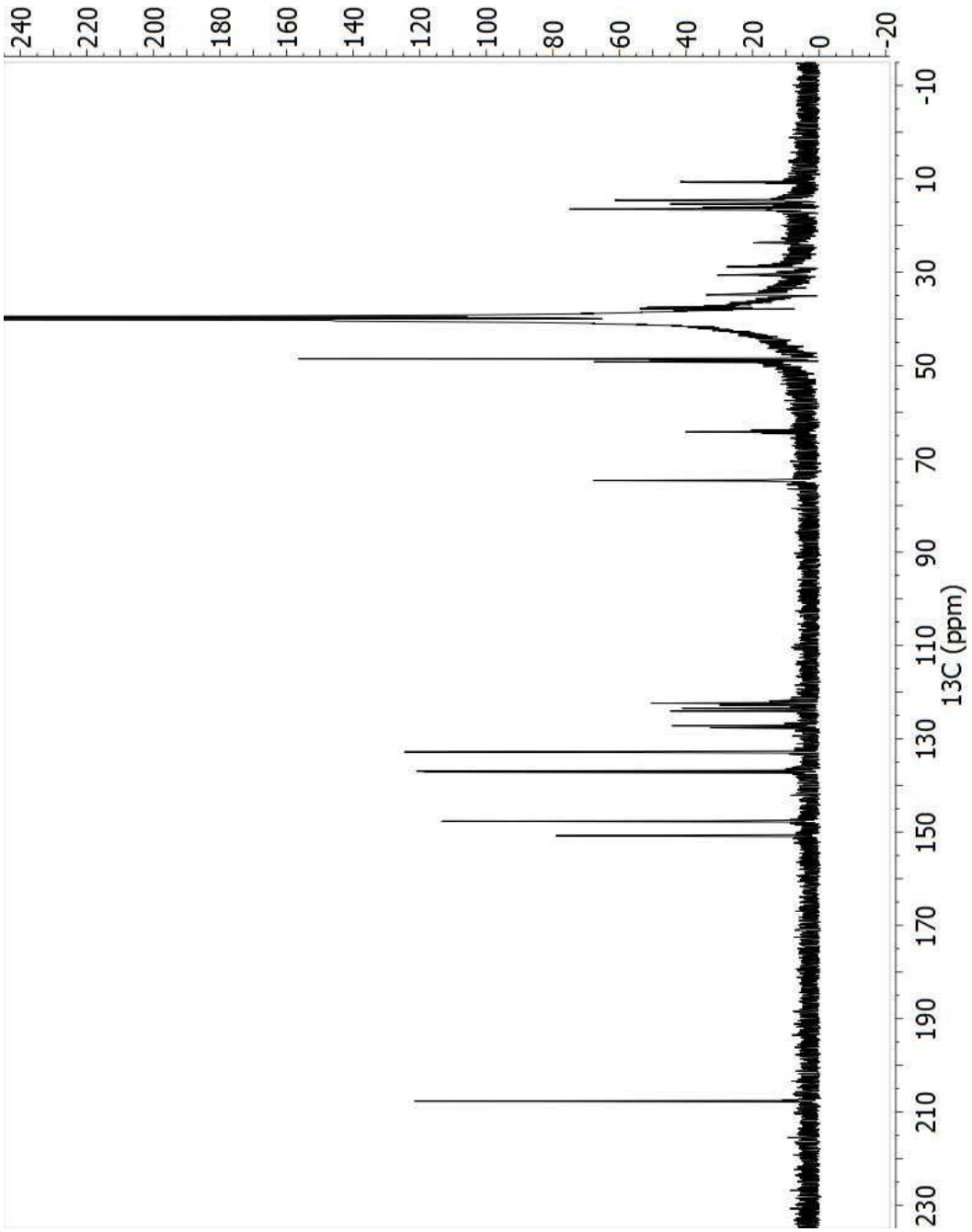


**Figure A23. $^{13}$C NMR for (-)-terpestacin**

### *A.1.8 Degradation of Asteltoxin and Derivatives*

Degradation of Asteltoxin and Derivatives

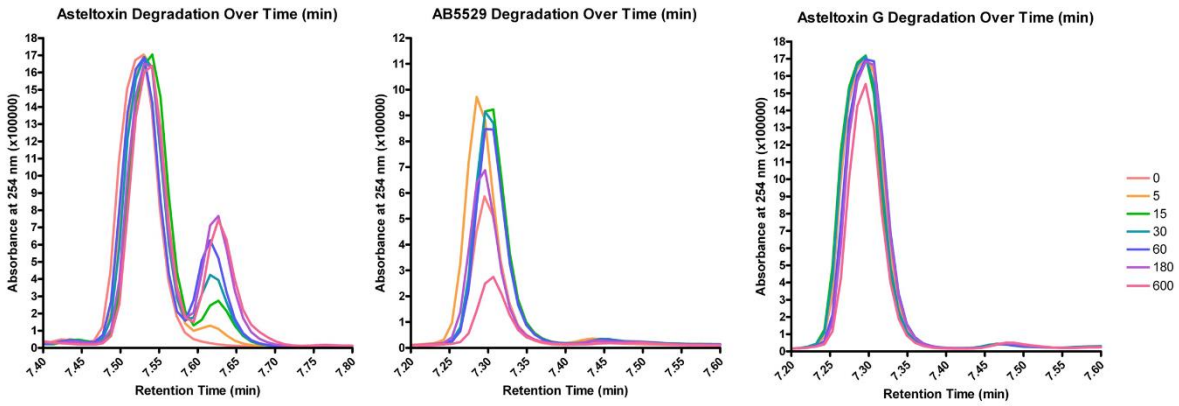


**Figure A24. Degradation of Asteltoxin and Derivatives.**

Degradation analysis of the three polyenic alpha-pyrones when exposed to light in DMSO. Degradation of asteltoxin was observed within 5 minutes exposure to light, while asteltoxin G only showed minimal degradation after 600 minutes. Considering degradation was also seen in AB5529 within 15 minutes exposure, the likely increased stability arose from the tricyclic furanose motif/decreased conjugation rather than the altered substitution of the pyrone.

## Appendix A.2: Chapter 5

### *A.2.1 Fungus Identification of Sephaceloma corylii*

Determined via ITS sequencing and compared to NCBI Blast

TCCTGACGTTTCGAAATTCTAACACGCCGGGGGTCGGTGCCTCGCCGATGCA
TTTCGGGCGGGCCGGCTCCCCCCTTTTGACGGGGGTGGATCCGGCCTGACGC
CTAATACCAAGCGGGGCTTGATTGGTGAAATGACGCTCGAACAGGCATGCC
CCTCGGAATACCAAGGGGCGCAATGTGCGTTCAAAGATTCGATGATTCACT
GAATTCTGCAATTCACATTACTTATCGCATTTCGCTGCGTTCTTCATCGATGC
CAGAACCAAGAGATCCGTTGTTGAAAGTTTTAATTTGATTGTACAAAAGTAC
TCCGACAGTATAGTTAAAAACAGAGTTGATTTGGTCCTCCGGCGGGCGCTAT
CCGATCCGCGATGGGACCGGCCGGCCCTGTACCCCCCGGTGAGGGGGGGGA
GGGACGGGCCCGCCGAATCAACGTATTCACAACAGCAAAGGGTGGGGAGTT
CGCGCCCCTTTCGGGAACCCTTCCTCGTTACTGATCCTTCCGCAGGTTCACCT
ACGGAAACCTTGTTACAACTTTTACTT

*A.2.2 Initial Isolation Scheme*

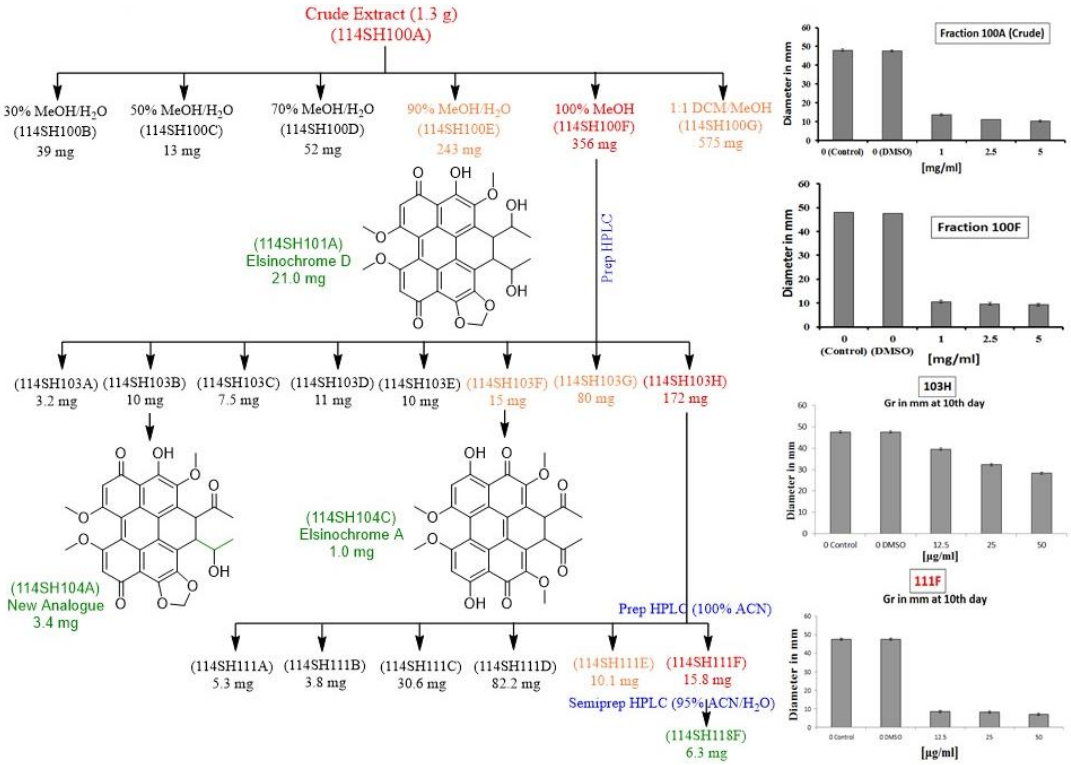


**Figure A25. Initial Isolation Scheme** using bioassay guided fractionation. Three elsinochromes were isolated as well as persephacin A.

### *A.2.3 Optimized Isolation Scheme*

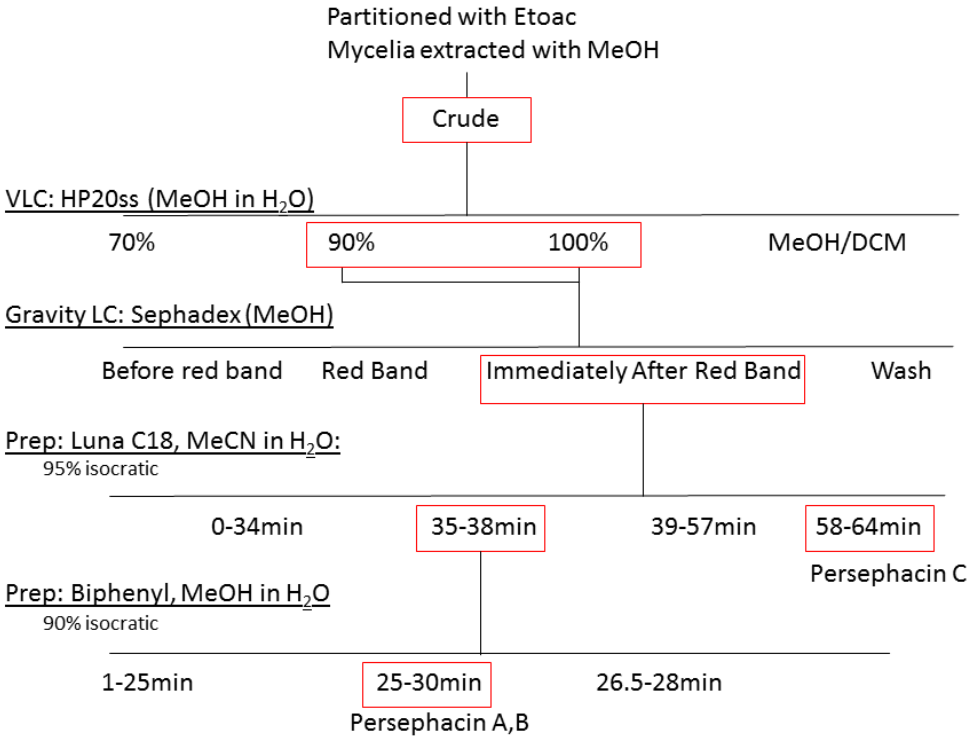


**Figure A26. Optimized Isolation Scheme.** Larger quantities of extract can be more easily purified using the following method.

### *A.2.4 Elsinochrome A*

NMR data were recorded on "Varian VNMR spectrometers (400 and 500 MHz for $^{1}$H, 100 and 125 MHz for $^{13}$C) with broad band and triple resonance probes at 25 ±0.5 ˚C.

Samples dissolved in dDMSO

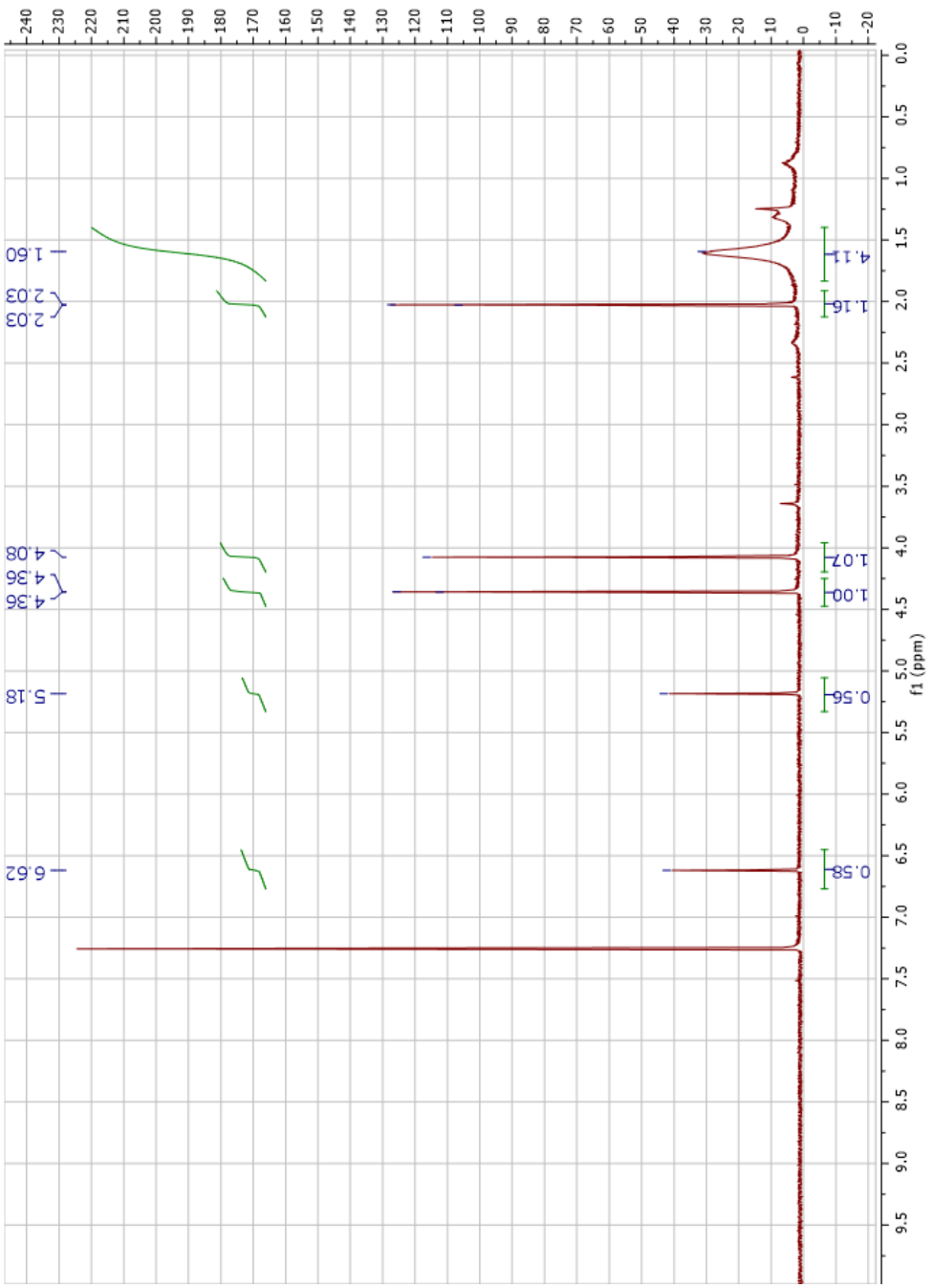


**Figure A27. $^{1}$H NMR for Elsinochrome A**

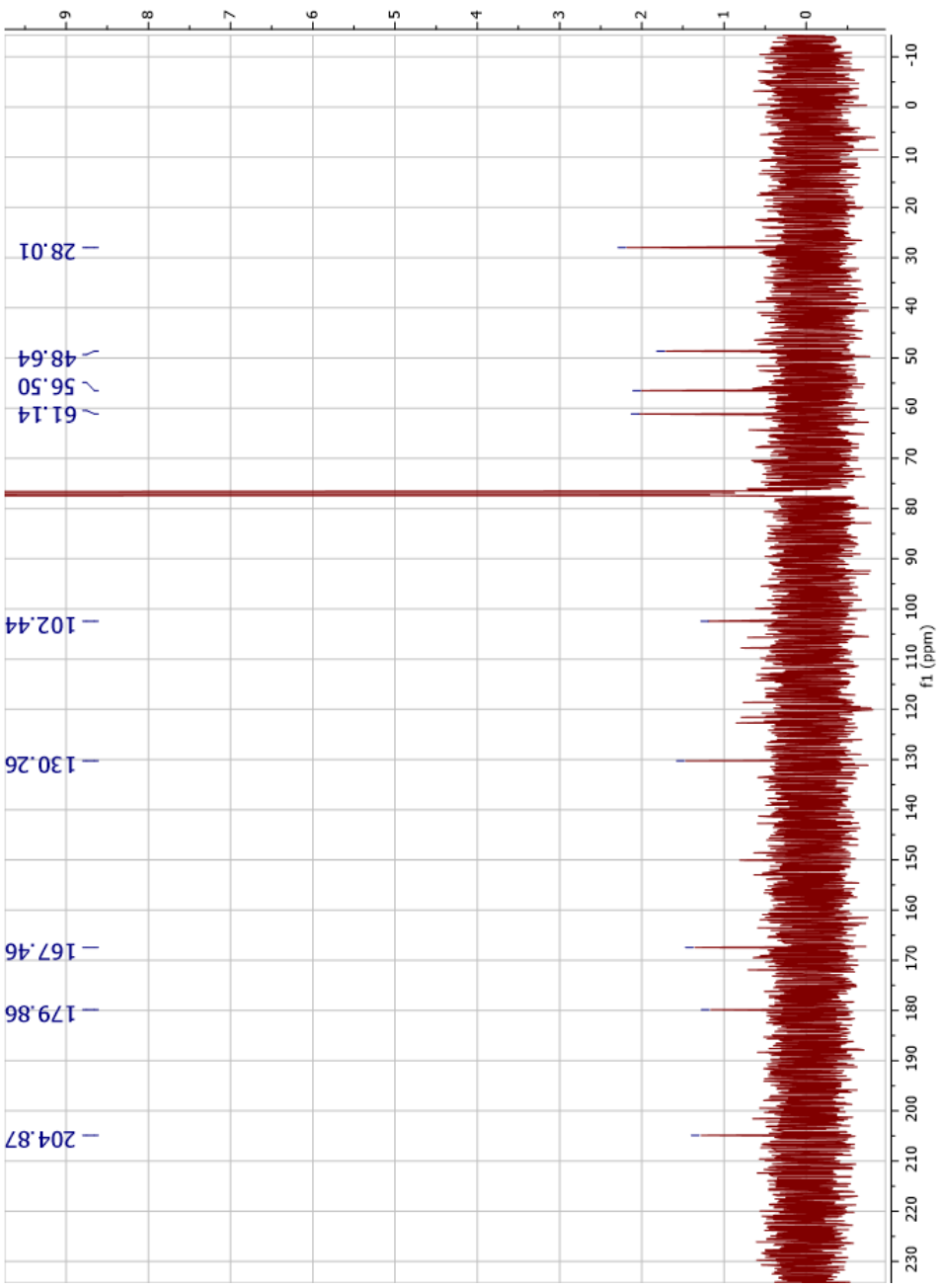


**Figure A28. $^{13}$C NMR for Elsinochrome A**

### *A.2.5 Elsinochrome D*

NMR data were recorded on "Varian VNMR spectrometers (400 and 500 MHz for $^{1}H$, 100 and 125 MHz for $^{13}C$) with broad band and triple resonance probes at 25 ±0.5 ˚C.

Samples dissolved in dDMSO

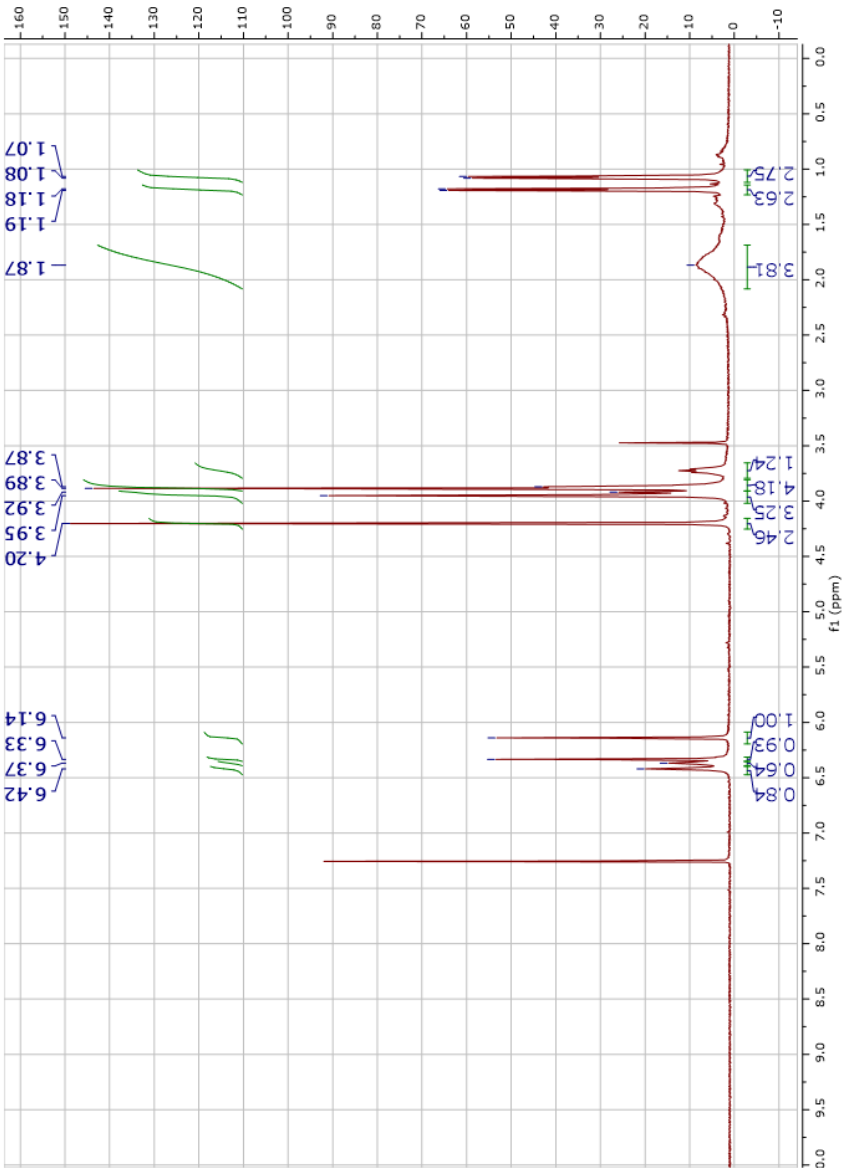


**Figure A29. $^{1}H$ NMR for Elsinochrome D**

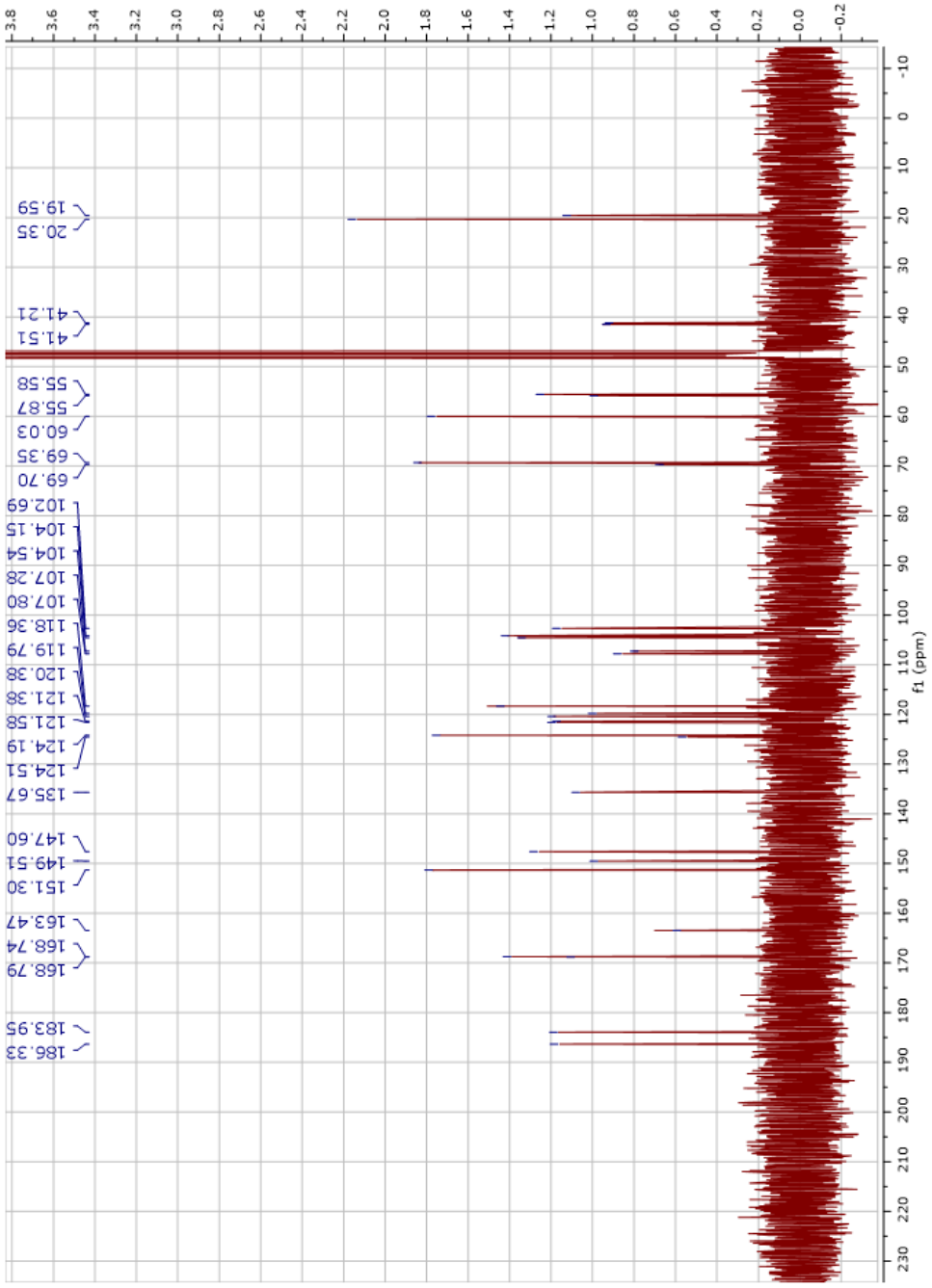


**Figure A30. $^{13}$C NMR of Elsinochrome D**

### *A.2.6 Elsinochrome E*

NMR data were recorded on "Varian VNMR spectrometers (400 and 500 MHz for $^{1}H$, 100 and 125 MHz for $^{13}C$) with broad band and triple resonance probes at 25 ±0.5 ˚C.

Samples dissolved in dDMSO

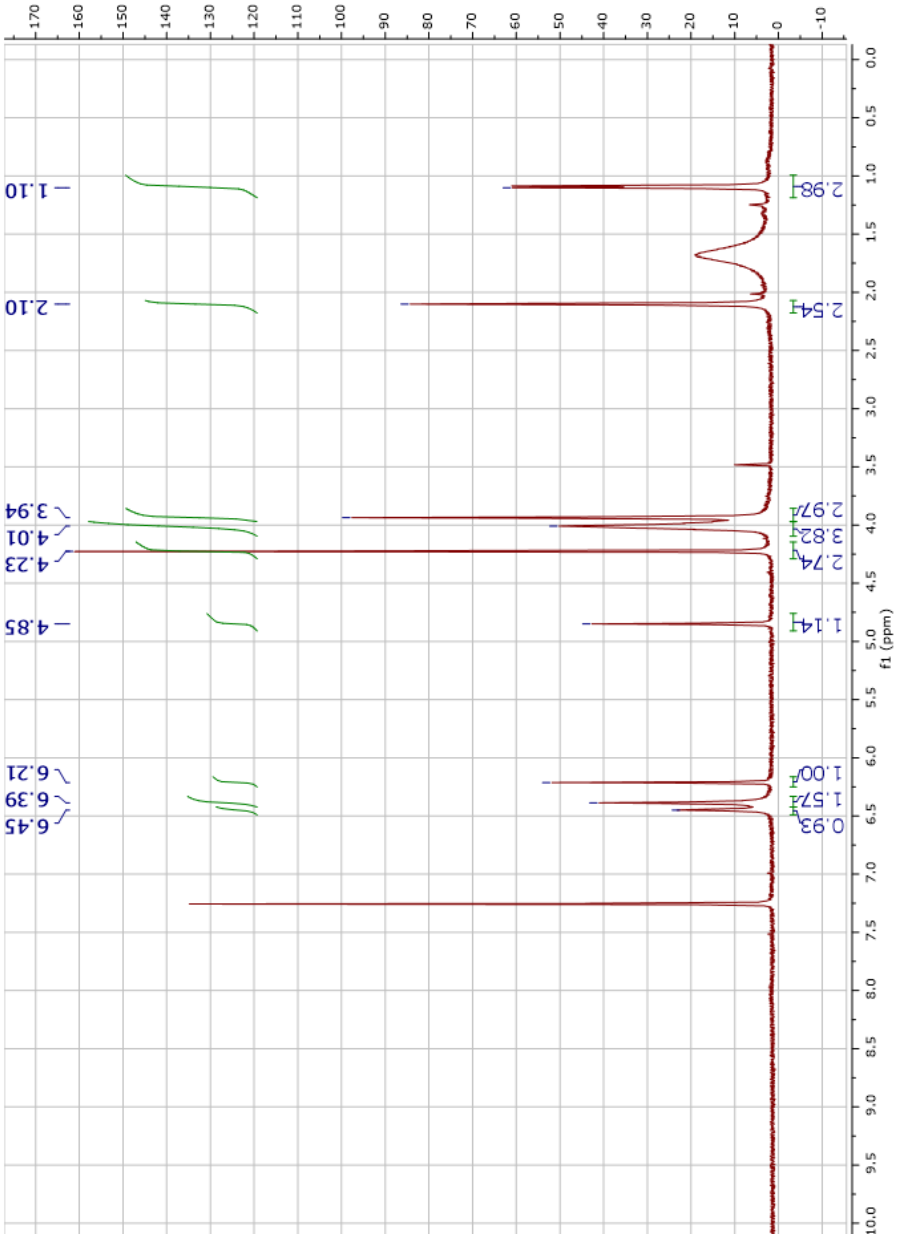


**Figure A31. $^{1}H$ NMR of Elsinochrome E**

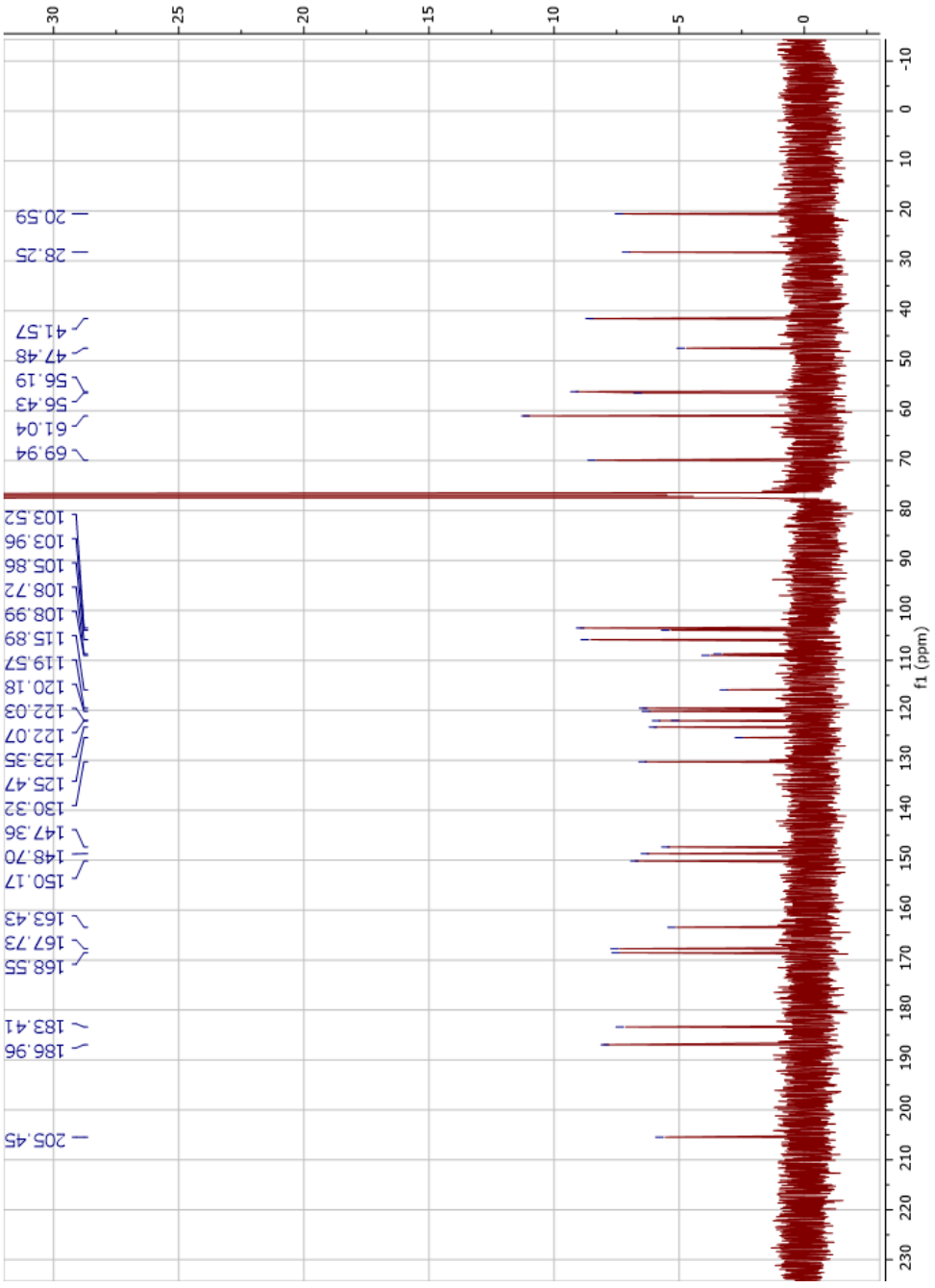


**Figure A32. $^{13}$C NMR of Elsinochrome E**

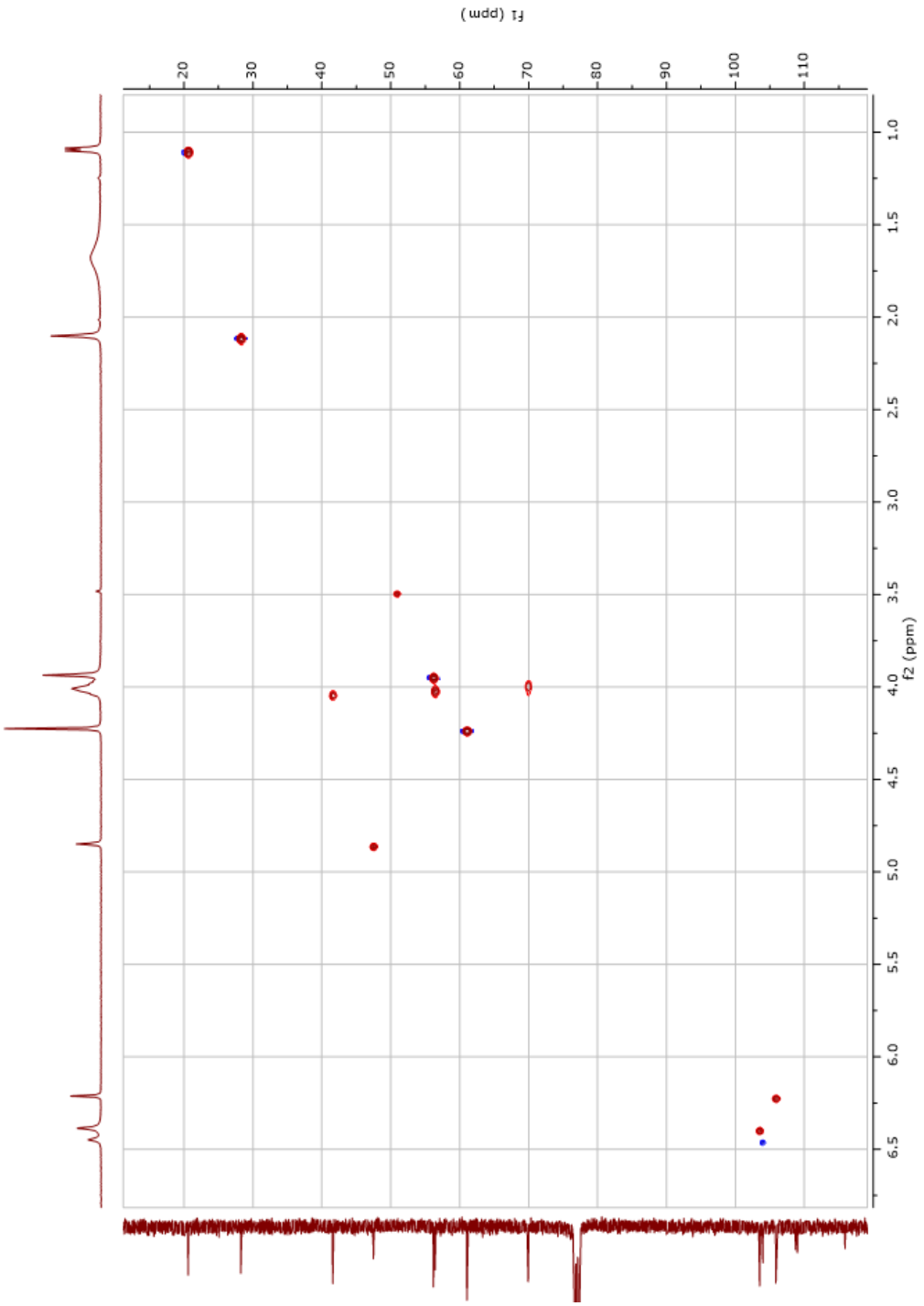


**Figure A33. HSQC of Elsinochrome E**

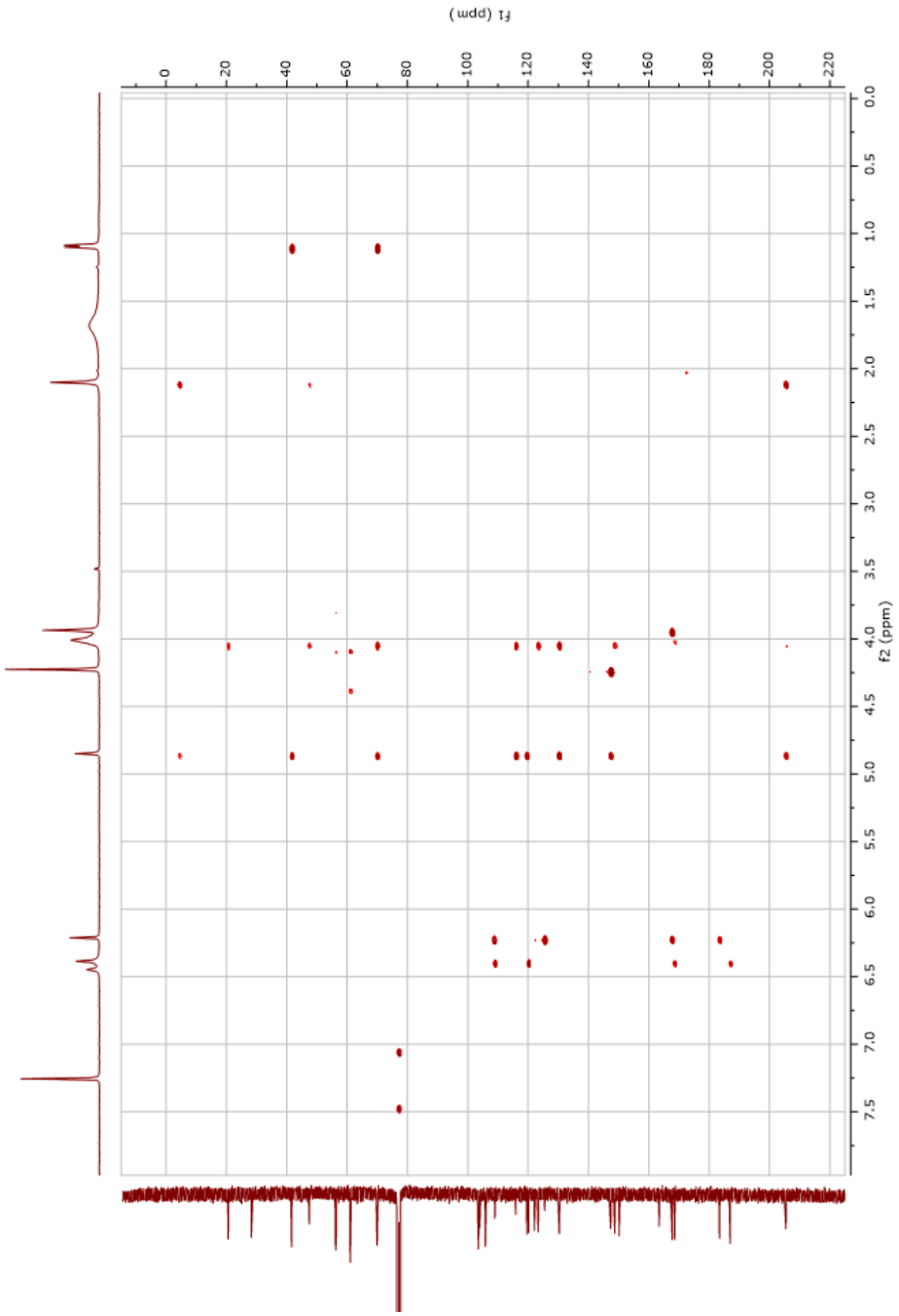


**Figure A34. HMBC of Elsinochrome E**

### *A.2.7 Persephacin A*

NMR data were recorded on "Varian VNMR spectrometers (400 and 500 MHz for $^{1}H$, 100 and 125 MHz for $^{13}C$) with broad band and triple resonance probes at 25 ±0.5 ˚C. Samples dissolved in dDMSO

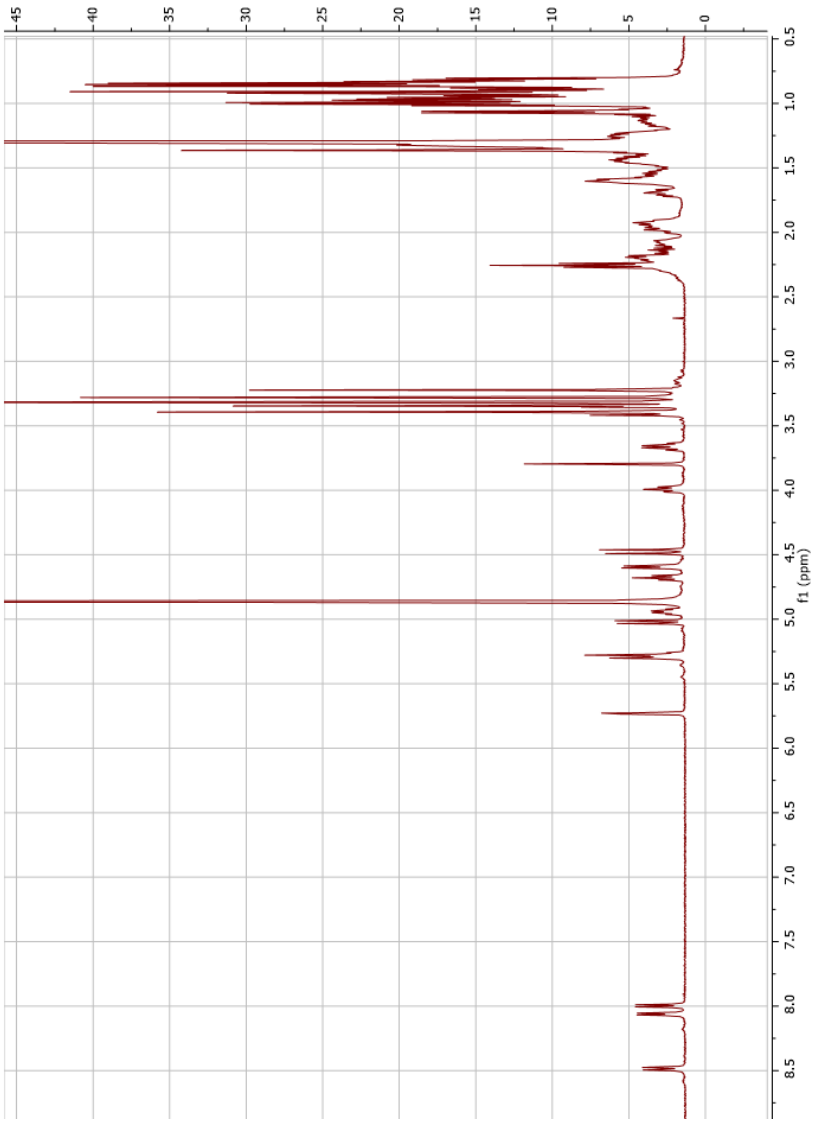


**Figure A35. $^{1}H$ NMR of Persephacin A**

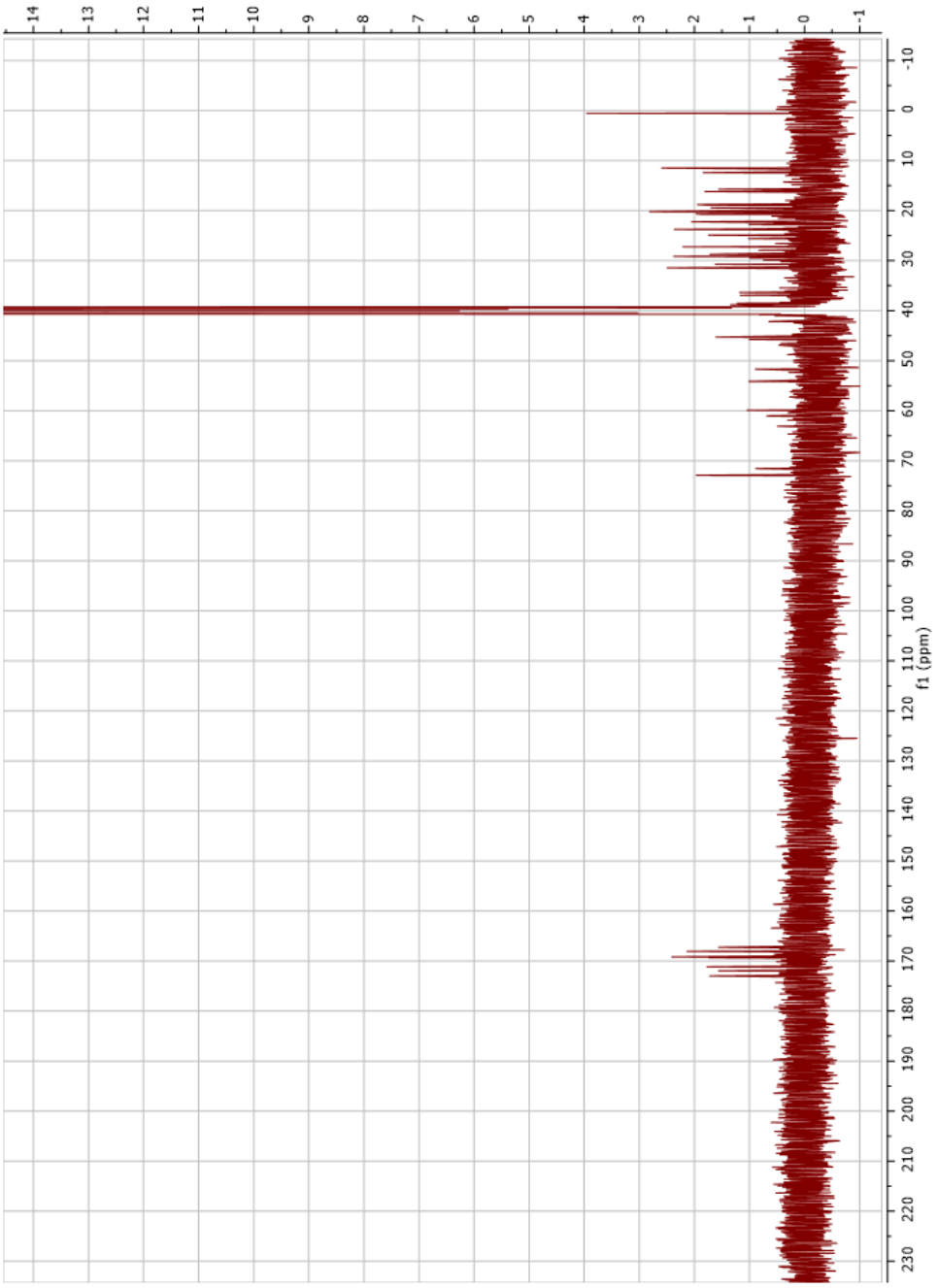


**Figure A36. $^{13}$C NMR of Persephacin A**

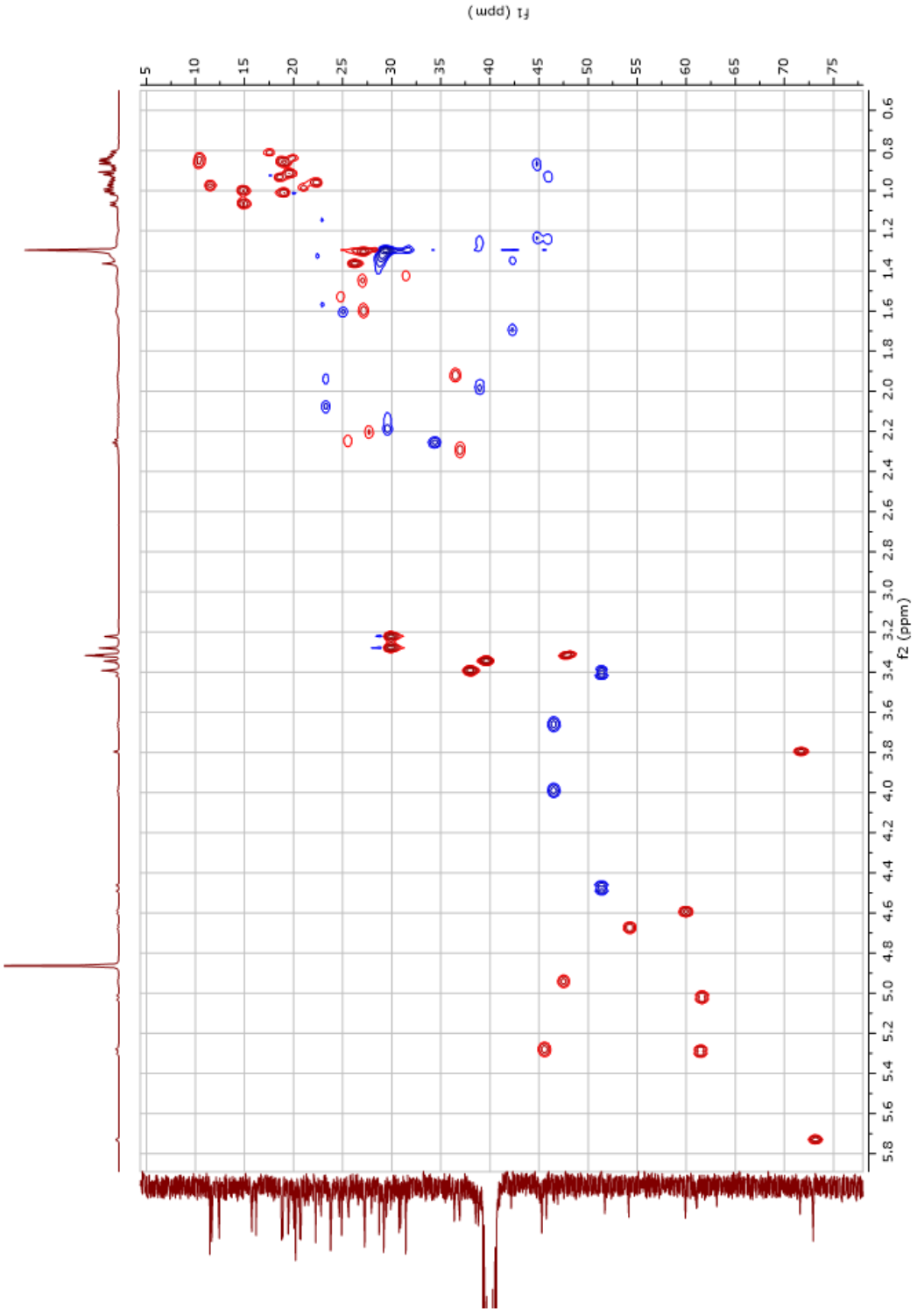


**Figure A37. HSQC for Persephacin A**


**Figure A38. HMBC for Persephacin A**

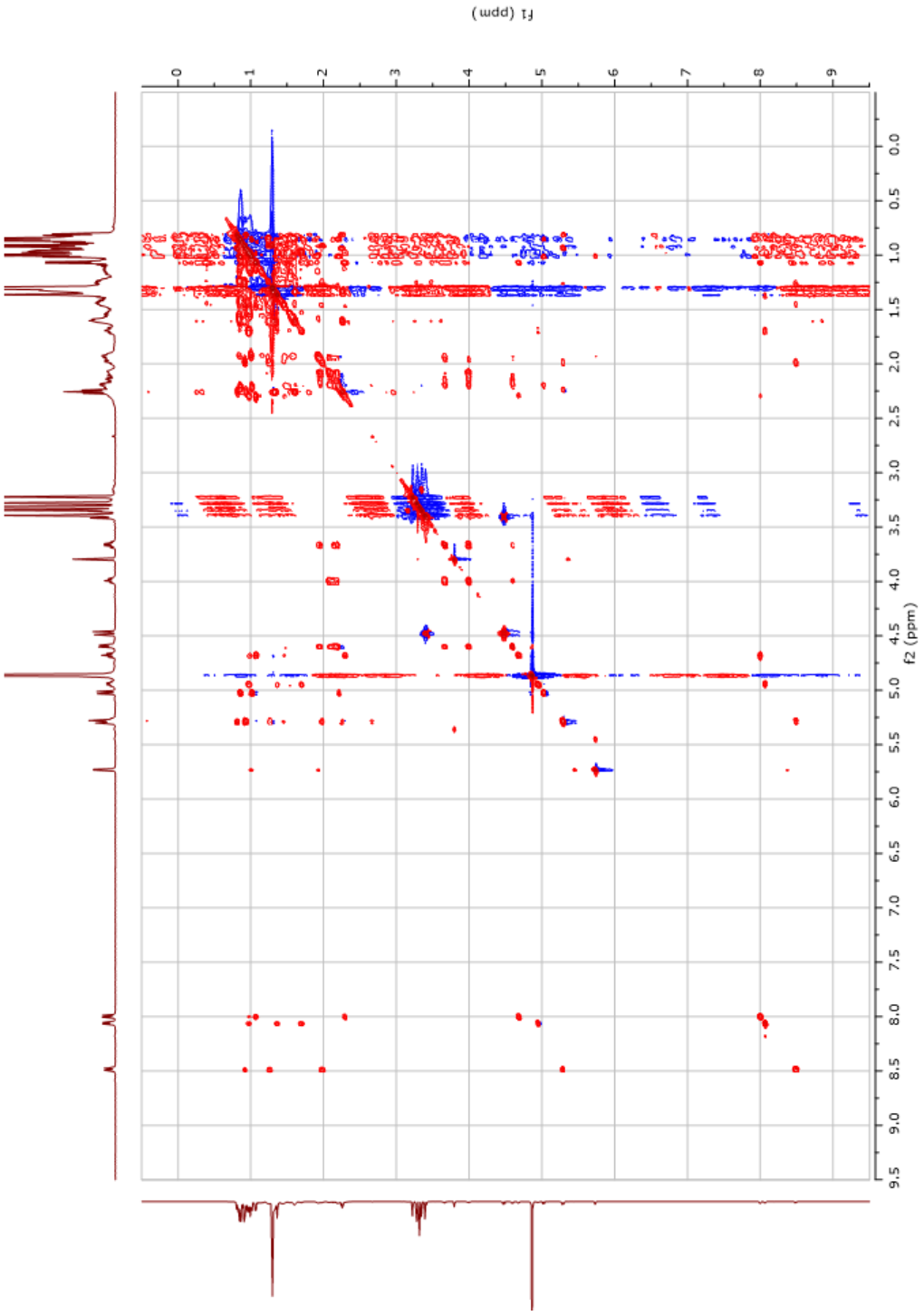


**Figure A39. TOCSY for Persephacin A**

*A.2.8 Persephacin B*

NMR data were recorded on "Varian VNMR spectrometers (400 and 500 MHz for $^{1}H$, 100 and 125 MHz for $^{13}C$) with broad band and triple resonance probes at 25 ±0.5 ˚C.

Samples dissolved in dDMSO

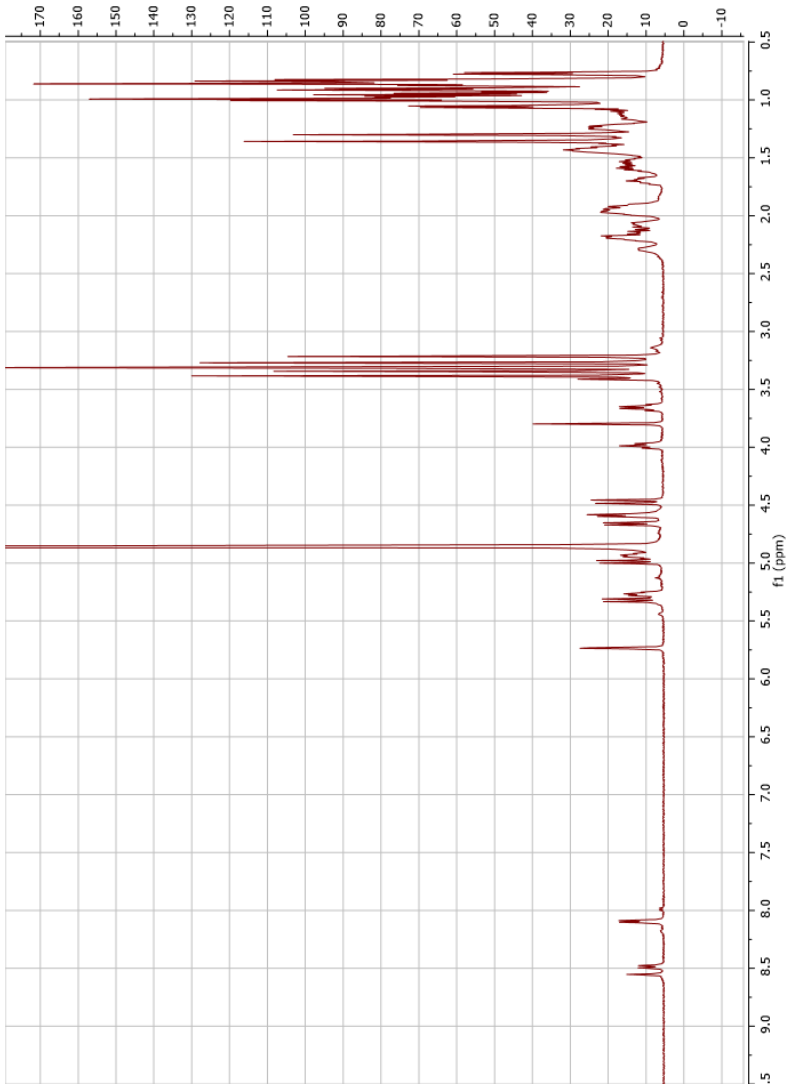


**Figure A40. $^{1}H$ NMR for Persephacin B**

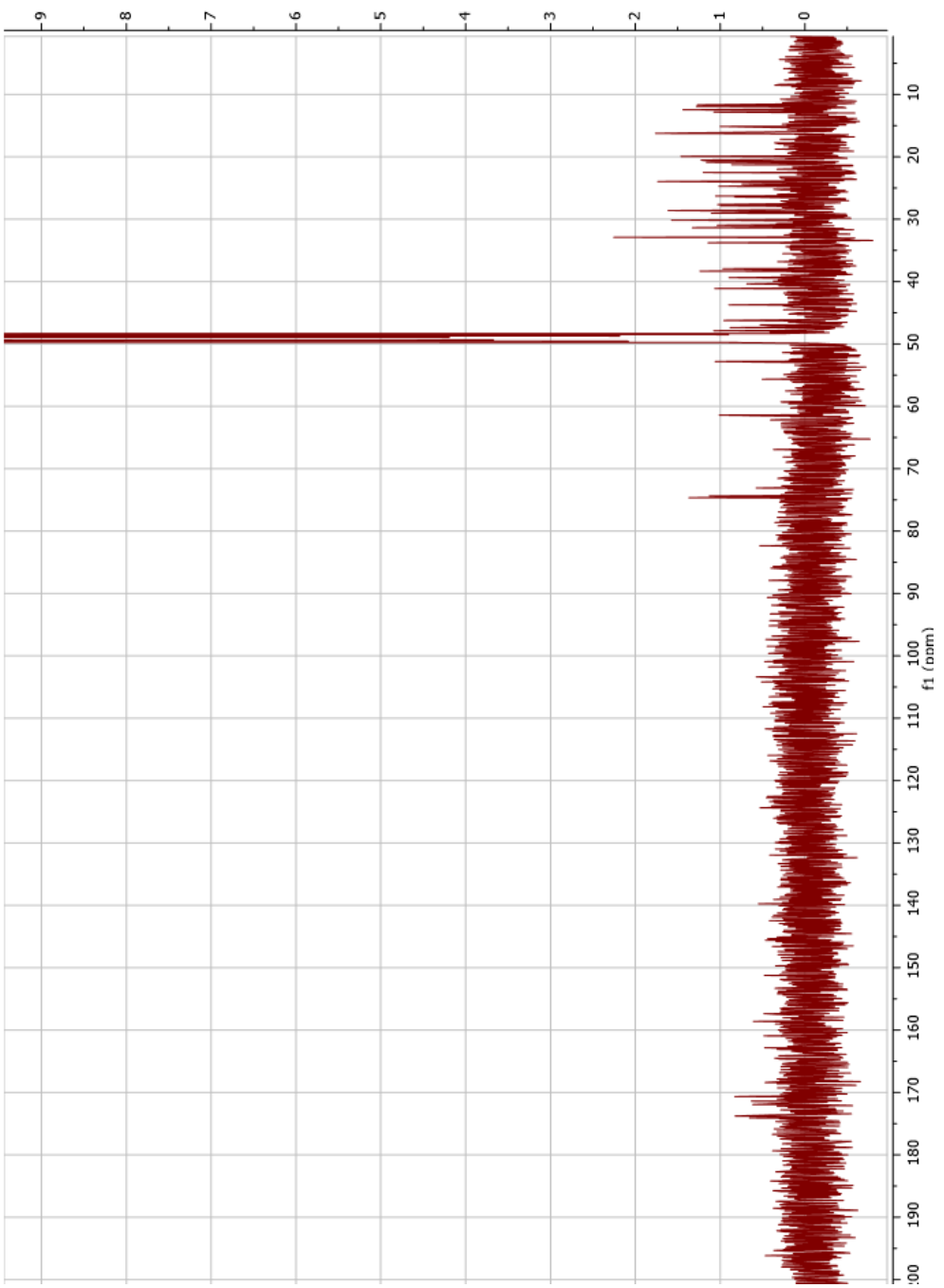


**Figure A41. $^{13}$C NMR for Persephacin B**

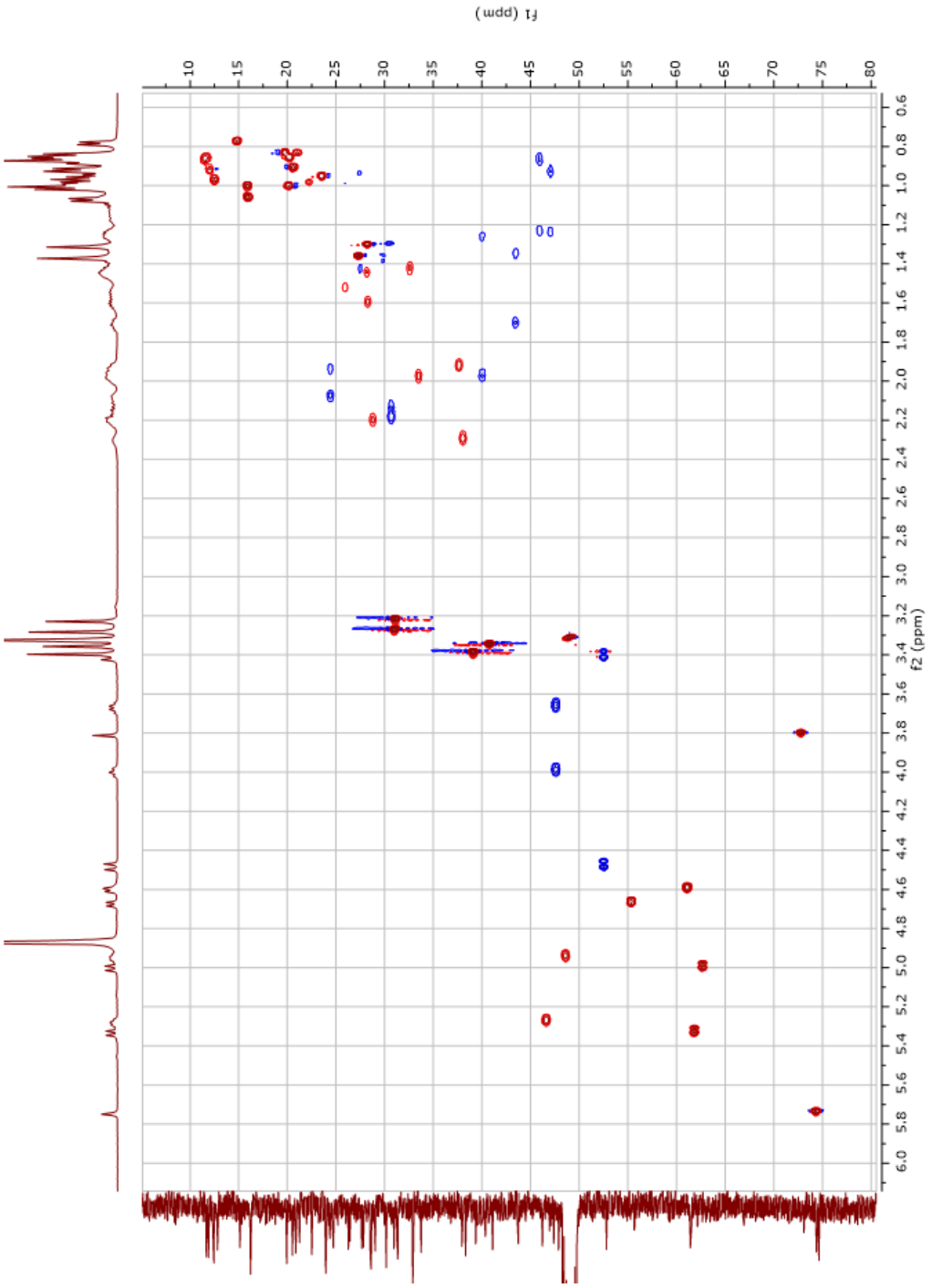


**Figure A42. HSQC for Persephacin B**

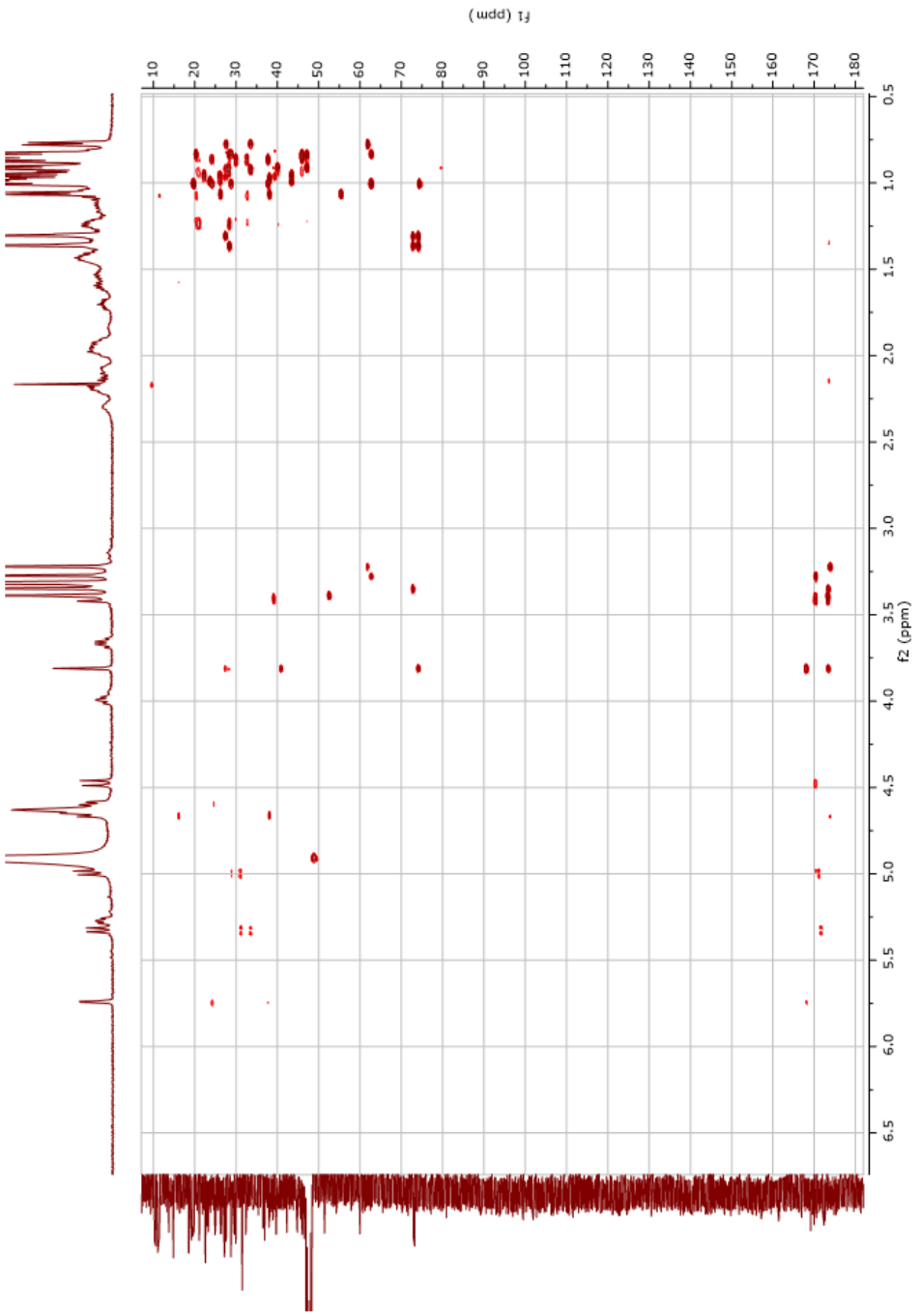


**Figure A43. HMBC for Persephacin B**

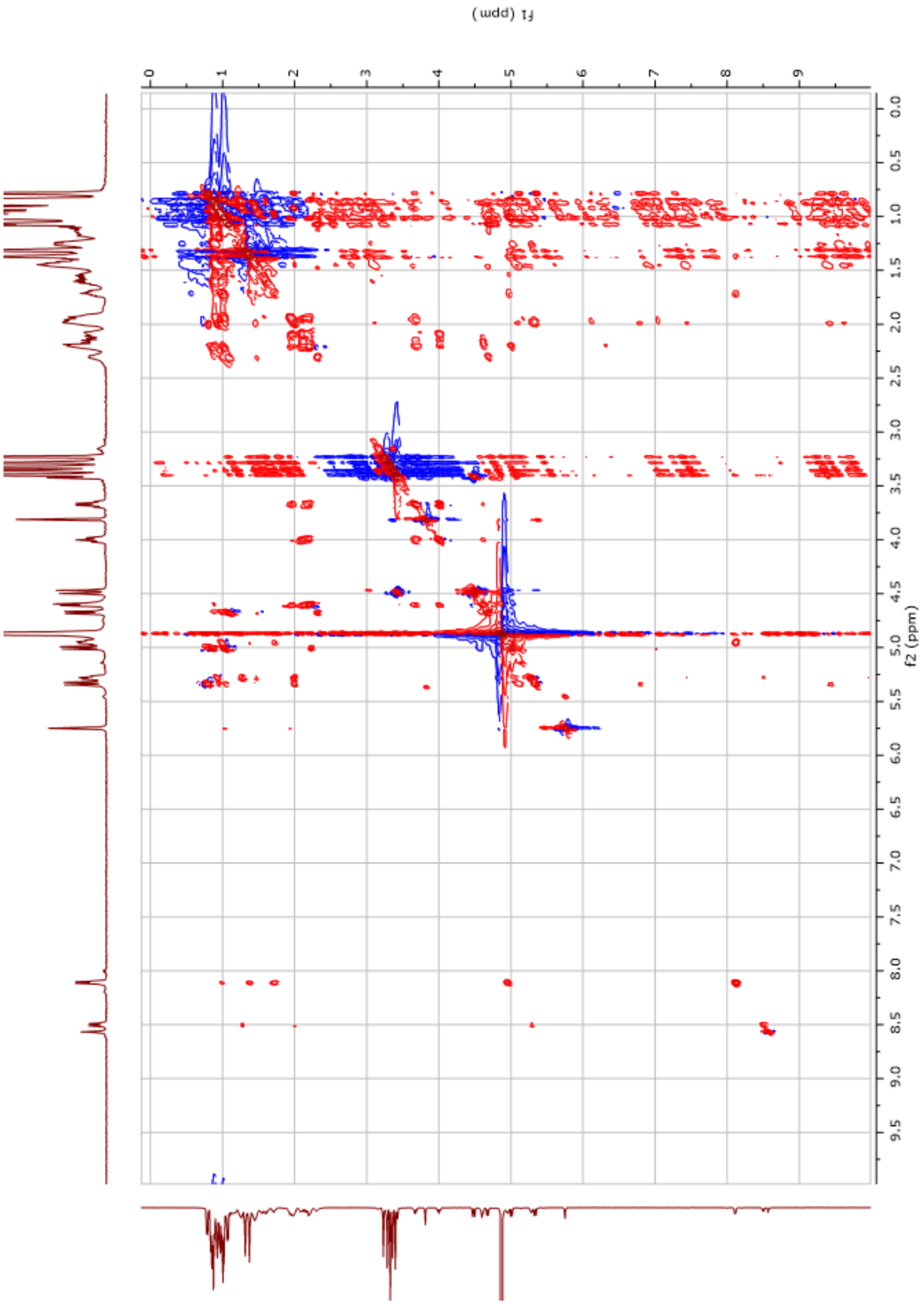


**Figure A44. TOCSY for Persephacin B**

### *A.2.9 Persephacin C*

NMR data were recorded on "Varian VNMR spectrometers (400 and 500 MHz for $^{1}H$, 100 and 125 MHz for $^{13}C$) with broad band and triple resonance probes at 25 ±0.5 ˚C.

Samples dissolved in dDMSO

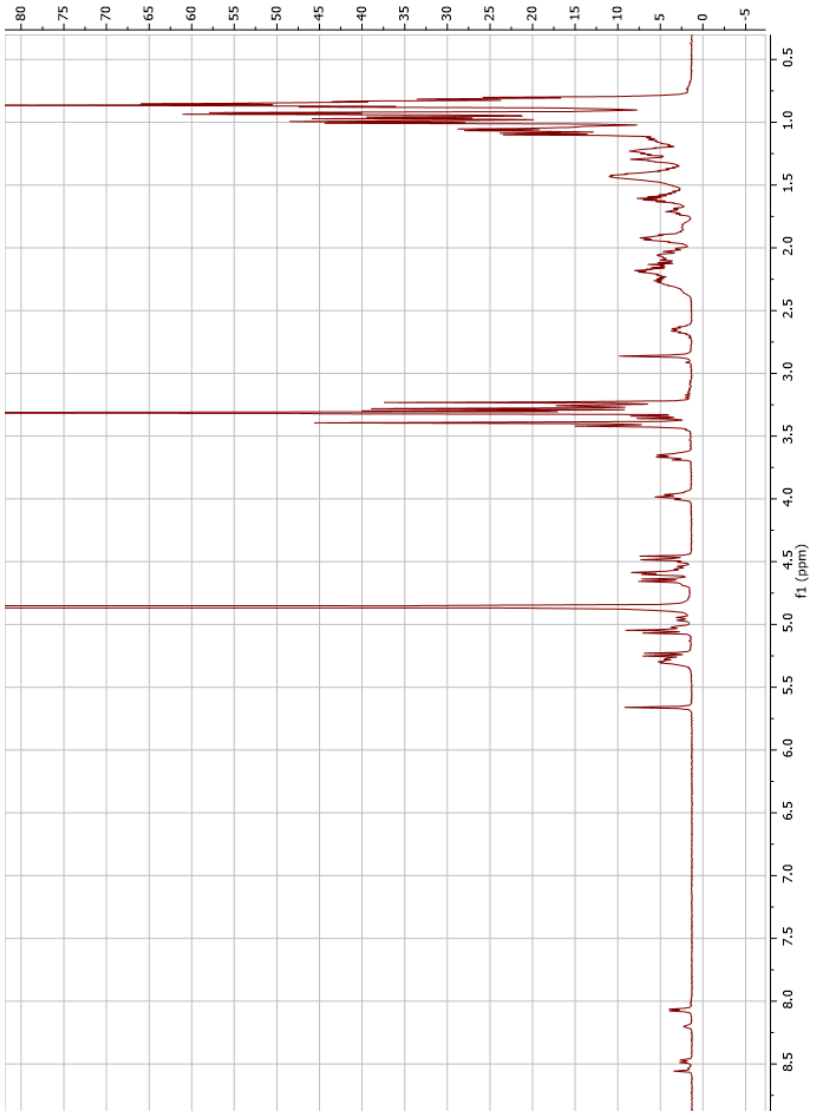


**Figure A45. $^{1}H$ NMR for Persephacin C**

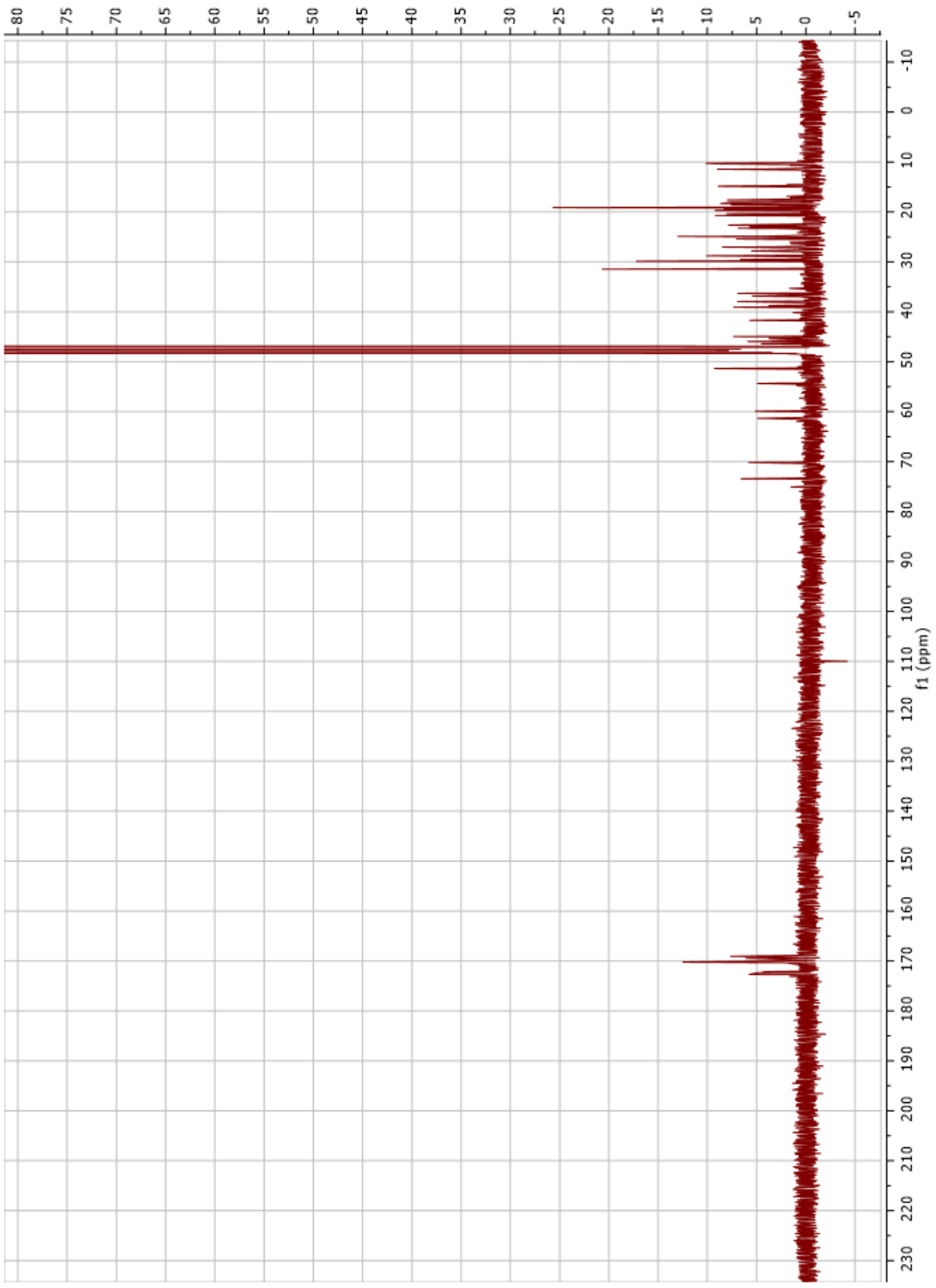


**Figure A46. $^{13}$C NMR for Persephacin C**

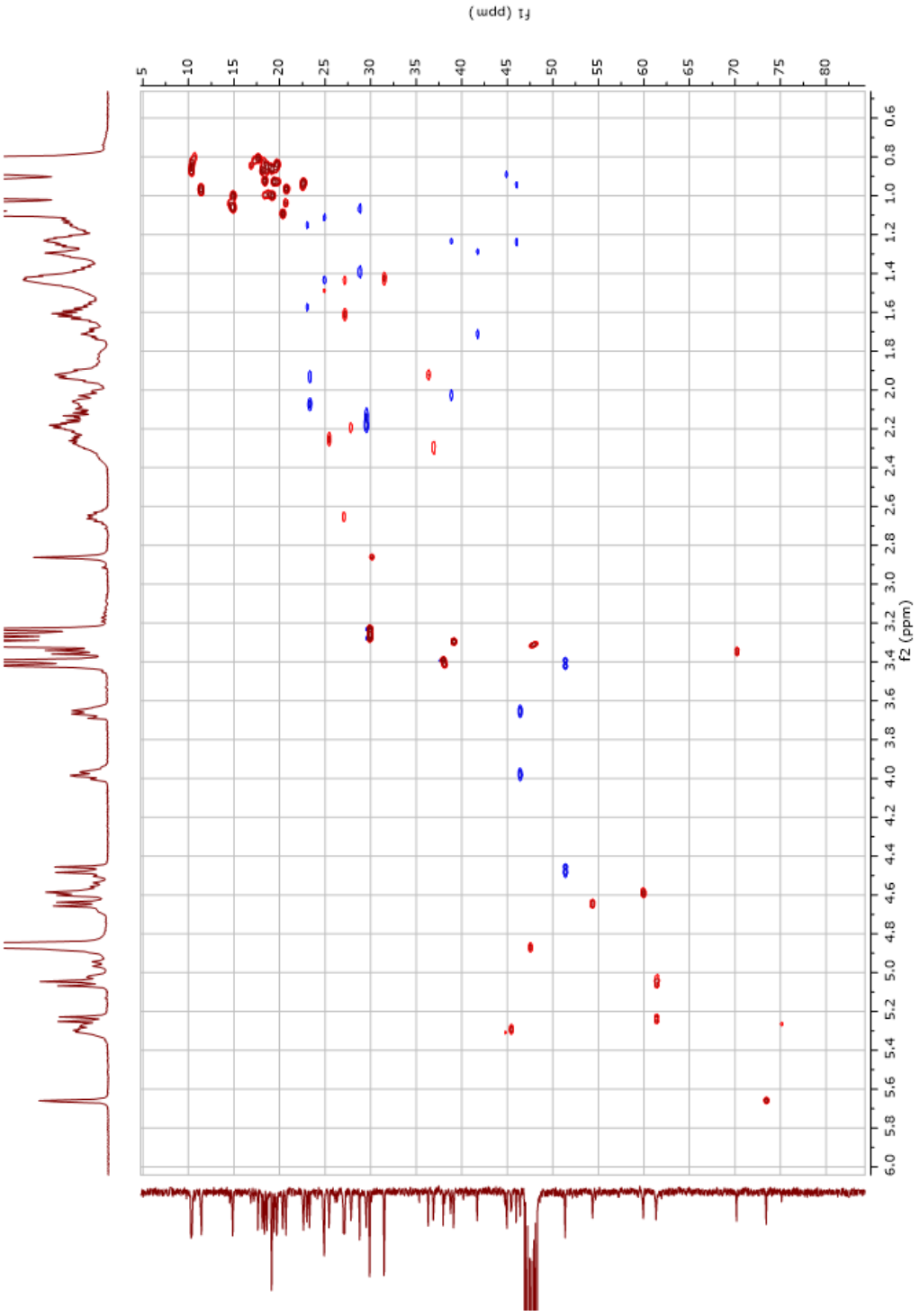


**Figure A47. HSQC for Persephacin C**

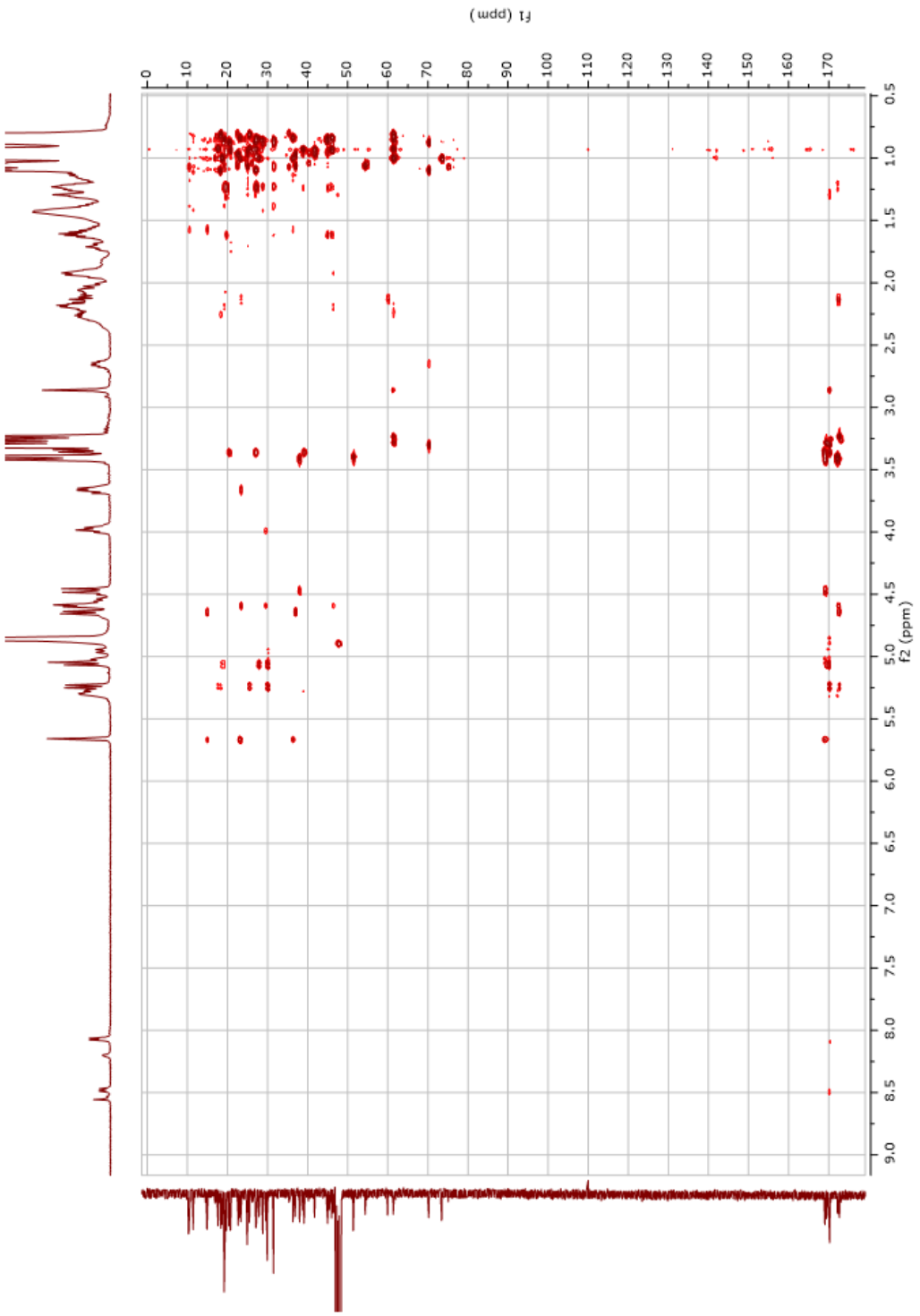


**Figure A48. HMBC for Persephacin C**

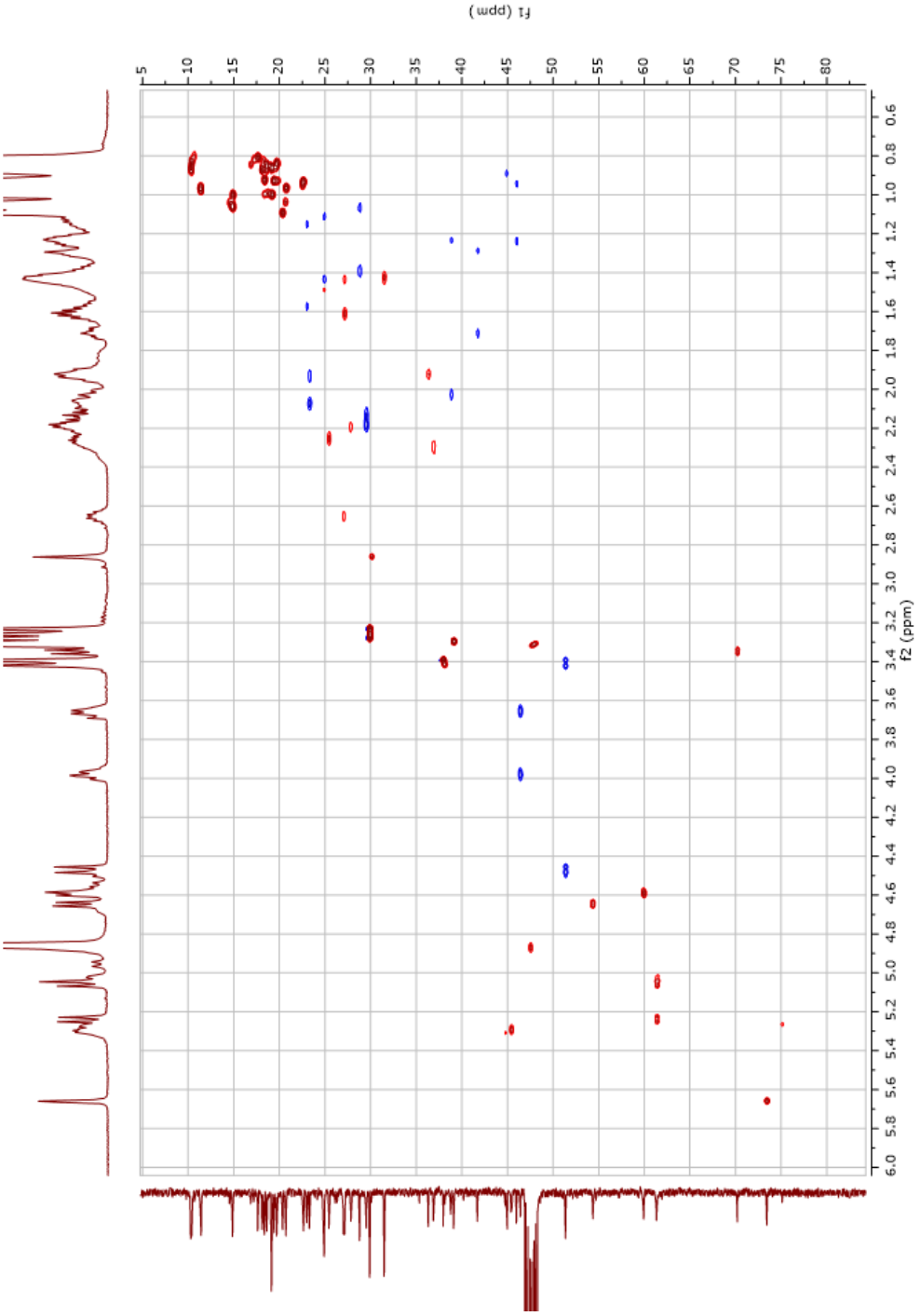


**Figure A49. TOCSY for Persephacin C**

*A.2.10 Media Optimization - Cheerios*

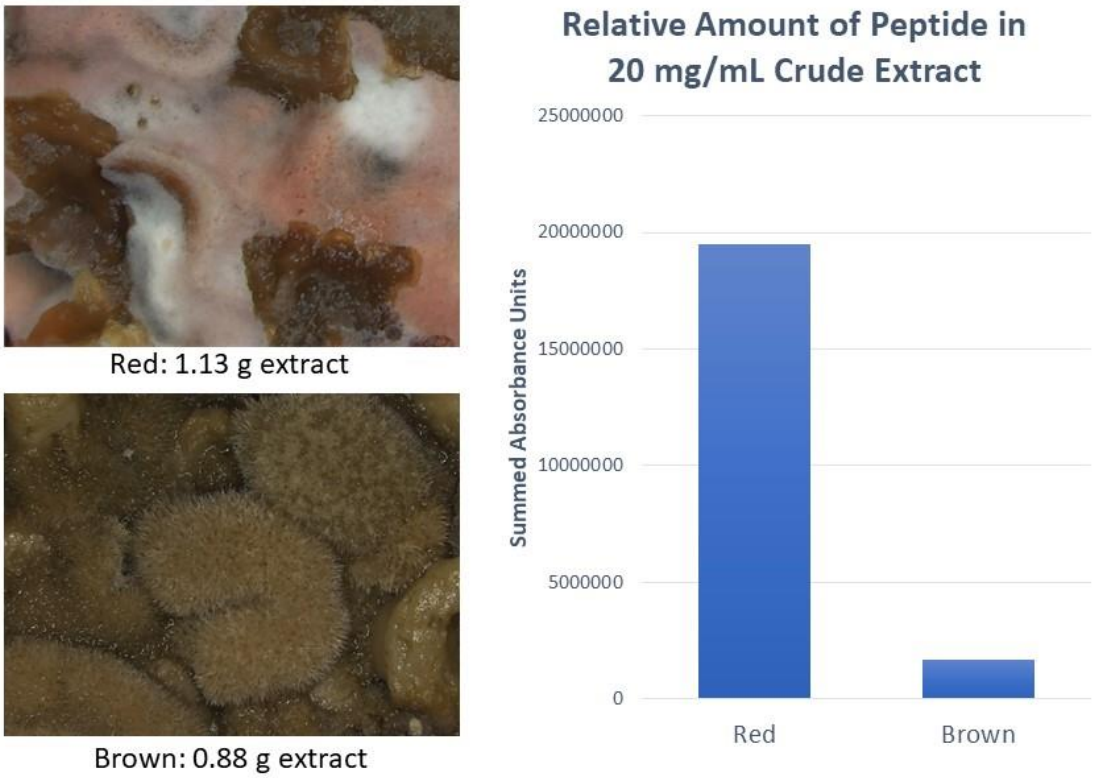


**Figure A50. Color Difference and Relative Persephacin A Yield**

While growing on Cheerios, a color and morphology change was noticed on some areas of the fungus. These were separated, extracted separately and compared for persephacin growth. It was determined that persephacin was present in a higher concentration when red was also present.

*A.2.11 Media Optimization – Roller Bottles*

In an attempt to increase surface area to determine the effect on persephacin production, we attempted to grow *Spaceloma corylii* in roller bottles with either 100mL or 200mL in various media. Samples were grown for 4 weeks and extracted by

partitioning ethyl acetate. The PDB condition had the greatest yield of persephacin A. However the flasks were inconsistent at the 200 mL volume. The agar of the 100 ml/bottle had the second highest yield. The 100mL flasks had the most consistent yield.

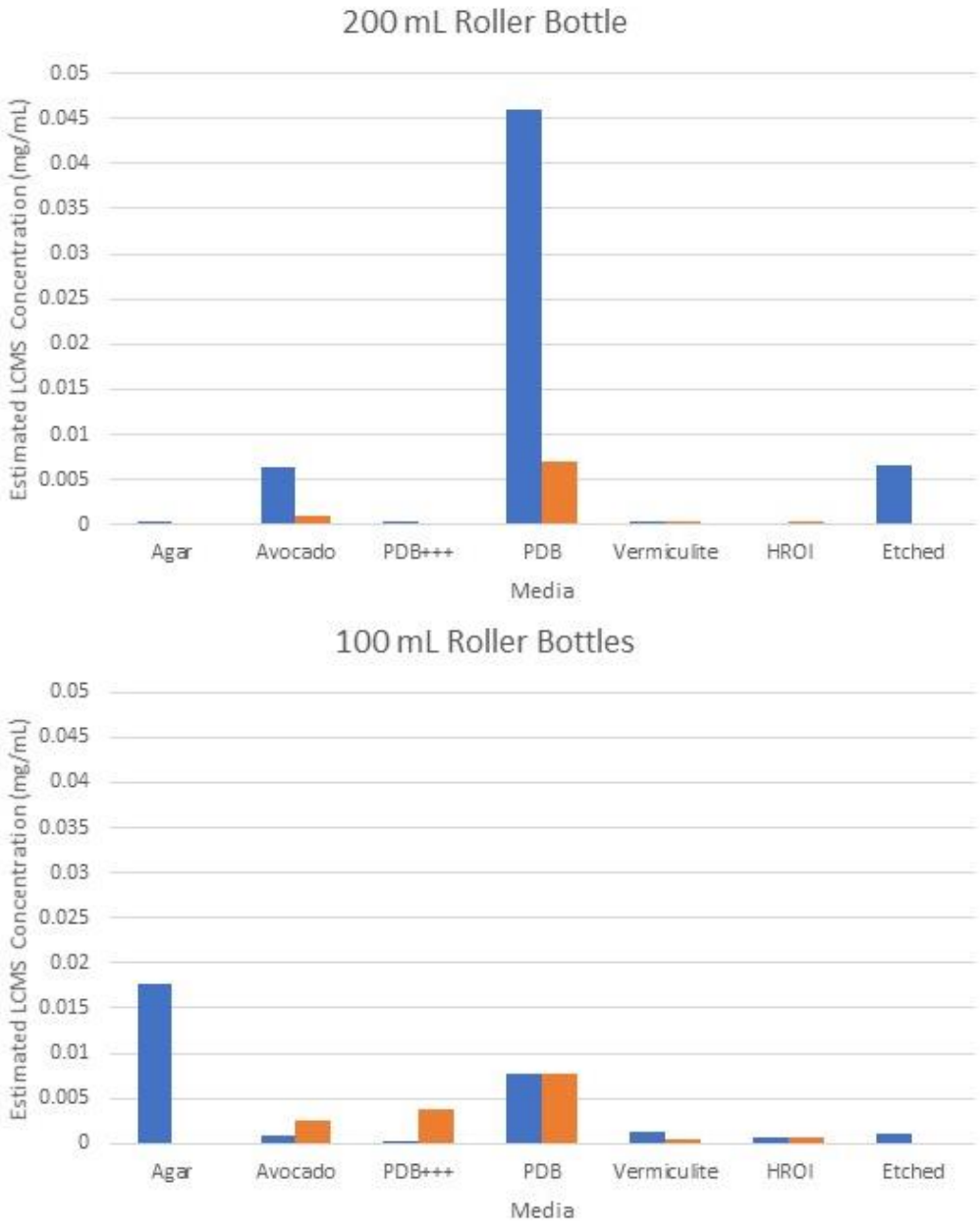


**Figure A51. Yield of Persephacin A in Roller Bottles with Varying Media Types.**

**Figure A52. Roller Bottles After 4 Weeks of Growth**

*A.2.12 Media Optimization – Bioreactor*

A bioreactor was filled with 10L of PDB+++ media and stirred for 4 weeks. Every week, 1L distilled and autoclaved water was added to account for that lost due to the high air flow. Upon extraction, and estimated yield of 89 mg of Persephacin A was calculated from LCMS and the calibration curve.

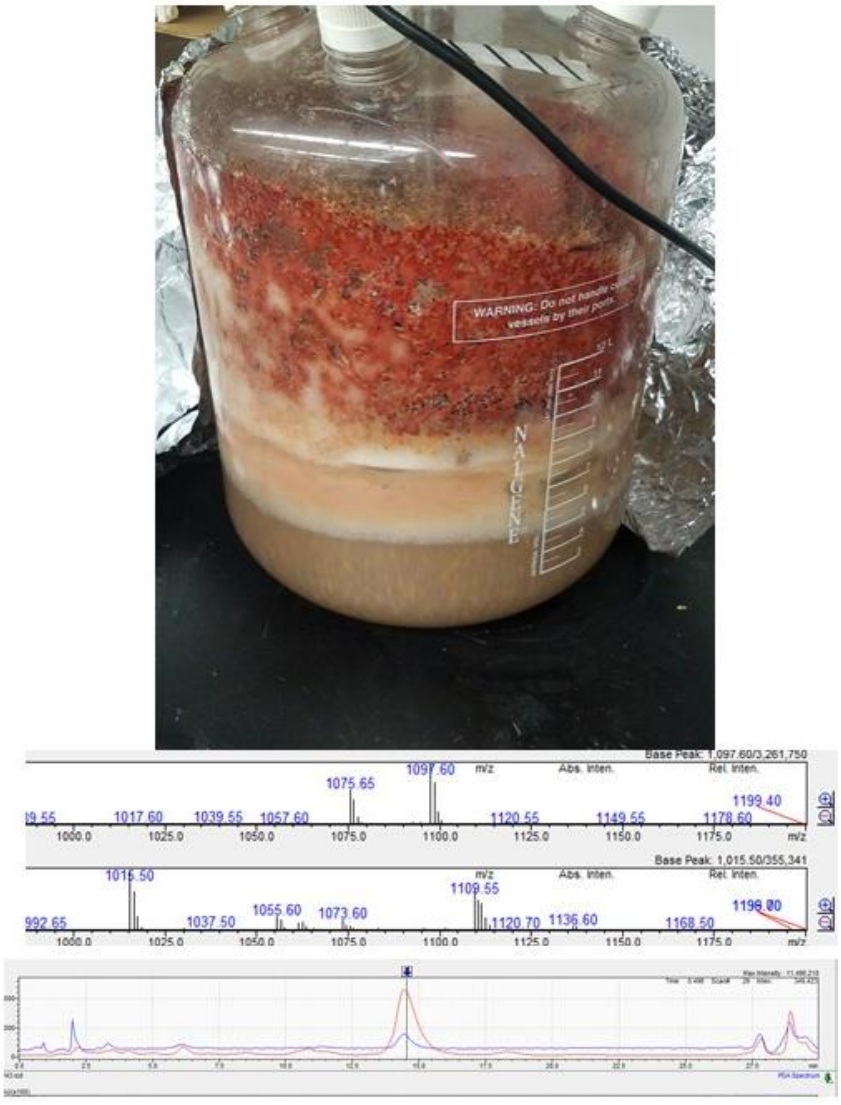


**Figure A53. Bioreactor and LCMS Chromatograms Showing the Quantification of Persephacin A**

*A.2.13 Bioassay Data – A. brassicicola*

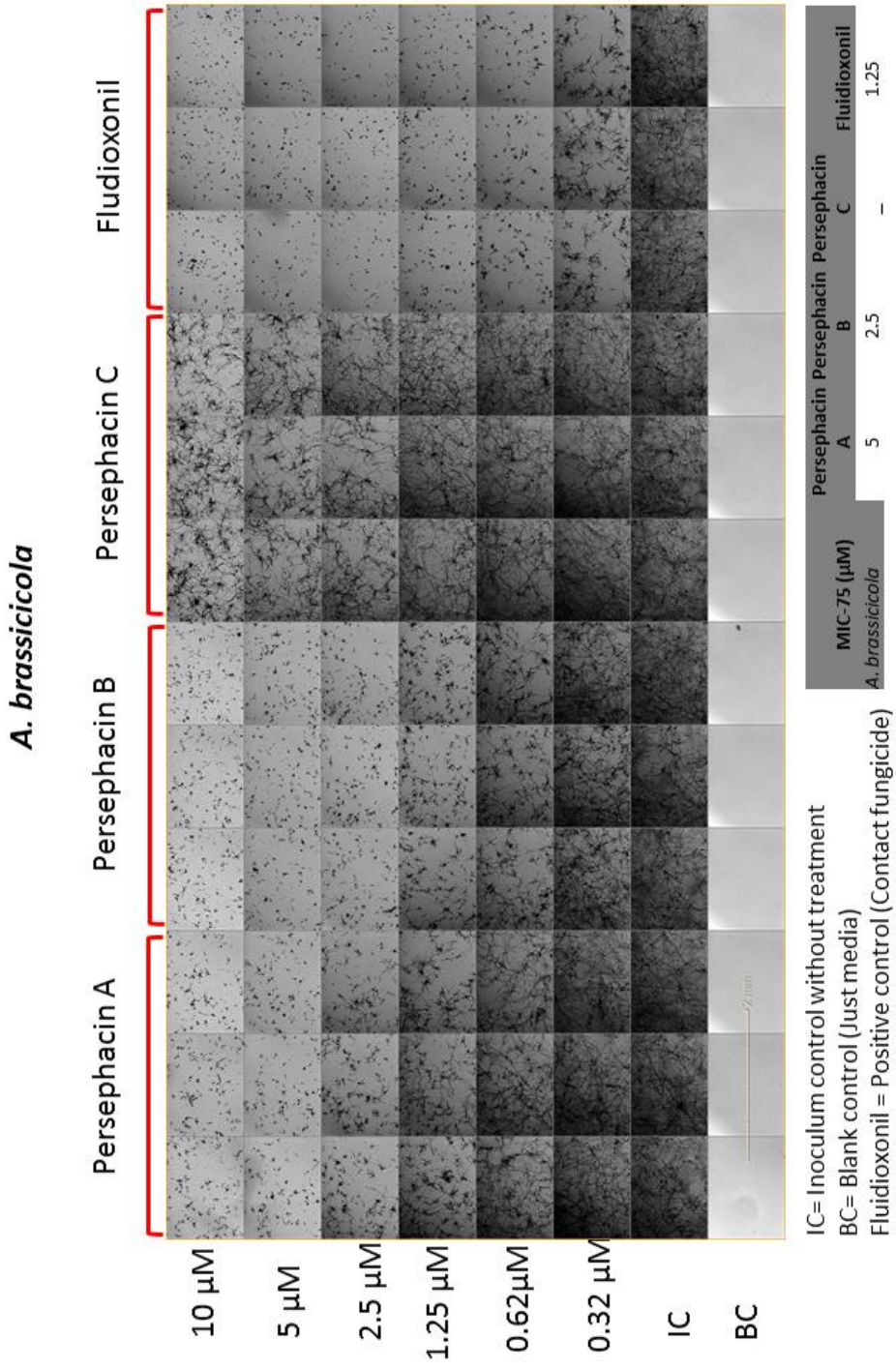


**Figure A54. Bioassay Data for *A. brassicicola***

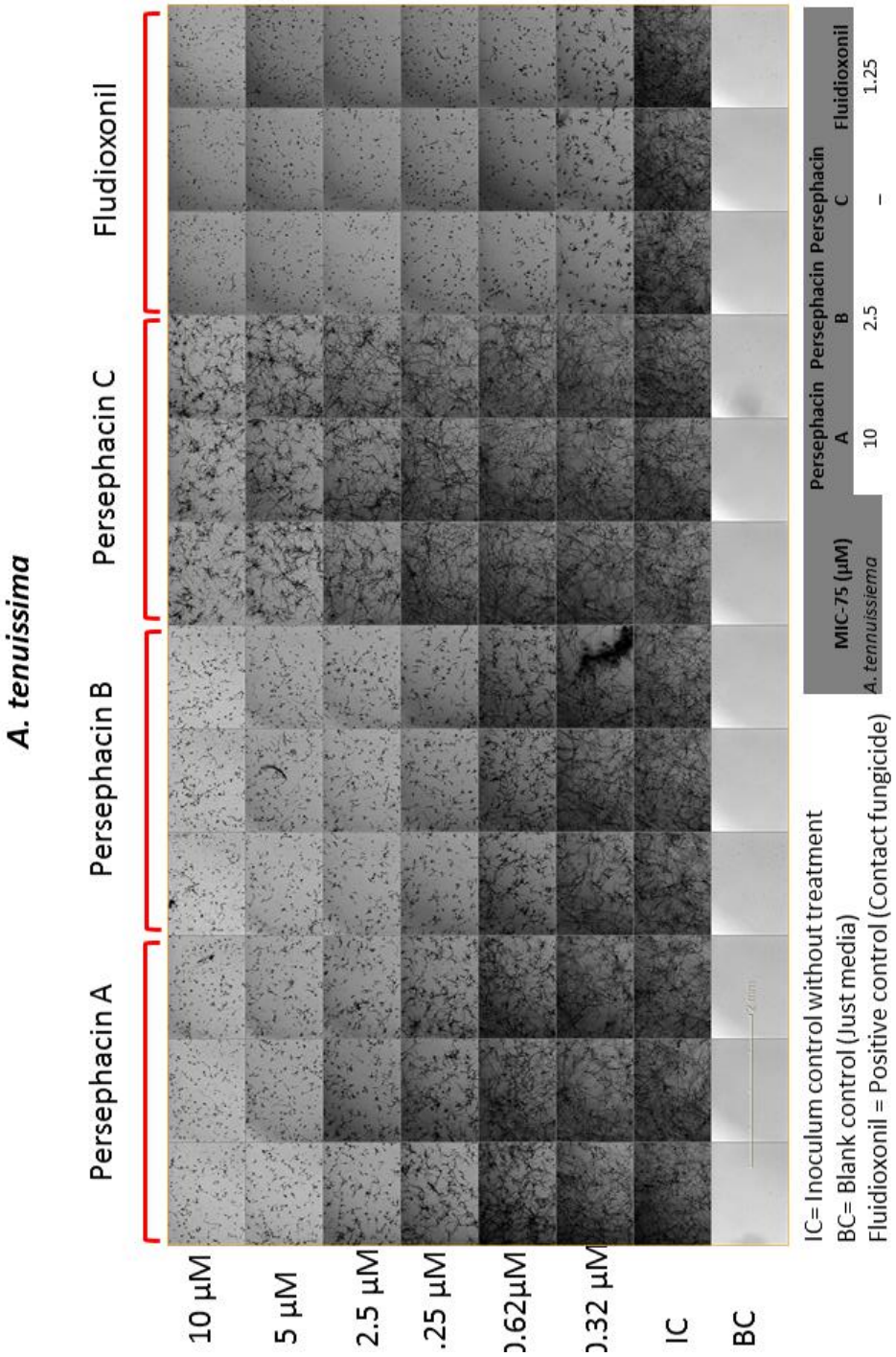


**Figure A55. Bioassay Data for *A. tenuissima***

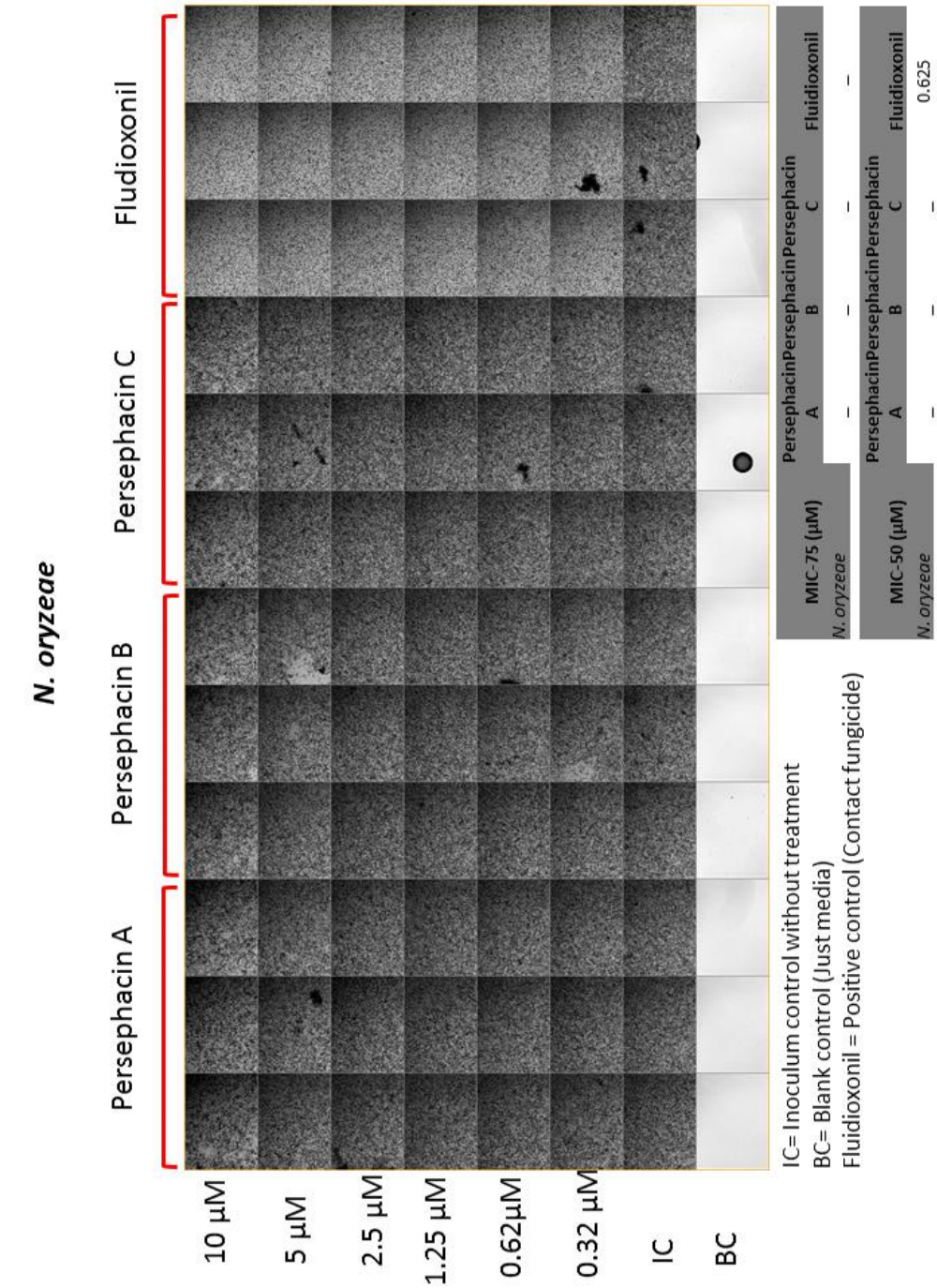


**Figure A56. Bioassay Data for *N. oryzeae***

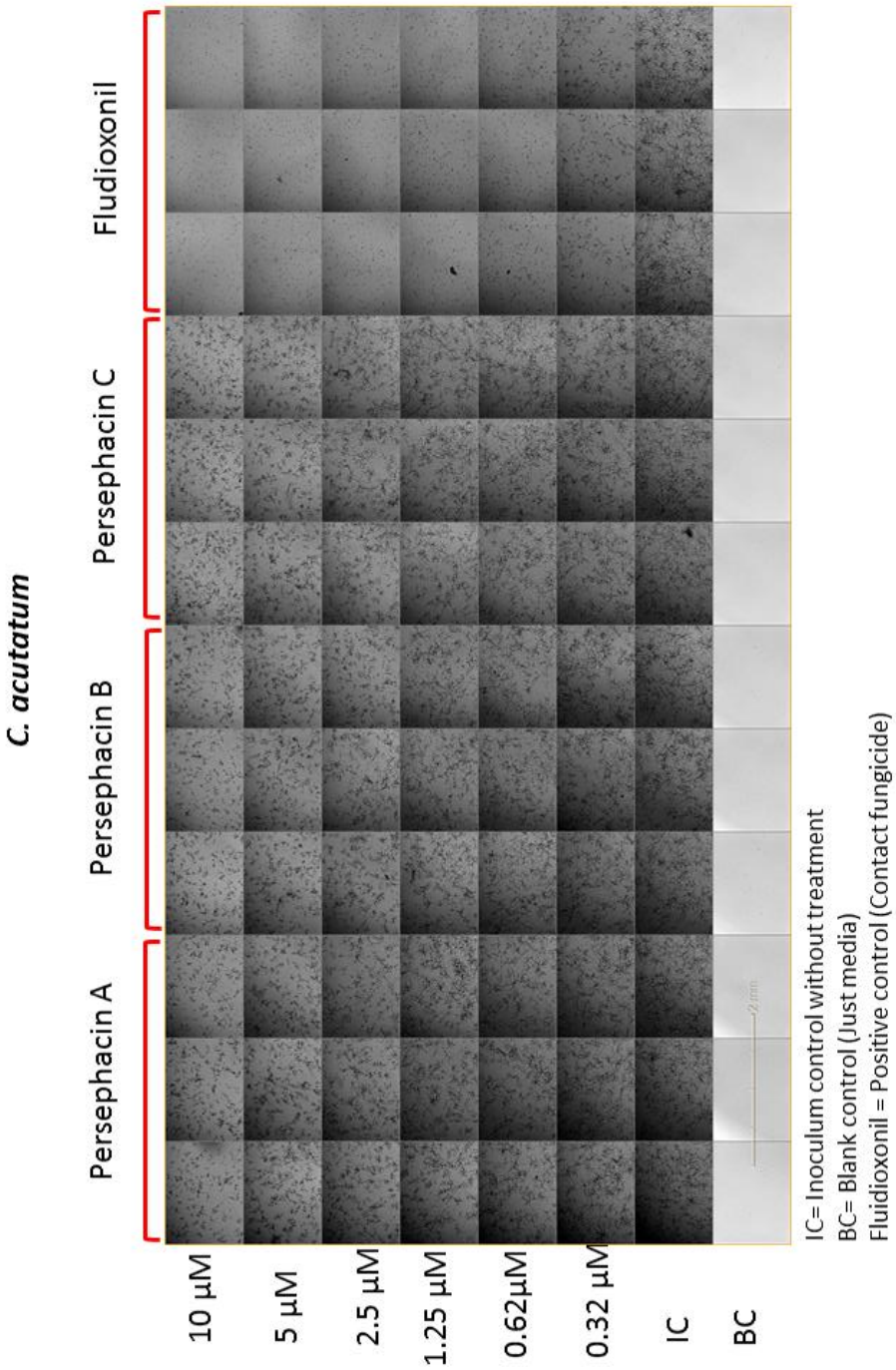


**Figure A57. Bioassay Data for *C. acutatum***

*A.2.17 Bioassay Data – N. odulosporium*

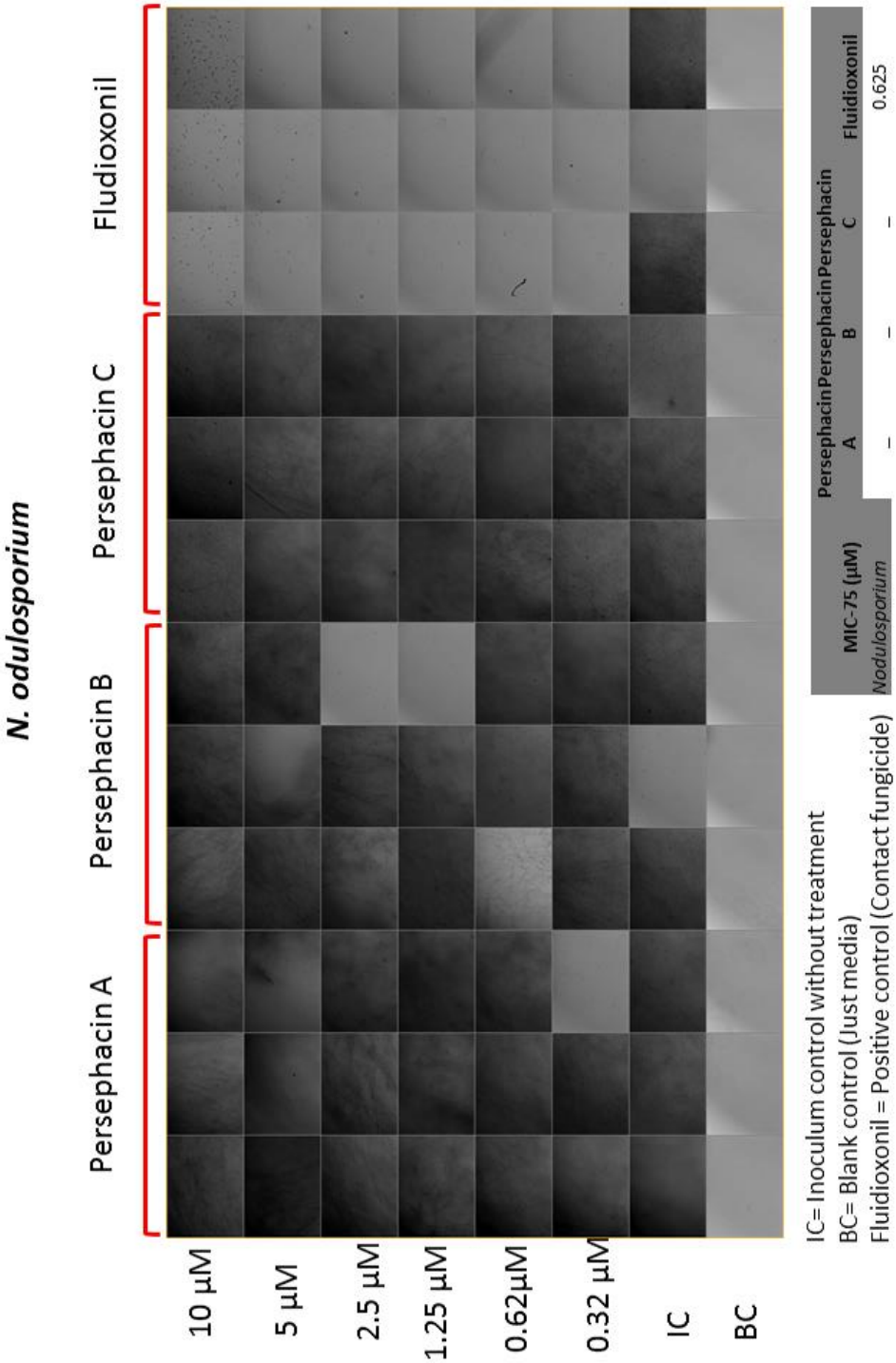


**Figure A58. Bioassay Data for *N. odulosporium***

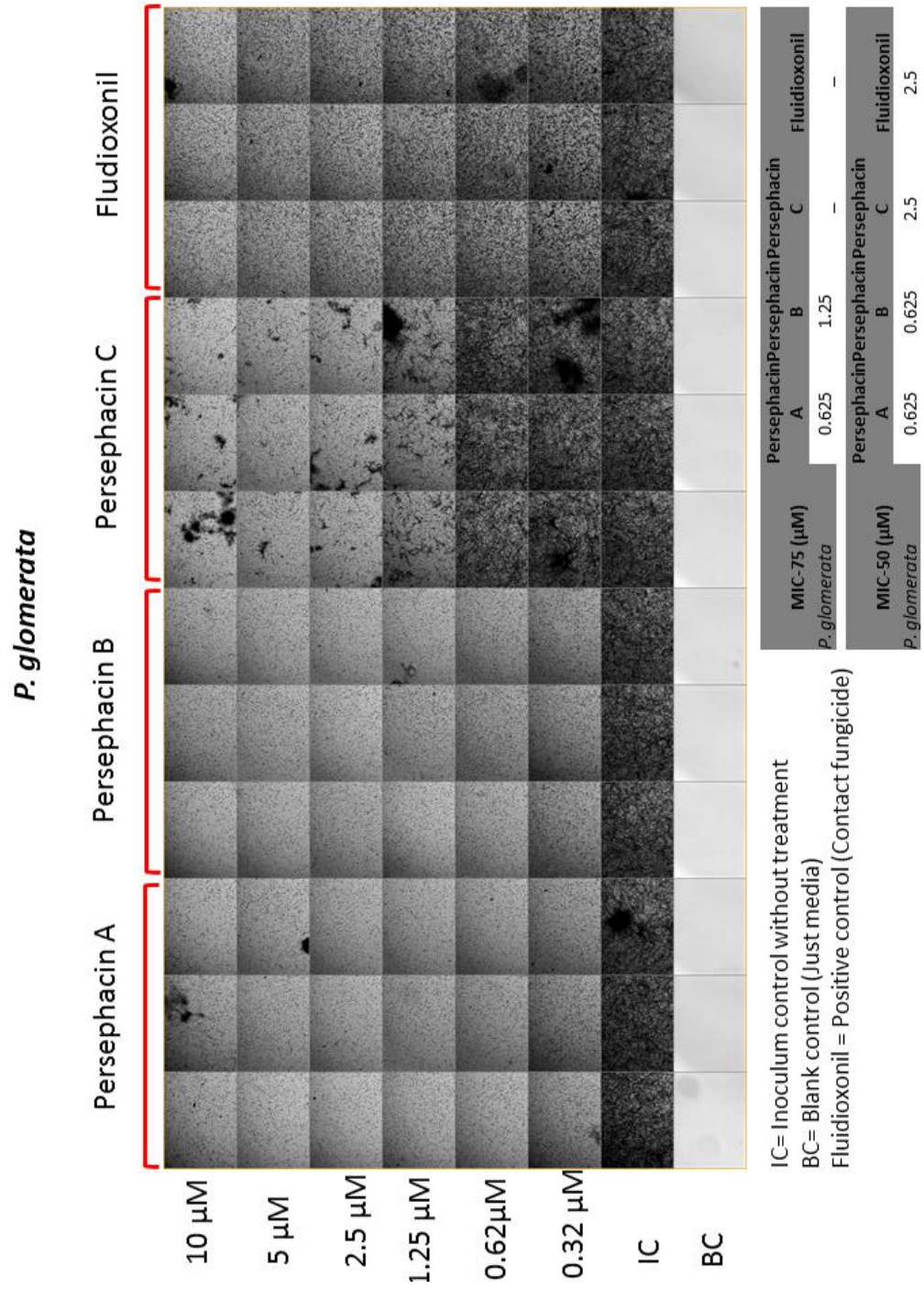


**Figure A59. Bioassay Data for *P. glomerata***

*A.2.19 Marfey's Analysis*

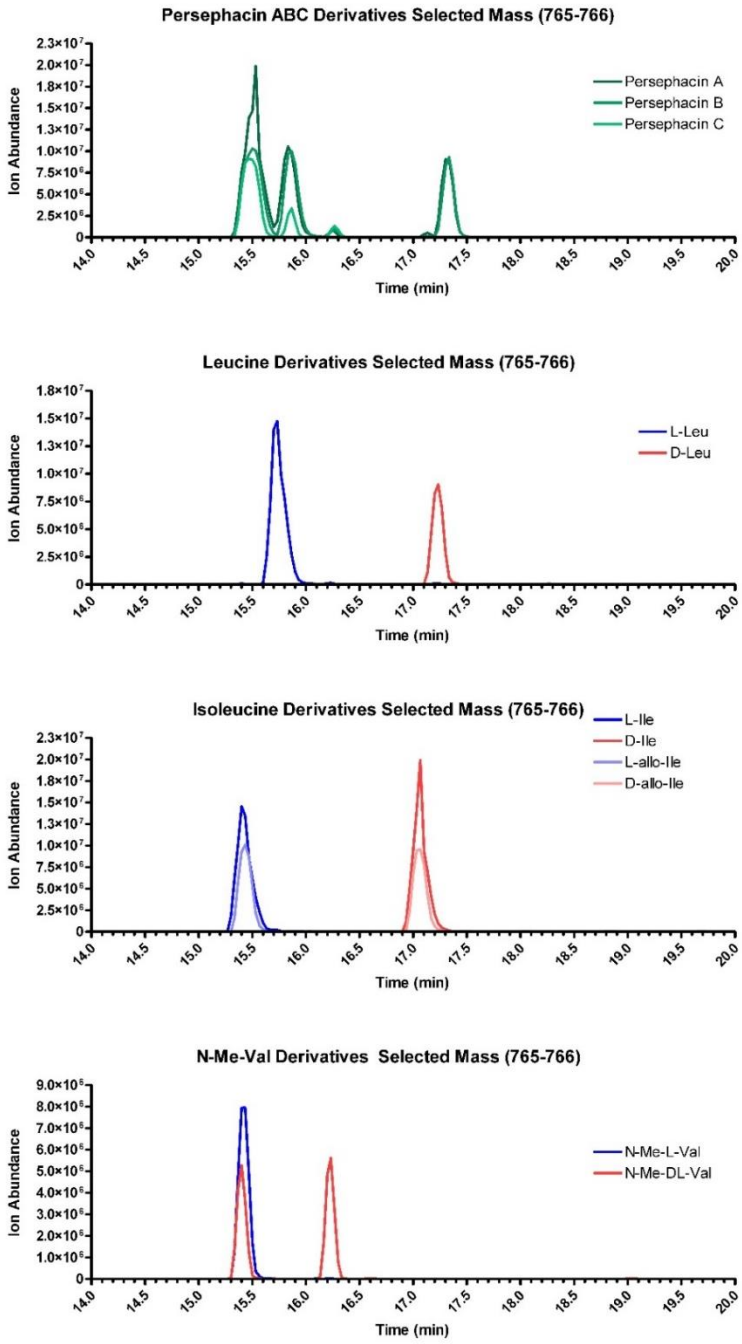


**Figure A60. Marfey's Analysis.** Showing the extracted mass Range for persephacins A-C in comparison with standard marfey reagents leucine, isoleucine, and *N*-Me-valine

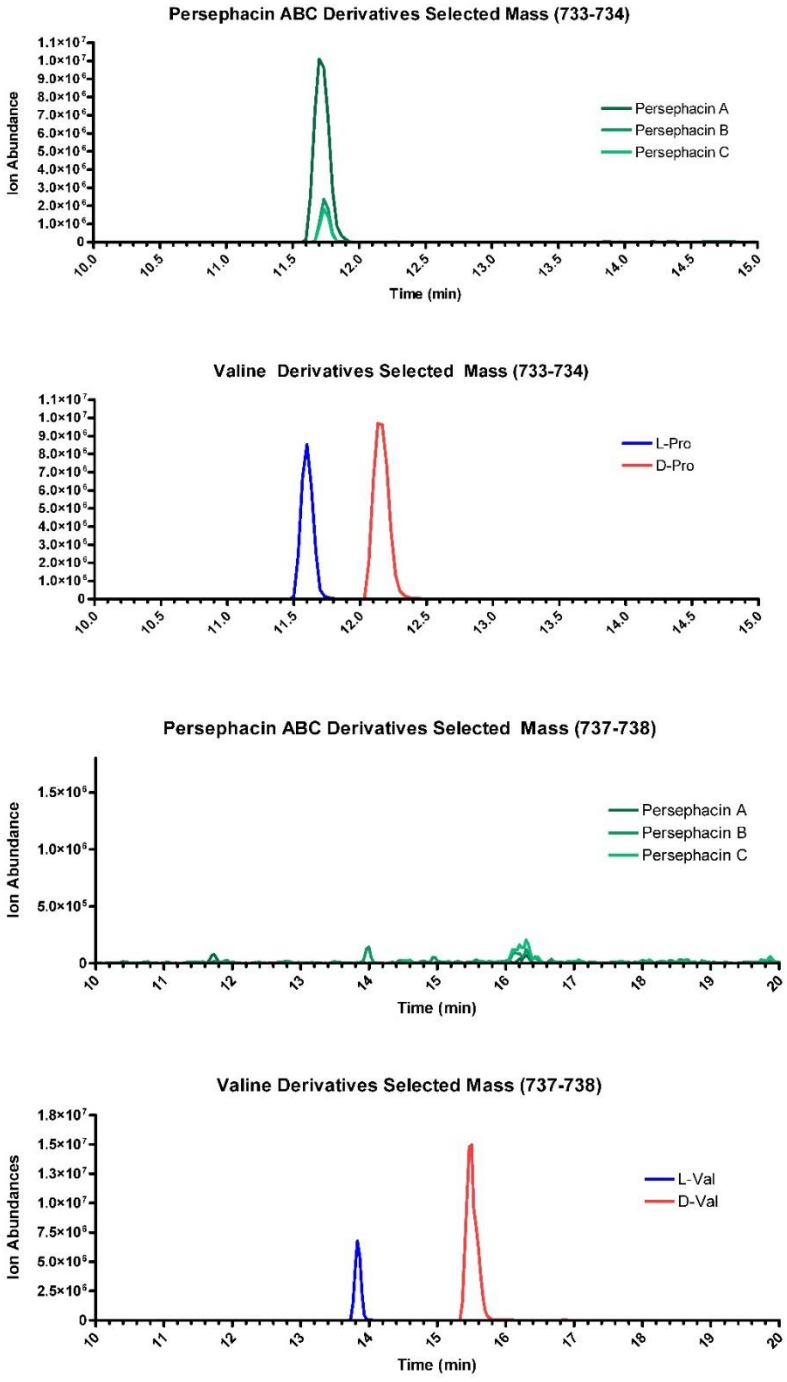


**Figure A61. Marfey's Analysis.** Showing the extracted mass Range for persephacins A-C in comparison with standard marfey reagents proline and valine